UNIVERSITY OF LIVERPOOL

Stephenson Institute for Renewable Energy

Encapsulated Salt Hydrate Phase Change Materials for Thermal Energy Storage

Thesis submitted in accordance with the requirements of the University of Liverpool for the Degree of Doctor in Philosophy

Michael Graham

Supervisor: Prof. Dmitry Shchukin

September 2017

Abstract

Man-made climate change is the biggest threat to humanity and other species inhabiting planet Earth. As technological advancement becomes ubiquitous with modern life, energy demand has increased immensely. It is vital to develop sustainable sources for energy production. Around 80% of worldwide energy is currently produced by fossil fuels. Coal, natural gas and oil are huge contributors to the release of CO_2 and methane into the atmosphere, which has led to a global average temperature increase of 0.8°C since the Industrial Revolution. Much research has been undertaken in developing renewable energies, with great recent advancements made on solar, wind and hydropower amongst others. Renewable energies garner much attention, both within the scientific community and mainstream media. However, renewable energies suffer from intermittency and cannot be used continuously. An often overlooked yet essential component of renewable energies is thermal energy storage, which will vastly improve their continued use and efficiency.

Chapter 1 provides a literature overview of the current world energy problem and energy storage. Thermal energy storage is currently achieved using sensible heat storage materials, which store heat as they increase in temperature. They have low volumetric energy capacity, especially when compared to latent heat storage materials, which store and release energy as they change phase. These materials are known as phase change materials (PCMs), of which organic paraffin waxes and inorganic salt hydrates (also known as crystallohydrates) are the most promising candidates. PCMs not only have the potential to improve efficiency of renewable energy sources, they may also be used for applications such as passive thermal regulation. Thermal regulation can greatly reduce air conditioning demands of buildings, and increase lifetimes of photovoltaics and electronics. Unfortunately, PCMs are not available for use in their bulk state due to several drawbacks which lead to short lifetimes. Numerous approaches have been made to increase their lifespan. Encapsulation within a polymer shell is considered the best approach, as it gives numerous advantages whilst employing simple reaction methods, allowing for industrial scale-up. Reducing

capsule diameter to the nanometre range hugely increases surface area to volume ratio, which can eliminate several inherent drawbacks of PCMs.

Salt hydrates are the most promising PCM, due to their very high volumetric energy storage density. However, they are also the most problematic PCM to work with. They are corrosive, incongruently melt and are prone to supercooling. Due to their hydrophilicity, they are also difficult to encapsulate. Our initial approach to confine them on the nanoscale was to produce water-in-oil emulsions using surfactants. Chapter 2 details how we found that several surfactant combinations could be used to provide an initial shell with salt hydrates solubilised within them. However, a more robust shell was required for full analysis.

To fully stabilise the salt hydrates, a polymer shell needs to form around the emulsion droplets. Chapter 3 details the use of poly(ethyl-2-cyanoacrylate) (PECA) for the formation of nanocapsules containing magnesium nitrate hexahydrate and sodium sulphate decahydrate. The salt hydrates showed vastly increased stability and thermal properties once encapsulated. Hydration level of the salts could be maintained by employing ultrasound to create miniemulsions, whilst supercooling was greatly reduced. The PECA nanocapsules were stable for at least 100 cycles, with results suggesting they would be stable for many more. This is in stark contrast to the bulk PCMs which were stable for less than 10 cycles.

Developing several polymer shells for encapsulation is of benefit as capsules can then be tailored to suit different applications. We used polyurethane (PU), one of the most commonly used polymers in industry, which displays great versatility. Chapter 4 documents how micro- and nanocapsules can be synthesised with a PU shell. Initial results have been promising, with the materials stable for at least 10 cycles when encapsulated. PU also displays better thermal stability and chemical resistance compared to PECA. Our results demonstrate the potential of salt hydrates for use in thermal energy storage applications.

Contents

List of Figures

List of Tables

Abbreviations

%wt – Weight percentage

ΔH – Latent heat

AOT – Aerosol OT (dioctyl sulfosuccinate sodium salt)

C_s – Specific heat capacity

CLHS – Cascaded latent heat storage

CSP – Concentrated solar power

DBDL – Dibutyltin dilaurate

DSC – Differential scanning calorimetry

DTA – Differential thermal analysis

EA – ethyl acrylate

ECA – ethyl-2-cyanoacrylate

EDX – Energy dispersive X-ray analysis

EE – Encapsulation efficiency

FTIR – Fourier transform infrared spectroscopy

LbL – Layer-by-layer assembly

LHS – Latent heat storage

MDI – methylene diphenyl diisocyanate

MMA – Methyl methacrylate

O/W – Oil-in-water emulsion

PACA – Poly(alky cyanoacrylates)

PAH – polyallylamine hydrochloride

PCM – Phase change material

PECA – Poly(ethyl-2-cyanoacrylate)

PEFC – Polymer electrolyte fuel cell

PEG – Polyethylene glycol

PEMA – Poly(ethyl methacrylate)

PHU - Polyhydroxyurethane

PMMA – Poly(methyl methacrylate)

PSS – Poly(sodium styrene sulfonate)

PU – Polyurethane

PUMC – Polyurethane microcapsule

PUNC – Polyurethane nanocapsule

PV – Photovoltaic

PVP – poly(vinylpyrrolidone)

SA/V – Surface-area-to-volume ratio

SEM – Scanning electron microscopy

SHS – Sensible heat storage

TCS – Thermochemical energy storage

TEM – Transmission electron microscopy

TES – Thermal energy storage

TEOS – Tetraethyl orthosilicate

TGA – Thermogravimetric analysis

TPV – Thermovoltaic cell

T_M – Melting temperature

T_F – Freezing temperature

W/O – Water-in-oil emulsion

W/O/W – Water-in-oil-in-water emulsion

XPS – X-ray photoelectron spectroscopy

XRD – X-ray diffraction

Dedication

I dedicate this thesis to Kathleen Halpin (24/09/34-15/08/2014) & John Graham (24/04/1930-15/08/2017), my dear grandparents who died whilst I was undertaking my PhD. I am fortunate to have great memories with each of them. I would also like to dedicate the thesis to my other grandparents Shane Halpin (14/08/35-23/10/2003) and June Graham, who is the last one standing!

Acknowledgements

Firstly, I want to thank my supervisor Prof. Dmitry Shchukin, who has helped me greatly over the past 4 years and allowed me to develop as a scientist. I hope I have repaid your faith with some good results.

Many thanks go to Dr. Paula Felix de Castro, who joined the group just before me and has been an invaluable help. I also thank the great group of people who have been in the Shchukin group during my PhD – Marios, Dan, Zhaoliang, Lorena, Xiaolei, Maria, Hongqiang, Claudia, Vicente, Mar, Yanli, Simona and Stewart.

The Stephenson Institute has been a great place to work and I don't know how I would have pulled through without the people in it. Firstly, my gratitude goes to 2 of my very best friends Mark Forster and Tom Galloway, who I had the pleasure of living with for 3 years. Our nights in the pub, hilariously aggressive political arguments, bizarre YouTube videos and times at Glastonbury Festival I will never forget. To the other guys who have helped me through the last 4 years I thank you all, we've had some great times and I'm sure we'll have many more!

Where would I be without music. I must thank Stars of the Lid, I have listened to literally hundreds of hours of their music whilst I've been reading and writing. Any other stuff I've been listening to - like Bing & Ruth, Jon Hopkins, William Basinski, Floating Points, Boards of Canada, Dawn of Midi, Leon Vynehall, Max Richter, thank you also for helping me concentrate. The National, my favourite band, I feel like we are best friends. No matter whether I've been happy, sad, angry, whatever – whenever I hear Matt Berninger's voice I feel better! My heart also goes out to my other favourites Radiohead, Yo La Tengo, Red House Painters/Sun Kil Moon, Nirvana, Sonic Youth, Pink Floyd, Velvet Underground, Sleater-Kinney, Godspeed You Black Emperor; and to Deafheaven, Mastodon, Drive Like Jehu, Inter Arma, Metallica & Sannhet amongst others for tearing my ears to shreds.

I thank the EPSRC and University of Liverpool for funding and for providing good facilities and working environment. Thanks to Karl Dawson, Tobias Heil and Keith Arnold at NiCaL for help with SEM and TEM measurements. Thanks to José Coca-Clemente for XPS data and Elena Shchukina for DSC measurements.

To my mum Sharon & dad Mark, thank you for all you have ever done for me. There's no way I would be where I am today without both of you. To my only sibling Chris, Britain's strongest man under 25, thank you for your utterly bizarre and hilarious anecdotes, and I will forever be fascinated with your ability to eat 12000 calories in a day.

Finally, to my wonderful girlfriend Becki, who still smiles every time she looks at me after 9 years (don't know how you do it!!!). I thank you for all you do for me.

1.

Introduction

1.1 Energy: Our most important resource and greatest problem

With each passing year, energy becomes more crucial in modern society. Rapid technological expansion and a growing population lead to increased electricity demand. A one third increase in demand is predicted by 2035[1]. There is a correlation between higher energy usage and higher literacy rates in countries[2]. As the developing world improves their technological infrastructure, their energy demands will increase. More developed countries will also increase their energy demand as artificial intelligence improves. Many common jobs will soon be performed by computers or involve more computing, and innovations such as self-driving cars will become widespread. Increased efficiency of energy production and use is crucial moving forwards.

Fossil fuels have been humanity's greatest energy resource since the dawn of the Industrial Revolution. In 2001, global consumption of energy was 4.25×10^{20}J, of which 86% was produced by fossil fuels[3]. Global energy demand will rise by approximately 33% from 2011-2035, according to the World Energy Outlook report in 2014[1]. However, oil, coal and natural gas reserves are not infinite, and have had an enormous impact on our environment. Atmospheric levels of carbon dioxide have risen from around 250ppm in the early 1800s to above 400ppm in 2016, while levels of methane have also soared. Large amounts of greenhouse gases in the atmosphere lead to the global warming effect, along with acidification of the oceans. Due to the lack of natural removal mechanisms for CO_2, it is predicted that it will remain in the atmosphere for 400-2000 years once absorbed[3]. Environmental change can already be observed by the behaviour of wild plants and animals, with their behaviour and geographical distribution already being affected[4,5]. Since the Industrial Revolution, average global temperatures have risen by approximately 0.8^{o}C, with the subsequent destruction of habitats contributing to the dramatic recent increase in the rate of extinction amongst species[6]. Global warming has also lead to increased melting of land based ice such as glaciers. Rising sea levels will eventually have grave consequences for life on land, especially due to the coastal location of many settlements which are rapidly growing in population[7]. Fossil fuels also lead to major

political problems. Their uneven distribution can lead to interdependencies between countries and may even lead to conflict[8].

Despite the catastrophic consequences of consuming fossil fuels, it is not currently an option to stop. The use of smartphones, the Internet and cars are now ubiquitous in modern life. More people have a mobile phone than proper toilet facilities, for instance. Energy consumption is vital for continuing technological development. Therefore, it is important to develop cleaner energy sources. The best possible energy sources are renewable energies. They are unlimited in the amount of energy they can supply, and often produce zero greenhouse gases. They are also cheap once equipment used to harvest the energy is built, as renewable sources are often free and require little to no sourcing of feedstock. Unfortunately, renewable energies suffer from several deficiencies which must be overcome for their widespread use. Renewable energies, combined with energy storage, carbon capture and geoengineering technologies can go a long way in helping prevent further man-made climate change[9,10].

Energy policy has become an increasingly important political issue, due to its humanitarian and environmental impacts. For example, the EU's energy strategy states that members must reduce greenhouse gas emissions by 40% and increase energy efficiency by 27% by 2030. Resulting from the focus on energy, a large amount of funding has been granted to many researchers working in the field. There are many ways in which energy can be harvested and stored, which will now be discussed.

1.2 Current Energy Production & Energy Storage Technologies

Fossil fuels provide most of the energy that we use and are an extremely large business, worth $4.65 trillion in 2014. In 2016, Forbes listed 6 oil companies as part of the top 10 most valuable businesses in the world. However, this economy will soon collapse due to the rapidly declining value and availability of oil. It is predicted that supplies of oil, coal and natural gas will expire by around 2050, 2060 and 2100, respectively; although including undiscovered and unconventional (such as shale, tar sands and methane clathrates) fossil fuels could have over a thousand years left[3]. However, the greenhouse effect would become catastrophic far more quickly. Nuclear power is an alternative power source, but there is concern about its use due to potential disaster, nuclear waste products and the high price of decommissioning. Unfortunately, due to the high demand for immediate power, renewable energies are not currently reliable or economically viable enough to fully replace oil, coal and natural gas. Therefore, it is vital to develop energy storage systems to ensure clean energy can be provided round the clock. Large amounts of research have been undertaken on energy storage. Lithium-ion[11] and lithium-air[12] batteries can be used to store electricity, while carbon nanotubes[13] and metal organic frameworks[14] can act as storage media for hydrogen. These measures have great potential to reduce emissions from the transport sector. Electric cars running on lithium batteries are now widely available. Lithium-air batteries suffer from reliability issues due to chemical instability and sensitivity to moisture, but theoretically can provide as much power as a traditional petrol driven engine[15–17]. Despite this progress, electric cars are only as green as their power source. For example, most energy in India is provided by coal-fired power plants. An electric vehicle in India will therefore be more polluting than a regular one, due to the increased emissions during production. In Paraguay and Iceland, almost 100% of electricity is produced from hydropower and geothermal energy. Therefore, an electric vehicle manufactured in Paraguay or Iceland will produce no emissions aside from those associated with the manufacturing process. Clearly, clean renewable energies are the key to future energy security and economy, along with prevention of further climate change.

While there are many types of renewable energy, reliability remains their main drawback. Hydropower is the most successful current renewable, due to its far superior reliability. It is extremely effective and can be up to 85% efficient, and was producing 19.8% of electricity in Europe as of the year 2000[18]. Hydro-electric plants use the energy of falling water to drive a turbine. Some utilise pumped hydropower where 2 reservoirs are used, with water being pumped to the reservoir of higher elevation. Pumped hydropower actually uses more electricity than it produces but is useful for electricity production during peak periods when demand outweighs production. Many more hydropower dams are planned[19] despite opposition to new developments, often from environmentalists due to the destruction of habitats. The number of sites available for hydropower are not unlimited however, so other renewable sources are also required. Due to effects from flooding on local vegetation, hydropower reservoirs may also release methane, a greenhouse gas.

Compressed air energy storage (CAES) is another renewable energy source. Air is compressed and stored in underground caverns. The air can then be heated during peak demand for electricity, making it a reliable source of energy. Air expansion during heating drives a turbine. Only 2 CAES plants have ever been constructed; the first in Germany in 1977, the second in Alabama, USA in 1991. Despite its reliability, Lund *et al* determined it was unlikely CAES is economically viable on a wide scale[20]. However, more CAES plants are currently under construction.

As can be seen from Fig 1.1, renewable energy provides a reasonable chunk of the world's energy (19.8% in 2013). However, around half of this is from burning biomass. Although renewable, burning biomass sources such as wood creates carbon emissions. Despite their minimal current production, solar and wind are the most promising renewable energies moving forward. The percentage of electricity produced by these means is rapidly increasing. Wind power is intermittent and requires many large turbines. The turbines are mounted on a tower to take advantage of faster and less turbulent wind. The turbines rotate due to air flow around the blades. The rotation spins a shaft which in turn drives a generator to produce electricity. Turbines are considered an eyesore by the

general public and generate noise pollution, so are usually limited to off shore wind farms. This negative perception is the major issue for wind power, although countries such as Denmark have found great success with its use. Energy storage to combat intermittency is also an issue for wind power. Excess wind energy must be stored in batteries or flywheels, the technology for which is currently very expensive. Solar power is more widely accepted as a major energy source. Huge amounts of research have been undertaken into improving the efficiency of solar power. Although many issues remain, technologies are under development which will greatly increase the potential of solar energy.

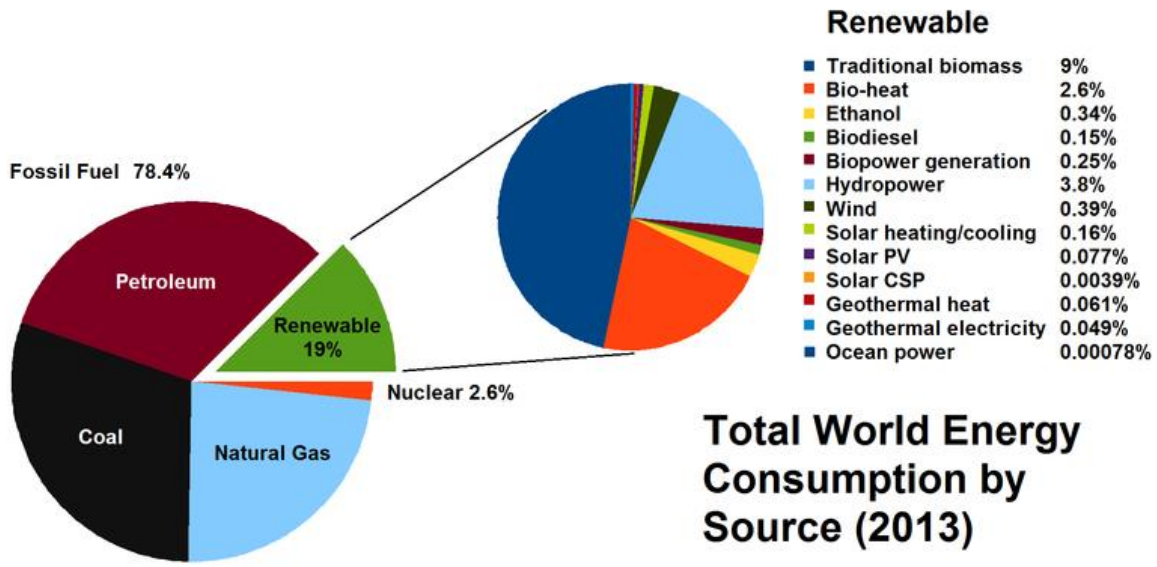

Fig 1.1 Chart displaying a breakdown of worldwide energy sources in 2013, taken from REN21 Renewables 2014 Global Status Report, http://www.ren21.net/Portals/0/documents/Resources/GSR/2014/GSR2014_full%20report_low%20res.pdf

1.3 Solar Power

Solar power is considered the most promising renewable energy due to its abundance, zero cost and lack of emissions[21]. The sun provides an unlimited source of energy which dwarfs that available from all other energy sources combined - in 2006 the US Department of Energy calculated that the worldwide consumption of energy in 2001 could be met with less than 1 and a half hours of sunlight[22]. Space missions have relied on solar energy for many years[23]. There are numerous ways to utilise solar power. Photovoltaics (PV) convert light into energy using semiconductors which display the photovoltaic effect. As the semiconductor absorbs photons, electron-hole pairs are created. An electrical potential difference can then be set up at the interface between two materials[24]. Doped silicon is traditionally used as semiconductor. The next generation of PV solar cells are being developed using halide perovskites[25–27] or polymers[28,29], with the new materials displaying excellent light harvesting abilities and potential improved efficiency. PV cells are often used to power smaller-scale applications such as single houses, although PV power stations have been built, consisting of many PV panels. Excess energy produced by PV can be stored by batteries in the form of electricity.

Concentrated solar power (CSP) allows large amounts of energy to be produced using the sun's rays, by concentrating the solar beam to create large amounts of thermal energy. It is the most promising way of utilising solar energy, due to its future cost effectiveness once the technology has been sufficiently improved. There are several different designs for CSP, which will be discussed below. All types operate by focusing sunlight which heats up water, creating steam. The heat can also be collected by an energy storage material for later use, an advantage over PV - which is difficult to incorporate energy storage into[1]. The steam created is used to drive a turbine to produce electrical energy, akin to a coal or natural gas-fired power station. CSP will be discussed in further detail later (page 26).

The major drawback of solar power is its intermittency - when the sun isn't shining, no electricity can be produced. This is where thermal energy storage is of great importance. Instead of producing

steam, excess thermal energy can be stored using an energy storage media, which acts as an energy sink. The energy can then be released during peak hours to meet demand, known as peak shifting. Despite the minimal publicity energy storage systems receive in comparison to other renewable technology, they are crucial in solving the intermittency problem. There is a distinct lack of successful storage options currently. On 8th June 2017, BBC reported that despite over 50% of energy in the UK being provided by renewables for the first time on the previous day, only 1% of it was produced from stored energy. Although there is a continued reliability issue with renewables, progress is rapidly being made. In late 2016, Portugal provided its entire energy supply for 4 days in a row using only renewables. Solar power is fast becoming the cheapest available energy source, a great improvement from the early days of photovoltaics when they were extremely expensive (around $77 per Watt in 1977 compared to $0.30 per Watt now). PV technology has been favoured over CSP despite the lower amount of energy production. This is due to the large amount of land and near perfect conditions (no cloud or haze) required for CSP to operate. CSP is therefore only suitable for wide scale energy production, while PV is more effective on a smaller scale.

CSP does have an advantage over other power plants in that destruction of habitats during construction can be minimal, although extreme heat produced from the parabolic mirrors can kill birds and other wildlife passing by during energy harvesting. CSP plants need large areas with no obstruction of sunlight for maximum exposure. Deserts are an excellent choice, providing large areas which contain minimal wildlife or human settlements. Indeed, the largest CSP plant currently built is the Ivanpah facility in the Mojave Desert, California (shown in Fig 1.2). Morocco has pledged to produce 42% of its electricity through renewables by 2020, and built the Ouarzazate CSP facility in 2015. Phase 2 and 3 of the project will open in 2017 and 2018, giving the facility a total energy production of 580MW.

Fig 1.2 The Ivanpah CSP plant in California, producing 390MW of energy

Renewable energies suffer not only from issues of reliability and energy production, but also from scepticism over climate change from some of the general public and high-ranking politicians (often with conflicts of interest!), despite a near unanimous consensus from climate scientists. Noam Chomsky described the Republican party of the USA as “the most dangerous organisation in human history” due to their refusal to tackle climate change. It is crucial that funding in renewable energies is continually increased and made a top priority, to reduce further climate change and increase future energy security.

Although the most important factor in the improvement of renewable energies is their efficiency, energy storage is a solution that can be developed more quickly. Due to the high temperatures involved, thermal energy storage is ideal for use in conjunction with CSP. Firstly, a suitable heat storage material must be selected. Factors involved in the selection of heat storage materials include cost, storage density and reliability. The various forms of thermal energy storage will now be discussed.

1.4 Thermal Energy Storage Media

1.4.1 Sensible Heat Storage (SHS)

Sensible heat refers to heat that can be detected ('sensed') by a temperature change. As materials heat up they store energy in a linear relationship with temperature (as seen in Fig 1.3). All materials can store heat sensibly, although some are more effective than others. The heat stored is dependent on the specific heat capacity (C_s) of the material in question. Water has a high C_s, and is widely used for SHS due to its low toxicity and availability. Rock or concrete are often used as solid SHS media, these store heat more uniformly than water but have lower heat capacity[30]. As temperature increases, thermal conductivity of rock decreases. At higher temperatures, rocks containing quartz will expand rapidly, affecting thermal cycling stability[31].

SHS is the simplest and most developed form of heat storage, and is the only heat storage method to be industrialised. However, it suffers from several issues, such as low energy density and loss of thermal energy at any temperature[32]. Large containers are required to house enough material to store heat effectively. This increases costs and maintenance requirements. The mediocre heat storage capacity of SHS has led to research into other storage materials to improve economic feasibility. SHS is still useful due to its simplicity, and can be used in conjunction with other energy storage methods such as latent heat storage to improve heat transfer[33].

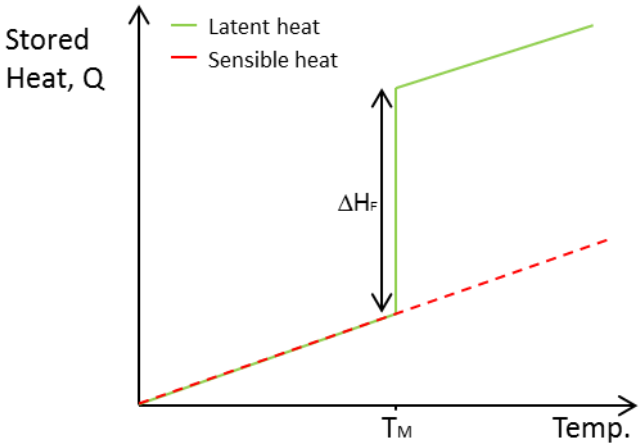

Fig 1.3 Comparison between SHS and LHS, ΔH_F is the latent heat of fusion during melting

1.4.2 Latent Heat Storage (LHS)

Latent heat storage (LHS) refers to heat transfer associated with phase transitions, which cannot be detected with a thermometer. LHS stores more energy, is more efficient and has a far superior storage density than SHS. This phenomenon was discovered by Joseph Black in 1761, during research into finding the optimum quantities of fuel and water for a whisky distillation process. He noticed that ice took in heat energy without increasing its temperature. Materials which can utilise LHS are known as phase change materials (PCMs). Examples of phase transitions include melting and freezing (solid-liquid), evaporation and condensation (liquid-gas) or changes in crystalline structure (solid-solid). Essentially, the energy associated with these changes corresponds to the numbers of chemical bonds broken. Therefore, solid-gas transitions store the highest amount of energy. However, the large volume change of these transitions means pressurised containers are required, and therefore they are not suitable for practical use. Solid-solid transitions are useful due to the lack of volume change (hence they are known as 'form-stable' PCMs), but can only store small amounts of energy. Solid-liquid PCMs give a good balance between high energy capacity and acceptable volume change upon melting; these are seen as the most promising PCM type. As can be seen from Fig 1.3, LHS materials store heat sensibly up to the melting point (T_M). During melting, a large

amount of heat is stored almost isothermally. Once the material freezes, this heat energy is released again. PCMs are far more efficient than SHS materials, especially over the small temperature range associated with their phase transition. It is also advantageous for PCMs to have good specific heat capacity to provide additional SHS whilst the material is not undergoing a phase change.

In 1983, Abhat[34] outlined the ideal properties for a PCM:

Thermodynamic

- T_M in desired application range
- High latent heat of fusion
- High density
- High specific heat for additional SHS
- High thermal conductivity
- Congruent melting
- Small volume changes during phase transition

Kinetic

- No supercooling

Chemical

- Chemically stable over long periods
- Non-corrosive to container materials
- Non-flammable, non-toxic and non-explosive

Economic

- Low cost
- Available in large quantities

However, there are no PCMs to date which fit all these criteria. Practical applications and classification of PCMs will be further discussed in more detail below (see page 17)

1.4.3 Thermochemical Energy Storage (TCS)

In terms of thermal energy storage, storage density is of great importance. Hence, LHS is of great interest as an improvement over SHS. Meanwhile, TCS gives the highest energy density of all, around 5 to 10 times greater than LHS and SHS respectively. TCS relates to energy stored and released during controlled reversible reactions. Thermal energy is stored during the endothermic forwards reaction and released during the exothermic backwards reaction, for example:

1. $MX.nH_2O \rightleftharpoons MX + nH_2O$

2. $M(OH)_2 \rightleftharpoons MO + H_2O$

3. $MCO_3 \rightleftharpoons MO + CO_2$

Eq 1.1-1.3 Examples of reversible thermochemical reactions **1.** Dehydration of a metal salt **2.** Metal hydroxide to metal oxide reaction **3.** Metal oxide to metal carbonate reaction

Equations 1-3 demonstrate some examples of thermochemical reactions. The temperature at which the reaction spontaneously occurs needs to match the temperature of the application. Eq. 1 shows a typical dehydration of a salt hydrate to give a salt and water. The case of salt hydrates is an interesting one, as they are usually thought of as an LHS material, but can demonstrate thermochemical properties if the sorption and desorption of water is utilised. Donkers *et al*[35] prepared a study of many TCS reactions of salt hydrates, finding that very few are currently suitable for practical use. Sorption reactions have the highest energy density of any storage media, and can

refer to adsorption or absorption. It is defined as the capture of a gas or vapour by a substance in the solid or liquid state[36]. Sorption can be a physical or chemical process, with chemisorption giving higher energy densities but may be irreversible. Adsorbent materials for use in these reactions are usually porous materials such as zeolites or silica gels[36]. Eq. 2 is the hydration/dehydration of a metal hydroxide. Magnesium oxide has been proposed as a useful example for storage between 90-110°C with good durability[37]. In 1977, Ervin[38] showed magnesium oxide had a conversion decrease from 95% to 60% over the first 40 thermal cycles before it stabilised. Eq. 3 shows the decarboxylation of a metal carbonate. Calcium carbonate is the most studied material for this reaction, which has shown reasonable cycling stability and can be improved with additives[39].

TCS has been outlined as especially important for long term energy storage over many months, with a theoretically unlimited storage period due to zero thermal losses. SHS and LHS are not as ideal for long-term storage as they progressively lose energy[40]. For use in practical applications, suitable TCS reactions must first be identified. Factors such as the rate of reaction, reversibility and the effects of temperature and pressure must be considered. Unlike with LHS where gas phase reactions are undesirable, TCS can take advantage of the extra energy density of solid-gas reactions. Posern and Kaps[41] utilised a mixture of $MgCl_2$ and $MgSO_4$ salts impregnated into attapulgite, based on their hydration/dehydration reactions. The two salts were selected due to their differences in deliquescent relative humidities (DRH) – $MgSO_4$ is more hydrothermally stable, so has a higher DRH than $MgCl_2$ (90% compared to 33% at 30^{o}C). They found increasing the ratio of $MgCl_2$ had a positive effect. Although $MgCl_2$ has a lower ΔH_f, the increase in the rate of water vapour condensation due to the lower DRH increases heat of sorption overall. This interesting effect should be considered when using salts as TCS materials. A drawback of their approach was that the increase in water vapour led to leakage out of the porous attapulgite. They hypothesised new porous host materials with differing pore sizes could be utilised in future to prevent leakage. Another drawback was that low desorption temperatures must be used, as higher temperatures led to increased corrosion. Neises *et al*[42] tested a solar heated rotary kiln utilising the redox reaction of cobalt oxide. They found the

reaction had good thermal storage abilities at temperatures between 800-900°C, the reaction being followed by a measure of the oxygen concentration at different temperatures. A complex reactor design would be necessary for larger scale use, however.

Despite the progress made with TCS and its potential for high temperature applications, like LHS it has issues with long-term stability but to a larger degree. Reactions must have constant conversion efficiency without degradation of energy storage capacity over long periods of time[43]. This is especially difficult when dealing with gas and liquid phase reactions. A potential solution to leakage could be to encapsulate the reactants in a shell material. It has been shown that organic reactions can be improved by encapsulating the reactants for example[44]. TCS also currently requires high cost materials for long-term storage[40], improved heat transfer[43] and complex reactor design[40], meaning SHS and LHS are preferable for now. Essentially, the major problem for TCS is the lack of research and understanding. Currently, SHS has been developed to an industrial level, LHS to pilot plant scale, while TCS has only been tested on a laboratory scale[39]. TCS may be valuable in future, but LHS should be the focus for immediate research as a solution to energy storage issues.

1.5 Phase Change Materials (PCMs)

1.5.1 PCM Classification

There are many kinds of PCM, as seen in Fig 1.4. PCMs can be classified according to the specific phase transitions they undergo. The possible transitions that yield LHS are solid-solid, solid-liquid, solid-gas and liquid-gas. While sublimation and evaporation give the highest latent heat of fusion, they are not practical due to the large volume change and need for specialised containment to prevent material losses. Solid-liquid PCMs are viewed as the most practical, as they give a good balance between high latent heat of fusion and manageable volume change.

1.5.2 Solid-Solid

Solid-solid PCMs have pseudo-phase transitions arising from a rearrangement of the crystal structure. The main advantage of these materials is that they have almost zero volume change during phase transition, meaning they require no encapsulation. A downside to this is that the latent heat of fusion is relatively low. Solid-solid PCMs can only be cost effective if the low cost of not having to contain the material can be balanced by a relatively high latent heat and energy storage density.

Polyurethane polymers are commonly synthesised as solid-solid PCMs. Du and collaborators[45] synthesised a hyperbranched polyurethane as a PCM. Hyperbranched structures increases phase change enthalpy compared with linear polymers due to the increased number of possible arrangements of the compound. Even so, they found the latent heat was lower than that of PEG 6000, a solid-liquid PCM. The lower latent heat and high cost of synthesis mean it is unlikely solid-solid PCMs will ever be seriously considered for large scale use.

1.5.3 Solid-Liquid

From now on, all PCMs described in the thesis will be solid-liquid. As described earlier, solid-liquid are most useful for practical applications. Due to the volume changes upon melting, suitable containment is necessary. Solid-liquid PCMs can be classified according to whether they are organic or inorganic materials (Fig 1.4). Organic PCMs include paraffin wax, fatty acids and polyethylene glycol (PEG), whilst inorganic PCMs can be salt hydrates, salts or metallic.

Paraffin waxes are the major organic PCM. They are linear alkanes containing between 8-40 carbon atoms. Longer carbon chains give higher T_Ms, in a relatively linear fashion (Fig 1.5). Paraffins often display additional LHS in the form of solid-solid transitions associated with different crystalline phases. They have several advantages, including good thermal and chemical stability, good latent heat of fusion (ΔH_F), congruent melting and no supercooling. Disadvantages include low thermal conductivity, bad odour, flammability and high cost. It has been shown that the cost of paraffin wax is so great, that a storage tank for a CSP plant would cost more to maintain than the value of the energy stored. Paraffin waxes are also non-renewable, as they are refined from petroleum. With regard to their low thermal conductivity, Javani *et al*[46] simulated a PCM heat exchanger with octadecane to control the battery pack temperature of an electric car. They found that improving the thermal conductivity to a practical level using finned tubes to increase heat transfer area was impossible, as the tubes would be too long to fit in the car. Conductive particles would be required instead.

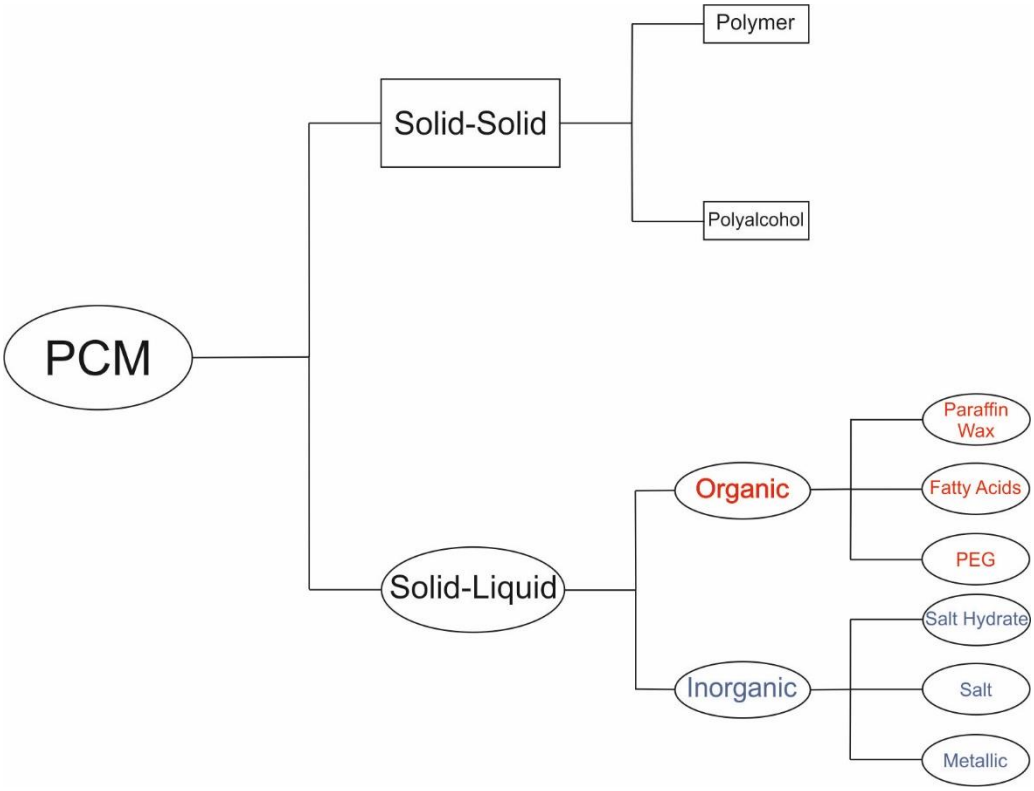

Fig 1.4 Classification of various solid-solid and solid-liquid PCMs

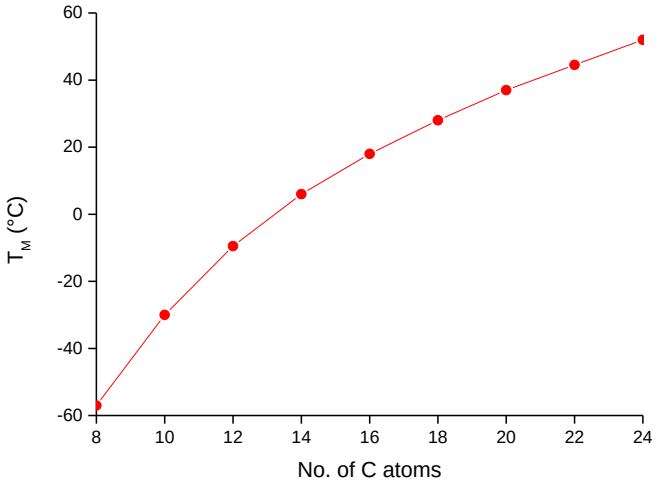

Fig 1.5 Graph showing how carbon chain length affects T_M in paraffin waxes[47]

Fatty acids have similar properties to paraffin waxes, such as reasonable latent heat and poor thermal conductivity. They have additional advantages such as non-flammability and no bad odour. However, their high cost (even higher than paraffin waxes) has rendered them unusable in practical applications. Due to the large volume change on melting, they must also be contained. Several attempts at synthesising form-stable fatty acids have been made, which is discussed later (see page 24).

Salt hydrates (also known as crystallohydrates) are the major class of inorganic PCM, and most promising PCM overall due to their high latent heat, high energy storage density, low cost, abundance, reasonable thermal conductivity and wide range of T_Ms in the domestic application range (5-130°C). Their favourable properties compared to paraffin waxes are displayed in Table 1.1. They have the general formula M.$n$$H_2O$ where M is a metal salt and n is the hydration number. The hydration number has a profound effect on the T_M of the salt hydrate. The lower the hydration number of a particular salt, the higher the T_M. This is due to the mechanism by which they melt. As salt hydrates reach the T_M, water molecules free themselves from the crystal structure. The liquid

water then dissolves the salt. Therefore, the less water molecules available to dissolve the salt, the higher the T_M. For example, magnesium nitrate hexahydrate has a T_M of 89^oC, whereas its dihydrate form has a T_M of 129^oC. Especially, salt hydrates' high energy density is attractive as less material is required. Smaller containers are therefore needed, reducing costs further. Salt hydrates have densities in the region of 1500-2000 $kg \cdot m^{-3}$, whereas paraffin waxes have densities of around 900 $kg \cdot m^{-3}$. Combined with their higher latent heats of around 200-250 $J \cdot g^{-1}$ compared with 150-200 $J \cdot g^{-1}$ for paraffins[48], their energy storage ability is far greater. Some paraffin waxes have latent heat values equal to that of some salt hydrates. However, when the latent heat per unit volume is quoted, salt hydrates will demonstrate greater energy storage ability. Salt hydrates have energy densities of around 250-400 $J \cdot dm^{-3}$ compared with around 125-200 $J \cdot dm^{-3}$ for paraffin waxes[34,49,50]. Data for energy density in $J \cdot dm^{-3}$ is sparse in the literature, but is very useful when considering container sizes. It is also a good illustration of why more research into salt hydrate PCMs is beneficial. Salt hydrates have a greater range of T_Ms (5-130^oC) for use in domestic applications compared with paraffin waxes (5-80^oC). They can be as cheap as <100$/ton in the case of sodium sulphate decahydrate[51]. The research presented in this thesis is based around salt hydrate PCMs.

When interest in PCMs first arose after the oil crisis of the 1970s, most investigations were centred on salt hydrates. However, their use leads to numerous problems that could not be solved at the time, and paraffin waxes became the most frequently investigated PCM. Disadvantages of salt hydrates include incongruent melting, phase separation, supercooling and corrosiveness towards container materials, especially metals. Incongruent melting is incomplete melting of the salt hydrate, leading to the irreversible formation of a salt of lower hydration number. This salt then precipitates at the bottom of the melt, known as phase separation[34]. These effects reduce ΔH at the desired T_M, and will eventually lead to zero latent heat, and also rendering salt hydrates chemically unstable, often after very few melting/freezing cycles. Supercooling is also a major problem. It is a phenomenon where a material must be cooled far below its T_F in order to freeze, caused by poor heat transfer and lack of nucleation[34]. This can be as much as 40^oC. Salt hydrates also display

corrosiveness towards container materials, and several studies have been undertaken to understand which materials can be used to contain them[52,53]. In hermetically sealed vessels it is possible to stabilise salt hydrates with minimal losses of latent heat for many cycles[54]. However, other factors such as corrosion, supercooling and volume changes must be considered. Some commercial salt hydrates have been produced which are stable over very many cycles (>10000), made possible using additives. These are roughly 10x more costly than pure salt hydrates[51] though, and encapsulation is still necessary. More cost-effective methods need to be found.

Table 1.1 Comparison of key properties of paraffin wax and salt hydrate PCMs. Data taken from Zalba *et al*[48] and Abhat[34]

	Paraffin Wax	**Salt Hydrate**
Energy Density	*125-200 J·dm^{-3}*	*250-400 J·dm^{-3}*
Latent Heat	*150-200 J·g^{-1}*	*150-250 J·g^{-1}*
T_M Range	*-60-80^{o}C*	*5-130^{o}C*
Thermal Conductivity (Solid Phase)	*0.2 W·m^{-1}K^{-1}*	*0.7-1 W·m^{-1}K^{-1}*
Supercooling	*No*	*Yes*
Congruent Melting	*Yes*	*No*

An advantageous property of salt hydrates that is yet to be fully realised is the formation of mixtures and eutectics. When salt hydrates are mixed, their T_M is lowered due to the inhibition of crystallisation of the components. The ratio which results in the lowest possible T_M, always lower than both of the component compounds, is known as a eutectic. At this ratio, a single crystalline phase develops while phases of the single crystallohydrates disappear. Eutectics have a higher latent heat than other mixture ratios due to the formation of a single phase. This ability to adjust the T_M with a simple procedure is highly advantageous to tailor PCMs for specific applications. Unfortunately, little research has been done on salt hydrate eutectics, although eutectic mixtures of non-hydrated salts are used for SHS in CSP. Research into eutectics is particularly useful as there are few known pure crystallohydrates with a T_M in the optimal range for applications such as air conditioning[51].

Other major classes of inorganic PCMs are salts and metals, which are the most suitable for high temperature applications. They have the widest range of melting temperatures, salts from -86°C for a 24.8 weight percentage (%wt) HCl and water eutectic mix[55], up to 500+°C. Several metals and alloys have T_Ms lower than 100°C; others have T_Ms of 1000°C+. The major advantage of metallic

PCMs is their high thermal conductivity[56], but they have low storage density. The high mass of metals must also be considered for any practical applications such as their use in building materials, and also makes them unsuitable for transportation of heat energy[57]. Low temperature metallic PCMs such as Gallium (T_M = 29.8°C) have been used to cool computer chips[58] and USB memory drives[59]. It is anticipated in future that encapsulation techniques for high temperature PCMs will be developed, which will make them available for applications such as storage for CSP or reusing waste heat[57].

Another class of PCM which may be of use are clathrate hydrates. Clathrate hydrates are compounds in which guest molecules are entrapped by a network of hydrogen bonded water. A similar compound to a clathrate is the 'organic hydrate' pinacol, which can be found in monohydrate and hexahydrate forms. It has rarely been investigated as a PCM, although Rathgeber *et al*[60] showed that it combined advantages of inorganic and organic PCMs, with high volumetric latent capacity and lack of corrosion. However, they did not demonstrate prolonged cycling stability and pinacol is expensive.

1.5.4 Form-Stable PCMs

Form-stable PCMs are solid-liquid PCMs which have been combined with a structural support, usually a polymer such as polyurethane (PU) or polymethyl methacrylate (PMMA), so that they keep their shape even after melting. Organic or polymeric PCMs can be made form-stable. Essentially, the PCM is embedded into a polymer matrix, thereby preventing leakage and preserving latent heat capacity. This provides several other advantages, such as removing the need for further containment, reducing thermal resistance caused by any shell material that would otherwise be required and preventing reaction with any external materials[61]. It is possible to load the PCMs into the polymer up to around 80 %wt, meaning the latent heat remains high[62]. Several researchers have formulated fatty acid-based form-stable PCMs. Sari and collaborators have made numerous fatty

acid blends for use as form-stable PCMs[61,63,64]. They confirmed the PCMs had reasonable latent heat and were suitable for use without further encapsulation. Despite some positives of form-stable PCMs, leakage remains a problem at high loading, and the need for a large amount of structural support means form-stable PCMs are not cost-effective.

1.6 PCM Applications

Broadly speaking, there are two major applications PCMs can be used for. They are thermal energy storage and thermal regulation. Thermal energy storage (TES) can be used to store excess thermal energy produced from CSP, as mentioned previously, or also waste heat from urban zones[54]. It can also be used for applications such as 'smart tarmac'[65], which stores heat during summer and can then keep roads or runways free of ice during the winter. Thermal regulation can be used as a passive form of air conditioning in buildings or clothing, or for cold storage. PCMs may also be used as a hydraulically powered engine, with the expansion and contraction of the material powering a generator, known as a PCM engine[66]. The conversion efficiency for these engines is currently poor (around 2.5-7.5%). This review will focus only on thermal applications that PCMs are better suited for. Following is an in-depth discussion of potential and current PCM applications.

1.6.1 Concentrated Solar Power Storage

Concentrated solar power (CSP) involves the direct use of sunlight to create heat energy, by concentrating the solar beam onto a single point using mirrors. This creates high temperatures which can be used to create steam to drive a turbine. High heat produced from the concentration of sunlight is usually transferred to a heat transfer fluid (HTF), which can be used to transport the heat energy to a power block[1]. Higher temperatures lead to higher Rankine cycle efficiency. A Rankine power cycle is the model used for steam-driven turbines. It consists of four processes - 1. A high-pressure liquid is pumped into a boiler and heated to saturation temperature 2. Vapour expands to drive the turbine; this work can be converted to electricity 3. The vapour leaving the turbine is condensed at low pressure 4. The condensate is pressurised in the feed pump to be re-used. Typical Rankine cycle efficiencies are around 40% for fossil fuel fired plants, a figure which is achievable for CSP in future[67]. The major loss in efficiency is during the conversion of heat to electricity.

USA and Spain are the leading countries in the development of CSP, although many other countries are building or have expressed interest in using CSP. Indeed, any country except those above latitude 45°N or below 45°S are well-placed to utilise solar energy. The countries between these two latitudes have average irradiation of at least 1.6MWh/m^2. Numerous 'hot spots' exist, including the Sahara, Kalihari, Atacama and Mojave deserts; the Middle East and north west Australia[68]. To illustrate its potential, if only 1% of the land area with the required solar radiation were used for CSP, the energy production would still be higher than the total world energy supply for the year 2000[69]. CSP has relied on government subsidies in order to be cost effective[70], so improving efficiency and output is a must. There are various types of CSP plant designs. These are linear Fresnel, parabolic dish, parabolic trough and power tower[68], visualised in Fig 1.6. All kinds of CSP depend on their solar collectors, as they are the means to focus the solar beam. Each design has its own set of advantages and disadvantages, which will now be discussed.

The power tower CSP design has been highlighted as the most promising. A recent example is the Gemasolar plant in Seville, Spain. It has an operating capacity of 74% the total theoretical energy yield. This compares with 41% for previously developed parabolic trough plants[67]. A large number of heliostats focus the sunlight onto a central tower. Heliostats are mirrors which follow the sun by means of electronic operation, in order to focus the solar beam onto a single point – the power tower. Heliostats have the added advantage of using flat glass, which is cheaper than the curved glass used in parabolic mirrors. This heat is transferred to the HTF, which can either create steam directly, transfer it to an energy storage material or store the energy itself. Power towers have several advantages, such as the creation of high temperatures – producing higher efficiency and reduced storage costs; and a flexible setup allowing the choice between various HTFs, heliostats and receivers. Due to the improved tracking of the sun by heliostats, they are more effective at producing energy in winter than other CSP plants[67]. Over a third of planned CSP plants are of the power tower design.

Parabolic trough systems form a large majority of operational CSP plants[71], such as the Solana Generating Station in Arizona and the Solnova Solar Power Station near Seville, Spain. The collectors are parabolic reflectors which reflect onto an absorber tube attached along the parabola. The absorber consists of a metal tube and glass covering, separated by air or vacuum to reduce thermal losses. The reflectors and tubes move consistently with the sun. Again, with this method it is possible for direct steam generation or storage with the use of a HTF. Main advantages of this design are that it is easily scalable, and the troughs only require two dimensional tracking of the sun, whereas other designs require three dimensional tracking[72].

Linear Fresnel systems are similar to parabolic trough collectors, but consist of a series of flat mirrors with a downward facing absorber tube, which is fixed to a tower and lies above the reflectors. Puerto Errado 1 in Murcia, Spain is a small capacity Linear Fresnel power plant. The main advantage in this method is its simplicity which lowers costs and allows direct steam generation. However, it has a lower efficiency than other CSP designs[73] and energy storage is difficult to incorporate.

Parabolic dish collectors are single collectors with the heat absorber located above the dish. Both components move in tandem to react to track the sun. They have a higher efficiency than the other CSP collectors and do not require a HTF. Their major disadvantages are their expense due to the large number of different dish collectors required. Each dish produces electricity independently, meaning hundreds or thousands of them are needed to create a CSP plant. It is also difficult to incorporate energy storage to the parabolic dish design. Despite their deficiencies, several parabolic dish power plants are under construction[74].

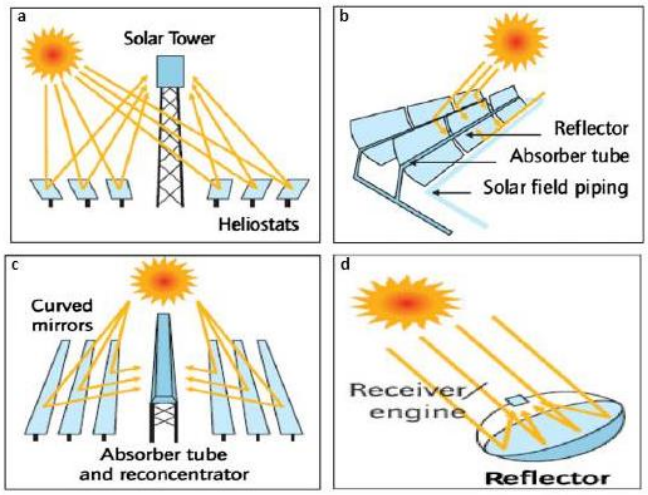

Fig 1.6 Different designs for CSP collectors **(a)** solar power tower **(b)** parabolic trough **(c)** linear Fresnel **(d)** parabolic dish. Taken from Zhang *et al*[68]

The ability to store energy for CSP is essential. When there is no sunlight at night or during cloudy periods, direct steam generation is not possible. Stored thermal energy can then be released from the storage media to produce electricity, in effect producing electricity 24 hours per day. The storage energy and direct energy are independent, providing 2 efficient Rankine cycles to deliver energy. Excess energy produced at times of low demand is stored to be used during peak demand, known as peak shifting. This ensures there is no difference between supply and demand for energy. Increased reliability of renewable energies means consumers have increased confidence in buying, causing the technology to become profitable.

Current state of the art energy storage for CSP plants is SHS using molten salt eutectics. They are useful due to their high C_s and ability to be used as heat transfer fluid (HTF) as well as energy storage media. Mineral oil was the original storage material for early CSP plants, but molten salts can be used at much higher operating temperatures (currently up to 565^{o}C, compared with 393°C for mineral oil). Higher operating temperatures improve Rankine cycle and thermodynamic efficiency of the CSP plant. Molten salts currently used are usually nitrates[75], for example Solar Salt, a 60:40 mix

of sodium nitrate and potassium nitrate. At temperatures above 600°C, nitrate salts degrade and release highly corrosive nitrogen oxide[76], causing problems with containment and mass loss. Current solar power tower plants can produce temperatures of up to 950°C[77], so new materials are required for higher temperature storage. Molten salts have high T_Fs (e.g. Solar Salt T_F = 220°C), meaning anti-freeze measures are required which use lots of energy. Freezing results in an unwanted discharge of large amounts of energy, and can lead to blockages and damage to the system[67]. Current CSP plants must burn fossil fuels to quickly reach operating temperatures each day. Also, due to the inferior heat storage SHS provides, large tanks are required to house the molten salts. Larger containers and amounts of storage material increase costs. Problems also remain with corrosion and salt decomposition[78]. Current production of the commonly used SHS nitrate salts is not sufficient to supply the proposed number of CSP plants in future - 30 times the current production would be required to supply CSP plants by 2050[1], so the development of new thermal storage materials is crucial. An ideal solution would be to develop a high temperature PCM of T_M at least 300-550^{o}C to improve the Rankine efficiency of the energy cycle, along with increased energy density of storage. HTFs and other components must also be developed for use at these temperatures[76]. The cost of keeping the PCMs above their T_M would be offset by the better energy storage capacity compared to SHS materials. The candidates for high temperature PCMs are inorganic salts and metals.

Inorganic salts proposed as high temperature PCMs include nitrates, chlorides, sulphates and carbonates. They have fewer problems with supercooling and phase separation than salt hydrates, although still have low thermal conductivity. Volume changes upon melting of salts can exceed 10%, which must be taken into account when designing containers to house them[79]. Liu *et al*[80] found salts with higher T_Ms generally have higher heat storage capacity, and therefore give lower costs per kWh of energy produced. Fluoride salts have good heat capacity, especially some eutectics, but have higher costs and are less compatible with containment materials.

Metals have higher thermal conductivity than salts, but much lower energy storage per unit weight. Relatively few studies have been undertaken on understanding their properties. A study in 1994[81] found the major advantage of the high thermal conductivity, using aluminium as PCM. The Al was encapsulated in a stainless steel capsule 4cm in diameter. They found a uniform temperature throughout the metal core, whilst identical tests with salts resulted in a thermal gradient depending on the proximity of the salt to the capsule shell. Blanco-Rodriguez *et al*[82] investigated a eutectic alloy of 49 %wt magnesium and 51 %wt zinc, which had a T_M of 342°C, for use in CSP storage. The material had minimal supercooling, due to its high thermal conductivity of 75 $Wm^{-1}K^{-1}$ at 300°C, which is 2 orders of magnitude higher than any inorganic salt. Despite this, the metal alloy had a higher cost and much lower energy storage than salts. Metallic PCMs also have an issue with corrosion in the liquid phase[83]. Investigators have attempted to solve this problem by coating in other metals, such as coating a copper PCM in an iron shell[84]. Of course, other safety issues arise from the use of molten metal.

Datas *et al*[85] *c*onceptualised a high-temperature LHS system using silicon as PCM. Silicon has very high latent heat (1800 $J \cdot g^{-1}$), high thermal conductivity, low cost ($2/kg) and a high T_M of 1414^oC. They simulated a system which directly converted the stored energy into electricity using thermovoltaic cells (TPV). They discovered the TPV would have discharge efficiencies of 20-45%, which would lead to electric energy densities in the range of the best performing Li ion batteries. The problem with adapting this potential technology for use with CSP, is safety and practicality in working with such high temperatures. Containers and other equipment would have to be stable at temperatures approaching 2000^oC.

Some researchers have proposed combining high temperature PCMs with additional SHS storage materials. Laing and collaborators[86] designed a prototype utilising sodium nitrate LHS for steam generation combined with concrete-based SHS for preheating and superheating. They proposed using aluminium fins in the PCM containers to increase heat transfer to the salt. Future CSP plants

should be multi-purpose, able to not only produce electricity but also sustainably produce hydrogen, convert CO_2 into methane and methanol and also desalinate water (Sattler *et al*, DLR presentation on thermochemical energy storage, 2013 - https://energy.gov/sites/prod/files/2014/01/f6/tces_workshop_2013_sattler.pdf). Ozturk *et al*[87] suggested combining a solar power tower CSP plant with coal gasification to produce syngas. Their calculations showed the system would have good Rankine cycle efficiency and waste heat recovery abilities. The increased heat storage efficiency PCMs provide would make CSP as valuable as coal or gas-fired power stations. Solutions must be found to combat poor thermal conductivity, supercooling, container corrosion and incongruent melting.

1.6.2 Waste Heat Storage

Thermal energy is produced as a by-product of a huge number of industrial processes, and usually considered as 'waste heat'. Waste heat at varying temperatures is created by different processes, for example in steelmaking it is between 150°C and 1500°C[88]. The US Department of Energy defined waste heat <230°C as 'low-temperature heat'[66]. These processes contribute to a phenomenon known as 'urban heat islands'. Urban areas are hotter than rural areas due to several other factors, such as the differing heat capacities of asphalt and concrete compared with green spaces, tall buildings reflecting/absorbing sunlight and the reduced amount of vegetation. It is also possible increased urban heat contributes to global warming, although this is disputed. Waste heat can be utilised for applications such as space heating or to drive small power stations like the Riverside power plant in London, which is run on transported waste heat. The International Energy Agency in 2014 stated that waste heat utilisation was key in achieving a low-carbon future.

PCMs are a good solution to reduce urban heating by recycling waste heat. Industrial applications produce waste heat at a wide range of temperatures. Salt hydrates are suitable for use at

temperatures from 60-120°C. At higher temperatures, salts may be considered for use. Despite great potential for utilising waste heat, several impeding factors persist such as lack of nearby heat sinks, interference with industrial operation and lack of financial returns with current technology[89]. With TES systems in place, it is possible to either reuse waste heat, or transport the waste heat elsewhere to an off-site purchaser for applications such as greenhousing[66]. Thermoelectric generators are devices which can convert waste heat to electricity, which can be especially useful in cars[90,91]. TES offers a flexible approach to the usage of excess heat.

Other contributors to the urban heat phenomenon are applications such as fuel cells which may be used to drive cars etc. Polymer electrolyte fuel cells (PEFCs) emerged as a promising energy generation system in the 2000s, usually producing waste heat at a temperature of 60-100^{o}C[92]. Clearly for applications such as powering cars, thermal energy storage must be compact. PCMs are therefore a good choice due to their high storage density. Nagano *et al*[54] investigated the use of magnesium nitrate hexahydrate ($Mg(NO_3)_2.6H_2O$) as a suitable PCM for PEFCs. $Mg(NO_3)_2.6H_2O$ has a T_M of 89^{o}C, a latent heat of 160.2 $J \cdot g^{-1}$ and is cheap compared to other PCMs in that temperature range. In order to modulate the T_M, they added magnesium chloride hexahydrate ($MgCl_2.6H_2O$). Adding a 2nd PCM with the same base metal eliminates the chance of any unwanted reactions that may occur between the two salts, and resulted in a minimal loss of latent heat. When calcium nitrate tetrahydrate was used as an additive, the latent heat significantly declined. With the use of additives, the T_M could be modulated between 56^{o}C (eutectic point, 40% $MgCl_2.6H_2O$) and approximately 80^{o}C (10% $MgCl_2.6H_2O$). They also noted that cheaper industrial grade materials behaved similarly to pure reagents, making salt hydrates even more cost effective. The use of crystallohydrate mixtures for the modification of T_M will be further discussed in the section 'Controlling T_M' (see page 46).

1.6.3 Thermal Regulation

Most of the energy we use leads to increased emissions. To combat this, other than developing electricity sources which result in no emissions, passive systems which reduce the overall energy demand can be developed. A great example of this is thermal regulation, which accounts for a huge amount of energy use, especially in more developed nations. Thermal regulation is probably the most researched application for PCMs, as most of these applications require low temperature PCMs - ideal for paraffin waxes and salt hydrates. Thermal regulation can be used for many applications to keep them within a specific temperature range, or to prevent overheating. Applications benefitting from thermal regulation include air conditioning/space heating in buildings[93–95], electronics[96,97], lithium batteries[98–101], photovoltaics[99,102,103], spacecraft/spacesuits[104] and textiles[105–107]. As melting is an endothermic process, energy is withdrawn from the surrounding area, having a cooling effect on the surroundings. Once the temperature falls and the PCM freezes, this energy is then released and the surroundings heat up again, thus temperature is controlled within the desired range. A classic example of thermal regulation using PCMs is ice in a drink. As the ice melts, the drink is continuously kept cool. Ice exemplifies the energy storage density of PCMs compared with SHS materials such as liquid water: if the energy required to melt ice was applied to an equivalent volume of water, the water temperature would increase by 82^{o}C[52]. Snow is still used today, and can be stored for use in applications such as food storage and cooling systems[108]. This is especially useful in places such as Scandinavia and parts of Japan, where snow is abundant and must be removed from cities and towns at a high cost. Transporting this snow for use elsewhere in practical applications minimises monetary losses.

1.6.3.1 Thermal control of space equipment and textiles

The use of PCMs as thermal regulation materials was pioneered by NASA, who helped produce the Phase Change Materials Handbook in 1971[109]. They needed to protect their spacecraft and astronauts from the extreme temperatures of space, which can range from approximately -150°C to 120°C. A large amount of the equipment used requires stable temperature control to combat temperature fluxes[110]. As recently as September 2016, a heat exchanger module containing the paraffin wax pentadecane was installed in the International Space Station for thermal control. PCMs are ideal for compact storage which is especially important for outer space applications, as materials cost approximately $20000 per kg to launch[104].

Short term high heat-flux is a major cause of components failing on spacecraft[111]. Technologies often employed such as capillary pumped loops have proved fairly effective, however are not suitable for future challenges in space technology[110]. Wu *et al*[111] simulated a PCM designed to protect multi-layer insulation on spacecraft. This insulation material is applied externally on almost the entire spacecraft and so is highly exposed to radiation. Their simulated results showed that the PCM kept the insulation within the desired operating temperature. They also found adding graphite as an additive to increase thermal conductivity helped with the temperature regulation. Paraffin waxes were used as PCMs for these applications for many years, however more recent research has focused on new materials to improve thermal conductivity. In 2007, NASA developed lithium nitrate trihydrate with carbon fillers as a PCM for potential use in a Mars rover[112]. As the carbon filler is hydrophobic, a surfactant was required for use with the hydrophilic lithium nitrate. They also doped the lithium nitrate with zinc nitrate hexahydrate which greatly reduced the supercooling. The resulting material had a heat storage capacity of 40 $J \cdot g^{-1}$ and prevented large heat-fluxes even with high power input. This shows salt hydrates can be used for thermal regulation when sufficiently modified, although the heat storage capacity is not yet satisfactory.

Thermal management of textiles is one of the major applications that PCMs have been commercially available for. PCMs have been used in outdoor wear such as coats, along with underwear, bedding and sleeping bags etc[106]. They react to changes in environmental temperature to automatically heat or cool the user, whilst preventing discomfort associated with large temperature fluxes[105,113]. Encapsulated PCMs incorporated in textiles can have minimal effect on the fabric properties[114], although this may be problematic at high loading capacity[115]. It is important therefore, that PCMs incorporated into textiles have good latent heat so a small volume may be used. Companies such as BASF and Samsung have used PCMs in their products. There are numerous methods to apply PCM materials into textiles, such as knife over roll[116], dip coating[117] and screen printing[106]. PCMs incorporated into textiles run the risk of being removed or damaged during washing. Studies by Shin *et al*[115,118] showed fabrics loaded with melamine formaldehyde capsules containing eicosane retained only a quarter of their heat storage capacity after 10 cycles. A potential solution to this problem is to first attach the PCM to a support material such as nanocellulose fibres, which can act as an anchor to prevent material loss.

1.6.3.2 Passive air conditioning

Passive air conditioning can be considered the primary application for low-temperature PCMs. Buildings account for approximately 40% of global energy usage[119–121]. Air conditioning is a large part of this energy demand. This is especially true of modern buildings, whose lightweight construction leads to large temperature swings due to a lack of thermal mass[122]. Many recent skyscrapers and other buildings have been built with large amounts of glass for example, making them unbearably hot in summer and meaning they must be heavily air conditioned. It is possible to reduce these fluctuations with the addition of PCMs to various parts of the building. PCMs increase the thermal mass of buildings whilst taking up a relatively small volume[123]. To keep internal temperature within the range of human comfort, a PCM with a T_M of 20-25^oC is required. Using a passive air conditioning

system, it is possible to reduce space heating energy requirements by up to approximately 90%. An EU directive has called for all new buildings to be zero net energy by 2020, PCMs can be of great value in achieving this goal. A building erected in 2012 at the University of Washington in Seattle, USA used a 'bioPCM' in its walls. They estimated that the 1.25cm thick layer of bioPCM had the same thermal insulation effect as a 25cm thick concrete wall.

Once PCM technology for thermoregulation is developed, new buildings can be constructed accordingly. A major problem is the improvement of existing buildings to reduce their energy demands. Retrofitting PCM components *i.e.* replacing existing building parts, is a potential solution[124]. Replacing whole walls or roof spaces is not economically viable; a method to get around this is to add PCMs to smaller building components which can more easily be retrofitted. Drywall (wallboard) is a good candidate for the addition of PCMs. Drywall is a lightweight material made of gypsum and is used for wall interiors. It is possible to directly incorporate PCMs into gypsum. In 1991, Feldman *et al*[125] fabricated gypsum plaster containing butyl stearate as PCM. The incorporated PCM had no impact on the physical properties of the wallboard, and increased the energy storage capacity tenfold. Sari *et al*[126] used a form-stable eutectic blend of capric and stearic acids to add to wallboards, while Shilei *et al*[127] found the same mixture had good thermal stability. Using a similar procedure with commercial PCMs, Kuznik and collaborators[128] found the temperature inside a test cell were kept 2-3°C lower when using a PCM wallboard compared with regular wallboard. Several investigations have determined PCMs need to be encapsulated for addition to building materials to prevent leakage or interaction with the walls[122,129]. Capsules must have sufficient surface area in order to deliver acceptable heat transfer through the building[123]. Hexadecane-loaded capsules with a diameter of 5-20μm incorporated into gypsum was shown to keep temperatures in the level of human comfort for far longer than conventional wallboards[130]. PCMs are most effective in tropical climates, as space cooling is required every day of the year, unlike many countries such as the UK which have both warm and cold seasons. A simulation based on the tropical weather in Singapore displayed that an ideal PCM could reduce heat gains within a building by 21-32% during a year[131].

A new solution to the retrofitting problem is the development of PCM 'thermopaint'. PCMs can be combined with commercial paint which, when added to a surface such as a wall, will thermally regulate the internal building area. PCM paints have not yet been developed. Due to the issues outlined earlier, it is not possible to simply add PCMs directly to the paint. They must firstly be contained, of which currently there are no mass-scale or cost-effective methods. Other energy saving paints such as Insuladd and SuperTherm have been available since the late 1990s. These paints act as thermally reflective coatings due to hollow structures in their composition which reduce heat transfer through the coating. This allows the paint to reflect heat either inside or outside of the building. The main drawback is that the paint must be uniformly applied so that there is a perfect angle between the heat source and insulating surface. If the heat source changes angle the efficiency is decreased. These paints, although partially effective, do not allow control over indoor temperature. PCM thermopaint would allow an ideal indoor temperature to be chosen. The space will be kept at approximately the PCMs T_M, as the PCM will melt or freeze depending on external temperature. Although still a passive system requiring zero energy, thermal energy is stored and released based on the PCM melting and freezing, rather than reflection of any heat source. As the heat storage relies on temperature rather than reflection, the paint can be applied anywhere in the building with the same thermal regulation effect.

Another interesting 'new' technological development is the erection of wooden skyscrapers. Wood fell out of favour as a building material due to disasters such as the Great Fire of London in 1666. Contrary to popular belief, wood is more resistant to fire than steel, which most modern constructions are made of. Wood chars during fire, forming a layer of carbon which restricts oxygen supply to timber underneath. This protects internal layers and maintains structural stability. In contrast, steel will bend and buckle after reaching a critical temperature. As an example of the new trend in using wood, the Hoho building in Vienna has been constructed in 2017. At 84m, it is the tallest wooden building ever made. The major issue with wooden buildings is rot due to moisture. It

is feasible that thermopaint could be used to help prevent wood rot in addition to temperature control – paint is used on cars for rust prevention, for instance.

Older buildings which tend to be made of concrete do not suffer temperature fluctuations to the same extent as more lightweight buildings. This is due to their high thermal mass. Walls impregnated with PCM have been shown to outperform concrete whilst requiring less wall thickness. As a further advantage, porous materials used in buildings which can be impregnated with PCMs are low cost and easy to fabricate[132]. A numerical simulation showed that calcium chloride hexahydrate outperformed paraffin wax and concrete when comparing indoor temperatures. The 0.08m thick calcium chloride impregnated wall kept the room temperature between 18-22°C, compared to 15-25°C when using a 0.05m thick paraffin wax impregnated wall or a 0.2m thick concrete wall[133]. The simulation demonstrates the additional energy density salt hydrates provide, leading to the prevention of large temperature fluctuations.

1.6.3.3 Passive cooling systems

Refrigeration systems can also benefit from the use of PCMs. Refrigeration is very widely used in such applications as transportation of food, vaccines and ice[55]. Refrigerated trucks using PCMs have been tested for effectiveness. Refrigeration units used currently rely on diesel engines for cooling, which consume energy and produce emissions. Temperature fluctuations within the refrigerator lead to reduced product quality or possible destruction[134]; PCMs reduce these fluctuations as well as decreasing energy requirements. Transportation conditions are dependent on the contained material, so a range of PCMs with differing T_Ms should be developed. Ahmed *et al*[135] used a paraffin with a T_M of 7°C concealed in copper pipes, which were incorporated into regular truck panels. During tests, the PCM panels reduced peak heat transfer by an average of 29.1% compared with the regular panels. Liu *et al*[136] developed a PCM with T_M of -26.8°C for refrigerating raw meat, which is

usually stored at -18°C. The PCM used was an inorganic salt and water solution. They found the system could reduce energy requirements by up to 86% compared to using a diesel driven coolant. Melone and collaborators[137] produced an encapsulated PCM/cellulose composite for refrigeration. They developed a mathematical modelling simulation, which showed the PCMs effectiveness in food preservation.

Large amounts of research have been devoted to the thermal management of electronics, Li-ion batteries and photovoltaics. Most failures of these products are due to overheating[99], which PCMs can help prevent with no additional energy input. Traditional cooling technologies such as active air and liquid cooling are ineffectual due to low heat transfer rates[138], and also consume energy. Many modern technologies such as smart phones are small closed systems, meaning active air cooling using bulky fans is not practical[139].

Numerous studies have shown loss of capacity in Li-ion batteries is highly temperature dependent[140–143]. Temperatures which are either much lower or much higher than the optimum operating temperature will cause rapid degradation of the battery. Khateeb *et al*[98,144] first designed a thermal management system for Li ion batteries in an electric scooter using simulated results, followed by experimental tests. Simulations showed that a paraffin wax PCM module alone was not enough to continuously cool the battery, due to poor thermal conductivity. This was improved by the addition of aluminium fins to increase the heat transfer area. Experimental and simulated values were similar, and confirmed that a finned configuration was necessary in hot conditions to improve performance.

PVs have an optimum working temperature of around 25°C. Less than 20% of the solar energy they receive is converted to electricity, the rest is converted to heat which causes efficiency losses. It has been estimated than PVs lose around 0.4-0.65% K^{-1} power output upon heating[145,146], due to alteration of the working voltages[99]. PCMs can provide better thermal management of PV than other systems[147]. In a series of studies, Huang *et al*[148–151] determined through both simulations and

experimental data, that PCMs were highly effective at preventing temperature rises in PV modules. PV integrated into buildings especially require thermal regulation as their temperatures rise up to 9% higher than regular PV[150]. The temperature was reduced by as much as 30°C in some cases compared to regular PV design. Also suggested was the use of finned configurations to apply a more uniform temperature, while salt hydrates were found to be more effective at reducing temperatures than fatty acids.

1.7 Improvements to PCMs for Practical Applications

The practical use of PCMs is hindered by their limitations. For instance, the solid-liquid transition must be suitably contained to prevent leakage. No known PCM fulfils all of their ideal criteria (outlined by Abhat[34] and listed on page 13). The main drawbacks of salt hydrates are incongruent melting and phase separation. These can be improved by additives. The 'extra water principal' involves adding extra water to the salt hydrate melt, preventing change in hydration number and maintaining T_M. The idea is that once melted, salt hydrates may lose water due to evaporation. With more water in the mix, they are able to remain in the correct hydration state. This effect was investigated by El Sebaii *et al*[152], who showed calcium chloride hexahydrate ($CaCl_2.6H_2O$) could be kept stable over 1000 cycles with minimum loss of ΔH simply by adding extra water at intervals. Nucleators can be added to prevent incongruent melting, while thickeners can be used to stop phase separation. It must be noted that the use of additives reduces ΔH, as there is less salt hydrate in the mix. Even with the use of nucleators and thickeners, PCMs will still degrade over time[152], so they are not an ideal solution for solving the problems associated with PCMs. Following is a discussion of the numerous ways in which researchers have approached enhancing the thermal conductivity and chemical stability of both organic and inorganic PCMs.

1.7.1 Enhancing Thermal Conductivity

PCMs in general suffer from low thermal conductivity (aside from metallic PCMs). There are ways to improve this, such as the use of conductive particles. Many studies have shown that a very small number of conductive particles can cause large increases in the thermal conductivity. A simulation in 2002[153] showed addition of copper or aluminium particles considerably increased the thermal conductivity of a PCM melt. As an increase in the number of conductive particles results in lower latent heat, an optimum number of particles must be determined. A compromise is required

between high latent heat, material stability and conductivity. Oya *et al*[154] enhanced the conductivity of erythritol using both nickel and graphite particles. When using only 15 %wt of expanded graphite particles, the thermal conductivity of the PCM was increased by 640%. Qi *et al*[155] produced a sample of PEG impregnated with graphene oxide as a support material, with graphite nanoplatelets as conductivity enhancer. With only 4 %wt graphite nanoplatelets in the mix, thermal conductivity was 490% that of regular PEG. Latent heat was minimally affected, reduced by only 1.8%.

Metal foams provide high surface area, increasing contact with the PCM to provide conductivity enhancement. Mathematical modelling has shown foams cause faster melting times for paraffins[156]. Experimental results using metal foams have shown the thermal conductivity can be increased by a factor of 3[157], while heat transfer increases by a factor of 3-10[158].

Finned configurations of containers are another method of increasing heat transfer contact with the PCM. It is simpler than using metal foams as no chemical synthesis is required. Zhang and Faghri[159] used a numerical simulation to show the effect of fins, and found it was an efficient way of conductivity enhancement for HTFs which have low thermal conductivity. It was found to be especially useful for PCMs which suffer from a large degree of supercooling. Agyenim *et al*[160] used fins to increase the conductivity of erythritol. Longitudinal fins gave the best results, achieving complete melting due to better thermal response during charging, and reduced supercooling during discharge. A combination of these approaches to increase thermal conductivity could be highly effective for heat storage systems of the future.

1.7.2 Cascaded and Thermocline LHS

A chemical engineering approach to improving the use of PCMs is changing the arrangement of the PCMs in a heat storage unit. The cascaded LHS (CLHS) is an energy storage tank with a packed bed of PCMs in decreasing order of T_M with respect to the flow of the HTF during charging, as shown in Fig

1.7. It has been shown both theoretically and experimentally that this approach improves heat transfer characteristics of the PCM melt. This idea could also be expanded to the use of encapsulated PCMs. Having different PCMs also allows storage over a larger temperature range, increasing capacity. This would be especially useful for applications with larger temperature swings. Using a single PCM for macroscale heat storage results in heat transfer problems and inefficiency. As the HTF flows over the PCM, its temperature decreases. This results in a large temperature difference between HTF and PCM, which decreases heat flow between the two. Using the cascaded approach, the temperature difference and heat flow can be kept relatively constant[80,161]. Michels and Pitz-Paal[162] showed the advantages of CLHS (a mixture of $NaNO_3$ (T_M = 306°C), KNO_3/KCl (T_M = 320°C) and KNO_3 (T_M = 335°C)) compared with a single PCM system (all $NaNO_3$). Far more of the PCM went through a full melting/freezing cycle for the CLHS, with 92% melting and 67% freezing, compared with 100% and 2% respectively for the single PCM. They showed that due to the improved efficiency, a lower mass of salt was required for CLHS to get the same storage capacity as a single PCM system.

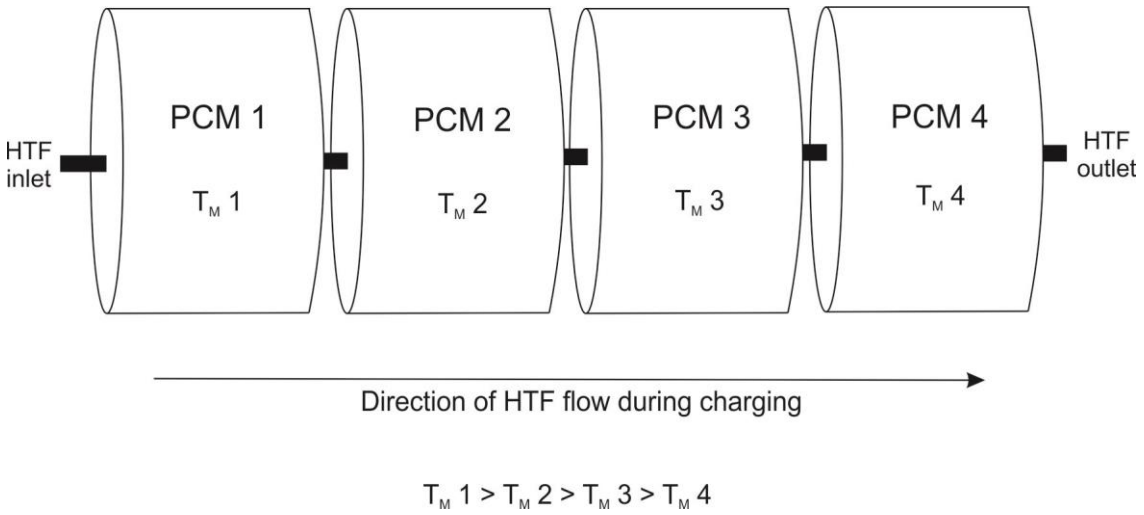

Fig 1.7 Representation of CLHS system, with PCMs set in order of decreasing T_M with regards to HTF flow during charging.

Thermocline energy storage consists of a porous bed of heat storage filler material with the HTF flowing through. As most of the storage tank is filled with the solid material, less HTF is required. It is possible to use PCM capsules with this method. Thermocline works due to thermal stratification, where hot fluid rises to the top of the tank and cold fluid to the bottom, creating a thermal gradient known as a thermocline[163]. The filler material helps maintain the gradient. It is possible to utilise PCMs within this setup, by adding them between layers of solid filler. A cascaded approach can also be used, with higher T_M PCMs added as a top layer, with alternating layers of solid filler and lower T_M PCMs below. Galione *et al*[163] ran a simulation which determined this kind of cascaded thermocline was more efficient than a regular CLHS system, using only 20% mass of the PCM but storing 83% of the energy compared to the CLHS. However, the thermocline system used far more filler material, so a cost analysis would be required.

CLHS has great potential, especially for large scale heat storage such as that used in CSP, due to improved melting and freezing characteristics. Further thermal conductivity enhancement may be necessary for complete melting and freezing, such as using finned containers. It is also feasible CLHS could be used at lower temperatures and for smaller scale applications. It could be useful for passive

air conditioning for example, especially if atmospheric temperatures fall outside the melting range of a single PCM. CLHS may be the approach used once PCM systems are adopted for use in CSP storage.

1.7.3 Controlling T_M

The key property for any PCM is the T_M. The T_M must be in the range of the application temperature, otherwise no energy storage will be possible. Therefore, a method of altering the T_M to suit any application would be highly advantageous. For paraffin waxes, longer carbon chains give higher T_Ms. Paraffins only have a small range of useful temperatures in which they can be used in. Salt hydrates and salts can be mixed together to tailor the T_M to the desired range. A mixture of two compounds with the lowest possible T_M is known as a eutectic. This effect is caused by the compounds inhibiting the crystallisation of each other[164]. At any ratio other than the eutectic point, the two compounds are separate phases. At the eutectic point, a single phase is formed with a defined T_M lower than that of the single components[41,165]. A typical phase diagram for a eutectic system is shown in Fig 1.8. Eutectic mixtures also have higher latent heat in comparison to other mixtures[54], potentially boosted by additional thermochemical heat[41]. For salt hydrates, the latent heat for mixtures other than the eutectic will be lower than that of the single components, due to the release of water.

Although eutectics and mixtures have these advantageous properties, they are not well researched with regards to crystallohydrates. They also retain the disadvantages that are inherent in single crystallohydrates, such as supercooling. More research is needed on the creation of salt hydrate eutectics. It has been suggested that molecules with similar crystal structures form eutectics better than others. Phase behaviour can also be studied. Due to the huge number of available crystallohydrates, it would be of use to develop some molecular modelling or other screening software to determine which mixtures have good potential. Zeng and collaborators[166] computationally determined phase diagrams of several ternary salt-water mixtures. This allows the

development of new heat storage materials and reduces the required amount of experimental work, saving time and money. The software was accurate in predicting phase diagrams for known salt mixtures, showing this can be useful in future eutectic work. In a further study[167], they calculated phase diagrams for manganese nitrate hydrates (tetrahydrate T_M = 26°C, hexahydrate T_M = 37°C) doped with 10 different salts, giving T_Ms between 11 and 32°C. Alteration of the T_M opens up new applications for salt hydrates. The modulation of manganese nitrate hydrate T_M has also been done experimentally[168]. It was found that when zinc nitrate hexahydrate and potassium nitrate were added, a eutectic of T_M 18-21°C is formed with a reasonable latent heat of 110 $J \cdot g^{-1}$. They also found suitable nucleating agents and thickeners to prevent supercooling and phase separation, respectively.

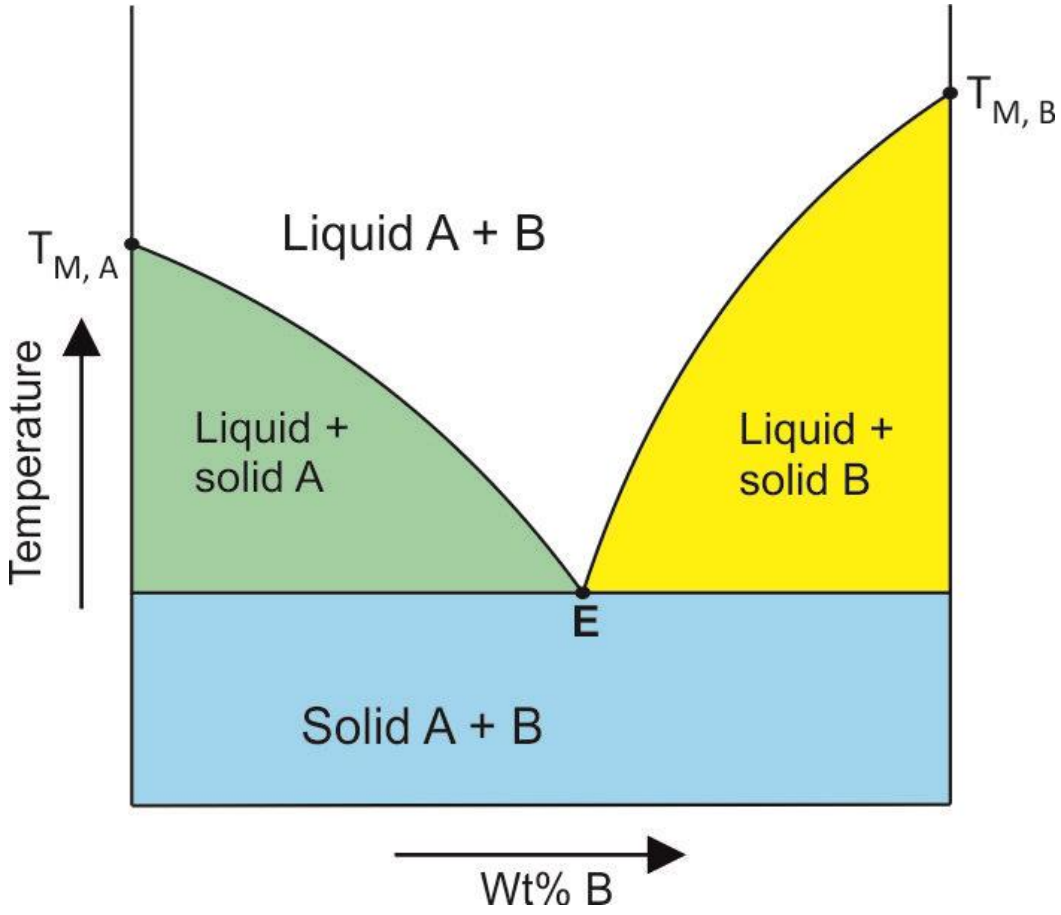

Fig 1.8 Typical phase diagram for a eutectic system. E is the eutectic point; at all other compositions two phases are present

1.8 Encapsulation of Active Materials

The most promising way to improve PCM properties is by encapsulation within a composite shell material. Encapsulation is a widely used technique to protect materials such as corrosion inhibitors, drugs, pesticides and DNA. Capsules can be macro- (>1000μm), micro- (1-1000μm) or nanosized (1-1000nm). Smaller capsules greatly increase the surface-area-to-volume-ratio of the material, which improves heat transfer. For example, it has been predicted that encapsulating PCMs in capsules 1mm in size would increase the surface area by 300m^2 per m^3 when compared with the bulk PCM[1]. Reducing their diameter to the nanometre range would vastly increase this. Other advantages of encapsulating PCMs include prevention of both leakage and reactions with the external environment, corrosion protection for container materials, control over volume change upon melting and improved thermal cycling stability[122,169]. All these properties are crucial to PCM usage in practical applications, so encapsulation can almost be thought of as a 'one size fits all' solution. The shell is usually made up of a polymer, as they give a good balance between strength and flexibility. Inorganic shells can also be used, which have higher thermal conductivity (silica is a good example of an inorganic shell for PCMs due to its enhanced heat transfer) but are more brittle. Polymer shells are more favourable due to their prolonged durability and low cost.

To create capsules containing active materials, it is first important to understand the basic chemistry and processes that contribute to encapsulation. To fabricate a capsule, an emulsion of the desired droplet size must first be formed, followed by the formation of shell material at the emulsion droplet interface. The encapsulation of active materials and their specific effects on PCMs will now be discussed.

1.8.1 Emulsions

An emulsion is a liquid dispersed in another liquid in which it is not soluble or miscible. This is achieved with stabilisers called surface active agents, commonly abbreviated to surfactants. Surfactants spontaneously form a shell around the dispersed liquid to create droplets known as micelles. This 'dispersed phase' is dispersed through the 'continuous phase'. The spontaneity of micelle formation is due to the amphiphilic nature of surfactants. They consist of a hydrophilic head group and hydrophobic tail group, which arrange accordingly to minimise contact between the 2 emulsion phases. An emulsion can be oil-in-water (O/W) or water-in-oil (W/O), depending on the ratio of the two. The liquid of least volume is dispersed within the other liquid. O/W emulsions are more common as there is no need for selection of the continuous phase. A good example of an O/W emulsion is the use of soap. Surfactants in the soap surround hydrophobic dirt which can then be rinsed away. W/O emulsions require careful selection of the continuous oil phase and surfactants to give the highest solubilisation capacity for the dispersed phase[170,171]. W/O emulsions are also known as 'inverse emulsions'. Capsules provide protection and enhance the properties of many materials; emulsion droplets provide a template for capsules to form. The shell material can either polymerise around the droplets, or can be premade and deposited.

It is possible to reduce emulsion droplet size by an energy input. Common energy inputs include homogenisation and sonication. Droplet size is a key factor in capsule formation, determining the diameter of the resulting capsules. An emulsion with nanosized droplets formed with a high energy input is known as a miniemulsion (or nanoemulsion). This is in contrast with microemulsions, which also have nanometre sized droplets, but form spontaneously. Miniemulsions are kinetically stable while microemulsions are thermodynamically stable[172]. Microemulsions require a larger amount of surfactant than miniemulsions, usually at least 20 %wt of surfactants in the oil phase, whereas miniemulsions require 3-10 %wt[173]. Regular emulsions and miniemulsions are thermodynamically

unstable due to the spontaneous minimisation of interfacial area between the two immiscible phases[174]. ΔG_F for emulsion formation is positive:

$$\Delta G_F = \lambda \Delta A - T\Delta S_F$$

Eq 1.4 Gibbs free energy of formation for emulsion droplets

Where ΔG_F is free energy of emulsion formation, λ is surface tension, ΔA is surface area gained during emulsification, T is temperature and ΔS_F is the entropy of emulsion formation. The large interfacial energy term ($\lambda \Delta A$) outweighs the entropy of droplet formation in miniemulsions, hence they do not form spontaneously. Microemulsions, in contrast, display thermodynamic stability as the large amount of surfactants facilitate a decrease in λ, contributing to a negative ΔG_F. A comparison of the basic features of the 3 emulsions types are displayed in Table 1.2.

Flocculation is the main cause of destabilisation of O/W emulsions, for W/O emulsions it is Ostwald ripening. Flocculation is the aggregation of colloidal particles without coalescence, which then precipitate. Ostwald ripening is essentially the deposition of smaller particles onto larger ones, driven by the minimisation of interfacial area. Emulsions destabilise by coalescing into their bulk oil and aqueous phases. Miniemulsions are advantageous due to their great kinetic stability, which in effect overrides their thermodynamic instability. Flocculation is avoided due to the very small particle sizes. Other destabilisation mechanisms include creaming, droplet coalescence and sedimentation. A good indicator of miniemulsion stability is the transparency of the solution. The formation of nanoscale droplets causes the solution to become transparent, sometimes with a blue tint.

Due to the additional free energy needed to be applied to obtain a good dispersion of the miniemulsion, this must be applied using sonication or high-pressure homogenisation. Sonication is

a good option for lab scale experiments, but is not currently suitable for use on an industrial scale. Regular homogenisation (such as Ultraturrax) does not provide the required amount of energy to form a miniemulsion, as much energy is lost as heat due to friction[174]. Regular homogenisation is therefore only effective at producing microcapsules >1µm in size.

Table 1.2 Comparison of different types of emulsion, taken from Rao *et al* 2011[175]

Characteristics	***Emulsion***	***Miniemulsion***	***Microemulsion***
Thermodynamic Stability	No	No	Yes
Stability Lifetime	Seconds to months	Hours to months	Infinite
Droplet Size Range	1-10µm	20-200nm	10-100nm
Polydispersity	Low	Very Low	Very Low
Typical Particle Size	1µm+	100-300nm	30-100nm

It is possible to form emulsions without the use of surfactants, by creating a Pickering emulsion. These are stabilised by solid particles adsorbing to the liquid-liquid interface, dependent on particle wettability. When the contact angle is slightly less than 90^{o}, an O/W emulsion is formed; slightly above 90^{o} and the emulsion will be W/O[176]. A contact angle of 90^{o} provides no stabilisation as the particles become dispersed in either phase[177]. Pickering emulsions can provide an increase in thermal conductivity, for instance if silica nanoparticles are used as stabiliser. However, they are also more sensitive to external stimuli such as pH changes than regular emulsions.

1.8.2 Sonochemistry

The use of ultrasound for a wide variety of applications is a recent development in the field of materials chemistry. Due to the reverse piezoelectric effect, electrical energy can be converted to mechanical energy using an ultrasonic transducer[178]. Ultrasound is an advanced oxidation process, and has been used for applications including the removal of contaminants from water[179], driving reactions[180], materials synthesis[181], cleaning[182], creating new surfaces[183] and breaking up aggregates of particles[183]. Ultrasound is defined as sound at frequencies above 16 kHz, which is generally

inaudible to adult humans, and creates a huge amount of energy. Acoustic cavitation is the mechanism by which sonicators produce their energy. Hydrodynamic cavitation is usually something for engineers to avoid in most applications due to corrosion damage. By contrast, acoustic cavitation is favourable for sonochemistry as it can be controlled when applied to a liquid medium[182]. Although not fully understood, the phenomenon is caused by nanoscopic bubbles forming and rapidly collapsing, producing localised temperatures above 5000K and pressures of several thousand bars[184]. This process is shown in Fig 1.9. There are 3 major effects from acoustic cavitation[185]: primary sonochemistry – gas phase chemistry occurring inside the bubbles; secondary sonochemistry – solution phase chemistry occurring outside the bubbles; and physical effects associated with bubble collapse. Physical effects are perhaps the most notable. Bubble collapse near a surface results in the formation of a microjet which impacts the surface at incredibly high speed. Resultant erosion of the surface leads to the creation of nanostructures. The effects of the microjets can be seen clearly on ultrasonic horns after extended use. Pitting corrosion occurs on the horn which eventually requires replacement. If a bubble collapses away from a surface, a shockwave forms causing strong turbulent effects such as interparticle collisions.

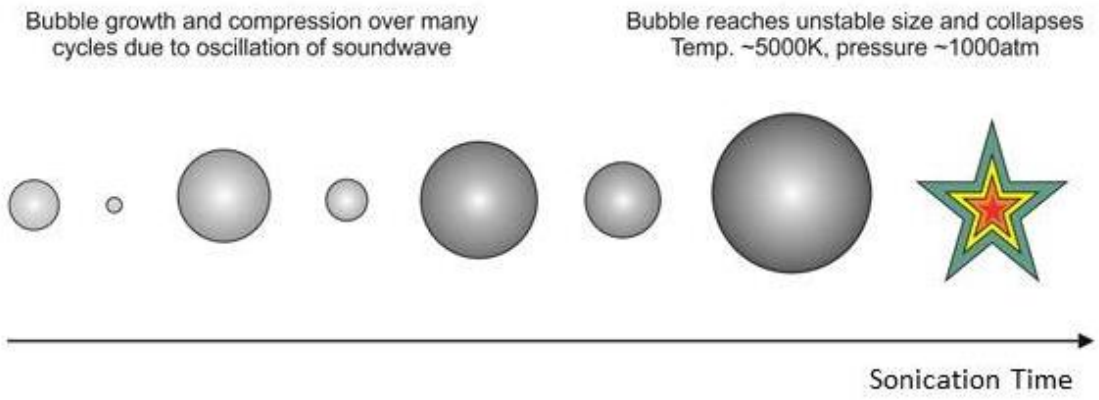

Fig 1.9 Growth and collapse of bubbles, arising from acoustic cavitation. Once the bubble reaches an unstable size it collapses, giving enormous local temperatures and pressures

Sonicators used in chemical synthesis are usually in the form of horns. Regular laboratory scale horns give out 10-100W of energy into the liquid during sonication. Ultrasonic baths deliver only a fraction of the energy produced by horns, but have found several uses. They are mainly useful for physical effects such as cleaning, activation of reactive metals such as Li, generating emulsions, exfoliating layered compounds[138] and aiding dissolution[185]. Ultrasound can be used to drive reactions under ambient conditions that may otherwise require high temperatures, high pressure or long reaction times. Sonication can initiate polymerisation reactions[186]. Teo *et al*[180] polymerised various methacrylate monomers using pulsed sonication to drive the reaction. They found a first-order mechanism, obtaining lower reaction and conversion rates with more hydrophilic monomers. However, if extremely high molecular weight polymers are desired, sonication may not be suitable as longer polymer chains can be degraded by energy from acoustic cavitation[183]. When water is used as a reaction medium ultrasound can produce HO· and H· radicals[187,188], shown in Eq 1.5, which may then react further. The production of radicals using ultrasound is known as sonolysis. This effect is especially useful when reducing noble metals such as Ag, Au and Pt to produce nanoparticles.

Sonolysis can be used to remove pollutants from water, which is especially effective when combined with other oxidation techniques such as photocatalysis[189].

$$H_2O \rightarrow H\cdot + HO\cdot$$

$$O_2 \rightarrow O + O$$

Eq. 1.5 Typical reactions producing radicals from water, driven by ultrasonic cavitation

Due to the fossil fuel energy problem, many countries are considering expanding nuclear energy generation. Despite negative public perception of the hazards involved, nuclear reactors can be invaluable if strict safety standards are enforced. Nuclear waste, such as spent fuel rods, presents a large problem however. Currently they must be safely stored for long periods until their radioactivity has significantly decreased. A potential use of sonochemistry is the treatment of spent nuclear fuel which can be recycled and reused. This is driven by the reaction of sonolytic products with actinide ions (such as uranium or plutonium ions)[190]. Recycling spent fuel rods makes the whole process more efficient and lessens the impact of radioactive waste.

In the context of PCM technology and other materials requiring encapsulation, the major application of sonochemistry is in generating emulsions. As mentioned above, the formation of miniemulsions requires a great deal of energy. Sonication is an ideal method to create them at laboratory scale. High pressure homogenisation produces results akin to sonication, however is mainly available on a large-scale. Regular homogenisers (such as Ultraturrax) are available for lab-scale use but are less effective than sonication. Emulsion droplet size is dependent on the shearing rate[32], with higher homogenisation speeds producing smaller droplets and narrower size distributions. Shearing an oil/water/surfactant mix with homogenisation or sonication will yield an emulsion or miniemulsion

(depending on the amount of energy applied) very quickly. Sonication can also be used to fully disperse other materials.

It is a common misconception that higher sonication power automatically leads to increased efficiency, which is not the case. Certain sonochemically driven reactions, such as the oxidation of iodide, have a maximum intensity value which gives the highest yield. At intensities higher than this maximum value, the yield is heavily reduced. This is attributed to the change in cavitation conditions[191]. All sonochemical applications require the optimisation of reaction conditions, such as the total time sonicating and amplitude. A suitable sized probe should also be used. The power delivered to the solution is dependent on probe size and amplitude. Selecting a suitable probe will prevent splashing or foaming of the liquid, allowing maximum power to be delivered to the solution. A photograph of a lab-scale sonicator is shown in Fig 1.10. It consists of a transducer, which converts electrical energy into mechanical vibration *via* the reverse piezoelectric effect; this travels through the probe to the tip, which rapidly expands and contracts rapidly based on the amplitude chosen by the user. Expansion and contraction of the tip causes cavitation. The diagram shows a sonicator equipped with a ½" tip. Larger or smaller probes may be chosen based on the sample size.

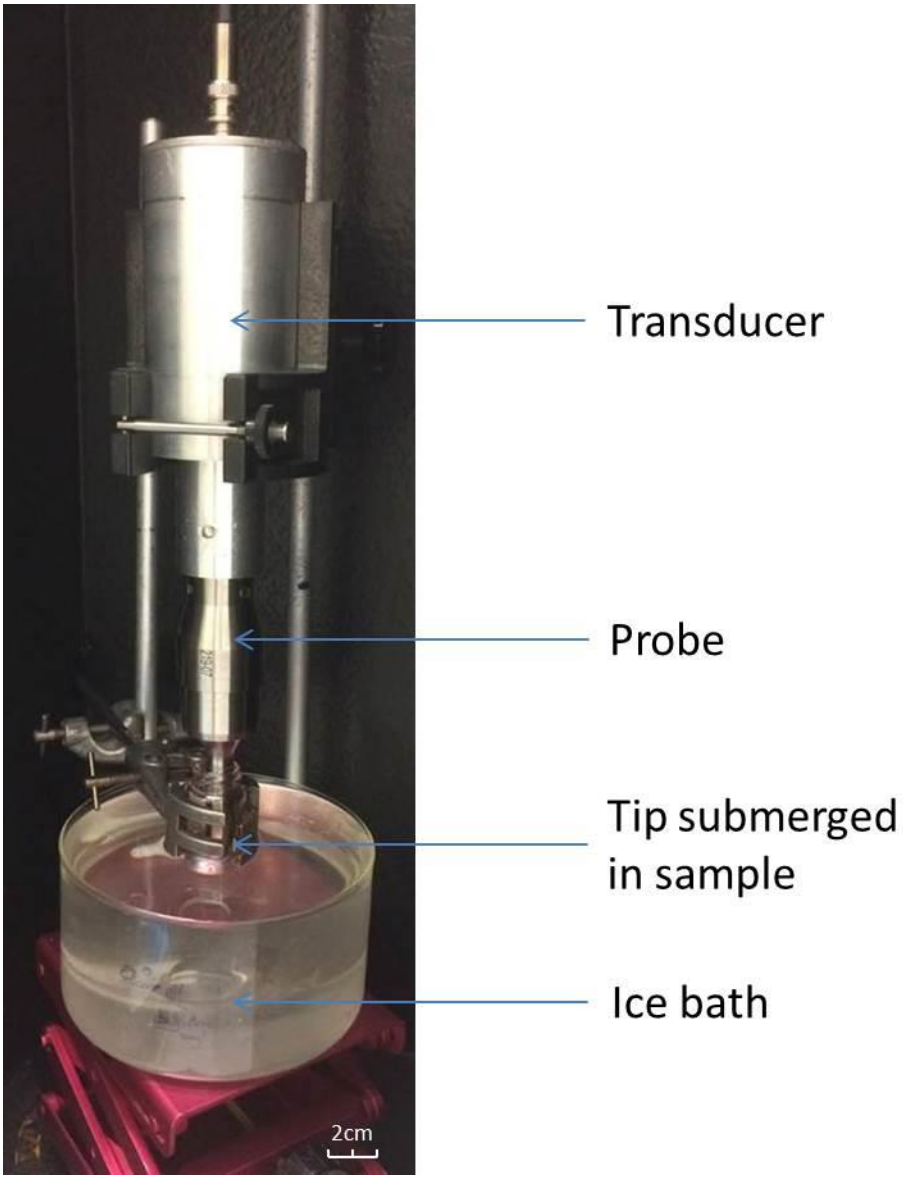

Fig 1.10 Photograph of a sonicator equipped with a ½" tip. The sample is cooled in an ice bath to prevent overheating

The major drawback of sonochemistry in an industrial sense is that it is not currently applicable for scale up. Health and safety issues with sonication include hearing damage and high temperatures produced due to cavitation. Problems would be multiplied if an industrial scale sonicator was developed, so must be taken into consideration along with factors such as efficiency and ultrasound frequency. A study was undertaken by Asakura *et al*[192] to determine how sonochemical efficiency was affected by the amount of liquid in the reactor. They found the optimum liquid height in the

reactor was approximately 15 times the height of the wavelength, with the ideal frequency being 200-600kHz. Lower frequencies mean too few bubbles for cavitation are formed, whereas greater frequencies result in many bubble collisions[189]. Bubble collisions lead to coalescence, where adiabatic compression leads to internal bubble temperatures being lower than that of smaller bubbles[193].

Another factor why current sonicator probes are not available for industrial scale-up is that they are designed in a tapering fashion, where power is concentrated at a small tip. This leads to an uneven cavitation field around the probe, meaning an uneven distribution of ultrasound[187]. The efficiency has been shown to be better with a more evenly distributed cavitation zone. Wei *et al*[194] designed a multi-stepped ultrasonic probe. They demonstrated that regular probes deliver the highest acoustic power in a small area below the probe, whereas their novel multi-stepped probe provided several high-power regions. Improved probe design can be combined with optimal reactor geometry[195,196] and favourable operating conditions[178,179,192] to suit industrial scale reactions. Industrial scale sonicators will be more efficient than the currently used homogenisers, which require numerous passes to achieve nanosized droplets[197].

Due to the high power, speed of reaction and efficiency that sonicators deliver, it is clear they can be a powerful tool for improving the properties of PCMs. By creating miniemulsions, PCM loaded nanocapsules may be formed. It is also possible for ultrasonic probes to be scaled up in the near future, as long as several factors of practicality and safety are taken into account. Polymerisation reactions based on emulsion chemistry will now be discussed.

1.8.3 Polymerisation

Capsules have found many uses in chemical industry, such as in food technology[198,199], dyes[200], catalysis[201,202], corrosion inhibitors[203,204] and drug delivery[205–209]. Their main purpose is to provide

protection for the core material from the external environment. Encapsulation is found throughout nature, for example egg shells and cell membranes. Synthesised capsules can be used to encapsulate many species, including drugs, enzymes[210], PCMs and DNA[211,212]. They can also be used as a reaction medium, for example Kang *et al* showed the rate of a Diels-Alder reaction could be rapidly sped up due to the vastly increased concentration of reactants inside the capsule[44]. Other interesting effects can be achieved using capsules. Capsules can be used to prevent corrosion[203,204,213], self-heal[214,215] and 'switch on' catalysts[202].

With technological advances over the last half century, preparing capsules with diameters from 1000μm down to around 40nm has become possible. Searching the literature using Web of Science, the first mention of microcapsules is from 1964 where Chang reported the encapsulation of enzymes[216]. Nanocapsules are referenced from 1976 onwards, with an early example being Couvreur *et al*, who demonstrated how polyacrylamide capsules 200nm in diameter could encapsulate fluorescein[217]. Capsule size can play a role in functionality. For instance, in drug delivery nanosized drug-loaded capsules have advantages over regular drugs. Certain membranes in the body only allow diffusion of molecules less than 100nm[218], and specific locations in the body can be targeted by specific particles[219–221]. Particle size is important for thermal energy storage materials due to its effect on thermal properties. Particle size is determined by factors including stirring rate of the emulsion, emulsifier content, initiators, core-to-shell ratio, polymerisation temperature and reaction time[222].

The interest in extremely small capsules is essentially an attempt to increase the surface-area-to-volume ratio (SA/V) of the active material. Increasing SA/V is the driving force for all nanotechnology and is inspired nature. The best example of enormous SA/V is the supercoiling of DNA – if uncoiled, the total length of DNA in one human body would be approximately twice the diameter of our solar system. A good example of increasing SA/V in technology is computer chips – the size of chips has rapidly decreased in accordance with the famous Moore's Law, allowing faster processing and

improved data storage. It has recently been proven that single atom data storage is possible by producing stable single atom magnets[223]. Higher SA/Vs give increased efficiency, for instance more finely ground substances will dissolve more quickly in a solvent. Along with increased SA, nanocapsules provide increased structural stability compared to microcapsules, which may break whilst being pumped round a system[169,224,225].

Many shell materials can be used to fabricate capsules. Most often, polymers are used due to their attractive mix of strength and flexibility[226]. As many different polymers can be used as shell material, it also allows scientists to select specific properties. Polymers have various inherent properties such as differing glass transition and melting temperatures and thermal conductivities. They may be hydrophilic, hydrophobic or amphiphilic. Typical polymers used as capsule shell material are polyurethane, polyurea, poly(methyl methacrylate), poly(lactic acid) and poly(alkyl cyanoacrylates). Polyurethane and polyurea are possibly the most ideal shell material, due to their good thermal resistance, chemical stability and their insolubility in many common solvents including water.

A problem with the adaptation of encapsulation methods to create PCM loaded capsules is that capsules are often used as a delivery mechanism. As a result, most capsules prepared are either deliberately designed for short lifetimes, or long lifespan may just not be taken into account. For instance, drug delivery capsules have shells designed to purposely degrade over a period of time for sustained release. Selection of shell materials is therefore important. As an example of lifetime requirements, a PCM incorporated into a building wall for air conditioning requires a life of at least 20 years. Assuming 1 melting/freezing cycle per day, the material must be stable for around 7300 cycles. Polymers are often very durable, so long lifetimes are possible although it is more difficult when a capsule shell may be only a few nanometres thick. If extended stability cannot be achieved, a postulated solution is the use of self-healing capsules. There a numerous examples in the literature of self-healing capsules which contain shell material in the core (e.g. diisocyanate in the core of a PU capsule[227]). The self-healing material is released when the shell is damaged. It may be possible to

combine this effect with PCMs in the capsule core to provide a longer lasting heat storage material. Self-healing materials will often be organic. Therefore, for a regular encapsulation reaction, only organic PCMs such as paraffin wax could be combined. The development of multi-compartmental capsules[228] may be of interest in order to use inorganic PCMs such as salt hydrates for heat storage in conjunction with self-healing.

There have been many reported techniques for creating micro- and nanocapsules. These include spray-drying[229,230], miniemulsion polymerisation[231,232], precipitation of pre-formed polymers[233], layer-by-layer assembly (LbL)[203,210], or other more advanced polymerisation reactions such as radical addition-fragmentation chain-transfer (RAFT)[234] and the creation of dendrimers[235]. Each of these techniques has their own advantages and disadvantages. While the deposition of pre-formed materials is a simple process, polymerisation reactions are generally more useful, as polymers of desired properties can be formed[175].

LbL is an interesting approach for its precise control over shell thickness. Oppositely charged polyelectrolyte layers are deposited successively[236]. Layers are generally a few nanometres thick, therefore simply by altering the number of layers deposited, a shell of desired thickness can be formed. The deposition can be easily followed by making zeta potential measurements, which will change from positive to negative based on the previous layer deposited. Sodium polystyrene sulfonate (PSS) and polyallylamine hydrochloride (PAH) are typical polyelectrolytes used for LbL, as polyanion and polycation, respectively. Often a sacrificial core is used as a template for deposition. The core can be dissolved once the desired shell thickness is achieved, leaving hollow capsules which can be loaded with a target material. Despite the simplicity of this method, the large numbers of steps required make it difficult for scale-up. Polyelectrolyte shells synthesised by LbL result in semi-permeable membranes which can allow smaller molecules to pass in and out, while large molecules such as proteins cannot diffuse across[237].

Polymerisation using a miniemulsion template is generally accepted to be the most reliable way to produce small capsules, especially when working in the nanometre size range. It is also feasible for scale up to industrial production[197], and requires less steps than methods such as LbL[238]. Traditional emulsion polymerisation is a type of free radical polymerisation, where polymerisation is started by radicals which enter monomer droplets[239]. By producing a miniemulsion, monomer droplets become much smaller (around 100nm compared to 1-10μm). This gives a far greater surface area, and therefore a better chance of radical initiation. The miniemulsion therefore provides an enormous number of parallel reactions – taking place inside 10^{18}-10^{20} nanodroplets[240]. Two other important types of polymerisation for encapsulating materials benefit from the use of miniemulsions. Miniemulsion droplets provide a template for the polymer shell to form. They are: interfacial polymerisation, where each of the dispersed and continuous phases contains a different monomer; and *in situ* polymerisation, where the monomer is only present in the continuous phase. Many examples of encapsulated PCMs appear in the literature.

1.9 Organic and Inorganic PCM Encapsulation – A Review

As mentioned previously, containment is crucial in giving PCMs the desirable properties for wide-scale use. PCM capsules provide the previously mentioned improvements compared to bulk PCMs, such as prevention of leakage, increased heat transfer area and decreased interaction with the external environment. Capsules come in various sizes, in the range of centimetres or millimetres (macroencapsulation), micrometres (microencapsulation) or nanometres (nanoencapsulation). As stated earlier, nanocapsules are most desirable due to the huge increase in surface-to-volume ratio, leading more pronounced improvements in heat transfer and structural strength. Various encapsulated PCM products are already on the market, although none are nanocapsules. The earliest example of an encapsulated PCM was a simulation by Theunissen and Buchlin[241], who determined a PCM storage system utilising $CaCl_2.6H_2O$ would require a volume 5 times less than that of an SHS rock bed, in order to store an equal amount of energy. The encapsulation process for that study simply consisted of a large tank, however modern technology allows for the fabrication of PCM capsules at the nanoscale. The positive effects of encapsulation have been proven with a huge number of journal articles on the encapsulation of paraffin waxes[242–245]. The most successful techniques for the fabrication of PCM-loaded capsules have been polymerisation reactions based on miniemulsions; these are miniemulsion, *in situ* and interfacial polymerisations, as described on the previous page.

1.9.1 Encapsulation of Organic PCMs

Much research has been done on the encapsulation of PCMs, mostly using paraffin wax as a core material. Paraffins must be contained due to potential reaction with external environment, difficulty in handling, large volume changes during melting, and their flammability. Additional fire retardant materials may also be added to the capsules[105]. Paraffin waxes have several advantages over salt

hydrates when it comes to their encapsulation. Firstly, O/W emulsions are more easily formulated. O/W emulsions are well researched; for example, it is well known sodium dodecyl sulphate (SDS, also known as sodium lauryl sulphate) can emulsify oils into aqueous solution, and is found in many common domestic cleaning products and is registered safe for use in food. Water being used as the continuous phase for O/W emulsions means costs are low. Paraffin waxes are comparatively easy to encapsulate compared to salt hydrates. Research into encapsulated paraffin waxes has proven the benefits of encapsulation in solving problems associated with PCMs.

Several researchers have synthesised capsules using melamine-formaldehyde or urea formaldehyde shells. The potential release of toxic formaldehyde into the environment means these shell materials are not suitable for use[246], especially as there are many inert and non-toxic polymer materials available to replace them.

Felix *et al*[32,246] fabricated docosane loaded microcapsules using PU as shell material. The capsules were stable over at least 100 cycles. They also found that by modifying homogenisation speed during the emulsion forming phase, capsules of different sizes could be made. An interesting effect was that the smaller capsules displayed higher latent heat compared with larger capsules. These effects show the benefits of reduced capsule size, resulting in higher encapsulation efficiency. Increased heat transfer to the core material also contributes to maximise latent heat. Another effect they found with decreasing capsule size was the distinct appearance of multiple crystalline phases during freezing. Spatial confinement clearly has a significant effect on PCM behaviour.

Zhang and collaborators[247] noted monomer effects on encapsulation. They used tolylene diisocyanate along with amines as crosslinkers for polyurea shell formation. Amines used were ethylene diamine, diethylene triamine and Jeffamine (amine-terminated polyoxypropylene). Longer chain amines formed capsules of larger diameter, along with better coverage of the core material. The authors state this is due to the hydrophilic amines requiring migration into the oil phase to react with the diisocyanate. Longer chains mean slower diffusion processes and so the emulsion remains

more stabilised during reaction. Due to the more complete coverage of shell material, the larger capsules had a higher EE and improved latent heat. Monomer selection is therefore an important factor to consider when fabricating PCM loaded capsules.

There have been several studies using acrylates as monomers for the polymerisation reactions. Acrylate-based polymers are particularly suitable for PCM encapsulation as they are softer than other polymers such as polystyrene. Increased flexibility allows them to withstand the volume changes of the solid-liquid transition. Yang *et al*[248] synthesised PMMA, poly(ethyl methacrylate) (PEMA) and polystyrene microcapsules containing tetradecane using *in situ* polymerisation, and found the acrylate capsules performed far better with regards to heat storage. Zhang *et al*[224] also made PEMA and PMMA capsules, but used sonication in order to perform a miniemulsion polymerisation. This resulted in nanocapsules 100-150nm in size, and encapsulated octadecane with a high efficiency of 89-95%. Both sets of researchers noted that supercooling of the paraffin was reduced once encapsulated. Sari *et al*[249] proved the durability of PEMA and PMMA capsules. They encapsulated nonadecane with 60.3% encapsulation efficiency (EE), with only a 5% loss in latent heat after 5000 cycles.

It has also been possible to synthesise capsules with full and partial inorganic shells. Yin *et al*[226] made a hybrid SiO_2/polystyrene/poly(divinyl benzene) shell using a Pickering emulsion template, resulting in capsules of approximately 100µm diameter. Modified SiO_2 particles were used as stabiliser and, due to the presence of -C=C groups on their surface, became embedded in the shell by covalent bonding. Other researchers have reported forming a full SiO_2 shell by hydrolysing tetraethyl orthosilicate (TEOS) to create an encapsulation precursor. This gave capsules of 8-15µm and a high encapsulation efficiency up to 87.5%[250]. Sol-gel processes can also be used to encapsulate paraffins with hydrolysed TEOS[251]. The authors reported capsules of 7-16µm, and noted the microcapsule thermal conductivity was 0.621$Wm^{-1}K^{-1}$ compared with 0.151$Wm^{-1}K^{-1}$ for bulk octadecane. They also

showed the silica shell has a conductivity of 1.296$Wm^{-1}K^{-1}$, compared with polymers which are around 0.20$Wm^{-1}K^{-1}$.

Although silica shells have given some promising results, especially with regards to thermal conductivity enhancement, their long-term stability is brought into question due to their brittleness. Despite good thermal and chemical stability, they may fracture due to stress brought about by PCM volume change. Besides, it is possible to impregnate polymer capsules with thermally conductive nanoparticles to increase thermal conductivity, without sacrificing shell flexibility.

Despite the great progress made with organic PCMs and their ongoing research, their low thermal conductivity and high cost mean other large-scale energy storage materials must be sought. Another issue to consider with the encapsulation and general use of organic PCMs is the possible release of carbon into the environment upon degradation. Encapsulated carbon release is an unknown quantity in environmental studies and may lead to unwanted side effects such as soil erosion[252].

1.9.2 Encapsulation of Inorganic PCMs

The major focus of the project that is the subject of this thesis was to nanoencapsulate salt hydrates and analyse their thermal storage abilities. It is important to account for historical and current research, to understand advantages and problems associated with their use. Several researchers have used salt hydrates in their bulk state for use in energy storage. More recently, some successful attempts at making salt hydrate capsules on the micro- and nanoscale have been achieved. Salt hydrates are difficult to encapsulate due to their hydrophilicity, tendency to alter water content and surface polarity[253,254]. Further added to these issues is their general chemical instability, which is well documented[34,255–259]. Another problem is that of washing and drying the capsules. Vacuum drying is not suitable as it may dehydrate the crystallohydrate core and therefore alter its T_M. Encapsulation

can promote improved stability due to effects described above, such as confinement of stoichiometry and improved heat transfer to decrease supercooling. It also acts as a barrier to prevent water loss from the crystallohydrate core, maintaining thermal characteristics. Ideal phase change behaviour for inorganic PCM capsules is described in Fig 1.11. Encapsulation of inorganic PCMs is currently more expensive than organic PCMs, due to the large amount of organic solvents required to form W/O emulsions[260]. The use of organic solvents may also be regulated due to health and safety concerns, so may not be suitable for industrial use[261,262]. It may be possible in future to reduce these costs by using waste products from industry, such as vegetable or other bio oils. The enhanced properties of inorganic PCMs compared with organics make further research into their encapsulation highly beneficial. Techniques to make aqueous core nanocapsules as cost effective as possible should be developed to maximise the benefit of energy storage using inorganic PCMs. Methodology for encapsulating salt hydrates requires a high EE to maximise heat storage potential. This is dependent on a good emulsification step[263], and also the viscosity of the continuous and dispersed phases. Increase in dispersion viscosity can prevent migration of the salt into the continuous phase[264]. Other factors influencing EE include polymer concentration[265,266], surfactant concentration[266,267], stirring rate during emulsification[267,268] and temperature[269,270].

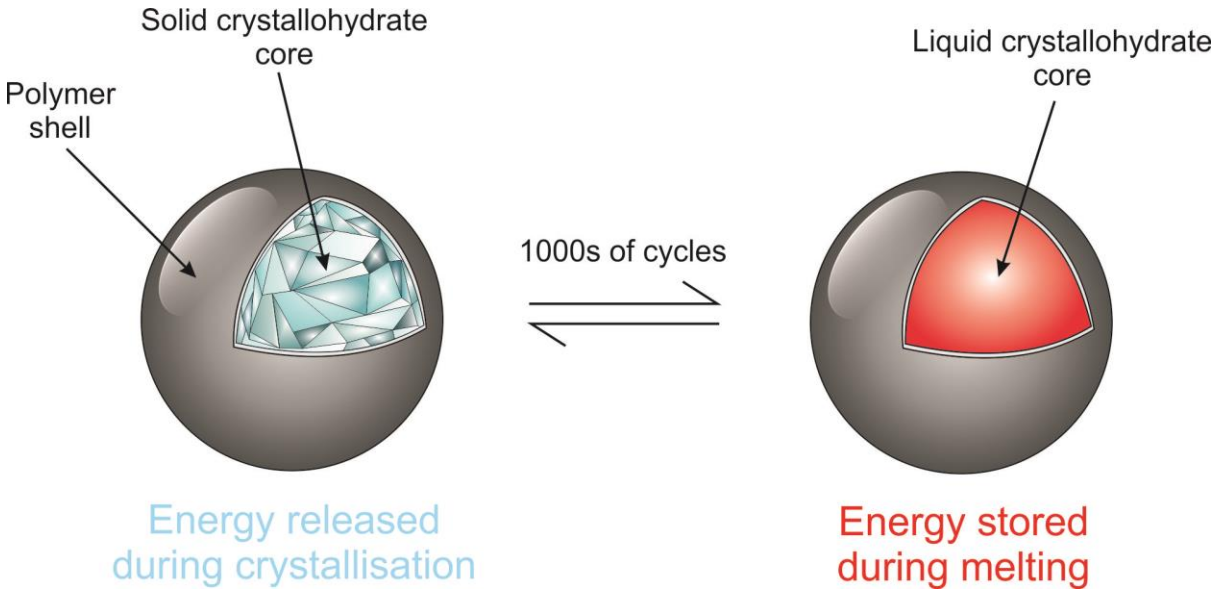

Fig 1.11 Cartoon showing ideal capsule behaviour for the salt hydrate core

In 2001, Gröhn *et al*[235] encapsulated chloroauric acid trihydrate within a dendrimer system, although this was not for energy storage purposes. To the best of the author's knowledge, the first attempted core-shell microcapsules containing salt hydrates specifically for energy storage were developed by Sarier and co-authors[261], to be used in thermally regulating fibres. They used a mix of PEG1000, hexadecane and sodium carbonate decahydrate ($Na_2CO_3.10H_2O$) as core material, encapsulated in a urea-formaldehyde shell. They noted the phase change behaviour resembled that of hexadecane and $Na_2CO_3.10H_2O$ didn't contribute. The same authors also developed a method of trapping PCM micelles inside a polyurethane foam[271]. One of the PCM combinations they used was octadecane and $Na_2CO_3.10H_2O$. However, they found that the $Na_2CO_3.10H_2O$ acted merely as a blowing agent due to its water content, and did not contribute to the latent heat. As these researchers were using O/W emulsions rather than W/O, the resulting capsules contained very little salt hydrate.

Salaün *et al*[263] encapsulated $Na_2PO_4.12H_2O$ with a polyurea/polyurethane shell. They used the solvent evaporation technique, using cellulose acetate butyrate as monomer which polymerised as the volatile solvent (chloroform) evaporated. They used MDI as the crosslinker to form the polyurea

shell. Unfortunately, they provided no results displaying thermal energy storage characteristics or accurate size measurements (only stating they were >1μm), although they did show the capsules contained a large amount of salt, up to 79%. In further research, they investigated the influence of the solvent on capsule properties. They found that changing the solvent for the dispersed and continuous phases had a profound influence on the characteristics of the microcapsules. Using chloroform as dispersed phase solvent instead of acetone facilitated the full coverage of the core with shell material. Using toluene as continuous phase instead of carbon tetrachloride reduced the rate of coacervation and produced better defined capsules. DSC results revealed most of the formed capsules had incomplete crystallisation processes, meaning that by the 2nd thermal cycle, no latent heat storage was possible. The most successful capsules were produced using toluene and chloroform as solvents, and produced capsules with a latent heat of melting of 140.4 $J \cdot g^{-1}$. However, the latent heat of crystallisation was only 48.9 $J \cdot g^{-1}$, suggesting long-term stability is not possible.

In another work, Salaün and co-authors[272] also made polymer nanocapsules containing $Na_2PO_4.12H_2O$, and added these to microcapsules containing paraffin wax mixtures. They found the addition of the nanoparticles decreased the thermal conductivity of the microcapsules, leading to a wider range of the T_M. They concluded this would have a positive effect for use as a 'thermal barrier'. It also shows how the low thermal conductivity of polymers can be a problem for LHS due to slower melting and freezing characteristics. The article proved that it was possible to encapsulate salt hydrates on the nanoscale, unfortunately no thermal data was provided for the salt hydrate containing nanoparticles alone.

Huang and collaborators made two attempts at encapsulating salt hydrates[253,273]. They also used $Na_2PO_4.12H_2O$ as core material. They used MMA as monomer, along with ethyl acrylate (EA) as crosslinker. The shell was made by a suspension polymerisation combined with solvent evaporation. They found that upon encapsulation the PCM was partially dehydrated to form $Na_2PO_4.7H_2O$ which resulted in an increase in T_M from 36ºC to 51ºC. They also made a follow up article[273], where they

compared their PMMA/EA capsules to urea-formaldehyde (UF) ones. The PMMA demonstrated much better thermal characteristics, with the UF capsules giving a very broad T_M with a peak at 41ºC. Broad T_Ms are unsuitable for practical when a narrow temperature range is required. They proved the shell material prevents water loss from the encapsulated salt hydrate by thermogravimetry measurements, therefore resisting dehydration and maintaining the T_M. Importantly, upon encapsulation the thermal conductivity was increased from 1.01$Wm^{-1}K^{-1}$ for pure $Na_2PO_4.12H_2O$ to 1.426$Wm^{-1}K^{-1}$ for the encapsulated $Na_2PO_4.7H_2O$, an increase of 29%[274].

Platte *et al*[254] encapsulated different mixtures of sodium sulphate, sodium phosphate and sodium carbonate which were hydrated by dissolving in water. They used a surface-thiol Michael addition polymerisation using ORMOCER polymers as shell material, which are biodegradable inorganic-organic hybrid polymers developed by Fraunhofer ISC. ORMOCERs are impermeable to water, which can be of great benefit to encapsulated salt hydrates to maintain the desired hydration state. Formed capsules were around 40µm in diameter. They noted the difficulty in maintaining the hydration state of the encapsulated crystallohydrates even when the shell formed has no defects, due to water permeation through the shell. Supercooling was still a problem, showing the microcapsules did not sufficiently improve heat transfer.

Schoth *et al*[275] developed a surfactant free method to encapsulate sodium sulphate decahydrate. They utilised the Pickering emulsion technique to create the initial emulsion. They made polyurethane nanocapsules with an average size of 750-1000nm, the first time a silica stabilised capsule had been made in that size range. It was shown that $Na_2SO_4.10H_2O$ could be encapsulated up to 20%wt, which is its solubility limit in water.

An interesting approach for salt hydrate encapsulation was the use of nanobowls, consisting of an SiO_2 matrix impregnated with $Na_2SO_4.10H_2O$[276]. The formation of the unusual bowl shape is due to non-synchronous rotation of droplets caused by viscosity differences between the liquid and solid phases. Of course, the SiO_2 matrix improved conductivity of the PCM, as well as reducing phase

separation. The sample also had high latent heat of 180.7 $J \cdot g^{-1}$ which was relatively unchanged after 60 cycles. However, supercooling was only marginally reduced.

One company, Capzo, has made commercial salt hydrate capsules known as Thermusol[277], showing future large scale developments in this area are viable. Despite this recent progress in encapsulating salt hydrates, issues remain with regards to their long-term stability, thermal characteristics and the expense and scale-up of encapsulation methodology.

High-temperature PCM encapsulation is also currently being researched. Gimenez-Gavarell and Fereres[278] developed borosilicate macrocapsules for encapsulating sodium nitrate salt, and metallic lead. The capsules performed well in the 300-400°C range, although some phase segregation was observed during melting. They also simulated results, which agreed with those experimentally determined. Smaller capsules will be developed in future. These high temperature PCMs are especially important for CSP energy storage systems.

1.10 Current research

Research for this thesis was based around the encapsulation of salt hydrates for LHS. Simple methods were sought, which may be scaled up in the future. Initial research focused on finding salt hydrates suitable as core materials, *i.e.* could be solubilised in a W/O emulsion. Once materials suitable for encapsulation were found, numerous methods were attempted for the creation of crystallohydrate-loaded capsules. Low temperature PCMs were chosen for investigation due to ease of handling and analysis.

We found numerous kinds of capsules with differing shell material could be formed once initial miniemulsions had been created. The materials synthesised were tested according to their thermal and chemical characteristics, paying specific attention to their stability over many thermal cycles. Long-term stability is the single biggest issue with crystallohydrate PCMs, we postulated this could be solved by nanoencapsulation, due to improved heat transfer and confinement of the PCM. Capsule characteristics were compared to the bulk salt hydrates. Salt hydrate PCMs are good candidates for use in low temperature applications such as passive air conditioning and thermal management of batteries. Results detailed in this thesis may also be of use to researchers studying other inorganic PCMs such as salts.

1.11 References

1 B. Xu, P. Li and C. Chan, *Appl. Energy*, 2015, **160**, 286–307.

2 S. Sargunanathan, A. Elango and S. T. Mohideen, *Renew. Sustain. Energy Rev.*, 2016, **64**, 382–393.

3 N. S. Lewis and D. G. Nocera, *Proc. Natl. Acad. Sci. U. S. A.*, 2006, **103**, 15729–15735.

4 G. Walther, E. Post, P. Convey, A. Menzel, C. Parmesan, T. J. C. Beebee, J. Fromentin, O. Hoegh-Guldberg and F. Bairlein, *Nature*, 2002, **416**, 389–395.

5 W. Thuiller, C. Albert, M. B. Araújo, P. M. Berry, M. Cabeza, A. Guisan, T. Hickler, G. F. Midgley, J. Paterson, F. M. Schurr, M. T. Sykes and N. E. Zimmermann, *Perspect. Plant Ecol. Evol. Syst.*, 2008, **9**, 137–152.

6 A. D. Barnosky, N. Matzke, S. Tomiya, G. O. U. Wogan, B. Swartz, T. B. Quental, C. Marshall, J. L. McGuire, E. L. Lindsey, K. C. Maguire, B. Mersey and E. A. Ferrer, *Nature*, 2011, **471**, 51–57.

7 G. McGranahan, D. Balk and B. Anderson, *Environ. Urban.*, 2007, **19**, 17–37.

8 M. Asif and T. Muneer, *Renew. Sustain. Energy Rev.*, 2007, **11**, 1388–1413.

9 M. I. Hoffert, K. Caldeira, G. Benford, D. R. Criswell, C. Green, H. Herzog, A. K. Jain, H. S. Kheshgi, K. S. Lackner, J. S. Lewis, H. D. Lightfoot, W. Manheimer, J. C. Mankins, M. E. Mauel, L. J. Perkins, M. E. Schlesinger, T. Volk and T. M. L. Wigley, *Science*, 2002, **298**, 981–987.

10 D. Y. C. Leung, G. Caramanna and M. M. Maroto-Valer, *Renew. Sustain. Energy Rev.*, 2014, **39**, 426–443.

11 A. S. Arico, P. Bruce, B. Scrosati, J.-M. Tarascon and W. van Schalkwijk, *Nat. Mater.*, 2005, **4**, 366–377.

12 G. Girishkumar, B. McCloskey, A. C. Luntz, S. Swanson and W. Wilcke, *J. Phys. Chem. Lett.*, 2010, **1**, 2193–2203.

13 A. C. Dillon, K. M. Jones, T. A. Bekkedahl, C. H. Kiang, D. S. Bethune and M. J. Heben, *Nature*, 1997, 386, 377–379.

14 N. L. Rosi, J. Eckert, M. Eddaoudi, D. T. Vodak, J. Kim, M. O'Keeffe and O. M. Yaghi, *J. Inorg. Organomet. Polym. Mater.*, 2003, **300**, 1127–1129.

15 T. Ogasawara, A. Débart, M. Holzapfel, P. Novák and P. G. Bruce, *J. Am. Chem. Soc.*, 2006, **128**, 1390–1393.

16 J. S. Lee, S. T. Kim, R. Cao, N. S. Choi, M. Liu, K. T. Lee and J. Cho, *Adv. Energy Mater.*, 2011, **1**, 34–50.

17 Z. Peng, S. A. Freunberger, Y. Chen and P. G. Bruce, *Science*, 2012, **337**, 563–566.

18 B. Lehner, G. Czisch and S. Vassolo, *Energy Policy*, 2005, **33**, 839–855.

19 C. Zarfl, A. E. Lumsdon, J. Berlekamp, L. Tydecks and K. Tockner, *Aquat. Sci.*, 2015, **77**, 161–170.

20 H. Lund and G. Salgi, *Energy Convers. Manag.*, 2009, **50**, 1172–1179.

21 V. Siva Reddy, S. C. Kaushik, K. R. Ranjan and S. K. Tyagi, *Renew. Sustain. Energy Rev.*, 2013, **27**, 258–273.

22 J. Tsao, N. Lewis and G. Crabtree, *US Dep. Energy*, 2006, 1–24.

23 M. S. Dresselhaus and I. L. Thomas, *Nature*, 2001, **414**, 332–7.

24 M. Grätzel, *Nature*, 2001, **414**, 338–344.

25 M. M. Lee, J. Teuscher, T. Miyasaka, T. N. Murakami and H. J. Snaith, *Science*, 2012, **338**, 643–648.

26 D. P. McMeekin, G. Sadoughi, W. Rehman, G. E. Eperon, M. Saliba, M. T. Horantner, A. Haghighirad, N. Sakai, L. Korte, B. Rech, M. B. Johnston, L. M. Herz and H. J. Snaith, *Science*, 2016, **351**, 151–155.

27 J. Burschka, N. Pellet, S.-J. Moon, R. Humphry-Baker, P. Gao, M. K. Nazeeruddin and M. Grätzel, *Nature*, 2013, **499**, 316–319.

28 S. H. Park, A. Roy, S. Beaupré, S. Cho, N. Coates, J. S. Moon, D. Moses, M. Leclerc, K. Lee and A. J. Heeger, *Nat. Photonics*, 2009, **3**, 297–302.

29 L. Huo, T. Liu, X. Sun, Y. Cai, A. J. Heeger and Y. Sun, *Adv. Mater.*, 2015, **27**, 2938–2944.

30 I. Dincer, S. Dost and X. Li, *Fuel Energy Abstr.*, 1997, **38**, 435.

31 R. Tiskatine, R. Oaddi, R. Ait El Cadi, A. Bazgaou, L. Bouirden, A. Aharoune and A. Ihlal, *Sol. Energy Mater. Sol. Cells*, 2017, **169**, 245–257.

32 P. Felix De Castro, A. Ahmed and D. G. Shchukin, *Chem. - A Eur. J.*, 2016, **22**, 4389–4394.

33 N. Nallusamy, S. Sampath and R. Velraj, *Renew. Energy*, 2007, **32**, 1206–1227.

34 A. Abhat, *Sol. Energy*, 1983, **30**, 313–332.

35 P. A. J. Donkers, L. C. Sögütoglu, H. P. Huinink, H. R. Fischer and O. C. G. Adan, *Appl. Energy*, 2017, **199**, 45–68.

36 H. Ö. Paksoy, *Thermal Energy Storage for Sustainable Energy Consumption*, 2007.

37 Y. Kato, J. Nakahata and Y. Yoshizawa, *J. Mater. Sci.*, 1999, **34**, 475–480.

38 G. Ervin, *J. Solid State Chem.*, 1977, **22**, 51–61.

39 P. Pardo, A. Deydier, Z. Anxionnaz-Minvielle, S. Rougé, M. Cabassud and P. Cognet, *Renew. Sustain. Energy Rev.*, 2014, **32**, 591–610.

40 K. E. N'Tsoukpoe, H. Liu, N. Le Pierres and L. Luo, *Renew. Sustain. Energy Rev.*, 2009, **13**, 2385–2396.

41 K. Posern and C. Kaps, *Thermochim. Acta*, 2010, **502**, 73–76.

42 M. Neises, S. Tescari, L. de Oliveira, M. Roeb, C. Sattler and B. Wong, *Sol. Energy*, 2012, **86**, 3040–3048.

43 P. Pardo, A. Deydier, Z. Anxionnaz-Minvielle, S. Rougé, M. Cabassud and P. Cognet, *Renew. Sustain. Energy Rev.*, 2014, **32**, 591–610.

44 J. Kang and J. Rebek, *Nature*, 1997, **385**, 50–52.

45 X. Du, H. Wang, Y. Wu, Z. Du and X. Cheng, *J. Appl. Polym. Sci.*, 2017, **134**, 1–8.

46 N. Javani, I. Dincer and G. F. Naterer, *J. Power Sources*, 2014, **268**, 718–727.

47 P. Zhang, Z. W. Ma and R. Z. Wang, *Renew. Sustain. Energy Rev.*, 2010, **14**, 598–614.

48 B. Zalba, J. M. Marin, L. F. Cabeza and H. Mehling, *Appl. Therm. Eng.*, 2003, **23**, 251–283.

49 S. A. Mohamed, F. A. Al-Sulaiman, N. I. Ibrahim, M. H. Zahir, A. Al-Ahmed, R. Saidur, B. S. Yılbaş and A. Z. Sahin, *Renew. Sustain. Energy Rev.*, 2017, **70**, 1072–1089.

50 R. Naumann and H. H. Emons, *J. Therm. Anal. Calorim.*, 1989, **35**, 1009–1031.

51 M. Kenisarin and K. Mahkamov, *Sol. Energy Mater. Sol. Cells*, 2016, **145**, 255–286.

52 L. F. Cabeza, J. Illa, J. Roca, F. Badia, H. Mehling, S. Hiebler and F. Ziegler, *Mater. Corros.*, 2001, **52**, 140–146.

53 F. C. Porisini, *Sol. Energy*, 1988, **41**, 193–197.

54 K. Nagano, K. Ogawa, T. Mochida, K. Hayashi and H. Ogoshi, *Appl. Therm. Eng.*, 2004, **24**, 221–232.

55 E. Oró, a. de Gracia, a. Castell, M. M. Farid and L. F. Cabeza, *Appl. Energy*, 2012, **99**, 513–533.

56 H. S. Ge, H. Y. Li, S. F. Mei and J. Liu, *Renew. Sustain. Energy Rev.*, 2013, **21**, 331–346.

57 T. Nomura, N. Okinaka and T. Akiyama, *ISIJ Int.*, 2010, **50**, 1229–1239.

58 K. Ma and J. Liu, *Front. Energy Power Eng. China*, 2007, **1**, 384–402.

59 H. Ge and J. Liu, *Front. Energy*, 2012, **6**, 207–209.

60 C. Rathgeber, H. Schmit, P. Hennemann and S. Hiebler, *Appl. Energy*, 2014, **136**, 7–13.

61 C. Alkan and A. Sari, *Sol. Energy*, 2008, **82**, 118–124.

62 Y. Hong and X. Ge, *Sol. Energy Mater. Sol. Cells*, 2000, **64**, 37–44.

63 A. Sari, C. Alkan, A. Karaipekli and A. Önal, *Energy Convers. Manag.*, 2008, **49**, 373–380.

64 A. Sari, C. Alkan, U. Kolemen and O. Uzun, *J. Appl. Polym. Sci.*, 2006, **101**, 1402–1406.

65 B. J. Manning, P. R. Bender, S. A. Cote, R. A. Lewis, A. R. Sakulich and R. B. Mallick, *Sustain. Cities Soc.*, 2015, **19**, 11–16.

66 M. T. Johansson and M. Söderström, *Energy Effic.*, 2014, **7**, 203–215.

67 R. I. Dunn, P. J. Hearps and M. N. Wright, *Proc. IEEE*, 2012, **100**, 504–515.

68 H. L. Zhang, J. Baeyens, J. Degrève and G. Cacères, *Renew. Sustain. Energy Rev.*, 2013, **22**, 466–481.

69 A. Fernández-García, E. Zarza, L. Valenzuela and M. Pérez, *Renew. Sustain. Energy Rev.*, 2010, **14**, 1695–1721.

70 D. R. Mills and G. L. Morrison, *Sol. Energy*, 2000, **68**, 263–283.

71 I. Llorente García, J. L. Álvarez and D. Blanco, *Sol. Energy*, 2011, **85**, 2443–2460.

72 Y. Tian and C. Y. Zhao, *Appl. Energy*, 2013, **104**, 538–553.

73 G. Morin, J. Dersch, W. Platzer, M. Eck and A. Häberle, *Sol. Energy*, 2012, **86**, 1–12.

74 U. Pelay, L. Luo, Y. Fan, D. Stitou and M. Rood, *Renew. Sustain. Energy Rev.*, 2017, **79**, 82–100.

75 K. Vignarooban, X. Xu, A. Arvay, K. Hsu and A. M. Kannan, *Appl. Energy*, 2015, **146**, 383–396.

76 C. K. Ho and B. D. Iverson, *Renew. Sustain. Energy Rev.*, 2014, **29**, 835–846.

77 P. D. Myers and D. Y. Goswami, *Appl. Therm. Eng.*, 2016, **109**, 889–900.

78 T. Bauer, N. Pfleger, N. Breidenbach, M. Eck, D. Laing and S. Kaesche, *Appl. Energy*, 2013, **111**, 1114–1119.

79 M. M. Kenisarin, *Renew. Sustain. Energy Rev.*, 2010, **14**, 955–970.

80 M. Liu, W. Saman and F. Bruno, *Renew. Sustain. Energy Rev.*, 2012, **16**, 2118–2132.

81 J. Yagi and T. Akiyama, *J. Mater. Process. Technol.*, 1995, **48**, 793–804.

82 P. Blanco-Rodríguez, J. Rodríguez-Aseguinolaza, E. Risueño and M. Tello, *Energy*, 2014, **72**, 414–420.

83 J. J. Park, D. P. Butt and C. A. Beard, *Nucl. Eng. Des.*, 2000, **196**, 315–325.

84 B. Ma, J. Li, Z. Xu and Z. Peng, *Appl. Energy*, 2014, **132**, 568–574.

85 A. Datas, A. Ramos, A. Martí, C. del Cañizo and A. Luque, *Energy*, 2016, **107**, 542–549.

86 D. Laing, C. Bahl, T. Bauer, D. Lehmann and W. D. Steinmann, *Sol. Energy*, 2011, **85**, 627–633.

87 M. Ozturk and I. Dincer, *Energy Convers. Manag.*, 2013, **76**, 1061–1072.

88 N. Maruoka, T. Mizuochi, H. Purwanto and T. Akiyama, *ISIJ Int.*, 2004, **44**, 257–262.

89 L. Miró, J. Gasia and L. F. Cabeza, *Appl. Energy*, 2016, **179**, 284–301.

90 M. A. Korzhuev and I. V. Katin, *J. Electron. Mater.*, 2010, **39**, 1390–1394.

91 S. Kumar, S. D. Heister, X. Xu, J. R. Salvador and G. P. Meisner, *J. Electron. Mater.*, 2013, **42**, 944–955.

92 Q. Li, R. He, J. Jensen and N. Bjerrum, *Chem. Mater.*, 2003, **15**, 4896–4915.

93 A. M. Khudhair and M. M. Farid, *Energy Convers. Manag.*, 2004, **45**, 263–275.

94 B. Zalba, J. M. Marín, L. F. Cabeza and H. Mehling, *Int. J. Refrig.*, 2004, **27**, 839–849.

95 S. A. Memon, *Renew. Sustain. Energy Rev.*, 2014, **31**, 870–906.

96 R. Kandasamy, X. Q. Wang and A. S. Mujumdar, *Appl. Therm. Eng.*, 2008, **28**, 1047–1057.

97 R. D. Weinstein, T. C. Kopec, A. S. Fleischer, E. D'Addio and C. A. Bessel, *J. Heat Transfer*,

2008, **130**, 42405.

98 S. A. Khateeb, S. Amiruddin, M. Farid, J. R. Selman and S. Al-Hallaj, *J. Power Sources*, 2005, **142**, 345–353.

99 Z. Ling, Z. Zhang, G. Shi, X. Fang, L. Wang, X. Gao, Y. Fang, T. Xu, S. Wang and X. Liu, *Renew. Sustain. Energy Rev.*, 2014, **31**, 427–438.

100 G. Jiang, J. Huang, Y. Fu, M. Cao and M. Liu, *Appl. Therm. Eng.*, 2016, **108**, 1119–1125.

101 N. O. Moraga, J. P. Xamán and R. H. Araya, *Appl. Therm. Eng.*, 2016, **108**, 1041–1054.

102 C. J. Smith, P. M. Forster and R. Crook, *Appl. Energy*, 2014, **126**, 21–28.

103 M. C. Browne, B. Norton and S. J. McCormack, *Renew. Sustain. Energy Rev.*, 2015, **47**, 762–782.

104 T. Y. Kim, B. S. Hyun, J. J. Lee and J. Rhee, *Aerosp. Sci. Technol.*, 2013, **27**, 10–16.

105 S. Mondal, *Appl. Therm. Eng.*, 2008, **28**, 1536–1550.

106 N. Sarier and E. Onder, *Thermochim. Acta*, 2012, **540**, 7–60.

107 X. Liu and Y. Lou, *Fibres Text. East. Eur.*, 2015, **23**, 63–67.

108 B. Nordell, *8 - Using ice and snow in thermal energy storage systems*, Woodhead Publishing Limited, 2015, vol. 8.

109 D. V. Hale, M. J. Hoover and M. J. O'Neill, 1971, 232.

110 T. D. Swanson and G. C. Birur, *Appl. Therm. Eng.*, 2003, **23**, 1055–1065.

111 W. F. Wu, N. Liu, W. L. Cheng and Y. Liu, *Energy Convers. Manag.*, 2013, **69**, 174–180.

112 M. Pauken, N. Emis and B. Watkins, *Sp. Technol. Appl. Int. FORUM - STAIF 2007*, 2007, **880**, 412–420.

113 B. A. Ying, Y. L. Kwok, Y. Li, Q. Y. Zhu and C. Y. Yeung, *Polym. Test.*, 2004, **23**, 541–549.

114 G. Nelson, *Int. J. Pharm.*, 2002, **242**, 55–62.

115 Y. Shin, D. I. Yoo and K. Son, *J. Appl. Polym. Sci.*, 2005, **97**, 910–915.

116 J. Kim and G. Cho, *Text. Res. J.*, 2002, **72**, 1093–1098.

117 C. Gao, K. Kuklane and I. Holmér, *Eur. J. Appl. Physiol.*, 2011, **111**, 1207–1216.

118 Y. Shin, D. I. Yoo and K. Son, *J. Appl. Polym. Sci.*, 2005, **96**, 2005–2010.

119 M. Kenisarin and K. Mahkamov, *Renew. Sustain. Energy Rev.*, 2016, **55**, 371–398.

120 H. Akeiber, P. Nejat, M. Z. A. Majid, M. A. Wahid, F. Jomehzadeh, I. Zeynali Famileh, J. K. Calautit, B. R. Hughes and S. A. Zaki, *Renew. Sustain. Energy Rev.*, 2016, **60**, 1470–1497.

121 N. Soares, J. J. Costa, A. R. Gaspar and P. Santos, *Energy Build.*, 2013, **59**, 82–103.

122 P. Schossig, H. M. Henning, S. Gschwander and T. Haussmann, *Sol. Energy Mater. Sol. Cells*, 2005, **89**, 297–306.

123 V. V. Tyagi, S. C. Kaushik, S. K. Tyagi and T. Akiyama, *Renew. Sustain. Energy Rev.*, 2011, **15**, 1373–1391.

124 F. Ascione, N. Bianco, R. F. De Masi, F. de' Rossi and G. P. Vanoli, *Appl. Energy*, 2014, **113**, 990–1007.

125 D. Feldman, D. Banu, D. Hawes and E. Ghanbari, *Sol. Energy Mater.*, 1991, **22**, 231–242.

126 A. Sari, A. Karaipekli and K. Kaygusuz, *Int. J. Energy Res.*, 2008, **32**, 154–160.

127 L. Shilei, Z. Neng and F. Guohui, *Energy Build.*, 2006, **38**, 708–711.

128 F. Kuznik and J. Virgone, *Appl. Energy*, 2009, **86**, 2038–2046.

129 F. Kuznik, D. David, K. Johannes and J. J. Roux, *Renew. Sustain. Energy Rev.*, 2011, **15**, 379–391.

130 S. H. Lee, S. J. Yoon, Y. G. Kim, Y. C. Choi, J. H. Kim and J. G. Lee, 2007, **24**, 332–335.

131 J. Lei, J. Yang and E.-H. Yang, *Appl. Energy*, 2016, **162**, 207–217.

132 A. G. Entrop, H. J. H. Brouwers and A. H. M. E. Reinders, *Sol. Energy*, 2011, **85**, 1007–1020.

133 A. J. N. Khalifa and E. F. Abbas, *Energy Build.*, 2009, **41**, 407–415.

134 E. Oro, L. Miro, M. M. Farid and L. F. Cabeza, *Int. J. Refrig.*, 2012, **35**, 984–991.

135 M. Ahmed, O. Meade and M. A. Medina, *Energy Convers. Manag.*, 2010, **51**, 383–392.

136 M. Liu, W. Saman and F. Bruno, *Appl. Energy*, 2012, **92**, 336–342.

137 L. Melone, L. Altomare, A. Cigada and L. De Nardo, *Appl. Energy*, 2012, **89**, 339–346.

138 K. Dai, L. Lu, Q. Liu, G. Zhu, X. Wei, J. Bai, L. Xuan and H. Wang, *Dalton Trans.*, 2014, **43**, 6295–6299.

139 F. L. Tan and C. P. Tso, *Appl. Therm. Eng.*, 2004, **24**, 159–169.

140 P. Ramadass, B. Haran, R. White and B. N. Popov, *J. Power Sources*, 2002, **112**, 606–613.

141 P. Ramadass, B. Haran, R. White and B. N. Popov, *J. Power Sources*, 2002, **112**, 614–620.

142 K. Amine, J. Liu and I. Belharouak, *Electrochem. commun.*, 2005, **7**, 669–673.

143 Y. Zhang, C. Y. Wang and X. Tang, *J. Power Sources*, 2011, **196**, 1513–1520.

144 S. A. Khateeb, M. M. Farid, J. R. Selman and S. Al-Hallaj, *J. Power Sources*, 2004, **128**, 292–307.

145 H. A. Weakliem and D. Redfield, *J. Appl. Phys.*, 1979, **50**, 1491–1493.

146 E. Radziemska, *Renew. Energy*, 2003, **28**, 1–12.

147 D. Du, J. Darkwa and G. Kokogiannakis, *Sol. Energy*, 2013, **97**, 238–254.

148 M. J. Huang, P. C. Eames and B. Norton, *Int. J. Heat Mass Transf.*, 2004, **47**, 2715–2733.

149 M. J. Huang, P. C. Eames and B. Norton, *Sol. Energy*, 2006, **80**, 1121–1130.

150 A. Hasan, S. J. McCormack, M. J. Huang and B. Norton, *Sol. Energy*, 2010, **84**, 1601–1612.

151 A. Hasan, S. J. McCormack, M. J. Huang, J. Sarwar and B. Norton, *Sol. Energy*, 2015, **115**, 264–276.

152 A. A. El-Sebaii, S. Al-Heniti, F. Al-Agel, A. A. Al-Ghamdi and F. Al-Marzouki, *Energy Convers. Manag.*, 2011, **52**, 1771–1777.

153 R. V Seeniraj, R. Velraj and N. L. Narasimhan, *J. Sol. Energy Eng. Asme*, 2002, **124**, 243–249.

154 T. Oya, T. Nomura, M. Tsubota, N. Okinaka and T. Akiyama, *Appl. Therm. Eng.*, 2013, **61**, 825–828.

155 G.-Q. Qi, J. Yang, R.-Y. Bao, Z.-Y. Liu, W. Yang, B.-H. Xie and M.-B. Yang, *Carbon N. Y.*, 2015, **88**, 196–205.

156 Z. Chen, M. Gu and D. Peng, *Appl. Therm. Eng.*, 2010, **30**, 1967–1973.

157 X. Xiao, P. Zhang and M. Li, *Appl. Energy*, 2013, **112**, 1357–1366.

158 C. Y. Zhao, W. Lu and Y. Tian, *Sol. Energy*, 2010, **84**, 1402–1412.

159 Y. W. Zhang and a Faghri, *Int. J. Heat Mass Transf.*, 1996, **39**, 3165–3173.

160 F. Agyenim, P. Eames and M. Smyth, *Sol. Energy*, 2009, **83**, 1509–1520.

161 M. Liu, N. H. S. Tay, S. Bell, M. Belusko, R. Jacob, G. Will, W. Saman and F. Bruno, *Renew. Sustain. Energy Rev.*, 2016, **53**, 1411–1432.

162 H. Michels and R. Pitz-Paal, *Sol. Energy*, 2007, **81**, 829–837.

163 P. A. Galione, C. D. Pérez-Segarra, I. Rodríguez, A. Oliva and J. Rigola, *Appl. Energy*, 2015, **142**, 337–351.

164 P. W. Stott, A. C. Williams and B. W. Barry, *J. Control. Release*, 1998, **50**, 297–308.

165 S. S. Chandel and T. Agarwal, *Renew. Sustain. Energy Rev.*, 2017, **67**, 581–596.

166 D. Zeng and W. Voigt, *Calphad Comput. Coupling Phase Diagrams Thermochem.*, 2003, **27**, 243–251.

167 D. Zeng, C. Fang and S. Chen, *Trans. Nonferrous Met. Soc. China*, 2004, 14, 1192–1198.

168 A. Efimova, S. Pinnau, M. Mischke, C. Breitkopf, M. Ruck and P. Schmidt, *Thermochim. Acta*, 2014, **575**, 276–278.

169 P. B. Salunkhe and P. S. Shembekar, *Renew. Sustain. Energy Rev.*, 2012, **16**, 5603–5616.

170 B. K. Paul and R. K. Mitra, *J. Colloid Interface Sci.*, 2005, **288**, 261–279.

171 K. Kundu and B. K. Paul, *Colloids Surfaces a-Physicochemical Eng. Asp.*, 2013, **433**, 154–165.

172 D. J. McClements, *Soft Matter*, 2012, **8**, 1719.

173 L. C. Peng, C. H. Liu, C. C. Kwan and K. F. Huang, *Colloids Surfaces A Physicochem. Eng. Asp.*, 2010, **370**, 136–142.

174 N. Anton, J. P. Benoit and P. Saulnier, *J. Control. Release*, 2008, **128**, 185–199.

175 J. P. Rao and K. E. Geckeler, *Prog. Polym. Sci.*, 2011, **36**, 887–913.

176 B. P. Binks, *Curr. Opin. Colloid Interface Sci.*, 2002, **7**, 21–41.

177 J. H. Schulman and J. Leja, *Trans. Faraday Soc.*, 1954, **50**, 598–605.

178 S. De La Rochebrochard, J. Suptil, J. F. Blais and E. Naffrechoux, *Ultrason. Sonochem.*, 2012, **19**, 280–285.

179 R. Xiao, Z. Wei, D. Chen and L. K. Weavers, *Environ. Sci. Technol.*, 2014, **48**, 9675–9683.

180 B. Teo, S. Prescott, M. Ashokkumar and F. Grieser, *Ultrason. Sonochem.*, 2008, **15**, 89–94.

181 J. H. Bang and K. S. Suslick, *Adv. Mater.*, 2010, **22**, 1039–1059.

182 T. J. Mason, *Ultrason. Sonochem.*, 2000, **7**, 145–9.

183 K. S. Suslick and G. J. Price, *Annu. Rev. Mater. Sci.*, 1999, **29**, 295–326.

184 K. S. Suslick and D. J. Flannigan, *Annu. Rev. Phys. Chem.*, 2008, **59**, 659–683.

185 H. Xu, B. W. Zeiger and K. S. Suslick, *Chem. Soc. Rev.*, 2013, **42**, 2555–67.

186 G. J. Price, *Ultrason. Sonochem.*, 2003, **10**, 277–283.

187 H. N. McMurray and B. P. Wilson, *J. Phys. Chem. A*, 1999, **103**, 3955–3962.

188 E. J. Hart and A. Henglein, *J. Phys. Chem.*, 1987, **91**, 3654–3656.

189 P. Sathishkumar, R. V. Mangalaraja and S. Anandan, *Renew. Sustain. Energy Rev.*, 2016, **55**, 426–454.

190 S. I. Nikitenko, L. Venault, R. Pflieger, T. Chave, I. Bisel and P. Moisy, *Ultrason. Sonochem.*, 2010, **17**, 1033–1040.

191 M. Gutierrez and A. Henglein, *J. Phys. Chem.*, 1990, **94**, 3625–3628.

192 Y. Asakura, T. Nishida, T. Matsuoka and S. Koda, *Ultrason. Sonochem.*, 2008, **15**, 244–250.

193 A. Henglein and M. Gutierrez, *J. Phys. Chem.*, 1990, **94**, 5169–5172.

194 Z. Wei, J. A. Kosterman, R. Xiao, G. Y. Pee, M. Cai and L. K. Weavers, *Ultrason. Sonochem.*, 2015, **27**, 325–333.

195 S. I. Nikitenko, C. Le Naour and P. Moisy, *Ultrason. Sonochem.*, 2007, **14**, 330–336.

196 G. Cravotto, G. Omiccioli and L. Stevanato, *Ultrason. Sonochem.*, 2005, **12**, 213–217.

197 J. M. Asua, *Prog. Polym. Sci.*, 2014, **39**, 1797–1826.

198 B. F. Gibbs, Selim Kermasha, Inteaz Al, *Int. J. Food Sci. Nutr.*, 1999, **50**, 213–224.

199 A. Madene, M. Jacquot, J. Scher and S. Desobry, *Int. J. Food Sci. Technol.*, 2006, **41**, 1–21.

200 L. Cheng, W. He, H. Gong, C. Wang, Q. Chen, Z. Cheng and Z. Liu, *Adv. Funct. Mater.*, 2013, **23**, 5893–5902.

201 P. M. Arnal, M. Comotti and F. Schüth, *Angew. Chemie - Int. Ed.*, 2006, **45**, 8224–8227.

202 A. C. Bijlard, A. Hansen, I. Lieberwirth, K. Landfester and A. Taden, *Adv. Mater.*, 2016, **28**, 6372–6377.

203 D. G. Shchukin, M. Zheludkevich, K. Yasakau, S. Lamaka, M. G. S. Ferreira and H. Möhwald, *Adv. Mater.*, 2006, **18**, 1672–1678.

204 D. G. Shchukin and H. Möhwald, *Adv. Funct. Mater.*, 2007, **17**, 1451–1458.

205 A. P. Kafka, B. J. McLeod, T. Rades and A. McDowell, *J. Control. Release*, 2011, **149**, 307–313.

206 D. Chitkara and N. Kumar, *Pharm. Res.*, 2013, **30**, 2396–2409.

207 S. Vrignaud, N. Anton, C. Passirani, J. P. Benoit and P. Saulnier, *Drug Dev. Ind. Pharm.*, 2013, **39**, 1706–1711.

208 J. Panyam and V. Labhasetwar, *Adv. Drug Deliv. Rev.*, 2003, **55**, 329–347.

209 C. E. Mora-Huertas, H. Fessi and A. Elaissari, *Int. J. Pharm.*, 2010, **385**, 113–142.

210 F. Caruso, D. Trau, H. Mo and R. Renneberg, 2011, 2324–2327.

211 H. Cohen, R. J. Levy, J. Gao, I. Fishbein, V. Kousaev, S. Sosnowski, S. Slomkowski and G. Golomb, *Gene Ther.*, 2000, **7**, 1896–1905.

212 H. Lomas, I. Canton, S. MacNeil, J. Du, S. P. Armes, A. J. Ryan, A. L. Lewis and G. Battaglia, *Adv. Mater.*, 2007, **19**, 4238–4243.

213 T. H. Tran, A. Vimalanandan, G. Genchev, J. Fickert, K. Landfester, D. Crespy and M. Rohwerder, *Adv. Mater.*, 2015, 3825–3830.

214 S. R. White, N. R. Sottos, P. H. Geubelle, J. S. Moore, M. R. Kessler, S. R. Sriram, E. N. Brown and S. Viswanathan, *Nature*, 2001, **409**, 794–797.

215 B. J. Blaiszik, N. R. Sottos and S. R. White, *Compos. Sci. Technol.*, 2008, **68**, 978–986.

216 T. M. S. Chang, *Science*, 1964, **146**, 524–525.

217 P. Couvreur, P. Speiser, P. Tulkens, M. Roland and A. Trouet, *FEBS Lett.*, 1977, **84**, 323–326.

218 J. Ballenger and R. Post, *Am. J. Psychiatry*, 1980, **137**, 782–790.

219 A. K. Gupta and M. Gupta, *Biomaterials*, 2005, **26**, 3995–4021.

220 S. M. S. M. Moghimi, A. C. A. C. Hunter and J. C. J. C. Murray, *Pharmacol. Rev.*, 2001, **53**, 283–318.

221 J. Rytkönen, R. Miettinen, M. Kaasalainen, V. P. Lehto, J. Salonen and A. Närvänen, *J. Nanomater.*, 2012.

222 T. Khadiran, M. Z. Hussein, Z. Zainal and R. Rusli, *Sol. Energy Mater. Sol. Cells*, 2015, **143**, 78–98.

223 F. D. Natterer, K. Yang, W. Paul, P. Willke, T. Choi, T. Greber, A. J. Heinrich and C. P. Lutz, *Nature*, 2017, **543**, 226–228.

224 G. H. Zhang, S. A. F. Bon and C. Y. Zhao, *Sol. Energy*, 2012, **86**, 1149–1154.

225 A. Jamekhorshid, S. M. Sadrameli and M. Farid, *Renew. Sustain. Energy Rev.*, 2014, **31**, 531–542.

226 D. Z. Yin, L. Ma, J. J. Liu and Q. Y. Zhang, *Energy*, 2014, **64**, 575–581.

227 J. Yang, M. W. Keller, J. S. Moore, S. R. White, N. R. Sottos, J. Yang, M. W. Keller, J. S. Moore, S. R. White and N. R. Sottos, 2008, **41**, 9650–9655.

228 X. Huang and B. Voit, *Polym. Chem.*, 2013, 435–443.

229 A. Soottitantawat, H. Yoshii, T. Furuta, M. Ohkawara and P. Linko, *J. Food Sci.*, 2003, **68**, 2256–2262.

230 A. Gharsallaoui, G. Roudaut, O. Chambin, A. Voilley and R. Saurel, *Food Res. Int.*, 2007, **40**, 1107–1121.

231 Y. W. Luo and X. D. Zhou, *J. Polym. Sci. Part a-Polymer Chem.*, 2004, **42**, 2145–2154.

232 F. Tiarks, K. Landfester and M. Antonietti, *Langmuir*, 2001, **17**, 908–918.

233 U. Paiphansiri, P. Tangboriboonrat and K. Landfester, *Macromol. Biosci.*, 2006, **6**, 33–40.

234 R. H. Utama, M. H. Stenzel and P. B. Zetterlund, *Macromolecules*, 2013, **46**, 2118–2127.

235 F. Gröhn, B. J. Bauer and E. J. Amis, *Macromolecules*, 2001, **34**, 6701–6707.

236 A. P. R. Johnston, C. Cortez, A. S. Angelatos and F. Caruso, *Curr. Opin. Colloid Interface Sci.*, 2006, **11**, 203–209.

237 G. B. Sukhorukov, A. A. Antipov, A. Voigt, E. Donath and H. M̈hwald, *Macromol. Rapid Commun.*, 2001, **22**, 44–46.

238 E. M. Rosenbauer, K. Landfester and A. Musyanovych, *Langmuir*, 2009, **25**, 12084–12091.

239 J. M. Asua, *Prog. Polym. Sci.*, 2002, **27**, 1283–1346.

240 K. Landfester, J. Eisenblätter and R. Rothe, *J. Coatings Technol. Res.*, 2004, **1**, 65–68.

241 P.-H. Theunissen and J.-M. Buchlin, *Sol. Energy*, 1983, **31**, 271–277.

242 A. Sari, C. Alkan, A. Karaipekli and O. Uzun, *Sol. Energy*, 2009, **83**, 1757–1763.

243 K. Tumirah, M. Z. Hussein, Z. Zulkarnain and R. Rafeadah, *Energy*, 2014, **66**, 881–890.

244 M. G. de Cortazar and R. Rodriguez, *J. Appl. Polym. Sci.*, 2013, **127**, 5059–5064.

245 Z. Zheng, J. Jin, G.-K. Xu, J. Zou, U. Wais, A. Beckett, T. Heil, S. Higgins, L. Guan, Y. Wang and D. Shchukin, *ACS Nano*, 2016, **10**, 4695–4703.

246 P. Felix De Castro and D. G. Shchukin, *Chem. - A Eur. J.*, 2015, **21**, 11174–11179.

247 H. Zhang and X. Wang, *Sol. Energy Mater. Sol. Cells*, 2009, **93**, 1366–1376.

248 R. Yang, H. Xu and Y. Zhang, *Sol. Energy Mater. Sol. Cells*, 2003, **80**, 405–416.

249 A. Sari, C. Alkan, A. Biçer, A. Altuntaş and C. Bilgin, *Energy Convers. Manag.*, 2014, **86**, 614–621.

250 G. Fang, Z. Chen and H. Li, *Chem. Eng. J.*, 2010, **163**, 154–159.

251 H. Zhang, X. Wang and D. Wu, *J. Colloid Interface Sci.*, 2010, **343**, 246–255.

252 R. Lal, *Environ. Int.*, 2003, **29**, 437–450.

253 J. Huang, T. Y. Wang, P. P. Zhu and J. B. Xiao, *Thermochim. Acta*, 2013, **557**, 1–6.

254 D. Platte, U. Helbig, R. Houbertz and G. Sextl, *Macromol. Mater. Eng.*, 2013, **298**, 67–77.

255 D. R. Biswas, *Sol. Energy*, 1977, **19**, 99–100.

256 A. E. Fouda, G. J. G. Despault, J. B. Taylor and C. E. Capes, *Sol. Energy*, 1980, **25**, 437–444.

257 M. M. Farid, A. M. Khudhair, S. A. K. Razack and S. Al-Hallaj, *Energy Convers. Manag.*, 2004, **45**, 1597–1615.

258 R. A. Taylor, N. Tsafnat and A. Washer, *Appl. Therm. Eng.*, 2016, **93**, 935–938.

259 D. C. Hyun, N. S. Levinson, U. Jeong and Y. A. Xia, *Angew. Chemie-International Ed.*, 2014, **53**, 3780–3795.

260 W. Su, J. Darkwa and G. Kokogiannakis, *Renew. Sustain. Energy Rev.*, 2015, **48**, 373–391.

261 N. Sarier and E. Onder, *Thermochim. Acta*, 2007, **452**, 149–160.

262 C. Y. Zhao and G. H. Zhang, *Renew. Sustain. Energy Rev.*, 2011, **15**, 3813–3832.

263 F. Salaün, E. Devaux, S. Bourbigot and P. Rumeau, *Carbohydr. Polym.*, 2008, **73**, 231–240.

264 C. Yan, J. H. Resau, J. Hewetson, M. West, W. L. Rill and M. Kende, *J. Control. Release*, 1994, **32**, 231–241.

265 R. Ghaderi, C. Sturesson and J. Carlfors, *Int. J. Pharm.*, 1996, **141**, 205–216.

266 Z. El Bahri and J. L. Taverdet, *Powder Technol.*, 2007, **172**, 30–40.

267 P. Sansdrap and A. J. Moës, *Int. J. Pharm.*, 1993, **98**, 157–164.

268 T. Mateovic, B. Kriznar, M. Bogataj and A. Mrhar, *J. Microencapsul.*, 2002, **19**, 29–36.

269 R. Jeyanthi, R. Mehta, T. BC and P. P. Deluca, *J. Microencapsul.*, 1997, **14**, 163–174.

270 G. Fundueanu, M. Constantin, E. Esposito, R. Cortesi, C. Nastruzzi and E. Menegatti, *Biomaterials*, 2005, **26**, 4337–4347.

271 N. Sarier and E. Onder, *Thermochim. Acta*, 2007, **454**, 90–98.

272 F. Salaün, E. Devaux, S. Bourbigot, P. Rumeau, P. O. Chapuis, S. K. Saha and S. Volz, *Thermochim. Acta*, 2008, **477**, 25–31.

273 T. Wang, J. Huang, P. Zhu and J. Xiao, *Colloid Polym. Sci.*, 2013, **291**, 2463–2468.

274 Y. E. Milián, A. Gutiérrez, M. Grágeda and S. Ushak, *Renew. Sustain. Energy Rev.*, 2017, **73**, 983–999.

275 A. Schoth, K. Landfester and R. Muñoz-Espí, *Langmuir*, 2015, **31**, 3784–3788.

276 J. Zhang, S. S. Wang, S. D. Zhang, Q. H. Tao, L. Pan, Z. Y. Wang, Z. P. Zhang, Y. Lei, S. K. Yang and H. P. Zhao, *J. Phys. Chem. C*, 2011, **115**, 20061–20066.

277 M. Delgado, A. Lázaro, J. Mazo and B. Zalba, *Renew. Sustain. Energy Rev.*, 2012, **16**, 253–273.

278 P. Gimenez-Gavarrell and S. Fereres, *Renew. Energy*, 2017, **107**, 497–507.

2. Results: Solubilising Salt Hydrates in W/O Emulsions

2.1 Introduction

Salt hydrate PCMs have great potential for use in wide scale applications for thermal energy storage and delivery. For practical use, they must be confined to a small volume to improve issues such as supercooling and incongruent melting. To do so, an initial salt hydrate loaded emulsion must be formed. Emulsions are the necessary first step for many encapsulation methods and may be used without further processing for certain applications, although a more robust shell is often added. Other encapsulation methods based on solid particle templates may be used, such as layer-by-layer deposition. However, emulsions require less steps, can be formed on a large scale and can often use cheap reactants. Emulsions are mixtures of a liquid dispersed through another liquid with which it is not miscible or soluble. Emulsions consist of a continuous phase, and a dispersed phase which consists of droplets dispersed through the continuous phase. For a hydrophobic active material, an oil-in-water (O/W) emulsion is required. For a hydrophilic core, a water-in-oil (W/O) emulsion needs to be created. Various types of emulsions are displayed in Fig 2.1. Salt hydrates are hydrophilic and therefore a combination of oil and surfactant suitable for W/O emulsions is required. Our aim was to solubilise as much water within the oil as possible, creating stable emulsions with nanometre sized droplets. Emulsions with submicron droplets are known as mini- or microemulsions, depending on the method of formation. Droplet size determines the size of any capsules which may be subsequently formed, and is influenced by factors such as emulsifier content and stirring rate[1]. For the synthesis of nanocapsules, nanometre sized droplets are a prerequisite. We wanted to use nanomaterials for our PCM systems to achieve the highest possible heat transfer area.

Dispersed emulsion droplets require a stabiliser to solubilise them. Without a stabiliser, the oil and water will separate due to gravitational energy reducing their surface energy according to their relative densities, with the least dense material on top. Surfactants are the classic stabilisers for emulsions. Stabilisers are necessary for long lasting emulsions, which can be stable for months or years. The surfactants are usually soluble in the continuous phase and non- or sparingly soluble in

the dispersed phase[2]. They consist of a hydrophilic head group and a hydrophobic tail, which arrange themselves according to the make-up of the solution. Surfactant stabilised emulsions have applications such as soap and other cleaning products, and enhanced oil recovery[3,4]. Droplets formed by the rearrangement of surfactants are known as micelles for O/W emulsions, and reverse micelles for W/O emulsions (W/O emulsions are also known as 'inverse' emulsions). Surfactants are often selected according to their hydrophile-lipophile balance (HLB), assigned based on the size and number of each of the functional groups present in the surfactant chain[5]. Emulsions can either be a precursor for the addition of a polymer shell material, or can be used as a delivery system itself. Although surfactants are most often used as emulsions stabilisers, it is possible to replace them with solid particles which adsorb onto the interface between the emulsion phases. These systems are known as Pickering emulsions.

Water-in-oil-in-water (W/O/W) emulsions have often been employed as a template for aqueous core capsules[6]. This consists of a W/O emulsion further dispersed in an aqueous phase. W/O/W emulsions have the advantage of being able to introduce incompatible compounds into the same system[7]. They are effective at protecting encapsulated active compounds from degradation catalysed by light[8] and enzymes[9]. Choice of emulsifiers is key in determining droplet size and characteristics of the double emulsion[10], as different surfactants are required to stabilise each of the phases. Jager-Lezer *et al*[11] found that drug release from the W/O/W droplets is achieved *via* a swelling mechanism followed by oil droplet breakdown. The lipophilic surfactant had a profound effect on behaviour, increasing its amount reduced drug release. By altering the amount of lipophilic surfactant present, the rate of release could be controlled, which is highly beneficial for drug delivery systems.

W/O/W emulsions have often been used in conjunction with poly(lactide-co-glycolide) (PLGA) as shell material. The PLGA is preformed and added to the oil phase, which is then solubilised in the external aqueous phase. The organic solvent is then removed by evaporation, leaving PLGA capsules

dispersed in water. PLGA has good biodegradability, low biotoxicity and has good mechanical strength, so is ideal for drug-loaded capsule applications[12]. Desai *et al*[13] investigated how the size of PLGA particles affected their uptake in Caco-2 cells. They found capsules of 100nm had an uptake rate 5.9 x 10^6 greater than particles of 10µm.

W/O/W emulsions suffer from several drawbacks however. They are not thermodynamically stable due to droplet coalescence, and the internal aqueous phase may diffuse into the external aqueous phase[7,10]. Capsules fabricated from a W/O/W template have less core material than those made from W/O emulsions, they are more expensive and require more processing. Further hindering research, the most promising polymer for making subsequent capsules is PLGA, which is very expensive. Stable W/O single emulsions can be formed instead and are more ideal for industrial scale-up, due to the simplicity and minimal processing required.

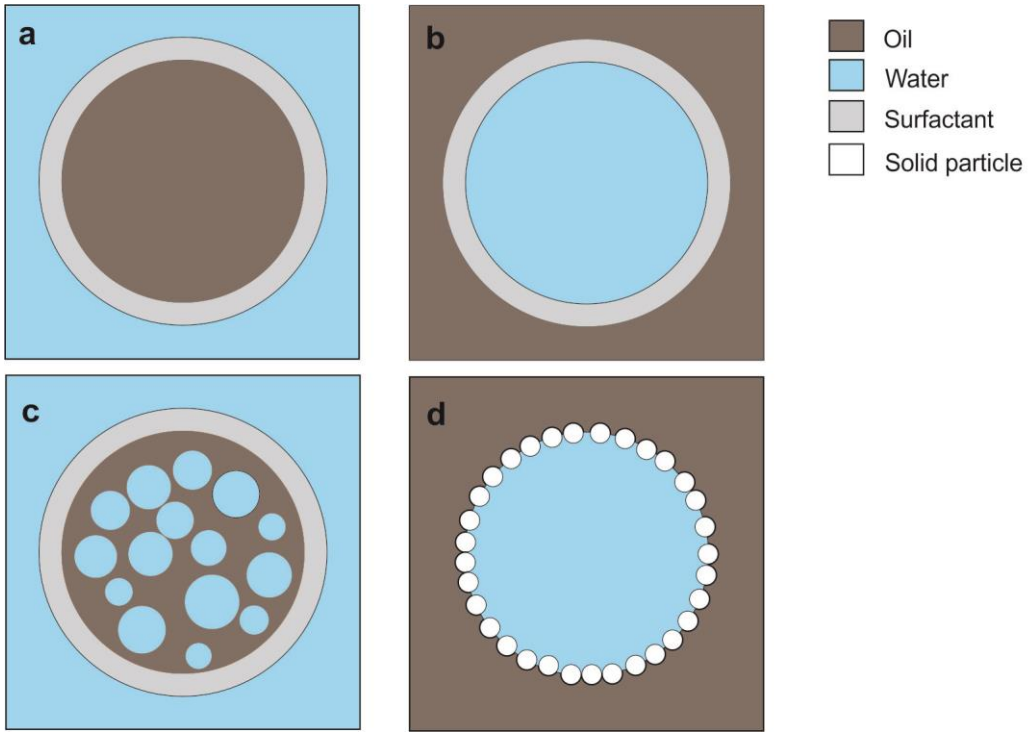

Fig 2.1 Cartoon depicting various types of emulsion droplets, **a** O/W **b** W/O **c** W/O/W **d** W/O Pickering emulsion

Many researchers have investigated how to maximise solubility of the dispersed phase within emulsions. Mini- and microemulsions are of great interest due to the nanometre sized droplets, whereas regular emulsions consist of droplets of micrometre diameters. Mini- and microemulsions differ in two ways: 1. Microemulsions are thermodynamically stable, miniemulsions are kinetically stable 2. Microemulsions are formed spontaneously by low energy methods with droplet sizes usually <100nm, miniemulsions by high energy shearing with droplet size of <300nm[14]. High shear is required by miniemulsions to overcome surface tension effects to force droplets into the nanoscale regimen[2]; microemulsions overcome this by use of a higher concentration of surfactants. Miniemulsions can be formed using high energy methods, such as sonication. Final droplet size is dependent on shearing rate or power, interfacial tension and the viscoelasticity of the emulsion fluid[15]. Miniemulsions are also known as nanoemulsions, with the terms usually being interchangeable[16]. However, some researchers describe nanoemulsions as a miniemulsion with

extremely small droplets <100nm[2]. Such small droplet sizes of mini- and microemulsions mean they avoid coalescence, a common cause of instability in classical emulsions[16].

To gauge the stability of mini- and microemulsions, several methods can be used. When W/O emulsions reach their solubilisation threshold, it may be accompanied by a large increase in electrical conductivity[17,18]. This percolation in conductance can be followed by measurements with a conductivity meter. The easiest method of observing mini-/microemulsion stability however, is simply looking at it by eye. When submicron droplets are formed, the solution will become transparent or translucent, in contrast with a regular emulsion which will be cloudy[19]. The transparency is due to very small particle size[20]. Using high energy input to form miniemulsions is valuable due to the fast speed of processing.

A problem with the use of high energy inputs during the creation of miniemulsions is that it can initiate possible degradation of the entrapped materials[21]. Low energy methods for microemulsion formation, such as the phase inversion temperature (PIT) method are an alternative. PIT is a phenomenon where an agitated O/W emulsion inverts to a W/O emulsion at a specific temperature. This is due to several effects, such as non-ionic surfactants becoming more hydrophilic when heated. Microemulsions are similar to miniemulsions but formed *via* low energy methods. However, these systems are complex and must be formulated using deep knowledge of surfactant chemistry; a large amount of surfactant is required to stabilise them. Due to the low energy methods used to form microemulsions, they are available for industrial scale up[22]. However, using large amount of surfactants proves problematic for processing and environmental reasons[15]. PIT requires good thermal control; although this can be achieved on an industrial scale, it requires large amounts of surfactant and a low solid content to produce nanometre-scale droplets. Increasing solid content of the active material can lead to micron-sized droplets[23], so the size of the subsequently formed capsules is limited to μm.

The usage of surfactants as stabilisers presents some problems. For instance, in the formation of polyurethane (PU), the hydrophilic alcohol monomer and the hydrophobic diisocyanate monomer will react with many polar groups. Side reactions between these monomers and the surfactant may occur, which may inhibit shell formation or weaken the shell[24]. To avoid this, other options may be sought, such as the formation of a Pickering emulsion – an emulsion stabilised by solid particles (often SiO_2) rather than surfactants. However, these are not as stable or flexible as micelles produced by surfactants. Another potential solution is to use 'surfmers', which are polymerizable surfactants used as both emulsifier and monomer. These surfactants are then covalently anchored within the shell, which provides additional strength and prevents permeability[25]. This approach can be particularly useful during high shear processes, as it helps prevent surfactant desorption from emulsion droplets. Surfmers suffer from several drawbacks however. They may need specific synthesis, increasing costs; and highly reactive surfmers will require a higher concentration than regular surfactants in order to stabilise emulsions[26]. We investigated both high energy (UltraTurrax homogenisation, sonication) and low energy (vortex mixing, mechanical stirring) methods, to test which gave stable emulsions. We anticipated the use of high energy input would be beneficial in order to reduce the amount of surfactants required for stabilisation.

Pickering emulsions are named after S.U. Pickering, one of the first scientists to describe them[27], and are stabilised by solid particles rather than surfactants. They can be O/W or W/O depending on wettability of the particles. Colloidal silica is the typical solid emulsifier chosen, however many other particles can be used[28]. Wettability is a key property of the solid stabiliser; for hydrophobic particles such as suitably treated silica, the contact angle is usually >90° and results in a W/O emulsion. For hydrophilic particles such as metal oxides, the contact angle is usually <90° and results in the formation of a O/W emulsion[29]. Although Pickering emulsions have been employed more rarely than conventional emulsions, researchers have found potential applications for them. Pickering emulsions avoid the drawbacks of using surfactants, such as irritancy or cytotoxicity found in some drug delivery systems[28]. Frelichowska *et al*[30] found that drug release from a Pickering emulsion was

slower compared with a conventional emulsion. A full coverage of the emulsion droplets with the stabilising solid particles is crucial or leakage will occur. Pickering emulsions can also be used as a template for polymerisation reactions[31–33].

In the context of PCMs, the inorganic solid stabilisers inherent in Pickering emulsions are attractive for their increased heat transfer. They have superior thermal conductivity in comparison with polymers. Despite their positive attributes, Pickering emulsions suffer from some drawbacks which will prevent their use with PCMs. First is that inorganic stabilisers are brittle, unlike their polymeric counterparts. During thermal cycling, PCMs undergo many phase changes, with volume increase during melting and decrease during solidification. This requires a flexible shell material; a Pickering shell may become fractured. Pickering emulsions are also susceptible to destabilisation caused by pH changes. Midmore[34] found that after addition of either strong acid or strong base, flocculation occurred in the emulsion. This was caused by acid/alkali catalysed cleavage of surface siloxane groups. Nanosized droplets are also difficult to form with Pickering emulsions, often droplet size is in the range of micrometres[28]. For the research presented in this thesis, we chose to use polymeric surfactants as emulsifiers due to their low cost and effective stabilisation.

Many researchers have investigated 'PCM emulsions', which are PCMs solubilised within the core of the dispersed emulsion droplets[35]. PCM emulsions have been of interest due to the simple one step procedure, without the need for further reactions such as polymerisation. Due to their fluid state and heat capacity greater than water, they are a good candidate as a HTF for a latent heat storage system[36]. Additional sensible heat can also be stored by the continuous phase[37]. PCM emulsion systems have been exclusively used with organic PCMs. A key property of phase change slurries (including both PCM emulsions and PCM microcapsule slurries) is the supercooling. According to nucleation theory, smaller volumes of material have a higher degree of supercooling[38], as there is a lower probability of any nucleating material required to start crystallisation being present[35]. Although supercooling may be increased by decreasing particle size, other factors must be

considered. Nucleation is a random process, so supercooling is difficult to predict. In a miniemulsion, each droplet requires a nucleation site, making simultaneous nucleation for the whole sample more difficult[39]. Huang *et al*[40,41] published two articles on PCM supercooling in emulsions. They found an increase in supercooling for PCM emulsions compared to the bulk material. The authors suggest that as the PCMs solidify in one emulsion droplet, the release of latent heat prevents nucleation at other sites due to the increase in local temperature. It was also noted that supercooling was altered with the use of different surfactants, due to the interaction of the surfactants with the PCM. Several researchers have made PCM nanocapsules without an increase in the supercooling however. Decreasing the droplet size can also have positive effects. Felix *et al*[42] showed that decreasing particle size has a profound effect on the core material, due to the confined volume and the increased heat transfer. Smaller capsules had larger latent heat due to the increase in heat flow to the core – PCM in the core therefore melted more uniformly and quickly. The confined volume also produced more distinct phases of the PCM.

It is also possible that differential scanning calorimetry (DSC) measurements give overstated supercooling values for some encapsulated PCM samples in the literature. As only small sample sizes are used, supercooling may increase. Due to low thermal conductivity of PCMs, sample temperatures will often not be uniform, potentially leading to inaccurate measurements. Investigating the thermal properties of the same material on a larger scale may demonstrate different properties. This is a factor that must be considered when determining the degree of supercooling. Heating rate also affects the T_M, so potential commercial PCMs should be tested at heating rates that replicate the application. DSC using the T-history method can be applied for bulk samples. Samples for this method are around 1000 times larger than regular DSC samples, which are around 5-10mg. T-history is therefore better placed to demonstrate bulk properties, although it is not as precise as regular DSC[43]. For T-history, a large amount of PCM is placed in a sample holder with a thermocouple placed in the centre of the sample. As the sample undergoes thermal cycling,

sample temperature is measured as a function of time. Combining the two types of measurement can be highly beneficial[44].

As the degree of supercooling in crystallohydrates is already very high, we anticipate that confining them to a small volume will be beneficial. The increased heat transfer, coupled with the higher thermal conductivity of inorganic PCMs in comparison with paraffins, should mean supercooling is reduced. As the crystallohydrate composition is confined, crystallisation may occur more freely. In addition to higher heat transfer, smaller droplets also have the added benefit of reducing the incidence of clogging any systems the PCMs may be used in. Zou and collaborators[45] designed a phase change emulsion with a working temperature of 80-90°C for use in domestic water heating systems. They used small droplet sizes to avoid agglomeration and therefore prevent any clogging. They also found that increasing the concentration from 20 %wt to 30 %wt of PCM, more agglomeration occurred, increasing viscosity which required increased pumping power. The system made less energy savings at 30 %wt compared to 20 %wt PCM due to this effect. Adding more PCM to increase latent heat capacity leads to increased viscosity and potential clogging.

Metal nanoparticles have been formed from or encapsulated in miniemulsions in several studies, and find use in applications such as heterogeneous catalysis, electrochemistry and sensing[46,47]. Bonnet *et al*[7] made W/O/W emulsions containing magnesium ions in order to treat magnesium deficiency, showing the emulsions were fairly stable. Yin *et al*[48] created bimetallic PdAu nanoparticles using oleic acid and oleylamine as surfactants. The average particle size was 7.4nm, achieving good monodispersity. Metal-containing compounds can also be synthesised or encapsulated in emulsion droplets. Winkelmann and collaborators[49] solubilised iron chloride within reverse micelles. The addition of hydroxide ions leads to iron oxide formation within the droplet cores, which could be precipitated as a nanosuspension once the water was removed by distillation. Zhao and collaborators[50] synthesised ZIF-8 metal organic framework nanocrystals within reverse micelle droplets. They found that by adjusting the initial inverse miniemulsion parameters, such as

changing concentration of reactants, crystal size could be tuned. The ZIF-8 crystals were shown to be useful for catalytic applications. From these studies, it is clear that W/O emulsions can solubilise metal salts, including salt hydrates[51].

2.2 Results - Microemulsions

O/W emulsions are well understood and simpler to formulate than W/O emulsions. For an O/W emulsion, the continuous phase will always be water. For a W/O emulsion, a vast number of oils may be used as continuous phase. Coupled with the need to select suitable surfactants, there are essentially infinite combinations to choose from. Optimisation of W/O emulsions is subsequently very time consuming. We chose surfactants based on numerous studies which had either looked at optimising the water solubilisation capacity of W/O emulsions, or had been used as a precursor to form polymer capsules.

The first surfactant we investigated to encapsulate salt hydrates was dioctyl sulfosuccinate sodium salt, more commonly known as Aerosol OT (AOT). The molecular structure of AOT and various other surfactants we used are shown in Fig 2.2. AOT has often been used in the creation of W/O emulsions. Hopwood and Mann[52] used AOT emulsions to prepare barium sulphate nanoparticles and nanofilaments, finding that AOT was more effective than other surfactants for filament formation.

Several researchers have found that adding an additional surfactant provides a synergistic effect in AOT W/O emulsions. Gonzalez-Blanco *et al*[53] probed the formation of AOT based W/O microemulsions with FTIR spectroscopy, finding the addition of poly(sodium styrene sulfonate) (PSS) or poly(vinylpyrrolidone) (PVP) even at low concentrations prevented aggregation of the reverse micelles in the W/O emulsion. When using solely AOT as surfactant, the reverse micelles displayed aggregation. Paul and collaborators[17,18,54,55] made multiple studies on AOT reverse micelles. They investigated both the influence of co-surfactants and oils of different properties used as the continuous phase on the resulting emulsions. They based their studies on the work of Shah *et al* in 1987[56–58], who made numerous observations on the formation of reverse micellar systems. They concluded the solubilisation of water in W/O microemulsions is determined by the curvature and elasticity of the interface, along with the total interfacial area. When the interfacial area is constant, solubilisation is proportional with droplet radii. Maximum solubilisation is achieved with optimal

interfacial curvature and elasticity values, which results in minimisation of bending stress and attractive force of the interface. Other factors contribute to the solubilisation of water within oil, including surfactant concentration, aqueous phase:oil phase ratio and type of oil. In a large study on W/O reverse micelles, Paul *et al*[17] found that cyclohexane was an excellent oil to use for W/O emulsions due to the high solubilisation capacity for water. Factors affecting the solubilisation capacity of specific oils include the oil's molar volume, polarity, viscosity and molecular structure.

We tested the solubilisation capacity of AOT solutions in both toluene and cyclohexane, and found cyclohexane was far more effective. The aqueous dispersed phase (pure water) was simply added to the AOT solution and vortexed. The weight percentage of AOT in the oil phase was varied. Solubilisation capacity is measured by recording the amount of aqueous phase added that results in a permanent turbidity *i.e.* no further water can be solubilised. Results are shown in Table 2.1. At 5 %wt concentration, both oils solubilise a similar amount of water (0.2 and 0.3mL). At increased concentrations, cyclohexane has almost doubled solubilisation capacity. At 40 %wt, toluene solubilised 2.4mL of water, whilst cyclohexane solubilised 3.8mL. An interesting effect is that doubling the weight percentage of AOT more than doubles the amount of water solubilised. This can be rationalised as increasing the amount of surfactants decreases interfacial tension, which in turn decreases Gibbs free energy and makes microemulsion formation more favourable, according to the equation:

$$\Delta G_F = \lambda \Delta A - T\Delta S_F$$

Eq. 2.1 Gibbs free energy of emulsion formation

Where ΔG_F is free energy of emulsion formation, λ is surface tension, ΔA is surface area gained during emulsification, T is temperature and ΔS_F is the entropy of emulsion formation.

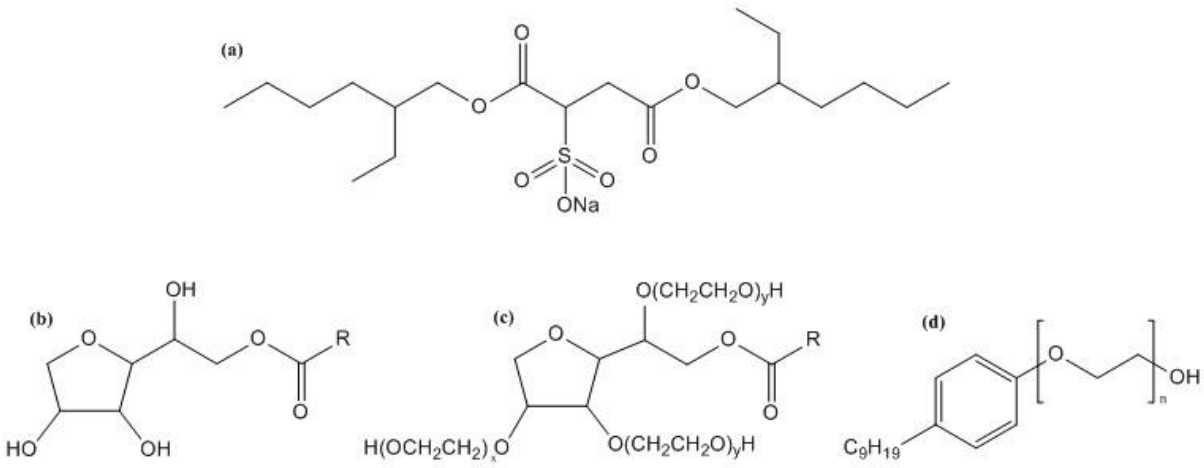

Fig 2.2 Molecular structure of various surfactants: **(a)** AOT, **(b)** Span (sorbitan esters), **(c)** Tween (polyethoxylated sorbitan esters) and **(d)** Igepal CO520

Table 2.1 Solubilisation capacity of different concentrations of AOT surfactant solutions (10g) in toluene and cyclohexane

[AOT] (%wt)	H_2O solubilised (toluene, mL)	H_2O solubilised (cyclohexane, mL)
5	0.2	0.3
10	0.4	0.7
20	1	1.6
40	2.4	3.8

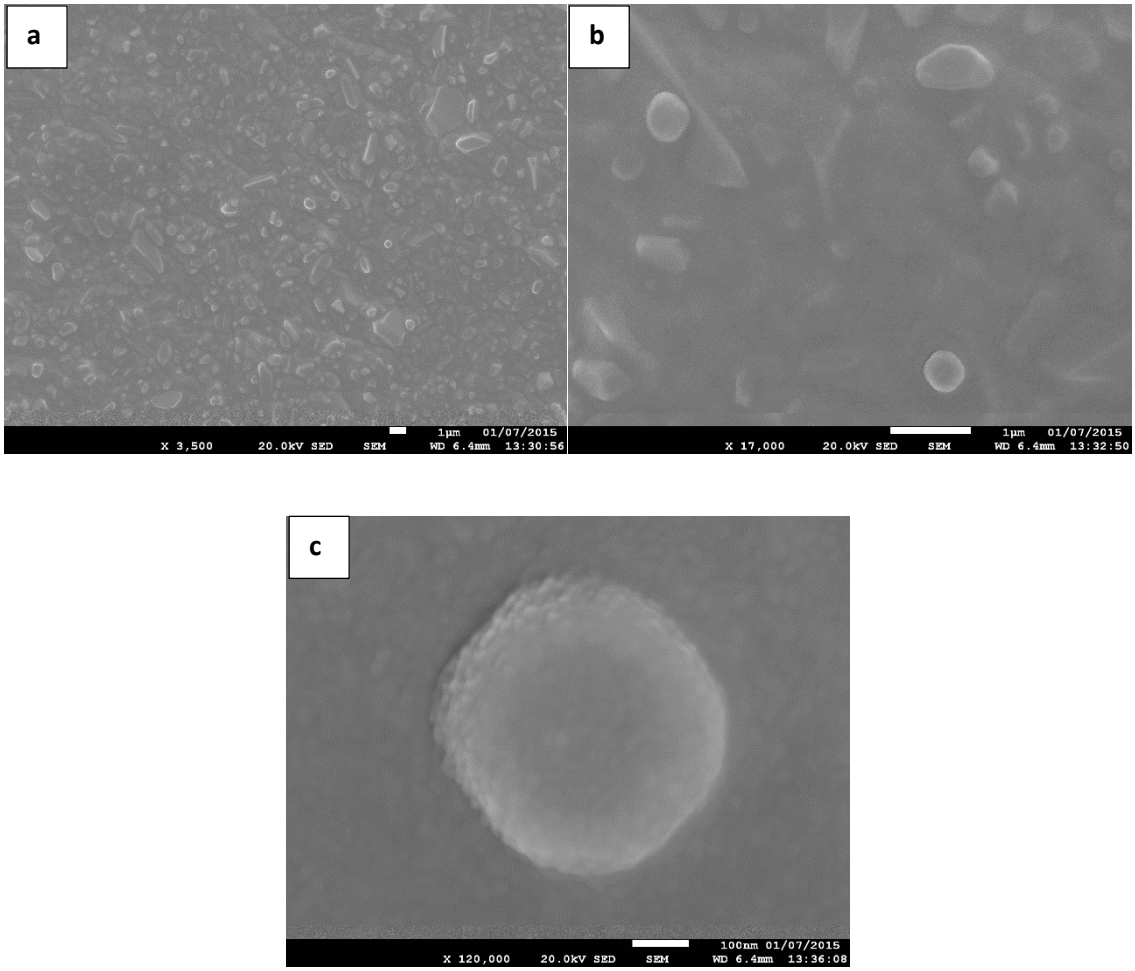

Fig 2.3 SEM micrographs of AOT microemulsions containing $Mg(NO_3)_2.6H_2O$. Scale bar for **(a)** and **(b)** is 1µm, for **(c)** is 100nm

It was also possible to produce AOT microemulsions containing salt hydrate. SEM images are shown in Fig. 2.3. Some reverse micelles can be observed, although they are much larger than results expected from literature: they are approximately 500nm in size, whereas according to the literature they should be <200nm[59]. This is due to swelling of the reverse micelles. It is also clear that the AOT shell is not strong enough to withstand the SEM high vacuum fully; most microemulsion droplets have collapsed, seen in Fig. 2.3a. In the close-up view of a reverse micelle in Fig. 2.3c, a rough surface can be observed. The difficulty of isolation means these PCM emulsions are difficult to fully analyse.

To test the synergistic effect of adding a cosurfactant to AOT, we used commercial surfactants Tween 80 (PEG sorbitan monooleate) and Igepal CO520 (nonyl phenol ethoxylate). They were added at the %wt that would give the maximum solubilisation capacity, according to Paul *et al*[17]. The ratio of surfactants used was 95:5 for AOT:Tween 80 and 60:40 for AOT:Igepal CO520. The overall %wt of surfactants in the continuous phase was 10%. Oil used was cyclohexane (90 %wt of continuous phase). As can be seen from Table 2.2, both cosurfactants lead to an increase in solubilisation capacity compared to only using AOT. Using only AOT at 10 %wt, 0.7mL of water was solubilised. With the addition of Tween 80 and Igepal CO520, this was increased to 0.8 and 1.1mL, respectively.

Commercially produced surfactants are widely used and cheap. Nonionic Tween and Span surfactants are amongst the most common. Nonionic surfactants have advantages over ionic surfactants, for example higher stability, lower reactivity and compatibility with more materials. Many researchers have combined Tweens and Spans, changing the HLB ratio to maximise solubilisation of oils or water. Span is the brand name of sorbitan esters, while a Tween is a polyethoxylated sorbitan ester i.e. a polyethoxylated Span. Their structures are shown in Fig. 2.2. The HLB value for Spans decreases with increasing esterification, giving better lipophilic solubility. Tweens are hydrophilic; increasing the degree of ethoxylation increases aqueous solubility.

Table 2.2 Amount of H_2O solubilised by solutions of AOT blended with cosurfactants (10g)

Surfactant Combination (total 10 %wt of continuous phase)	H_2O solubilised (mL)
95 %wt AOT, 5 %wt Tween 80	0.8
60 %wt AOT, 40 %wt Igepal CO520	1.1

We initially wanted to solubilise pure salt hydrate i.e. with no additional water added. We anticipated confining the crystallohydrate to the small volume in the emulsion droplets would allow it to maintain its hydration level, while using 100 %wt of the crystallohydrate as aqueous phase would maximise latent heat. To do this, we used a continuous phase of 60 %wt of a blend of 3:2 Tween:Span, with 40% toluene as oil. This continuous phase had been used by Kafka *et al*[60] who had used their emulsions to fabricate poly(ethyl-2-cyanoacrylate) (PECA) nanocapsules. To the continuous phase, we added salt hydrate and stirred overnight to yield a W/O microemulsion.

Initially we chose crystallohydrates with relatively high T_Ms in to make handling easier, as they will be solid at room temperature. Magnesium nitrate hexahydrate ($Mg(NO_3)_2.6H_2O$) and aluminium sulphate octadecahydrate ($Al_2(SO_4)_3.18H_2O$), which have T_Ms of 89 and 86°C respectively, were chosen. These PCMs also do not release any hazardous by-products upon dissolution, unlike other crystallohydrates. For instance, sodium sulphide nonahydrate ($Na_2S.9H_2O$) releases poisonous hydrogen sulphide, and this hinders its practical use. The T_M of around 90°C can be useful for domestic applications such as solar cooking. Domanski *et al*[61] investigated $Mg(NO_3)_2.6H_2O$ for this purpose, and found it was far more effective than a corresponding organic PCM, stearic acid. It was also beneficial to use our chosen PCMs as they have stable lower hydrated structures, meaning some heat storage capacity may be maintained even if they partially dehydrate during emulsification/polymerisation. This effect was observed by Huang *et al*[62], who found that upon encapsulation, $Na_2HPO_4.12H_2O$ was dehydrated to $Na_2HPO_4.7H_2O$ but still had good heat storage

capacity. We found that $Mg(NO_3)_2.6H_2O$ formed stable W/O emulsions with 60 %wt of a 3:2 blend of Tween:Span surfactants in toluene, simply by magnetically stirring. Even when solid $Mg(NO_3)_2.6H_2O$ was added, after stirring overnight it had 'melted' into the solution. On the other hand, $Al_2(SO_4)_3.18H_2O$ formed a precipitate without being emulsified.

Later, to study the universality of our methodology, we selected other salt hydrates to encapsulate. We chose PCMs with a T_M close to room temperature, which can potentially be used for passive air conditioning applications and therefore can be combined into thermally-regulating paints. Sodium sulphate decahydrate ($Na_2SO_4.10H_2O$) and calcium chloride hexahydrate ($CaCl_2.6H_2O$) were chosen, which have T_Ms of 32 and 30°C respectively. These are possibly the two most researched salt hydrates for thermal energy storage. We mainly used $Na_2SO_4.10H_2O$ for making emulsions, because it was compatible with $Mg(NO_3)_2.6H_2O$ to form crystallohydrate mixtures, while $CaCl_2.6H_2O$ was not as useful for this purpose (please see Chapter 3 for eutectics for PECA nanocapsules). $CaCl_2.6H_2O$ also may react with atmospheric CO_2 to form calcium carbonate. As shown by the results with AOT above, vortexing the solutions for a brief period is sufficient to prepare microemulsions containing a small amount of water. However, overnight magnetic stirring is required to solubilise crystallohydrates, especially as we wanted to solubilise a maximum amount.

Observations of the attempts to form microemulsions by magnetic stirring are shown in Table 2.3. $Mg(NO_3)_2.6H_2O$ was the only salt hydrate used that could form miniemulsions using this method. The other three selected crystallohydrates didn't solubilise into an emulsion, remaining as a separate solid phase in the form of a crystalline precipitate. Using 70 %wt $Mg(NO_3)_2.6H_2O$ and 30% water as aqueous phase gave a cloudy emulsion, whilst using 100 %wt led to a translucent emulsion. The cloudy effect is caused by the excess water saturating the emulsion, leading to some larger droplets. The emulsions also took on an orange/yellow colour due to the large amount of surfactants used (Tweens and Spans are viscous orange liquids at room temperature).

Table 2.3 Observations of PCM microemulsions prepared by mechanical stirring

		Continuous Phase (3:2 Tween:Span in toluene) (9g)		
		60 %wt surfactants	**40 %wt surfactants**	**20 %wt surfactants**
Aqueous Phase (1g)	*100 %wt $Na_2SO_4.10H_2O$*	Precipitate	n/a	n/a
	100 %wt $CaCl_2.6H_2O$	Precipitate	n/a	n/a
	100 %wt $Al_2(SO_4)_3.18H_2O$	Precipitate	n/a	n/a
	70 %wt $Mg(NO_3)_2.6H_2O$	Cloudy, no precipitate	n/a	n/a
	100 %wt $Mg(NO_3)_2.6H_2O$	translucent	Precipitate	Precipitate

Using this method, it was only possible to produce stable microemulsions with $Mg(NO_3)_2.6H_2O$ using 60 %wt surfactants with toluene as oil. Due to decreased surfactant solubility compared to toluene, cyclohexane was not suitable for the continuous phase. The lack of possible salt hydrates that can be solubilised by this method is a disadvantage, as the range of possible T_Ms is limited. The large amount of surfactants required is also a disadvantage, as previously described. We then opted for high energy methods to produce miniemulsions, as they give droplets of similar size and monodispersity to microemulsions. Miniemulsions require far fewer surfactants to stabilise, as the high energy input utilised in their formation overcomes the interfacial energy of the system. For a microemulsion, as there is no high energy input applied to the system, interfacial tension must be reduced by using extra surfactants.

2.3 Creating miniemulsions *via* high energy processes

To reduce the amount of surfactants required to stabilise emulsions, high energy equipment is needed. Reducing the volume of surfactants is beneficial as it reduces costs and prevents side reactions that may occur with surfactant functional groups. High energy processing on an industrial scale can be costly, but will produce miniemulsions quickly and with a high degree of monodispersity.

Lab scale homogenisers are useful for producing emulsions. In general, the higher the speed of homogenisation, the smaller the capsules produced. However, this conventional method of forming emulsions is not sufficiently powerful enough to obtain nanometre sized droplets. Nanodroplets lead to nanocapsules with improved structural strength, thermal transfer, reduced sedimentation and better thermal stability[63]. We initially used an Ultraturrax homogeniser to produce miniemulsions. After homogenisation, the resulting emulsions were cloudy, showing a stable miniemulsion had not been formed. Clearly, not enough power is delivered to overcome the interfacial tension effects. High pressure homogenisers, available for industrial applications, are more effective in reducing droplet size.

Sonicators deliver far more power than regular homogenisers, and are key in producing nanosized emulsion droplets. They are readily available and inexpensive for laboratory scale applications. Badnore *et al*[64] compared the synthesis of $CaCO_3$ nanoparticles using both conventional and sonochemical methods. Conventional synthesis gave nanoparticles 10-150nm in size with an 80% yield, while the sonochemical synthesis gave uniform 20nm particles and a 98% yield. This demonstrates the consistency sonication gives in producing small particle sizes, and increases yields without the need for extreme conditions. Reactions are driven with energy provided by ultrasonic cavitation.

Table 2.4 Observations of miniemulsions formed by sonication

		Continuous Phase (3:2 Tween 80:Span 80 in cyclohexane) (9g)		
		20 %wt surfs	**10 %wt surfs**	**5 %wt surfs**
Aqueous Phase (1g)	*70 %wt $Mg(NO_3)_2.6H_2O$*	Transparent	Transparent	Translucent
	20 %wt $Mg(NO_3)_2.6H_2O$	n/a	n/a	Translucent, cloudy
	20 %wt $Na_2SO_4.10H_2O$	n/a	n/a	Translucent, cloudy

Miniemulsions prepared with ultrasound are described in Table 2.4. Like with microemulsions, transparent solutions were desired after emulsification. The weight volume of surfactants in the aqueous phase was reduced compared to the microemulsions, where 60 %wt surfactants were required to stabilise. Starting with 20 %wt surfactants in the continuous phase and using 70 %wt $Mg(NO_3)_2.6H_2O$ in the aqueous phase, after only 5 minutes of sonication (1/2" tip, 50% amp., 30s on 10s off pulse regimen) a transparent emulsion was formed. It was possible to form stable miniemulsions down to 5 %wt surfactants. Miniemulsions prepared in the same way using 20 %wt $Mg(NO_3)_2.6H_2O$ and 20 %wt $Na_2SO_4.10H_2O$ were stable with no precipitate present, but were cloudier due to the additional water in the mixture. The miniemulsions formed were colourless due to the low volume of surfactants, in contrast to the orange/yellow microemulsions produced using 60 %wt surfactants.

The basic method was as follows – a crude macroemulsion was formed by stirring briskly for 30 min, which was very cloudy as the aqueous phase had not been fully solubilised and the emulsion contained large droplet sizes. After sonication, the miniemulsions became transparent or translucent, allowing light to pass through. Miniemulsions with 10 and 5 %wt surfactants in the continuous phase were prepared by 10 min of sonication (1/2" tip, 50% amp., 30s on 10s off pulse

regime). Other Tween and Span surfactants (e.g. Tween 20 and Span 20) gave similar results. We also found a blend of 5 %wt 2:1 Span 85:polyethylene glycol dioleate (PEGDO), used by Saihi *et al*[65] was effective at miniemulsion stabilisation.

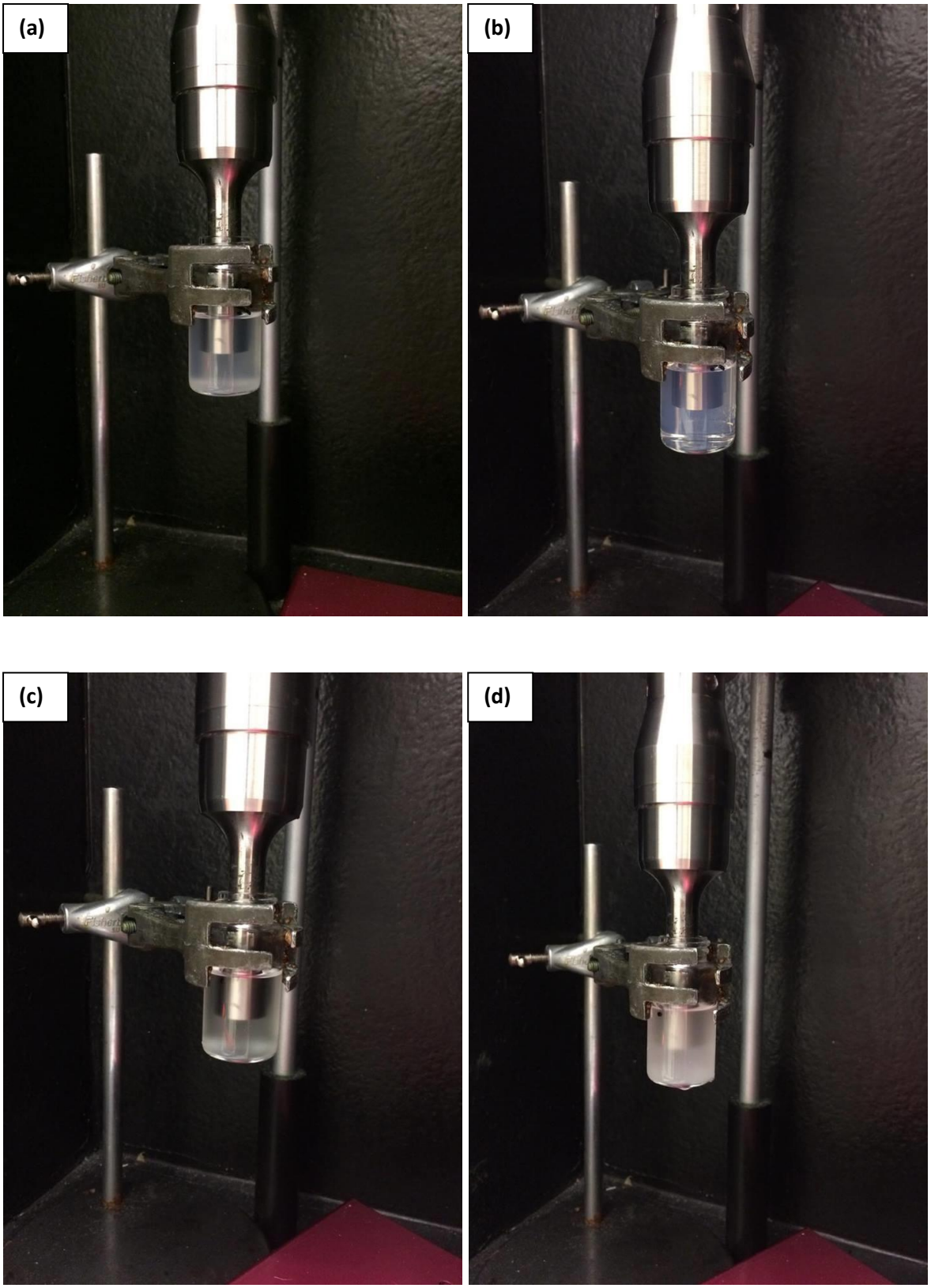

Fig 2.4 Miniemulsions before and after sonication with **(a)** and **(b)** 5 %wt surfactants; **(c)** and **(d)** 1 %wt surfactants with 70 %wt $Mg(NO_3)_2.6H_2O$ as aqueous phase

The effects of sonication on emulsification are shown by the photographs in Fig 2.4. Photographs on the left (Fig 2.4a and c) show sedimentation of the emulsions prior to emulsification, with the aqueous phase at the bottom of the vial due to density differences. After sonication, a homogeneous mixture is formed (Fig 2.4b and d). Using 5 %wt surfactants, the resulting miniemulsion was transparent with a blue tint (Fig 2.4b), showing the miniemulsion was stable against agglomeration. Reducing surfactants to 1 %wt of the continuous phase led to a cloudier miniemulsion (Fig 2.4d), as the aqueous phase is not fully solubilised.

Not only do these results show stable miniemulsions can be formed with a low concentration of surfactants, it was also possible to solubilise multiple crystallohydrates. It was not possible to solubilise pure 100 %wt $Mg(NO_3)_2.6H_2O$ in miniemulsions, however, unlike the microemulsion method. From results seen in Chapter 3 (PECA capsules), this was not a problem as additional water in the aqueous phase was proven crucial for improved phase change properties of the PCM during thermal cycling.

An interesting feature to note is that emulsions containing a large amount of the salt hydrates and a lower amount of water were more transparent. This is due to the salt hydrate acting as a 'superlipophobe', which stabilises the W/O emulsion[66]. Salts such as NaCl have been observed to increase water solubilisation in certain oils and surfactants due to this effect[17].

FTIR spectra for several emulsions are displayed in Fig 2.5. Span 80 and Tween 80 have similar spectra, with an O-H peak for the alcohol groups at 3391 and 3499cm^{-1}, 2 bands for C-H in the peaks at 2852-2923cm^{-1}, O-H in-plane bending at 1373 and 1348cm^{-1} and C-O peaks for esters at 1170 and 1083 for Span and 1247 and 1093 for Tween. $Mg(NO_3)_2.6H_2O$ has characteristic peaks for O–H stretching at 3356 cm^{-1},N=O bending at 1646 cm^{-1}, a mixture of N–O stretching and bending and N=O stretch in the broad peak at 1365 cm^{-1}, plus a sharp peak at 819 cm^{-1} for NO_3^-.

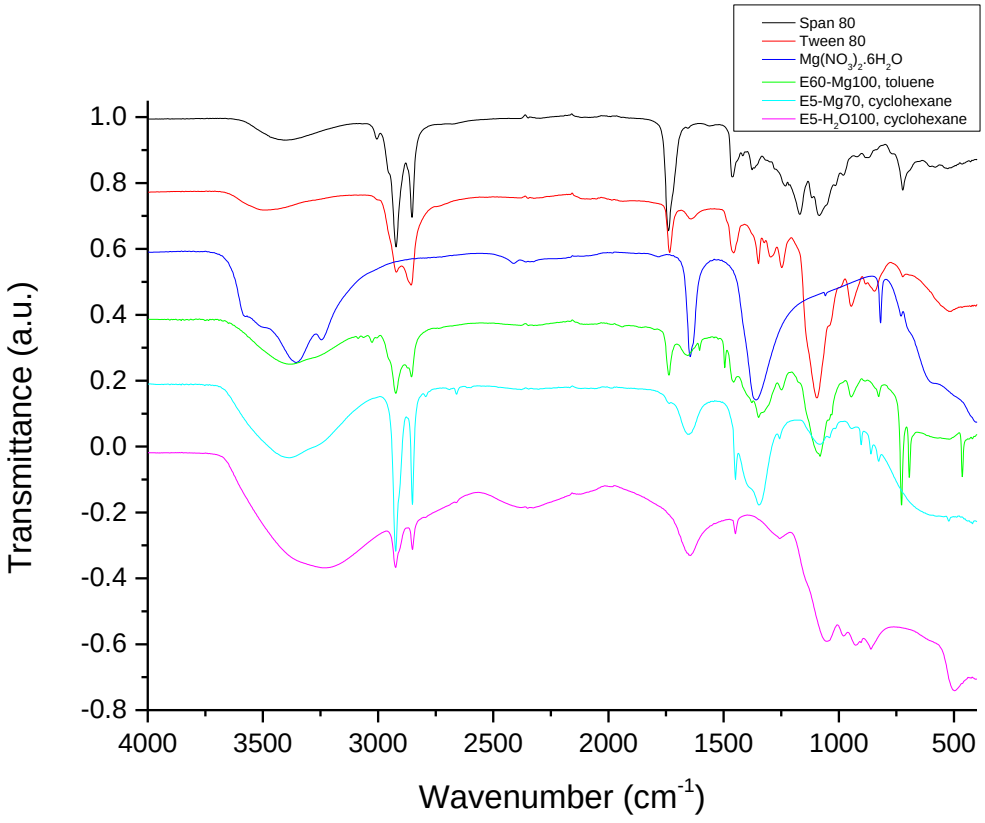

Fig 2.5 FTIR spectra for surfactant, salt hydrate and emulsion samples

Emulsions analysed were 60 %wt 3:2 Tween 80:Span 80 in toluene, with 100 %wt $Mg(NO_3)_2.6H_2O$ as aqueous phase (E60-Mg100, toluene), 5 %wt Tween 80:Span 80 in cyclohexane with 70 %wt $Mg(NO_3)_2.6H_2O$ (E5-Mg70, cyclohexane) and 100 %wt water (E5-H_2O100, cyclohexane) as aqueous phases. These emulsions contained all peaks attributed to Tween and Span. A key indication that $Mg(NO_3)_2.6H_2O$ had been solubilised was the peak at 827cm^{-1} for NO_3^-. It was present in the emulsions containing $Mg(NO_3)_2.6H_2O$, but absent from the emulsion containing only H_2O as aqueous phase. E60-Mg100, toluene also contained a peak at 693cm^{-1} corresponding to C-H bending and ring puckering of the toluene.

As PCM emulsion droplets are not stable enough to be isolated, they must be used in the form of a PCM slurry, i.e. the emulsion droplets dispersed through a liquid. Several mechanisms can contribute to emulsion destabilisation, such as creaming, flocculation, Ostwald ripening and phase inversion. It

is possible to prepare highly stable emulsions which avoid these problems, but most emulsions will separate. This is a serious problem for any practical applications of PCM emulsions. PCM slurries are used as both heat transfer fluid and energy storage material, making them highly beneficial. PCM slurries must be able to be pumped round a system, producing stress on the material. Therefore, strong materials are required to withstand any shell damage that may occur. Because of this, we wanted to add extra protection to our PCM emulsions, by fabricating a polymer shell around the droplets. PCM capsules can also be employed as a PCM slurry for heat transfer.

The additional shell material improves stability and allows isolation of the PCM capsules, which can then be characterised more easily. PCM capsules are also more versatile; they can be used in their isolated form, or as a slurry. We decided to make nanocapsules based on the initial miniemulsions we prepared. Numerous studies have shown microcapsules display lower structural stability than nanocapsules, especially when used in slurries which require pumping. Yamagishi *et al*[67] found that approximately 90% of capsules with an average diameter of 1000μm were broken after 500 thermal cycles. In contrast, 0% of capsules with an average diameter of 5μm were broken after 8000 thermal cycles. This clearly demonstrates the additional stability smaller capsules bring.

Our findings that we could form stable sub-micron emulsions containing salt hydrates were promising as a precursor for nanocapsule formation. Suitable polymerisation methods were then sought to form an additional shell. Any capsules formed using these emulsions as a template would necessarily contain crystallohydrate as core material. Polymerisations based on miniemulsions, such as *in situ* and interfacial polymerisations were researched. Once crystallohydrates are successfully encapsulated and the capsules isolated, thermal properties of the material can be measured. First attempts at encapsulation were made using methyl methacrylate (MMA) as monomer for the shell.

2.4 Attempts using poly(methyl methacrylate) as capsule shell material

Poly(methyl methacrylate) (PMMA) is a widely used polymer for shell material in micro- and nanocapsules. As it is a soft polymer, it is ideally suited to resist the volume changes of PCMs during melting. First attempts at making PMMA capsules crosslinked with ethyl acrylate (EA) containing crystallohydrates were based on the suspension polymerisation method of Huang *et al*[62,68]. They used Span as emulsifier with high energy input from an ultrasonic homogeniser. Despite washing the monomers with sodium hydroxide solution to remove any inhibitors present and using benzoyl peroxide as catalyst, we had trouble initiating the reaction. In later attempts, ultrasonic energy was used to attempt to initiate the reaction, a technique which has been used to prepare PMMA from O/W emulsions[69].

After the reaction was complete, the mixture was left to dry in a fume hood overnight. After evaporation of liquid, a white powder was left. As can be seen from FTIR spectra shown in Fig 2.6, this powder consisted of $Na_2SO_4.10H_2O$ only, no PMMA had formed. As the MMA and EA were left unreacted, they were still liquid and free to evaporate. It was clear the MMA/EA crosslinking reaction had not occurred.

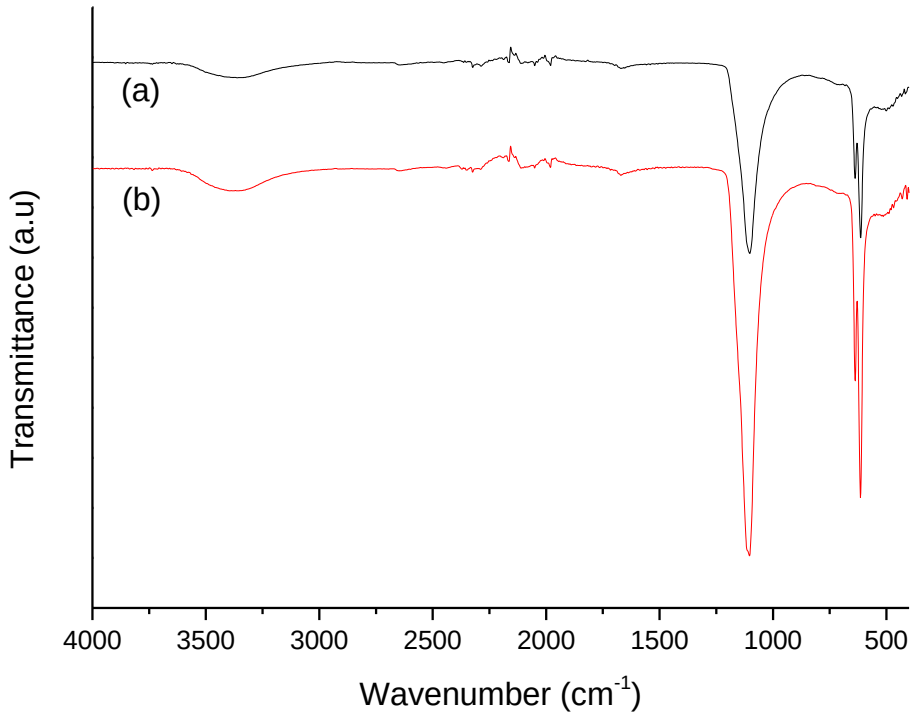

Fig 2.6 FTIR spectra of **(a)** $Na_2SO_4.10H_2O$ and **(b)** suspension polymerisation product

The precipitation of preformed polymers onto emulsion droplets is an alternative technique to emulsion polymerisations. It involves dissolving the polymer in a volatile solvent, and adding to an emulsion with a non-volatile continuous phase. During mechanical stirring, evaporation of the volatile solvent leads to polymer precipitation at the oil/water interface. It is a simple method, and can guarantee desirable polymer characteristics such as molecular weight. Paiphansiri and collaborators[70] used this technique to produce PMMA nanocapsules containing an antiseptic agent. We used their method to try to encapsulate crystallohydrates.

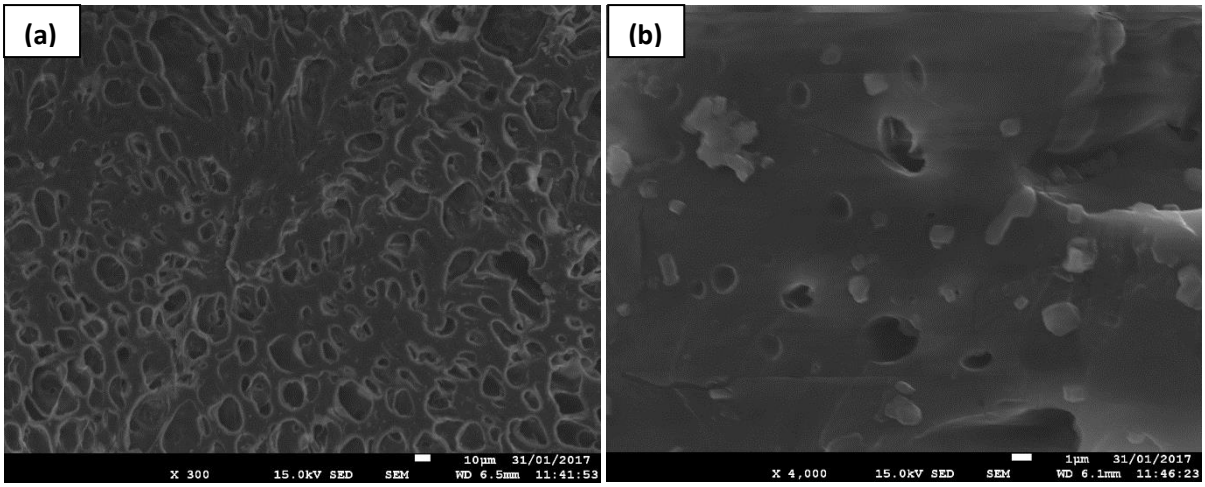

Fig 2.7 SEM images of attempts at PMMA nanoprecipitation at **(a)** x300 magnification (scale bar 10µm) **(b)** x4000 magnification (scale bar 1µm)

Upon evaporation of the chloroform, the PMMA coagulated into a solid block which was extremely rubbery. SEM images of the material are shown in Fig 2.7. As can be seen, the solid is a porous material, but no capsules have been formed. The pores are 1-50µm in size. In Fig. 2.7b, when zoomed into to x4000 magnification, small particles 0.1-2µm in size can be seen. These are particles of $Mg(NO_3)_2.6H_2O$ that have adsorbed to the surface.

A final attempt to use PMMA was made by 'inverting' the method of Zhang *et al*[71], who used PMMA to encapsulate octadecane. Octadecane was first emulsified in water by sonication, employing sodium dodecyl sulphate as surfactant. We made a W/O miniemulsion containing $Mg(NO_3)_2.6H_2O$ using a 2:1 blend of Span85:PEGDO as surfactants. Benzoyl peroxide was used as initiator for the polymerisation, which produces reactive benzoyl radicals at temperatures above 70°C. After leaving the mixture to react overnight, it was centrifuged. No capsules were observed.

With all PMMA samples, there have been issues with initiation of the reaction. Despite the favourable properties of PMMA such as softness and flexibility, all our attempts to use it for nanoencapsulation of crystallohydrates have failed. We moved on to other polymers with different

controls over initiation mechanisms, finding that poly(ethyl-2-cyanoacrylate) and polyurethane were useful in encapsulating salt hydrates, as discussed in the following chapters.

2.5 References

1 T. Khadiran, M. Z. Hussein, Z. Zainal and R. Rusli, *Sol. Energy Mater. Sol. Cells*, 2015, **143**, 78–98.

2 T. G. Mason, J. N. Wilking, K. Meleson, C. B. Chang and S. M. Graves, *J. Phys. Condens. Matter*, 2006, **18**, R635–R666.

3 A. Mandal, A. Samanta, A. Bera and K. Ojha, *Ind. Eng. Chem. Res.*, 2010, **49**, 12756–12761.

4 M. A. Ahmadi and S. R. Shadizadeh, *J. Pet. Sci. Eng.*, 2013, **110**, 66–73.

5 I. J. Lin, *J. Phys. Chem.*, 1972, **76**, 2019–2023.

6 R. Atkin, P. Davies, J. Hardy and B. Vincent, *Macromolecules*, 2004, **37**, 7979–7985.

7 M. Bonnet, M. Cansell, A. Berkaoui, M. H. Ropers, M. Anton and F. Leal-Calderon, *Food Hydrocoll.*, 2009, **23**, 92–101.

8 G. M. Tedajo, S. Bouttier, J. Fourniat, J. L. Grossiord, J. P. Marty and M. Seiller, *Int. J. Pharm.*, 2005, **288**, 63–72.

9 A. Silva-Cunha, J. Grossiord, F. Puisieux and M. Seiller, *Int J Pharm.*, 1997, **158**, 79–89.

10 D. Vasiljevic, J. Parojcic, M. Primorac and G. Vuleta, *Int. J. Pharm.*, 2006, **309**, 171–177.

11 N. Jager-Lezer, I. Terrisse, F. Bruneau, S. Tokgoz, L. Ferreira, D. Clausse, M. Seiller and J. L. Grossiord, *J. Control. Release*, 1997, **45**, 1–13.

12 R. A. Jain, *Biomaterials*, 2000, **21**, 2475–2490.

13 M. P. Desai, V. Labhasetwar, E. Walter, R. J. Levy and G. L. Amidon, *Pharm. Res.*, 1997, 14, 1568–1573.

14 D. J. McClements, *Soft Matter*, 2012, **8**, 1719.

15 C. Mabille, V. Schmitt, P. Gorria, F. Leal Calderon, V. Faye, B. Deminière and J. Bibette, *Langmuir*, 2000, **16**, 422–429.

16 T. Delmas, H. Piraux, A. C. Couffin, I. Texier, F. Vinet, P. Poulin, M. E. Cates and J. Bibette, *Langmuir*, 2011, **27**, 1683–1692.

17 B. K. Paul and R. K. Mitra, *J. Colloid Interface Sci.*, 2005, **288**, 261–279.

18 K. Kundu and B. K. Paul, *Colloids Surfaces a-Physicochemical Eng. Asp.*, 2013, **433**, 154–165.

19 M. J. Lawrence and G. D. Rees, *Adv. Drug Deliv. Rev.*, 2000, **45**, 89–121.

20 S. Cheng, S. R. S. Ting, F. P. Lucien and P. B. Zetterlund, *Macromolecules*, 2012, **45**, 1803–1810.

21 S. Vrignaud, J. P. Benoit and P. Saulnier, *Biomaterials*, 2011, **32**, 8593–8604.

22 S. Watnasirichaikul, T. Rades, I. G. Tucker and N. M. Davies, *Int. J. Pharm.*, 2002, **235**, 237–246.

23 J. M. Asua, *Prog. Polym. Sci.*, 2014, **39**, 1797–1826.

24 A. Schoth, K. Landfester and R. Muñoz-Espí, *Langmuir*, 2015, **31**, 3784–3788.

25 E. M. Rosenbauer, K. Landfester and A. Musyanovych, *Langmuir*, 2009, **25**, 12084–12091.

26 A. Guyot, *Macromol. Symp.*, 2002, **179**, 105–132.

27 S. U. Pickering, *J. Chem. Soc.*, 1907, **91**, 2001–2021.

28 Y. Chevalier and M. A. Bolzinger, *Colloids Surfaces A Physicochem. Eng. Asp.*, 2013, **439**, 23–34.

29 R. Aveyard, B. P. Binks and J. H. Clint, *Adv. Colloid Interface Sci.*, 2003, **100–102**, 503–546.

30 J. Frelichowska, M. A. Bolzinger, J. P. Valour, H. Mouaziz, J. Pelletier and Y. Chevalier, *Int. J. Pharm.*, 2009, **368**, 7–15.

31 K. Zhang, W. Wu, K. Guo, J. F. Chen and P. Y. Zhang, *Colloids Surfaces A Physicochem. Eng. Asp.*, 2009, **349**, 110–116.

32 Chen, Tao, Colver, Patrick J. and Bon, Stefan A. F., *Adv. Mater.*, 2007, **19**, 2286–2289.

33 S. A. F. Bon and P. J. Colver, *Langmuir*, 2007, **23**, 8316–8322.

34 B. Midmore, *J. Colloid Interface Sci.*, 1999, **213**, 352–359.

35 M. Delgado, A. Lázaro, J. Mazo and B. Zalba, *Renew. Sustain. Energy Rev.*, 2012, **16**, 253–273.

36 B. Chen, X. Wang, Y. Zhang, H. Xu and R. Yang, *Appl. Therm. Eng.*, 2006, **26**, 1238–1245.

37 L. Huang, M. Petermann and C. Doetsch, *Energy*, 2009, **34**, 1145–1155.

38 E. Gunther, T. Schmid, H. Mehling, S. Hiebler and L. Huang, *Int. J. Refrig.*, 2010, **33**, 1605–1611.

39 R. Montenegro, M. Antonietti, Y. Mastai and K. Landfester, *J. Phys. Chem. B*, 2003, **107**, 5088–5094.

40 L. Huang, E. Gunther, C. Doetsch and H. Mehling, *Thermochim. Acta*, 2010, **509**, 93–99.

41 E. Gunther, L. Huang, H. Mehling and C. Doetsch, *Thermochim. Acta*, 2011, **522**, 199–204.

42 P. Felix De Castro, A. Ahmed and D. G. Shchukin, *Chem. - A Eur. J.*, 2016, **22**, 4389–4394.

43 R. A. Taylor, N. Tsafnat and A. Washer, *Appl. Therm. Eng.*, 2016, **93**, 935–938.

44 C. Rathgeber, L. Miró, L. F. Cabeza and S. Hiebler, *Thermochim. Acta*, 2014, **596**, 79–88.

45 D. Zou, Z. Feng, R. Xiao, K. Qin, J. Zhang, W. Song and Q. Tu, *Sol. Energy Mater. Sol. Cells*, 2010, **94**, 2292–2297.

46 A. Martínez and G. Prieto, *Catal. Commun.*, 2007, **8**, 1479–1486.

47 X. Liu and D. Astruc, *Adv. Mater.*, 2017, **29**.

48 Z. Yin, D. Ma and X. Bao, *Chem. Commun.*, 2010, **46**, 1344–1346.

49 M. Winkelmann and H. P. Schuchmann, *Particuology*, 2011, **9**, 502–505.

50 X. J. Zhao, X. L. Fang, B. H. Wu, L. S. Zheng and N. F. Zheng, *Sci. China-Chemistry*, 2014, **57**, 141–146.

51 F. Gröhn, B. J. Bauer and E. J. Amis, *Macromolecules*, 2001, **34**, 6701–6707.

52 J. D. Hopwood and S. Mann, *Chem. Mater.*, 1997, **9**, 1819–1828.

53 C. González-Blanco, L. Rodriguez and M. Velazquez, *Langmuir*, 1997, **7463**, 1938–1945.

54 B. K. Paul and R. K. Mitra, *J. Colloid Interface Sci.*, 2006, **295**, 230–242.

55 K. Kundu and B. K. Paul, *J. Surfactants Deterg.*, 2013, **16**, 865–879.

56 M. J. Hou and D. O. Shah, *Langmuir*, 1987, **3**, 1086–1096.

57 R. Leung and D. O. Shah, *J. Colloid Interface Sci.*, 1987, **120**, 320–329.

58 R. Leung and D. O. Shah, *J. Colloid Interface Sci.*, 1987, **120**, 330–344.

59 L. Qi, *Encycl. Surf. Colloid Sci.*, 2006, 6183–6207.

60 A. P. Kafka, B. J. McLeod, T. Rades and A. McDowell, *J. Control. Release*, 2011, **149**, 307–313.

61 R. Domanski, A. A. El-Sebaii and M. Jaworski, *Energy*, 1995, **20**, 607–616.

62 J. Huang, T. Y. Wang, P. P. Zhu and J. B. Xiao, *Thermochim. Acta*, 2013, **557**, 1–6.

63 F. Cheng, Y. Wei, Y. Zhang, F. Wang, T. Shen and C. Zong, *J. Appl. Polym. Sci.*, 2013, **130**, 1879–1889.

64 A. U. Badnore and A. B. Pandit, *Chem. Eng. Process. Process Intensif.*, 2015, **98**, 13–21.

65 D. Saihi, I. Vroman, S. Giraud and S. Bourbigot, *React. Funct. Polym.*, 2005, **64**, 127–138.

66 D. Crespy, M. Stark, C. Hoffmann-Richter, U. Ziener and K. Landfester, *Macromolecules*, 2007, **40**, 3122–3135.

67 Y. Yamagishi, T. Sugeno, T. Ishige, H. Takeuchi and A. T. Pyatenko, *Energy Convers. Eng. Conf. 1996. IECEC 96. Proc. 31st Intersoc.*, 1996, **3**, 2077–2083 vol.3.

68 T. Wang, J. Huang, P. Zhu and J. Xiao, *Colloid Polym. Sci.*, 2013, **291**, 2463–2468.

69 B. Teo, S. Prescott, M. Ashokkumar and F. Grieser, *Ultrason. Sonochem.*, 2008, **15**, 89–94.

70 U. Paiphansiri, P. Tangboriboonrat and K. Landfester, *Macromol. Biosci.*, 2006, **6**, 33–40.

71 G. H. Zhang, S. A. F. Bon and C. Y. Zhao, *Sol. Energy*, 2012, **86**, 1149–1154.

3. Poly(ethyl-2-cyanoacrylate) Nanocapsules for Thermal Energy Storage

3.1 Introduction

If thermal storage capsules are to be widely used in building materials etc., they must be able to be produced on a large scale. For the industrial scale production of polymeric capsules, simple methods are important. Asua[1] described how miniemulsion polymerisation is the only method to create capsules <500nm in size on a wide scale, although it still faces challenges of cost-effectiveness, consistency and environmental issues. There are also safety concerns, such as the phenomenon of thermal runaways in batch reactors, which is a sudden and prolonged increase in polymerisation rate resulting in pressure increase. Other factors such as control over the size of the resulting capsules and reaction rates are also more complex with large amounts of material.

Alkyl cyanoacrylates are a group of hugely reactive monomers that have found use in producing aqueous core nanocapsules since the late 1970s. They had previously found use in the 1960s as novel plastic adhesives for use in such applications as surgery. Cyanoacrylates are the fastest reacting monomer currently known, driven by anionic polymerisation mechanisms (Fig 3.1a and b)[2]. They react extremely rapidly in the presence of nucleophiles, even mild ones such as water. Polymerisation reactions often require a catalyst, which can be toxic, expensive and may require removal from the final product[3]. That alkyl cyanoacrylates can undergo polymerisation initiated by only water is of great advantage. The highly reactive nature of alkyl cyanoacrylates ensures their polymerisations are simplistic.

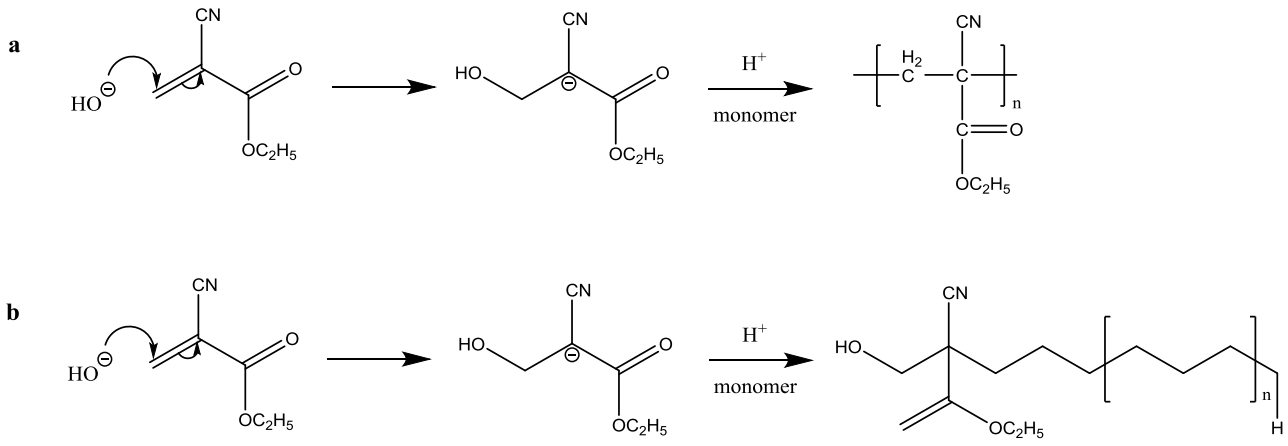

Fig 3.1 (a) and **(b)** Suggested mechanisms for the formation of PACA (the monomer shown is ethyl-2-cyanoacrylate). **(b)** was suggested by Behan *et al*[2]

Most poly(alkylcyanoacrylate) (PACA) nanocapsules have been fabricated for use as drug delivery systems. They have proved particularly efficient for the encapsulation of hydrophilic materials, particularly smaller molecules[4,5] – but have been less successful in trapping larger molecules such as proteins[6]. PACA polymers are also non-toxic and biodegradable. Drug entrapment is dependent on the type of PACA used, the concentration of the drug and pH[4,6]. Shorter chain lengths give better mechanical trapping due to faster polymerisation kinetics[6,7]. It is also possible for additional adsorption of any active material not trapped inside the capsules, onto the capsule outer surface. Materials adsorbed on the outside are released prior to degradation of the shell[8], whilst encapsulated material is released after the shell degrades. Hydrophilic drugs are often less stable than their hydrophobic analogues upon encapsulation, as they must be suspended in water for human consumption. Hydrophilic materials in the core may be released prematurely into the external aqueous phase by diffusion[9]. Strong and non-permeable shell materials are therefore desired for protection. In comparison to hydrophilic drugs, unwanted diffusion of core material may not be as prominent for hydrophilic PCMs, as they may be added directly to materials (e.g. wallboards, paints) for practical applications without the need for suspending in aqueous solution.

We chose ethyl-2-cyanoacrylate (ECA) as the monomer of choice to encapsulate salt hydrates due to the simple nature of the reaction, its availability compared to other cyanoacrylates and its prominence in the literature. Also, the short chain length of this monomer may lead to better trapping of core material, as stated earlier. Most people will have unknowingly used ethyl-2-cyanoacrylate at some time or another – it is believed to be the major component of superglue. Simple reactions are preferred for large scale applications, as more complex reactions have a higher cost[10]. Addition of ECA to a W/O emulsion will lead to spontaneous polymer shell formation at the oil/water interface. Cyanoacrylates form nanoparticles in the region of 100-300nm in diameter[2,8,11–14]. Some researchers have reduced the temperature or decreased the pH of the reaction mixture to slow down polymerisation. We found this was unnecessary, and performing the reaction at room temperature kept the procedure as simple as possible. Decreasing the pH has been found to reduce molecular weight of the resulting PECA shell anyhow, forming a weaker shell which will degrade more quickly[15]. ECA was dissolved in chloroform and added to the W/O emulsion. As the chloroform evaporates, a poly(ethyl-2-cyanoacrylate) (PECA) shell is formed.

Two separate methods were used, both based on the well-established procedure of PECA polymerisation. Kafka *et al*[11] employed a large amount of surfactant (60 %wt of the oil phase) as stabilisers. By simply adding $Mg(NO_3)_2.6H_2O$ and stirring, a W/O microemulsion was formed. In order to significantly reduce the amount of surfactant used, a high energy input is required. Musyanovych *et al*[12] used poly(butyl cyanoacrylate) as their shell material, creating miniemulsions using ultrasound, which required only 5 %wt surfactants in the oil phase. They also noted that a lower amount of surfactants led to a higher molecular weight shell, which should result in improved strength and stability. Using lower amounts of monomer also ensures the shell is of decreased thickness[15]; increasing shell thickness decreases thermal transfer due to the low thermal conductivity of the polymer. Increased stability of the shell is paramount, as after prolonged thermal cycling shell deterioration may occur. Shell deterioration leads to decreased diffusion tightness,

absorption of H_2O and potential release of active material[16]. Our inverse micro-/miniemulsion *in situ* polymerisation was found to be a simple yet effective method for encapsulation.

ECA has previously been used to encapsulate a PCM. Makuta *et al*[17] made cyanoacrylate covered microcapsules with a xylitol core using a novel method. They first made xylitol-in-oil and cyanoacrylate-in-oil emulsions before mixing them together. This resulted in capsule of 35µm average diameter, with a latent heat of 115 $J \cdot g^{-1}$. Their results show cyanoacrylates are suitable for use in thermal energy storage at temperatures up to 120°C. Looking at the synthesis of drug-loaded PECA nanocapsules, it was clear that if a W/O miniemulsion containing crystallohydrate PCMs within reverse micelle droplets was prepared, they could also be encapsulated at the nanoscale. Small capsules should lead to improved thermal properties for two reasons: 1. higher heat transfer due to increased SA:V ratio 2. confinement of the PCM into a nanosized core should assist faster melting and freezing due to the small amount of material present[18]. We found that nanoencapsulation improved physical and chemical properties of $Mg(NO_3)_2.6H_2O$[19,20].

3.2 Analytical methods for testing energy storage capsules

Synthesised capsules were characterised for their physical, chemical and thermal properties. The chosen techniques were readily available to us and gave the maximum amount of information on key capsule properties. Analytical techniques specific to PCMs are shown in the flow chart in Fig 3.2. For size and morphology measurements, scanning electron microscopy (SEM) and transmission electron microscopy (TEM) were used. Electron microscopes are far more powerful than light microscopes, which have a magnification limit of around x1000, and allow high resolution even at the nanoscale. This allows us to observe the capsule structure, for example whether the shell is smooth or rough, and whether complete coverage of the core is achieved. SEM produces images by use of an electron beam which interacts with the sample. As the sample interacts with the beam, secondary electrons are ejected by inelastic scattering. These electrons are accelerated so they have enough energy to create an image. TEM requires a very thin sample, which has an electron beam fired through it. As the beam interacts with the sample, some electrons disappear from the beam. Unscattered electrons are detected, giving rise to a 'shadow' image. The image appears darker or lighter depending on the density of materials present.

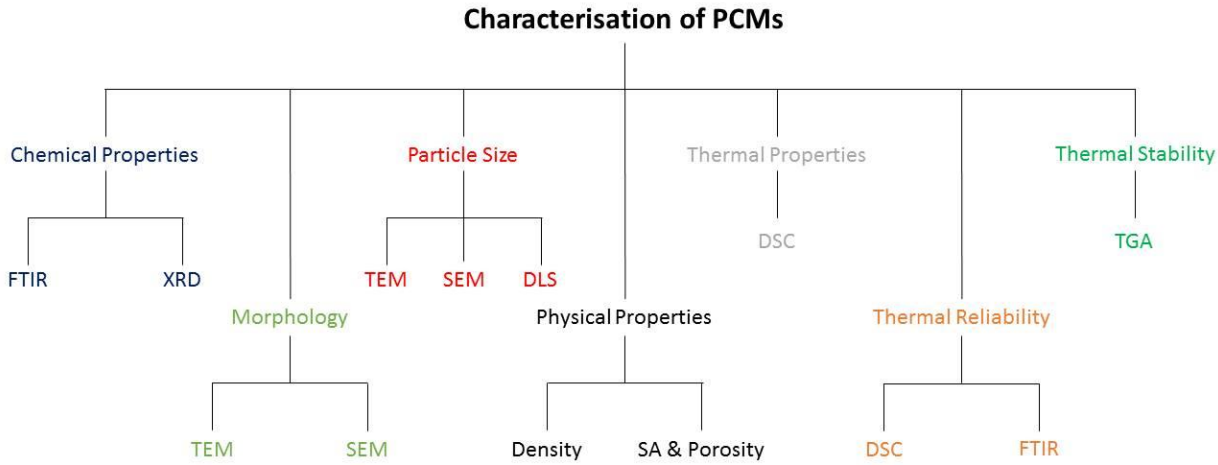

Fig 3.2 Flowchart describing techniques for thorough analysis of PCMs. Adapted from Khadiran *et al*[21]

Fourier transform infrared spectroscopy (FTIR) is a simple method to obtain the chemical structure of materials. It can also be used to observe mechanisms in chemical reactions. Samples are exposed to infrared light which molecules absorb, causing a change in dipole moment of certain functional groups. Molecules with no dipole moment, such as O_2, will not appear in the spectrum. Vibrational energy levels of the molecule are transferred from the ground state to the excited state upon absorption of infrared light. The vibrational energy gap determines the frequency of the absorption peak, which is inherent for particular functional groups and allows the user to determine the chemical structure of the sample. The commonly used wavenumber range for FTIR is between 4000-400 cm^{-1}, as most peaks for organic molecules and inorganic ions appear in this region.

Thermogravimetric analysis (TGA) is a common method of determining thermal stability, where changes in chemical and physical properties are monitored as temperature is increased. This can give information on changes of state such as decomposition and vaporisation. As the temperature

changes the material is constantly weighed and compared to a blank reference. The changes in mass can then be recorded and assigned to the phase transition that has occurred.

Differential scanning calorimetry (DSC) is a vital method of characterisation for heat storage materials, giving information on melting temperature (T_M), freezing temperature (T_F) and latent heat. DSC measures the difference in heat flow required to keep the sample at the same temperature as a blank reference. This is different from an earlier technique known as differential thermal analysis (DTA), which measures the difference in temperature between a reference and a sample when heat flow is kept constant. DSC gives a thermogram with endothermic (heating) and exothermic (cooling) curves. The area underneath the curves is the latent heat for the phase transition. The onset temperature ($T_{M,\ onset}$ for endothermic melting and $T_{F,\ onset}$ for exothermic freezing), peak temperature (T_M and T_F) and end temperature ($T_{M,\ end}$ and $T_{F,\ end}$), of the curves are important as they outline the temperature range in which the PCM may be used. DSC peaks arising from an ideal PCM would be sharp, give a large latent heat and have no supercooling. Sample sizes for DSC are around 5-10mg so may not give an accurate representation of larger samples required for practical applications. For instance, supercooling may be increased due to the small sample size. As a consequence, the T-history method was developed, which uses samples in the region of 10-100g. Sample sizes are approximately 1000 times larger than regular DSC samples, which are usually 5-10mg. Homemade instruments are used for T-history. They consist of a large tank containing the sample, with a thermocouple added so that it is probing the centre of the sample. The material is then thermally cycled and temperature changes recorded as a function of time[22]. As instruments used by different research groups are different, accurate comparisons between results are difficult[23]. Therefore, DSC must also be used in tandem. T-history gives a better representation of bulk properties, which can then be used alongside the more accurate regular DSC measurements. Good energy storage candidates then can be tested on a larger scale. For instance, PCMs for passive air conditioning may be tested by adding to panels in a test building to observe the changes in atmospheric temperature.

X-ray diffraction (XRD) is a commonly used technique for analysing crystalline structures, in which powder samples are bombarded with electrons. It is an uncommon technique for analysing PCMs. However, as salt hydrates are crystalline materials, we hypothesised their associated Bragg peaks should be detected in the XRD pattern of our nanocapsules.

X-ray photoelectron spectroscopy (XPS) is another technique not regularly used in examining polymer nanocapsules or PCMs, however provides valuable information about the %wt of each element present in the sample. This was useful for determining how much salt hydrate was present within synthesised nanocapsules. It was used in place of energy dispersive X-ray analysis (EDX), which is used in conjunction with SEM and can provide an elemental map of a site of interest in the sample. However, we found EDX was not sensitive enough to map the extremely small nanocapsules we fabricated. XPS works by exciting the surface of a powder sample using X-rays. The top 5nm of the sample is analysed – the energy of the emitted photoelectrons released from this region are analysed. From this binding energy and intensity of the resulting peak, the chemical identity and quantity of each element in the sample can be detected.

3.3 Results

3.3.1 Initial results

The first successfully synthesised capsules with a salt hydrate core had an aqueous phase made up of 2 %wt $CaCl_2.6H_2O$, 98 %wt water. Poor resolution SEM images of these nanocapsules are pictured in Fig 3.3, some capsule structures can be seen. Clearly, 2 %wt of the active material is not enough for heat storage, so ways of increasing the amount of core material were sought.

We found that using a large amount of surfactants, 60 %wt of Tweens and Spans, widely available commercial nonionic surfactants, stable miniemulsions could be formed simply by stirring. More detailed descriptions of PCM emulsions can be found in Chapter 2. Tweens and Spans worked better than AOT as a template for polymerisation reactions.

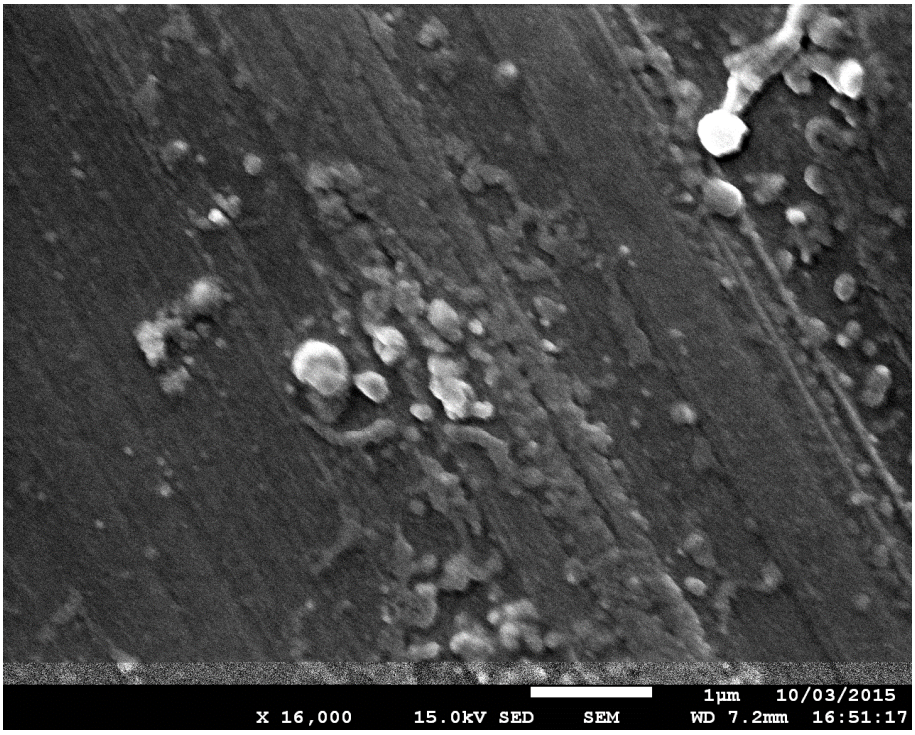

Fig 3.3 SEM image of PECA capsules with 2%wt $CaCl_2.6H_2O$ core, our first successful attempt at making salt hydrate-loaded capsules

Increasing the amount of PCM in the core was achieved for both $CaCl_2.6H_2O$ and $Mg(NO_3)_2.6H_2O$. $Mg(NO_3)_2.6H_2O$ was chosen for further analysis as its T_M (90°C) is way above room temperature, so phase transitions could more easily be detected on the thermal analysis equipment available to us. The T_M for $CaCl_2.6H_2O$ (29°C) is very close to room temperature. For rigorous analysis, 3 samples were chosen which would display the best parameters for the encapsulation of crystallohydrates with PECA. They were formed by different methods, described in Fig 3.4. The make-up of each NanoPCM sample is shown in Table 3.1.

Dissolving the ECA in chloroform prior to addition was a key step in formation of the nanocapsules. If ECA was added on its own, it immediately polymerised into a large colourless agglomerate. Dissolution in chloroform helps slow the reaction to the extent that the monomer will polymerise around emulsion droplets.

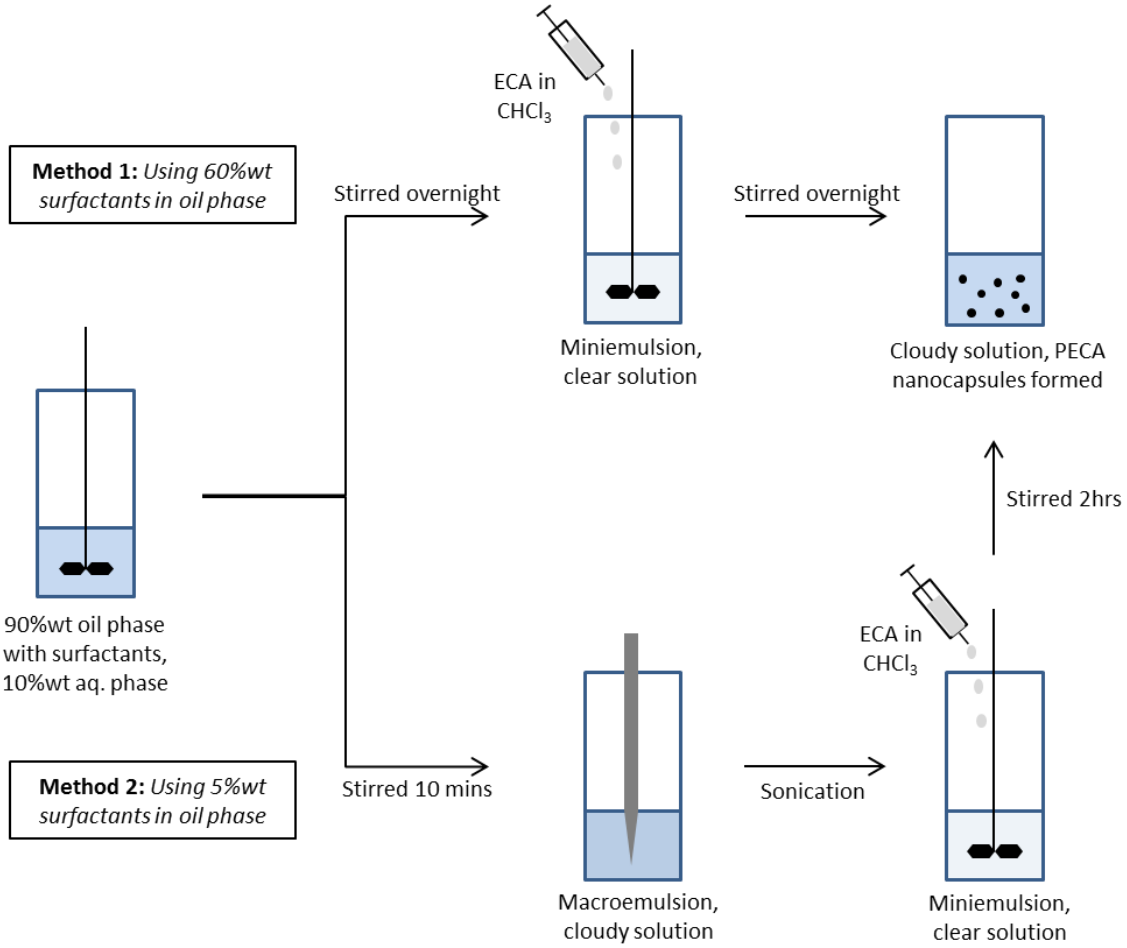

Fig 3.4 Synthesis of salt hydrate-loaded PECA nanocapsules by *in situ* polymerisation, employing mechanical stirring without (method 1) and with ultrasonic treatment (method 2)

Table 3.1 Composition of miniemulsion phases and amount of monomer added during preparation of $Mg(NO_3)_2.6H_2O$ capsules

Sample	Oil Phase (9g)	Aqueous Phase (1g)	ECA added (µL)
NanoPCM1	60 %wt surfactants, 40 %wt toluene	100 %wt $Mg(NO_3)_2.6H_2O$	600
NanoPCM2	60 %wt surfactants, 40 %wt toluene	70 %wt $Mg(NO_3)_2.6H_2O$, 30 %wt water	300
NanoPCM3	5 %wt surfactants, 95 %wt cyclohexane	20 %wt $Mg(NO_3)_2.6H_2O$, 80 %wt water	200

3.3.2 Crystalline Structure of $Mg(NO_3)_2.6H_2O$ and NanoPCM1

To observe crystallinity of bulk and encapsulated $Mg(NO_3)_2.6H_2O$, XRD was employed. Results are shown in Fig 3.5. $Mg(NO_3)_2.6H_2O$ is a crystalline solid, resulting in many sharp, intense peaks. PECA on the other hand is highly amorphous, leading to its characteristic broad peaks at approximately 12^o and 32^o. Similar XRD patterns have been reported by other researchers[24,25]. Amorphous samples, in contrast to crystalline substances, do not possess long range order. Therefore, sharp Bragg peaks are not possible, leading to the broad and noisy signal of PECA. In addition to these characteristic peaks, another small, broad peak appears at around 44^o. As this corresponds to signals from the bulk $Mg(NO_3)_2.6H_2O$, it can be concluded that these are peaks from salt hydrate in the nanocapsule core.

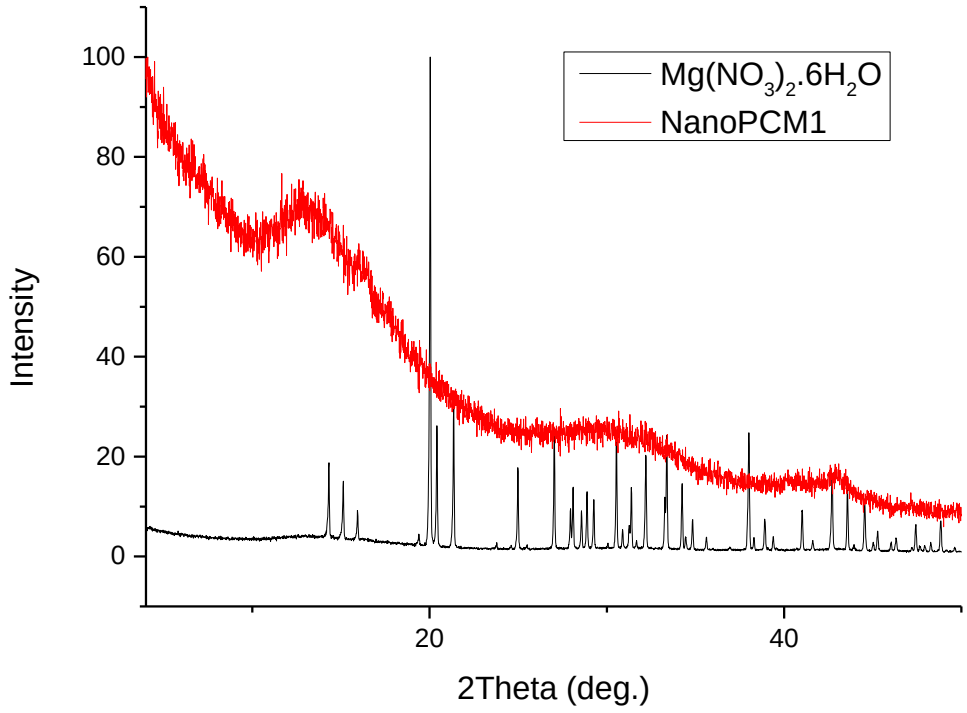

Fig 3.5 XRD patterns for $Mg(NO_3)_2.6H_2O$ and NanoPCM1

3.3.3 Morphology and size

Morphology and size of the capsules were measured by analysing SEM micrographs (Fig 3.6). Bulk $Mg(NO_3)_2.6H_2O$ appears either as crystalline solid (Fig 3.6a), with flakes of 10µm and above; or as large agglomerates in a sheet formation (Fig 3.6b). The large sheets are probably formed by partial melting of the $Mg(NO_3)_2.6H_2O$ during crushing. These images show how the structure of the salt hydrate completely changes after a melting/freezing cycle. The appearance of the nanocapsules is in stark contrast to the bulk $Mg(NO_3)_2.6H_2O$. As can be seen from Fig 3.6c-e, PECA nanocapsules aggregate upon drying, which is caused by residual monomer present in the product, and is common in PECA nanoparticles[13]. Aggregation of the capsules can be observed in the images. Single capsules can be made out, but some are 'glued' together. The dried agglomerates can be broken up by

dispersing using a bath sonicator. The micrographs show the capsules have a smooth surface with no pores present. Complete coverage of the core material is achieved, preventing leakage of the PCM cargo. The NanoPCMs are in the range of 100-200nm, which is consistent with insulin loaded PECA capsules[14]. Nanocapsules provide improved thermal performance due to increased SA:V ratio, and also may help create diffusion tight bonding, which is important for leakage prevention and maintaining hydration levels of the crystallohydrate[16]. Notable is that both microemulsion (NanoPCM1 and 2) and miniemulsion (NanoPCM3) *in situ* polymerisation methods lead to similarly sized capsules which are identical in appearance. Inverse micro-/miniemulsions created by both methods were therefore effective in solubilising salt hydrate. Capsules maintain a rounded shape even under the SEM high vacuum which indicates their high structural stability compared to larger capsules which may collapse under increased pressure[26]. Structural stability is crucial in practical applications which require that the capsules are pumped round a system.

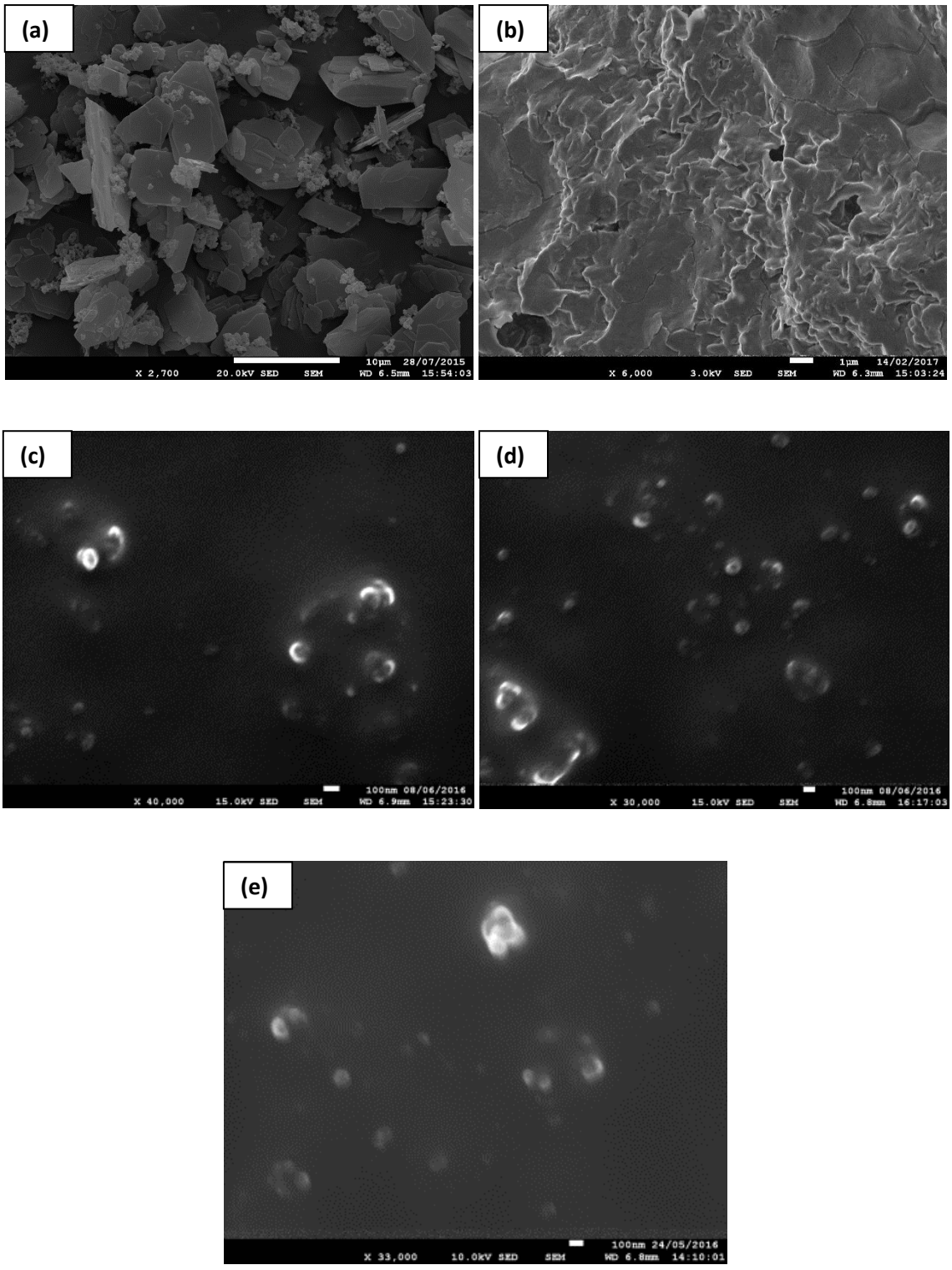

Fig 3.6 SEM images of $Mg(NO_3)_2.6H_2O$ - **(a)** Flaky solid **(b)** sheets after partial melting; **(c)** NanoPCM1, **(d)** NanoPCM2, **(e)** NanoPCM3. Scale bars are: for **(a)** 10µm **(b)** 1µm **(c)** – **(e)** 100nm

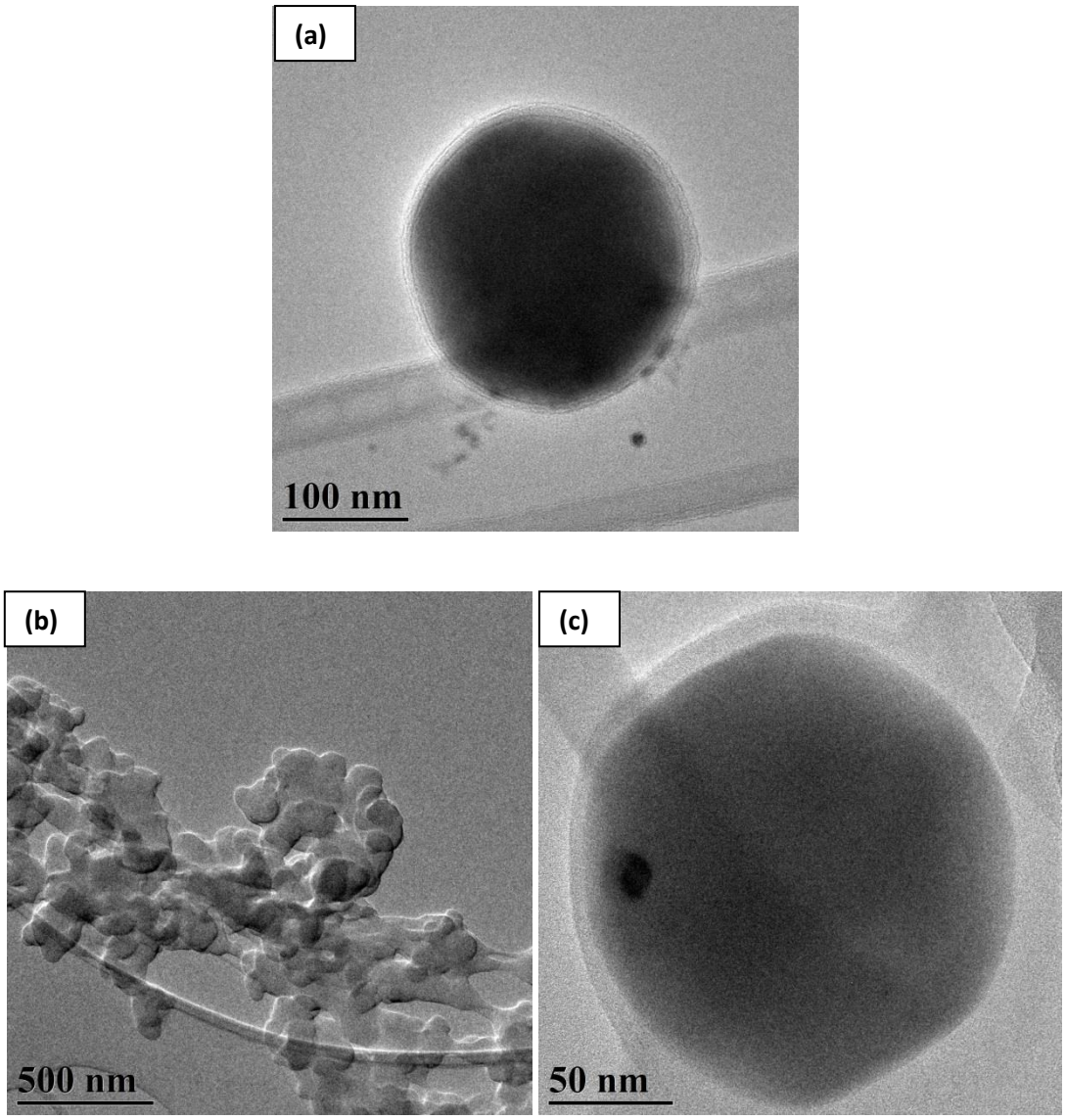

Fig 3.7 TEM images of **(a)** NanoPCM1, and **(b)**-**(c)** NanoPCM2.

TEM images of NanoPCM1 and 2 are shown in Fig 3.7. Single capsules can be observed in Fig 3.7a and c. They are approximately 200nm in diameter, identical to those seen in the SEM images. Darker areas appearing on the images are caused by difference in densities of the salt hydrate core and polymer shell. Fig 3.7b shows aggregated capsules of NanoPCM2.

3.3.4 Chemical Composition of NanoPCMs

Chemical composition of ECA, bulk $Mg(NO_3)_2.6H_2O$, ethyl cyanoacrylate and the NanoPCMs was probed by FTIR, spectra are shown in Fig 3.8. ECA has characteristic peaks for C-H at 2989 cm^{-1}, CN at 2240 cm^{-1}, C=O at 1730 cm^{-1}, C=C at 1616 cm^{-1}, 2 C-O peaks at 1287 and 1016 cm^{-1}, and =C-H bend at 803 cm^{-1}. $Mg(NO_3)_2.6H_2O$ has characteristic peaks for O-H stretching at 3356 cm^{-1}, N=O bending at 1646 cm^{-1}, a mixture of N-O stretching and bending and N=O stretch in the broad peak at 1365 cm^{-1}, plus a sharp peak at 819 cm^{-1} for the NO_3^- ion. NanoPCM1 and NanoPCM2 have identical spectra. Peaks for PECA are similar to ECA with the C-H stretch at 2927 cm^{-1}, C=O at 1745 cm^{-1} along with 2 C-O peaks at 1250 and 1013 cm^{-1} which signify the presence of an ester group. No peaks for CN appear in their spectrum, which may be masked due to the large amount of surfactants used in making the samples, although the peak is small in the spectrum for ECA anyway.

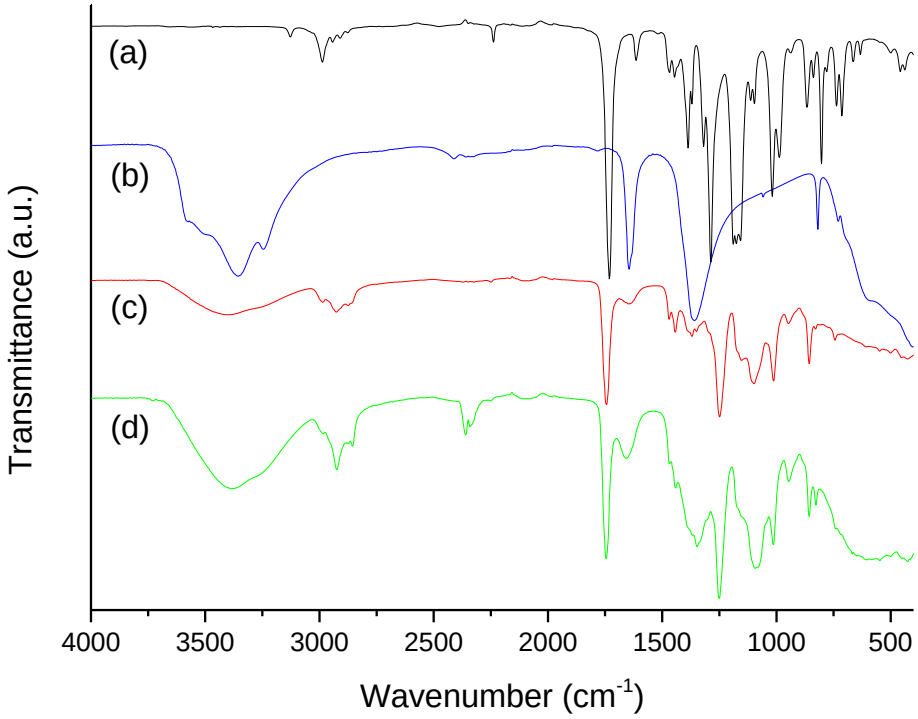

Fig 3.8 FTIR spectra for **(a)** ECA **(b)** $Mg(NO_3)_2.6H_2O$ **(c)** NanoPCM1 and **(d)** NanoPCM3.

NanoPCM3 has a similar spectrum with regards to NanoPCMs 1 and 2, confirming that the alternate methods produce nanocapsules that are chemically similar. It has peaks for PECA at 2923, 1745, 1253 and 1079 cm^{-1} respectively, corresponding to the previously mentioned functional groups. It also has a CN peak at 2360 cm^{-1}, due to residual ECA monomer. The peaks attributed to $Mg(NO_3)_2.6H_2O$ are more pronounced in the NanoPCM3 spectrum at 3373, 1643, 1345 and 827 cm^{-1}. Stronger peaks indicate that there is more $Mg(NO_3)_2.6H_2O$ present in the core and that the salt hydrate has a similar composition to that of the bulk material. The minor wavelength shifts for $Mg(NO_3)_2.6H_2O$ upon encapsulation are due to spatial confinement, which affects H-bonding. Spatial confinement effects on organic PCMs were noted in an article by Felix *et al*[27].

3.3.5 Thermal Analysis of NanoPCMs

Thermal properties of the capsules were studied by TGA and DSC. TGA curves are shown in Fig 3.9. The bulk $Mg(NO_3)_2.6H_2O$ starts mass loss at approximately 70°C. By 160°C, 36% mass has been lost, which corresponds to water loss and is in good agreement with the theoretical water content of 42%. The remaining mass is lost from 300 to 460°C. The decomposition of $Mg(NO_3)_2.6H_2O$ proceeds at 330°C according to literature, our TGA curve is in good agreement with Han *et al*[28]. 14% mass remains at 800°C, consisting mainly of magnesium oxide (MgO). Magnesium makes up 10% mass content of $Mg(NO_3)_2.6H_2O$ according to the stoichiometry, so the obtained values fit nicely.

NanoPCM1 and 2 have very similar curves, due to the almost identical synthesis. Both lose 4% mass by 150°C due to water evaporation. NanoPCM1 and 2 lose 65% and 60% mass, respectively, from 150-300°C. This is due to the PECA shell degrading, in agreement with previous research[28]. NanoPCM1s higher mass loss was due to a larger amount of shell material being present, which is to be expected as more monomer was added during synthesis. Further mass loss occurs from 330-400°C due to magnesium nitrate decomposition. After complete heating to 800°C, NanoPCM1 and 2 have 2% and 8% mass remaining, consisting of MgO and carbon residue. NanoPCM2's higher remaining mass shows there was more $Mg(NO_3)_2.6H_2O$ present in the core in comparison with NanoPCM1, which was confirmed by DSC thermal analysis.

NanoPCM3 was created using different methodology than NanoPCM1 and 2, leading to different thermal behaviour. It lost mass more rapidly between 30-150°C, with 15% mass loss attributed to water evaporation. The higher amount of water loss for NanoPCM3 can be rationalised as its aqueous phase contained a far larger amount of excess water than NanoPCM1 and 2. Mass loss increases at 150°C corresponding to the degradation of the PECA shell. Similar TGA curves have been obtained for pure PECA, with degradation starting at around 150°C[28,29]. Between 150-300^{o}C, NanoPCM3 loses 35% mass. Notable is that the PECA shell degrades much more slowly and has better temperature resistance than NanoPCM1 and 2. This is a good indication that a higher

molecular weight shell has been formed. Other researchers have shown that low amounts of surfactants and low volumes of added monomer lead to higher molecular weight shell[12], which is confirmed by the TGA curve for NanoPCM3. It is also possible the low amount of monomer prevents too much crosslinking from occurring in the polymer, which can be difficult to separate onto the emulsion droplet surface and hindering capsule formation[30]. Lower mass loss in comparison to NanoPCM1 and 2 is also due to the increased $Mg(NO_3)_2.6H_2O$ in the core of NanoPCM3, which was confirmed by DSC results. Upon degradation of the salt at 330°C, a further increase in mass loss occurs. After heating to 800°C, 14% mass remains, which is much higher than NanoPCM1 & 2. Again, this shows the increased level of crystallohydrate in the NanoPCM core, despite NanoPCM3 having a lower amount of $Mg(NO_3)_2.6H_2O$ added during synthesis. This can be explained by the fact NanoPCM3 also has a lower amount of monomer added, which leads to a thinner polymer shell. As NanoPCM1-3 are all of similar sizes, thinner shell material leads to a larger cavity in the core, solubilising more salt hydrate.

From 450-750^oC, NanoPCM3 has more remaining mass than bulk $Mg(NO_3)_2.6H_2O$. This can be explained by two factors. The error range of the TA Instruments SDT Q600 DSC instrument is ±2%. Also, the polymer shell may act as an intumescent. Intumescents swell during heating, leading to a volume increase. They act as a protective layer, and adding a hydrate core aids this effect by releasing water vapour which cools the material.

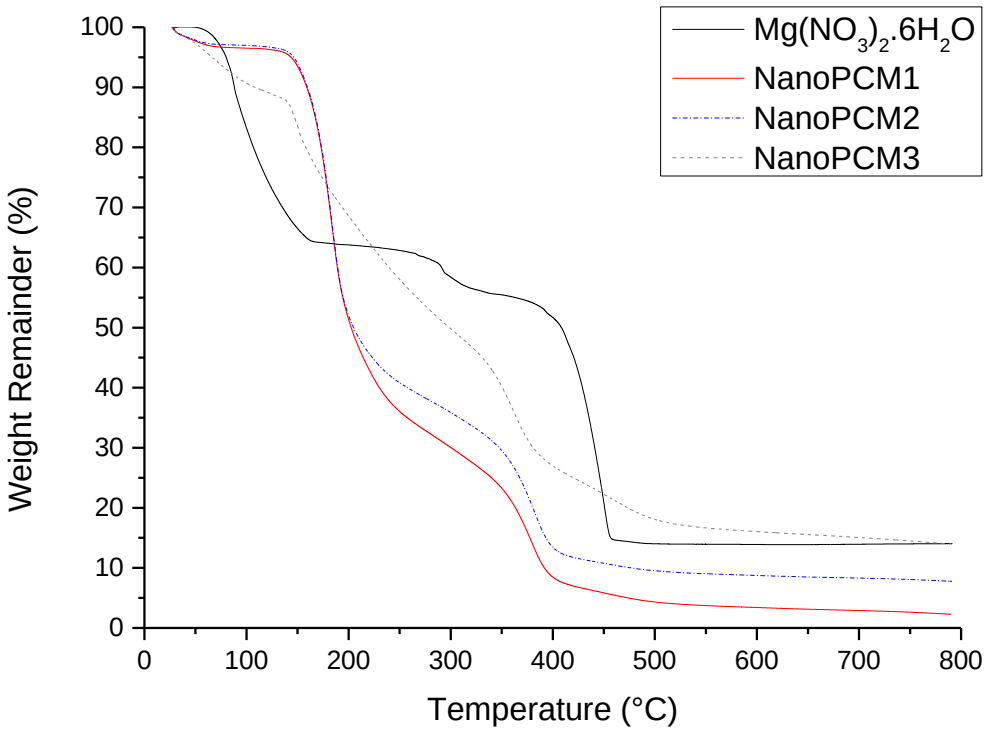

Fig 3.9 TGA curves for $Mg(NO_3)_2.6H_2O$ & NanoPCMs.

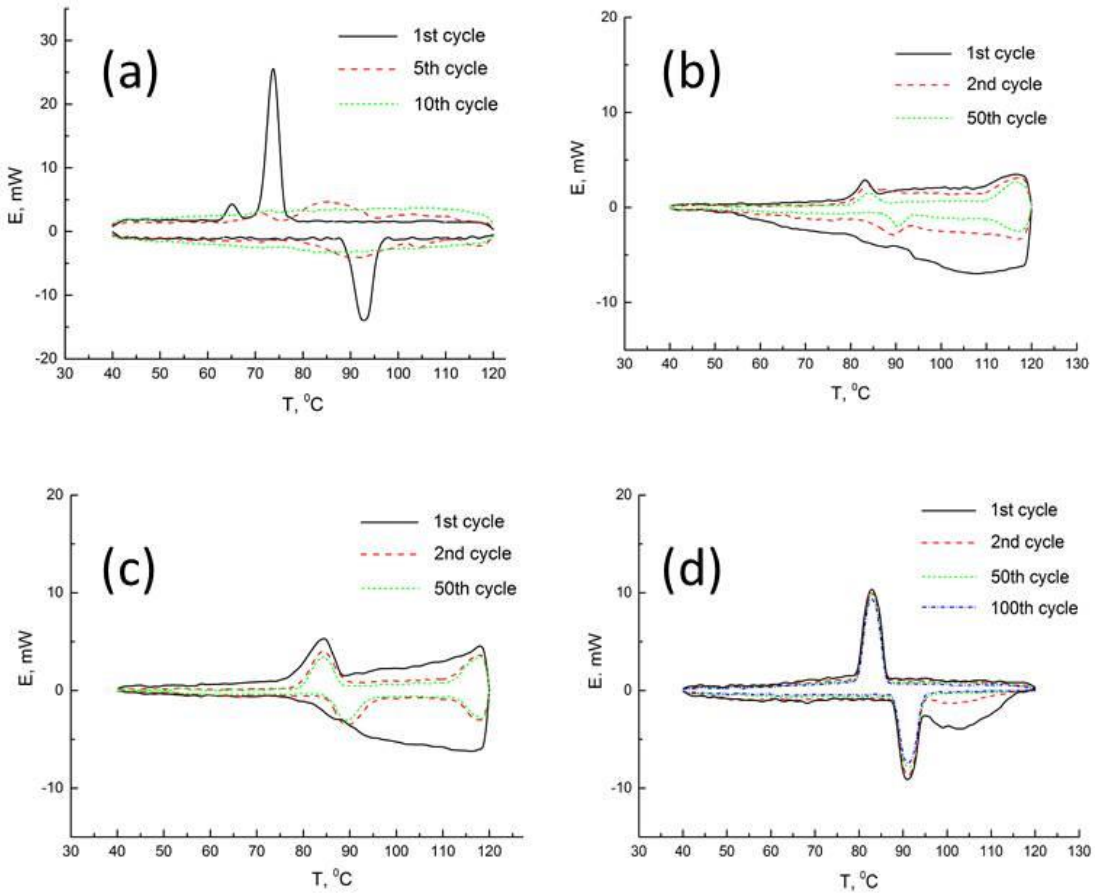

Fig 3.10 DSC thermograms for **(a)** bulk $Mg(NO_3)_2.6H_2O$ **(b)** NanoPCM1 **(c)** NanoPCM2 and **(d)** NanoPCM3.

DSC results show how the polymer shell vastly increases thermal cycling stability of the $Mg(NO_3)_2.6H_2O$. The thermogram for bulk $Mg(NO_3)_2.6H_2O$ (Fig 3.10a) shows the material has a latent heat of 160.2 $J{\cdot}g^{-1}$ and melting point with $T_{M,\,onset}$ = 88°C and T_M = 93°C. Values have a slight variation compared to those from literature of 162.8 $J{\cdot}g^{-1}$ and 89°C[31]. It has two freezing peaks, a major peak with $T_{F,\,onset}$ = 77°C and T_F = 74°C, and a smaller peak attributed to an additional solid-solid phase change at $T_{F,\,onset}$ = 68°C and T_F = 66°C. After only 5 cycles, the peaks are severely decreased; by 10 cycles, latent heat storage is no longer possible due to the complete dehydration of the salt. Chemical instability, along with supercooling (calculated by $T_M - T_F$) of 19°C demonstrate the inherent shortcomings of bulk salt hydrates as thermal energy storage materials.

By confining the $Mg(NO_3)_2.6H_2O$ within a nanocontainer, its chemical stability and heat transfer abilities are improved. In the first cycle for both NanoPCM1 and 2 (Fig 3.10b and c), a broad endothermic peak appears between 60-120°C and 80-120°C, respectively. This can be attributed to evaporation of excess water which is not associated to the salt hydrate. As the aqueous phase for NanoPCM1 consisted solely of $Mg(NO_3)_2.6H_2O$, any water that evaporates will necessarily dehydrate the salt to some extent. This process decreases its latent heat storage abilities; resulting in NanoPCM1 having the lowest latent heat capacity of all 3 NanoPCM samples. Excess water is still being lost from NanoPCM1 in the 2nd thermal cycle; for NanoPCM2, water evaporation only occurs on the first cycle. NanoPCM2 therefore has more water associated to the salt hydrate in the core. As the aqueous phase for NanoPCM2 contained extra water (30 %wt), it is clear extra water preserves the salt hydrate composition, an effect reported by several researchers[32,33]. Both NanoPCM1 and 2 have two melting and freezing peaks attributed to crystallohydrate. The peaks at approximately 90°C are due to the presence of $Mg(NO_3)_2.6H_2O$, whilst at 120°C the incomplete peaks are attributed to another stable hydrate, $Mg(NO_3)_2.2H_2O$ (T_M = 129°C). Lower hydrates are formed by incongruent melting, which is an irreversible process. The mechanism of incongruent melting for $Mg(NO_3)_2.6H_2O$ is shown in Eq. 3.1 and 3.2[34,35]. The presence of two hydrates is undesirable as it gives two T_Ms, both with low latent heat (after 50 cycles, ΔH_M for the peak at 90°C was 26.3 $J \cdot g^{-1}$ for NanoPCM1 and 39.4 $J \cdot g^{-1}$ for NanoPCM2). As PCM applications require a small temperature range, the incongruent melting effect limits effectiveness of salt hydrate PCMs.

$$Mg(NO_3)_2.6H_2O \underset{<90^oC}{\overset{90^oC}{\rightleftharpoons}} Mg(NO_3)_2 + 6H_2O$$

Eq 3.1 Congruent melting of $Mg(NO_3)_2.6H_2O$

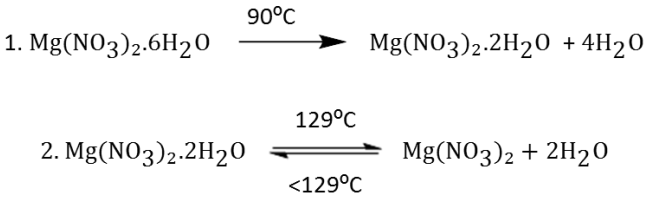

Eq 3.2 Incongruent melting of $Mg(NO_3)_2.6H_2O$, occurring in 2 stages.

NanoPCM3 displays improved characteristics (Fig 3.10d), with a latent heat of 83.2 $J \cdot g^{-1}$ after 50 cycles, with $T_{M,\ onset}$ = 87°C, T_M = 91°C and $T_{F,\ onset}$ = 86°C, T_F = 83°C. Encapsulation efficiency (EE) for PCM capsules is often measured by the equation:

$$\Delta H_{capsules}/\Delta H_{bulk\ salt\ hydrate} \times 100$$

Eq 3.3 Commonly used equation to determine encapsulation efficiency for PCM capsules

However, EE for drug delivery systems is simply defined as the amount of added drug that has been encapsulated. Using ΔH values means an EE of 100% could never be achieved due to the presence of the polymer shell. Also, any incongruent melting would lead to a lower EE, despite entrapment of the material. Results obtained using Eq 3.3 may better be described as 'thermal capacity', but will be described as EE in this work for consistency with other research. EE for NanoPCM3 is 51.9%. The high EE in comparison with the %wt of salt hydrate in the aqueous phase (51.9% EE compared to 20 %wt $Mg(NO_3)_2.6H_2O$ added to the aqueous phase) has been observed by other researchers[36]. This may be due to the salt hydrate acting as a 'superlipophobe', stabilising the W/O miniemulsion and favourably encapsulating the crystallohydrate[37]. Also, cyanoacrylates are efficient at encapsulating hydrophilic molecules due to the lack of diffusion processes by the monomer during polymerisation, thanks to the fast reaction kinetics. Like NanoPCM1 and 2, there is also loss of excess water in the 1st

cycle, explaining the broad peak at 95-120°C. The presence only a single T_M with high latent heat signifies that only the original salt hydrate, $Mg(NO_3)_2.6H_2O$, is present within the capsule core. Incongruent melting is avoided due to the constraint of the capsule core and the polymer barrier preventing water loss. The T_M for the capsules is 2°C lower than that of the bulk $Mg(NO_3)_2.6H_2O$. Decreased T_M in PCM capsules compared to the bulk material has been observed before with the fatty acid PCM stearic acid. The authors attributed this to the high surface area of the nanocapsules[38]. The T_M for NanoPCM3 remains constant at 91°C during prolonged cycling, despite other researchers reporting fluctuating T_Ms for organic PCMs after encapsulation[39]. Latent heat remains almost constant, with only a 3% decrease after 100 cycles. Encapsulation of the PCM in a PECA shell clearly promotes long term stability, with sufficient elasticity to control volume changes during phase transition. Supercooling is reduced to 8°C, with only a 1°C difference between $T_{M,\ onset}$ and $T_{F,\ onset}$. This is due to increased heat transfer area upon encapsulation. As demonstrated by TGA analysis, this method of producing nanocapsules leads to a higher MW shell, increasing EE and latent heat[6]. The superior properties of NanoPCM3 prove the value of sonochemistry in the preparation of miniemulsions during the encapsulation procedure. Using sonochemistry allows the amount of surfactants used to be reduced, leading to a thinner and higher molecular weight shell with improved thermal properties.

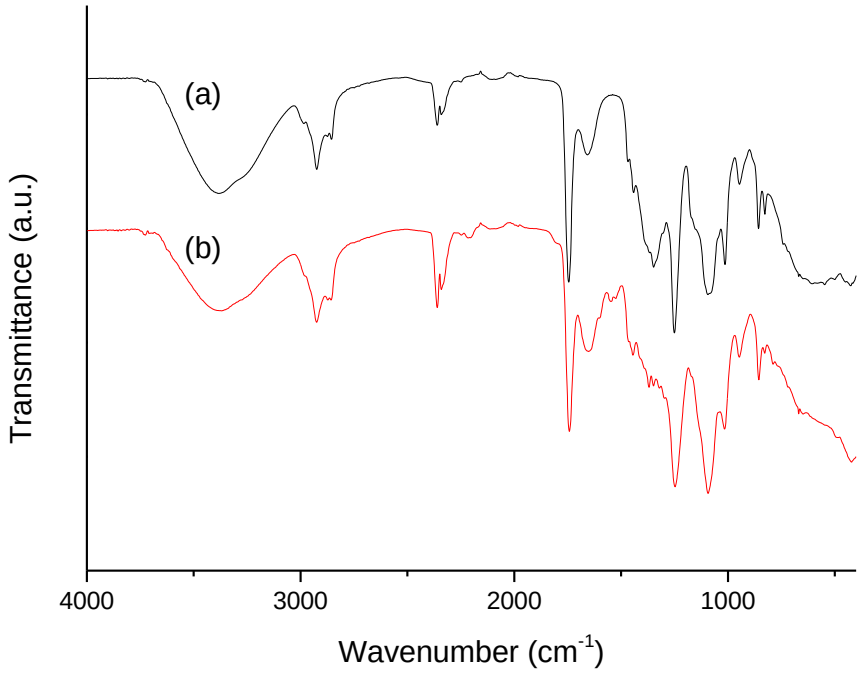

Fig 3.11 FTIR spectra for NanoPCM3 **(a)** before and **(b)** after 100 thermal cycles.

3.3.6 Chemical stability of NanoPCMs

Chemical stability is of great importance for crystallohydrate PCMs, so they can maintain heat storage properties over a vast number of cycles. Clearly this was demonstrated by DSC, especially by NanoPCM3. After 100 melting/freezing cycles between 50 and 120°C, the FTIR spectrum of NanoPCM3 was retaken to ensure the capsule and core material was chemically unchanged (Fig 3.11). Characteristic peaks of $Mg(NO_3)_2.6H_2O$ are present at 3373 cm^{-1} for O-H stretch, 1643 cm^{-1} for N=O bending, a mixture of N-O stretching and bending and N=O stretch at 1345 cm^{-1}, and NO_3^- at 827 cm^{-1}. Peaks for PECA are also unchanged, with C-H stretch at 2923 cm^{-1}, C=O at 1745 cm^{-1} and 2 C-O peaks at 1253 and 1079 cm^{-1}. The identical spectrum after 100 thermal cycles demonstrates the nanocapsule stability during the uptake and release of latent heat.

To observe the macroscale appearance of the NanoPCMs in comparison to bulk $Mg(NO_3)_2.6H_2O$ during thermal cycling, pictures were taken of the capsules before and after heating to 100°C. Results are displayed in Fig 3.12. $Mg(NO_3)_2.6H_2O$ is a crystalline solid before melting. After melting and refreezing, the material coagulates into a compact block surrounded by water. This demonstrates the volume change upon melting of a salt hydrate. This refrozen structure can limit the diffusion of water vapour[40], leading to dehydration of the salt hydrate. In contrast, the nanoencapsulated $Mg(NO_3)_2.6H_2O$ display no increase in volume or change in appearance after heating to 100°C. Absence of any leakage of the core material confirms the complete coverage of the core by the polymer shell. The salt hydrate is therefore fully protected from the external environment, helping prevent dehydration and leading to the increased thermal stability shown in the DSC thermograms.

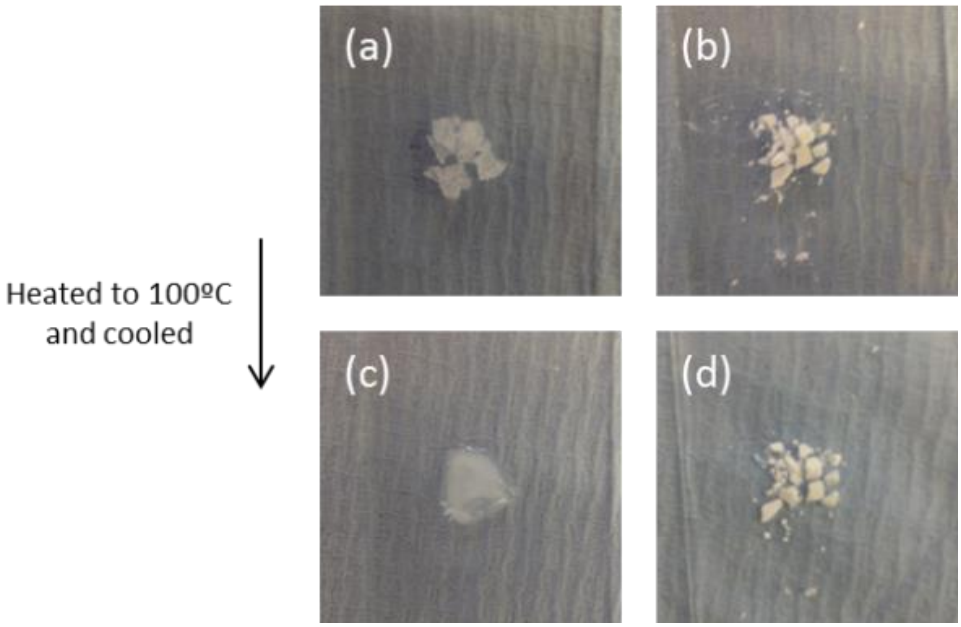

Fig 3.12 Photographs of $Mg(NO_3)_2.6H_2O$ **(a)** & **(c)** and nanoencapsulated salt hydrate **(b)** & **(d)** before heating to 100°C (top), and after letting them cool back to room temperature (bottom).

3.3.7 Encapsulation of Multiple PCMs

PECA is clearly a useful polymer for the nanoencapsulation of salt hydrates, as shown by the increased chemical and structural stability it provides. Two key steps were noted in the creation of effective thermal storage capsules: 1. The use of ultrasound in producing miniemulsions stabilised by low amounts of surfactant, which maximised encapsulation yield 2. The addition of extra water into the aqueous phase which stabilised the hydration level of the $Mg(NO_3)_2.6H_2O$, preventing incongruent melting and phase separation[41].

With the methodology optimised, the next stage was to show universality of the procedure. To do this, other salt hydrates must also be encapsulated. We chose sodium sulphate decahydrate ($Na_2SO_4.10H_2O$, also known as Glauber's salt), which is possibly the most well researched crystallohydrate of all, and is one of the cheapest. It has a T_M of 32°C, which is suitable for use in applications such as cooling of handheld electronics or photovoltaics. It is well known that $Na_2SO_4.10H_2O$ melts peritectically i.e. into both solid and liquid phases which leads to phase

separation[32]. With extra water added this process can be eliminated. NanoPCM3 was also remade to demonstrate reproducibility of the nanocapsules, which is highly important for capsules produced on an industrial scale. We also encapsulated mixtures of the two salts, described in more detail below. Composition of NanoPCM4-7 is shown in Table 3.2.

Table 3.2 Composition of the NanoPCMs for mixtures

Sample	Oil Phase (9g)	Aqueous Phase (1g)	ECA added (µL)
NanoPCM4	5 %wt surfactants, 95 %wt cyclohexane	20 %wt $Mg(NO_3)_2.6H_2O$, 80 %wt water	200
NanoPCM5		20 %wt $Na_2SO_4.10H_2O$, 80 %wt water	
NanoPCM6		20 %wt 1:1 $Mg(NO_3)_2.6H_2O$: $Na_2SO_4.10H_2O$, 80 %wt water	
NanoPCM7		20 %wt 1:2 $Mg(NO_3)_2.6H_2O$: $Na_2SO_4.10H_2O$, 80 %wt water	

3.3.8 Morphology and chemical analysis

SEM images show that NanoPCM4 and 5 look identical to previous NanoPCMs (Fig 3.13). They are between 100-300nm in size, with a smooth capsule surface and full coverage of the shell material. Again, this is imperative in prevention of water loss and reaction with the external environment. These capsules also aggregate upon drying, shown in Fig 3.13b, d, e and g. Some of these capsules have a non-spherical shape, which is due to crystallisation of the initially liquid crystallohydrate core during preparation of the nanocapsules, demonstrating the shells elasticity. Better images of single capsules were taken by obtaining a dispersion of the nanocapsules prior to drying *i.e.* before centrifugation of the nanocapsule suspension. These are shown in Fig 3.13c, e and h, and demonstrate how the single capsules are completely spherical, displaying their robustness to the SEM high vacuum. The TEM image in Fig 3.14 shows a NanoPCM4 capsule of approximately 120nm with a partly removed shell. The shell deformation is caused by electron beam damage[42].

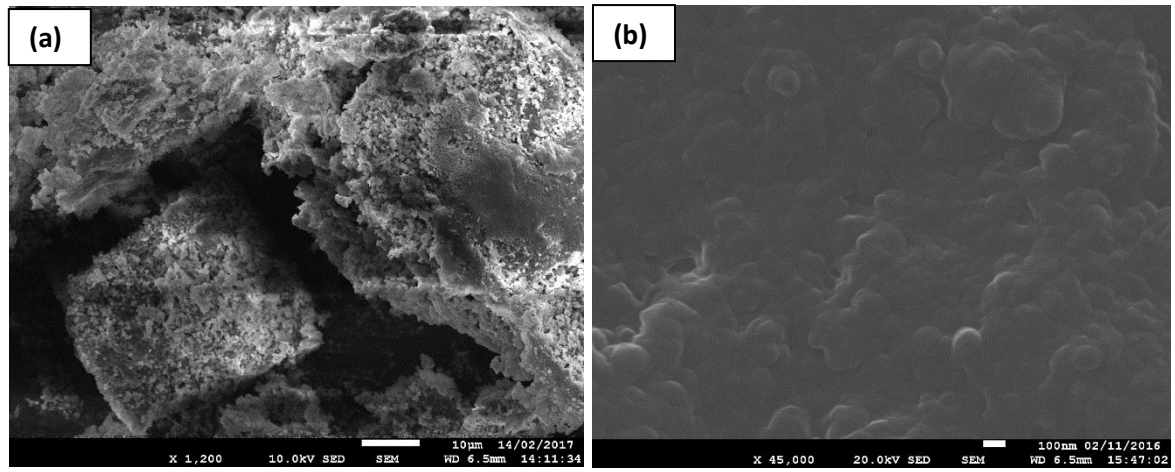
(a)
X 1,200 10.0kV SED SEM 10µm 14/02/2017 WD 6.5mm 14:11:34
(b)
X 45,000 20.0kV SED SEM 100nm 02/11/2016 WD 6.5mm 15:47:02
(c)
X 100,000 5.0kV SED SEM 100nm 25/04/2017 WD 5.8mm 11:37:07
(d)
X 90,000 20.0kV SED SEM 100nm 02/11/2016 WD 6.4mm 15:06:54
(e)
X 33,000 20.0kV SED SEM 100nm 02/11/2016 WD 6.5mm 15:22:10
(f)
X 12,000 5.0kV SED SEM 1µm 25/04/2017 WD 6.2mm 12:18:31

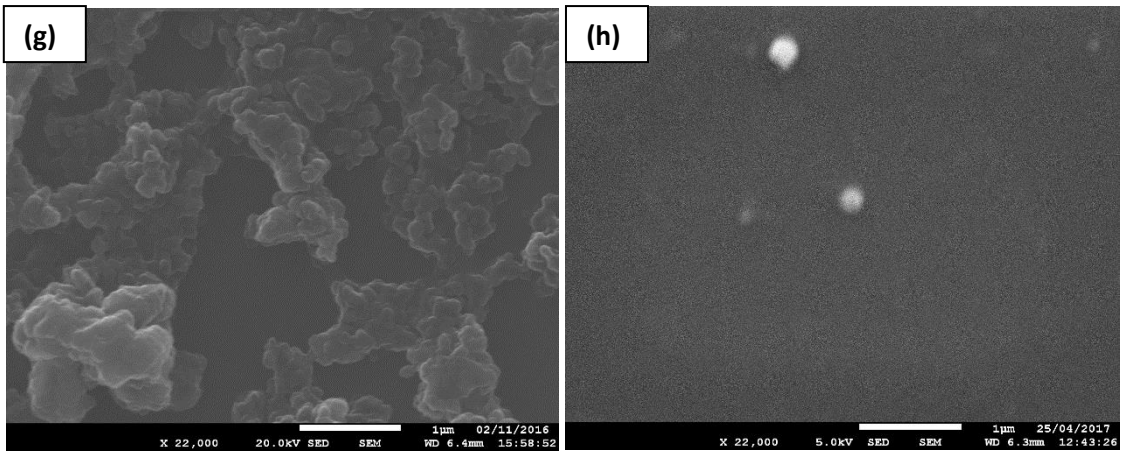

Fig 3.13 SEM images of **(a)** $Na_2SO_4.10H_2O$, **(b)** & **(c)** NanoPCM4, **(d)** NanoPCM5, **(e)** & **(f)** NanoPCM6 and **(g)** & **(h)** NanoPCM7. **(c)**, **(f)** and **(g)** were made by diluting a nanocapsules suspension x1000; all other samples were dispersions of the solid capsules after drying. Scale bars are: for **(a)** 10µm; for **(b)** – **(e)** 100nm; for **(f)** – **(h)** 1µm

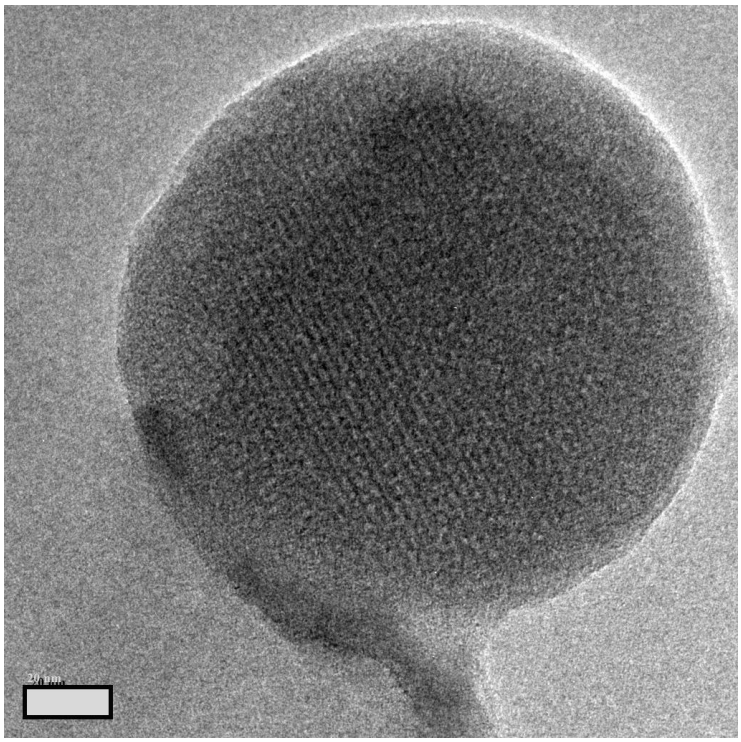

Fig 3.14 TEM image of NanoPCM4 sample with partly removed capsule shell (scale bar 20 nm).

FTIR spectra for the bulk salt hydrates and NanoPCMs is shown in Fig 3.15. Peaks for $Mg(NO_3)_2.6H_2O$ (Fig 3.15a) are described in the chemical analysis section for NanoPCMs 1-3. $Na_2SO_4.10H_2O$ (Fig 3.15b) has peaks for O-H at 3334 cm^{-1}, a mix of S-O and S=O at 1078 cm^{-1} and the SO_4^{2-} group at 613 cm^{-1}. All NanoPCMs were fabricated by identical methodology so form a similar capsule shell. PECA peaks are seen for all NanoPCMs (Fig 3.15c-f), C-H stretch at 2927 cm^{-1}, C=O at 1747 cm^{-1} and C-O ester peaks at 1249 and 1013 cm^{-1}. Only NanoPCM6 has a peak for CN at 2361 cm^{-1}, which can be explained by the presence of unreacted ECA residue in the capsule shell.

Peaks for the core material within the NanoPCMs correspond to the encapsulated salt hydrates. NanoPCM4 contains $Mg(NO_3)_2.6H_2O$, as shown by peaks a 3387 cm^{-1} for O-H, N=O bend at 1657 cm^{-1}, mix of N-O stretching and bending and N=O stretch at 1373 cm^{-1}, and NO_3^- at 827 cm^{-1}. NanoPCM5 contains $Na_2SO_4.10H_2O$, with a very small O-H peak at 3539 cm^{-1}, S-O and S=O in the broad peak at around 1121 cm^{-1} and SO_4^{2-} at 620 cm^{-1}. NanoPCM6 and 7 contain both $Mg(NO_3)_2.6H_2O$ and $Na_2SO_4.10H_2O$. They have peaks at 3259 and 3327 cm^{-1} respectively for O-H, 1651 and 1657 cm^{-1} for N=O bend, 1370 and 1373 cm^{-1} for a mix of N-O stretching and bending and N=O, 1084 cm^{-1} for S-O and S=O, and 613 cm^{-1} for SO_4^{2-}. NanoPCM6 has a small peak at 827 cm^{-1} for NO_3^-, this shifts to 830 cm^{-1} for NanoPCM7 with the increase of $Na_2SO_4.10H_2O$ in the core (described in more detail below). All FTIR signals reflect the core/shell composition of each nanocapsule sample. Deviations between wavenumbers for the bulk and nanoencapsulated crystallohydrates are due to spatial confinement effects, which influence H-bonding in the capsule core. Clearly, if a stable miniemulsion containing a salt hydrate or a mixture within the miniemulsion droplets is formed, it can be encapsulated to give the material improved thermal properties and chemical stability.

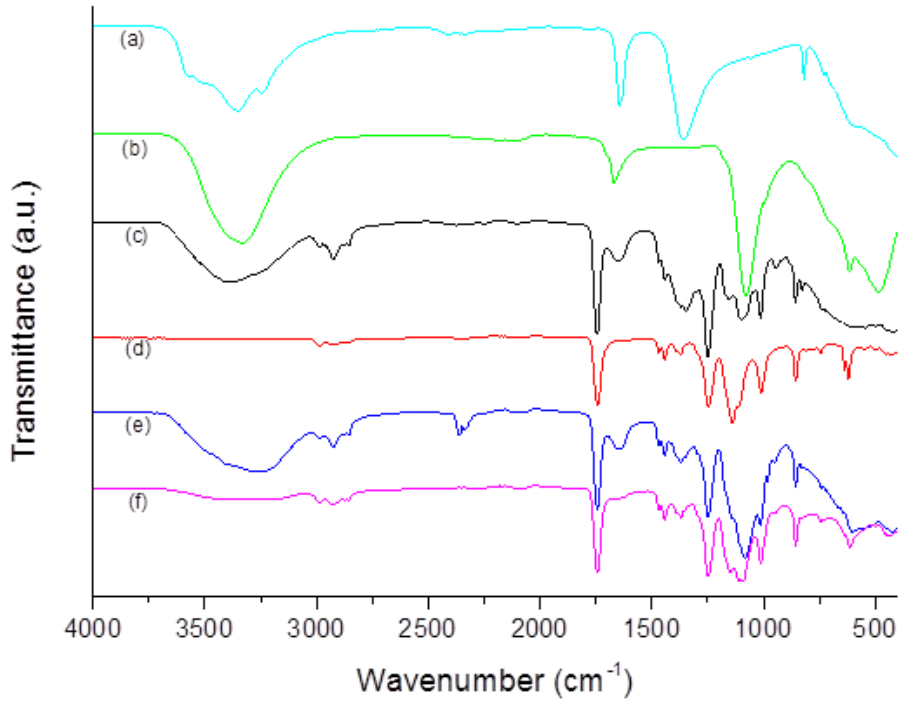

Fig 3.15 FTIR spectra for **(a)** $Mg(NO_3)_2 \cdot 6H_2O$, **(b)** $Na_2SO_4 \cdot 10H_2O$, **(c)** NanoPCM4, **(d)** NanoPCM5, **(e)** NanoPCM6 and **(f)** NanoPCM7

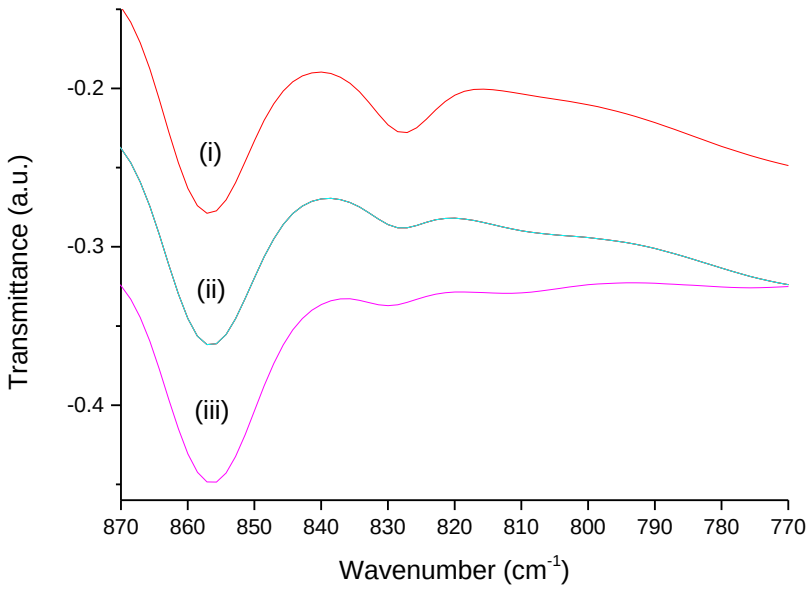

Fig 3.16 How the NO_3^- group peak is affected by core composition. NanoPCM4 **(i)** with pure $Mg(NO_3)_2.6H_2O$ and NanoPCM6 **(ii)** with 1:1 $Mg(NO_3)_2.6H_2O$:$Na_2SO_4.10H_2O$ have a peak at 827 cm^{-1}, while NanoPCM7 **(iii)** with 1:2 $Mg(NO_3)_2.6H_2O$:$Na_2SO_4.10H_2O$ in the core the peak shifts to 830 cm^{-1}

3.3.9 Spatial confinement and crystalline phase effects on the NO_3^- group wavenumber

Upon encapsulation, the NO_3^- group from $Mg(NO_3)_2.6H_2O$ is affected. In the bulk $Mg(NO_3)_2.6H_2O$ FTIR spectrum, a peak appears at 818 cm^{-1}. After encapsulation, it shifts to 827 cm^{-1}. In Fig 3.16, it can be seen that the ratio of the $Mg(NO_3)_2.6H_2O$:$Na_2SO_4.10H_2O$ also has an effect. As the amount of $Mg(NO_3)_2.6H_2O$ in the mix decreases, the size of the peak decreases due to the decrease in number of NO_3^- groups. For the 1:1 ratio, the peak remains at 827 cm^{-1}. At the eutectic ratio of 2:1, the peak shifts slightly to 830 cm^{-1}. At the eutectic ratio, a new single phase is formed which affects the bonding energies of NO_3^-, explaining this change.

3.3.10 Further Chemical Analysis

Further study was also made on the chemical composition of the NanoPCM samples, using XPS (Fig 3.17-3.19, Table 3.3). XPS confirmed the presence of all expected elements in the samples, with corresponding peaks labelled on the spectra. Values are consistent with thermal and chemical analysis. % values for C and O may be higher than expected due to the formation of carbonates. The PECA shell also chars due to the X-ray beam, which is common for polymers during XPS.

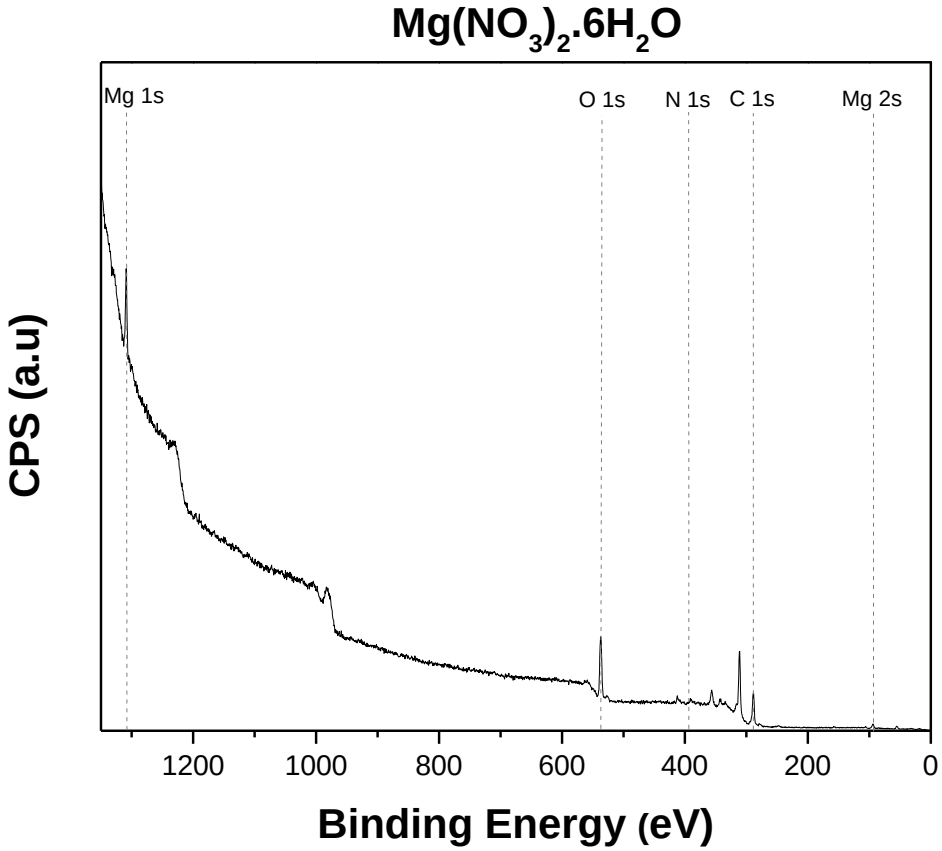

Fig 3.17 XPS spectrum for $Mg(NO_3)_2.6H_2O$

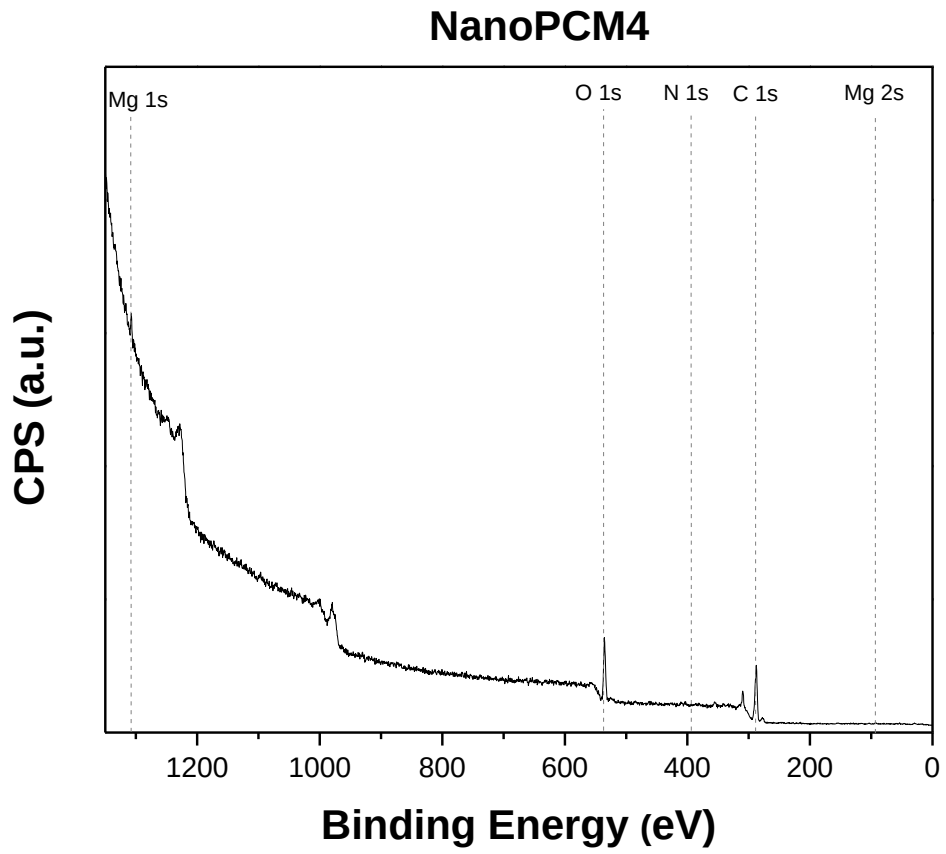

Fig 3.18 XPS spectrum for NanoPCM4

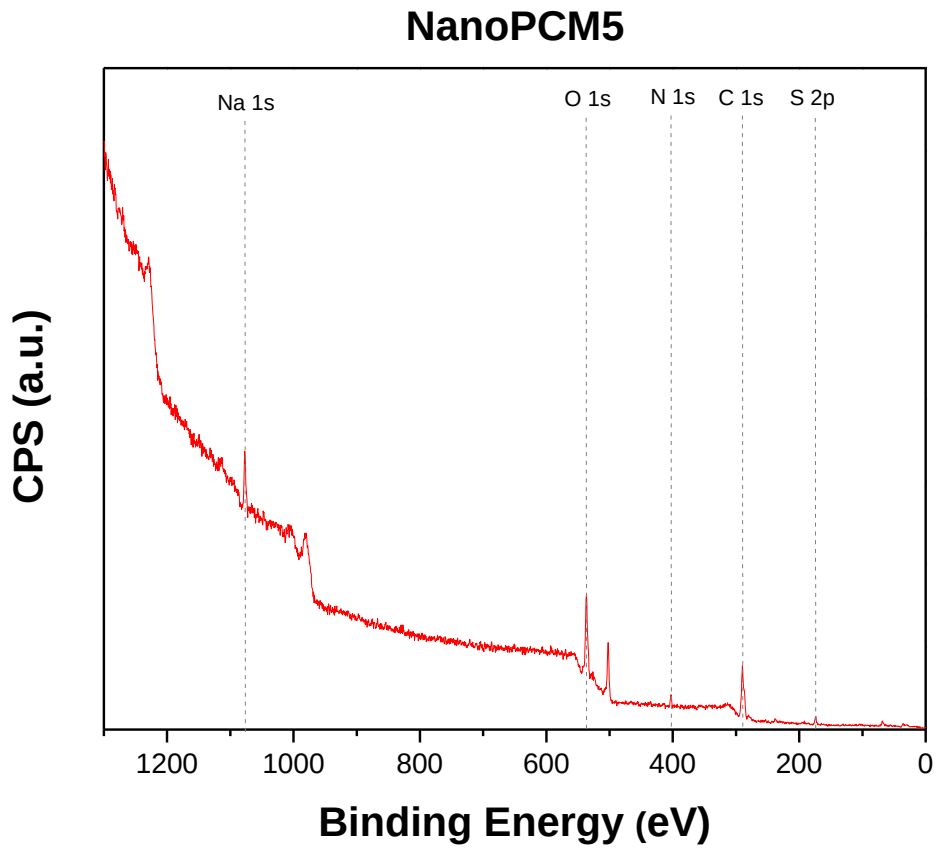

Fig 3.19 XPS spectrum for NanoPCM5

Table 3.3 Summary of XPS data.

Element	**NanoPCM4** (%wt)	**NanoPCM5** (%wt)
Mg	1.24	n/a
Na	n/a	6.30
C	77.91	63.41
O	19.40	25.42
N	1.44	3.83
S	n/a	1.03

3.3.11 Thermal analysis

TGA curves of both salt hydrates and NanoPCM4-7 are shown in Fig 3.20. Both salt hydrates display fast degradation in their pure state, starting at 40°C for $Na_2SO_4.10H_2O$ and 90°C for $Mg(NO_3)_2.6H_2O$, corresponding to their melting points – as soon as the material melts, water is free to evaporate. $Na_2SO_4.10H_2O$ loses all associated water by 120°C (55% mass), which fits nicely with the expected stoichiometric value of 55.9%. No further decomposition of the anhydrous Na_2SO_4 occurs by 600°C. $Mg(NO_3)_2.6H_2O$ showed nearly identical behaviour to the previous sample from above. It had lost 36% of its mass up to 250°C. Further mass loss occurred between 290 to 470°C due to $Mg(NO_3)_2$ decomposition. After heating to 600°C, 21% mass remains, mainly consisting of MgO.

All NanoPCMs have better thermal stability in comparison with the bulk salt hydrates, due to protection from the PECA shell. All NanoPCMs lose water up to 150°C, dependent on the quantity of free water remaining after capsule synthesis. TGA results are consistent with DSC results (see

below). NanoPCM4 loses 16% mass by 150°C, increasing the amount of $Na_2SO_4.10H_2O$ in the core reduces the amount of water loss over this temperature range. NanoPCM7 commences weight loss at a lower temperature than NanoPCM5 and 6, which is probably due to residual cyclohexane present in the sample. Mass loss is then accelerated for all samples at 150°C due to PECA disintegration, and additionally, the decomposition of magnesium nitrate into magnesium oxide. The TGA curves stabilise at 450°C, with minimal subsequent mass loss. Increasing the amount of $Na_2SO_4.10H_2O$ in the mixture increases the % mass remaining at 600°C. Remaining mass is 20% for NanoPCM4, 22% for NanoPCM6, 24% for NanoPCM7 and 29% for NanoPCM5.

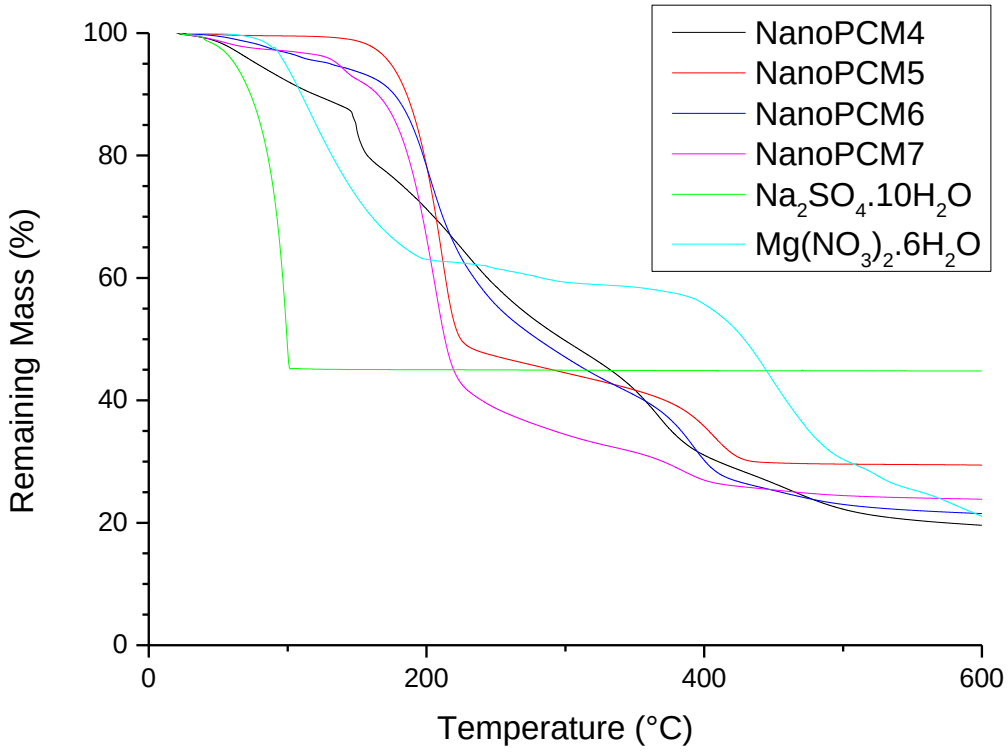

Fig 3.20 TGA curves for pure crystallohydrates and NanoPCM4-7

3.3.12 Thermal cycling stability of single crystallohydrate capsules

DSC thermograms of bulk salt hydrates and NanoPCM4 and 5 are shown in Fig 3.21. The pure crystallohydrates show poor thermal stability, decomposing after only 10 cycles. $Mg(NO_3)_2.6H_2O$ again had a similar thermogram to the sample previously shown, albeit with a wider melting point with $T_{M,\ onset}$ = 83°C and T_M = 93°C. The broad peak can be explained due to uneven sized crystallohydrate particles. Latent heat is 160.4 $J{\cdot}g^{-1}$. These values are similar to literature values of 89°C and 162.8 $J{\cdot}g^{-1}$. The main freezing peak has $T_{F,\ onset}$ = 60°C, T_F = 55°C. Supercooling is very large at 38°C. The bulk $Na_2SO_4.10H_2O$ has two endothermic peaks. The first has $T_{M,\ onset}$ = -2°C and T_M = 3°C, which can be assigned to either ice melting or a $Na_2SO_4.7H_2O/Na_2SO_4.10H_2O$ transition. The second has $T_{M,\ onset}$ = 26°C and T_M = 32°C, the solid-liquid transition for $Na_2SO_4.10H_2O$, which had a latent heat of 228.1 $J{\cdot}g^{-1}$. From literature[43], these values are 32.4°C and 254 $J{\cdot}g^{-1}$. The reverse exothermic

processes were found at $T_{F,\ onset}$ = 13°C and T_F = 4°C for the $Na_2SO_4.10H_2O$ liquid to solid transition, and another small peak at T_F = -11°C due to $Na_2SO_4.7H_2O$ and water crystallisation. $Na_2SO_4.10H_2O$ therefore also has a large supercooling of 28°C. The rapid decay in latent heat storage of each of the bulk crystallohydrates is due to dehydration, occurring after only 10 cycles. Signals are lost completely once the salts dehydrate to form anhydrous $Mg(NO_3)_2$ and Na_2SO_4, along with lower hydrates – most likely $Mg(NO_3)_2.2H_2O$ and $Na_2SO_4.7H_2O$. This rapid decaying of the advantageous thermal uptake and release processes, along with the large degree of supercooling, shows the inherent problems with using bulk salt hydrates in practical applications. Once additional factors such as corrosion are taken into account, the use of bulk salt hydrates becomes even more difficult.

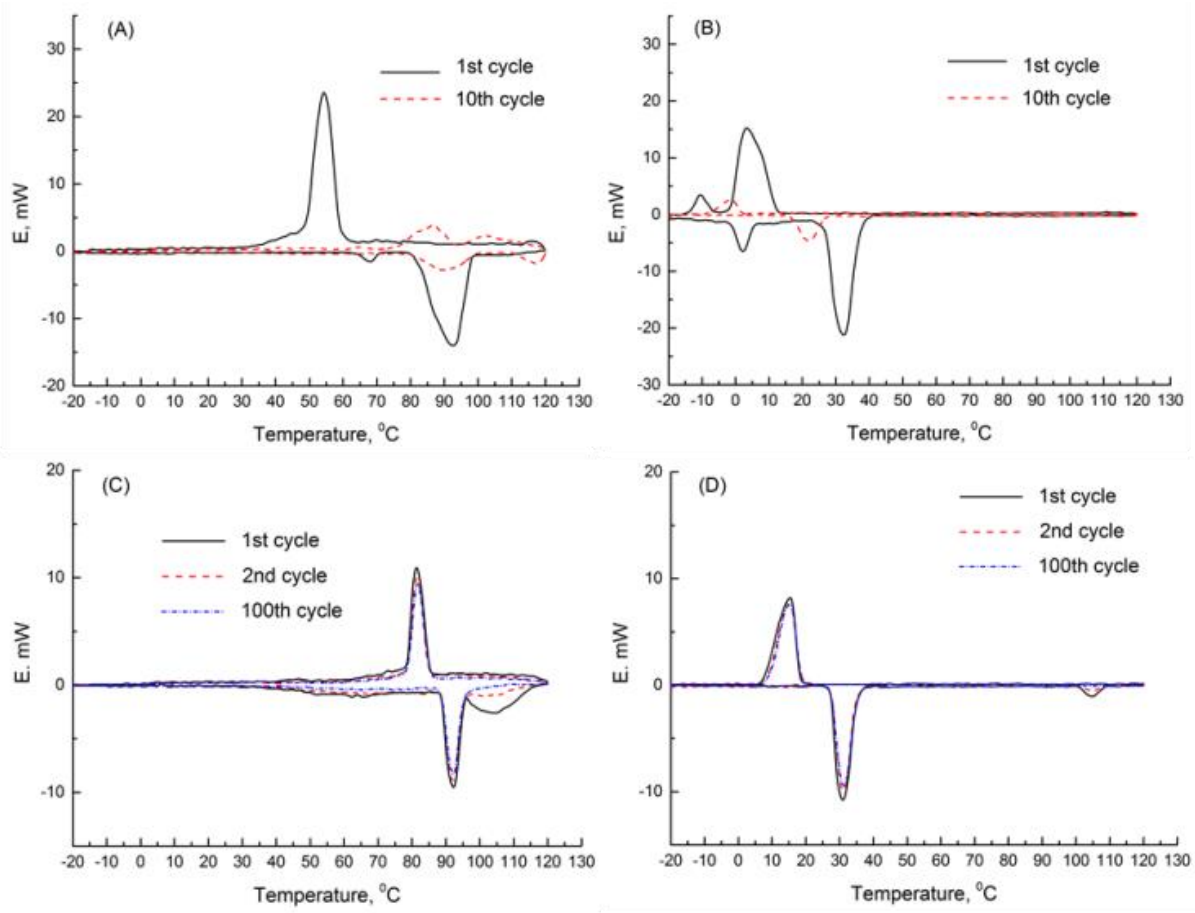

Fig 3.21 DSC thermograms for **(A)** bulk $Mg(NO_3)_2{\cdot}6H_2O$, **(B)** bulk $Na_2SO_4{\cdot}10H_2O$, **(C)** NanoPCM4, **(D)** NanoPCM5.

Encapsulation of each of the salt hydrates greatly increases their stability. DSC curves of NanoPCM4 and 5, containing $Mg(NO_3)_2.6H_2O$ and $Na_2SO_4.10H_2O$ respectively, are shown in Fig 3.21c and d. Both samples avoid thermal decomposition during thermal cycling. NanoPCM4 has a latent heat of 88.4 $J{\cdot}g^{-1}$ after 100 cycles, with $T_{M,\ onset}$ = 88°C, T_M = 92°C, $T_{F,\ onset}$ = 86°C and T_F = 82°C. Supercooling is reduced to 10°C, while $T_{M,\ onset}$ and $T_{F,\ onset}$ differ by only 2°C. The peak is sharper than the bulk $Mg(NO_3)_2.6H_2O$, due to increased heat transfer area of nanocapsules. On the first cycle, there is also a broad peak from approximately 100-110°C, attributed to the evaporation of excess water during synthesis. This peak disappears after 3 cycles. Water loss may also occur from any capsules with damaged shells. Thermal storage and release properties are almost unchanged after 100 cycles between -20 and 120°C, latent heat of melting decreases by only 3%.

NanoPCM5 also has highly stable thermal characteristics. The first DSC cycle has $T_{M,\ onset}$ = 26°C, T_M = 32°C, $T_{F,\ onset}$ = 21°C and T_F = 17°C. There is also a small endothermic peak attributed to water evaporation at 105°C. The DSC signals from other Na_2SO_4 phases that were present in the thermogram for bulk $Na_2SO_4.10H_2O$ have disappeared. Excess water added to the core material ensures it remains fully hydrated, preventing changes in T_M and latent heat. The latent heat value is 138.6 $J{\cdot}g^{-1}$ after 100 thermal cycles with only a 2% decrease from the first cycle. Supercooling is reduced to 15°C, the difference between the $T_{M,\ onset}$ and $T_{F,\ onset}$ is 5°C.

Both NanoPCM4 and 5 show increased thermal stability and decreased supercooling in comparison with the bulk salt hydrates, along with the stabilisation of the desired phases to keep T_M constant. Incongruent melting is further prevented by the capsule shell stopping water exchange with the external environment. EE is 54% for NanoPCM4 containing $Mg(NO_3)_2.6H_2O$, and 61% for NanoPCM5 containing $Na_2SO_4.10H_2O$. These results demonstrate the universality of this simple procedure to enhance the properties of valuable salt hydrate PCMs for heat storage.

3.3.13 Additive mixtures of NanoPCM4 and 5

After demonstrating universality of the PECA encapsulation procedure by encapsulating multiple PCMs, it is also necessary to demonstrate how they might be used in practical application. Cascaded latent heat storage (CLHS) is utilised to not only give heat storage abilities over a larger temperature range with good efficiency, but also to improve melting characteristics. However, CLHS has only been used at high temperatures, usually in association with energy storage for CSP[44–46]. We made additive mixtures of the capsules containing single salt hydrates (NanoPCM4 and 5) to test a multi-temperature CLHS system at low temperature <100°C. The ratios used were 2:1, 1:1 and 1:2 to test the effect on T_M and latent heat.

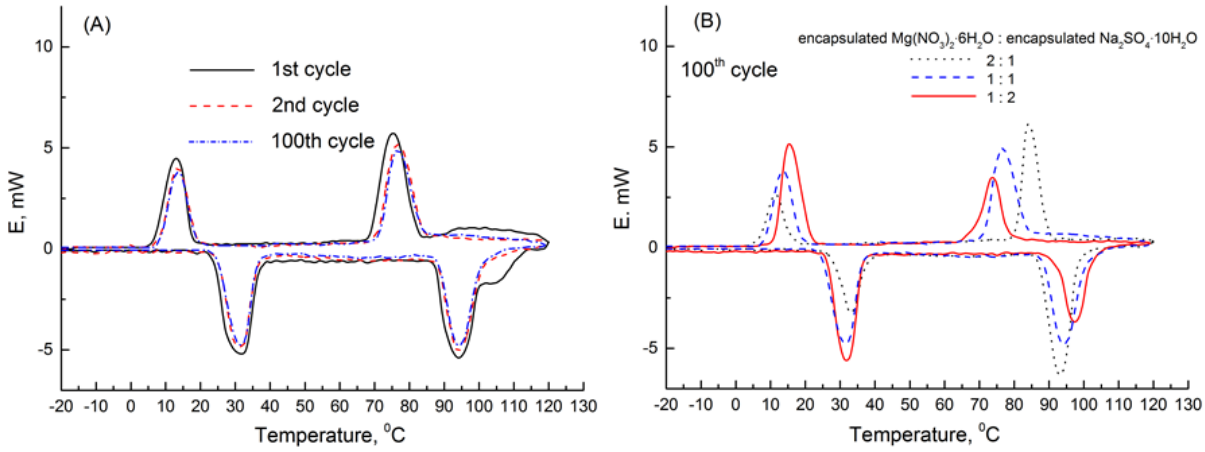

Fig 3.22 DSC thermograms for **(A)** 1:1 NanoPCM4:NanoPCM5 ratio at different cycles, **(B)** different NanoPCM4:NanoPCM5 ratio on 100th heat uptake/release cycle.

The 1:1 mixture of NanoPCM4:NanoPCM5 exhibited additive effects of each encapsulated salt hydrate (Fig 3.22a). The first cycle demonstrated the $Na_2SO_4.10H_2O$ phase transitions at $T_{M,onset}$ =24°C, T_M = 32°C, $T_{F,onset}$ = 19°C and T_F = 13°C. $Mg(NO_3)_2.6H_2O$ phase changes were also evident at $T_{M,onset}$ =87°C, T_M = 94°C, $T_{F,onset}$ = 84°C and T_F = 75°C. There is also a peak at 100-110°C related to the evaporation of any free water left after encapsulation, this peak vanishes on the 2nd cycle. No considerable changes to the thermogram appear after the 2nd cycle and the 1:1 mixture remains stable over at least 100 cycles. Latent heat was 67.2 J·g^{-1} for $Na_2SO_4.10H_2O$ and 44.1 J·g^{-1} for $Mg(NO_3)_2.6H_2O$. Supercooling for both salt hydrates in the mixture was 19°C, which is considerably higher than the single capsule samples for both NanoPCM4 (10°C, $Mg(NO_3)_2.6H_2O$ core) and NanoPCM5 (15°C, $Na_2SO_4.10H_2O$ core). Clearly heat transfer to the nanocapsules is reduced, giving higher supercooling values.

Supercooling is affected as the ratio of each NanoPCM changes. From Fig 3.22b, it can be observed that changing the PCM mixture ratio is accompanied by a change in latent heat values for both NanoPCM4 and 5. Decreasing the quantity of any nanocapsules component in the mixture leads to

an increase in supercooling for the minor component and a decrease in supercooling for the major component. A 2:1 mixture of NanoPCM4:NanoPCM5 resulted in T_M = 33°C and T_F = 12°C for $Na_2SO_4.10H_2O$; and T_M = 93°C and T_F = 84°C for $Mg(NO_3)_2.6H_2O$. Supercooling is therefore decreased in $Mg(NO_3)_2.6H_2O$ to 9°C and increased for $Na_2SO_4.10H_2O$ to 21°C. Latent heat values for the 2:1 mixture are 59.0 $J{\cdot}g^{-1}$:46.1 $J{\cdot}g^{-1}$ for NanoPCM4:NanoPCM5 respectively.

For the 1:2 mixture of NanoPCM4:NanoPCM5, the opposite effect occurs. Phase transitions for $Mg(NO_3)_2.6H_2O$ are T_M = 97°C and T_F = 74°C; while for $Na_2SO_4.10H_2O$ they are T_M = 32°C and T_F = 15°C. Supercooling for the encapsulated salt hydrates is therefore 23°C for $Mg(NO_3)_2.6H_2O$ and 17°C for $Na_2SO_4.10H_2O$. The latent heat also changed in accordance with the proportion of each crystallohydrate in the mixture, being 29.1 $J{\cdot}g^{-1}$:93.1 $J{\cdot}g^{-1}$ for NanoPCM4:NanoPCM5 respectively. In all additive mixtures, latent heat values are consistent with the ratio of each NanoPCM.

Supercooling is caused by low thermal conductivity of the PCMs during melting and freezing, and the changes in supercooling in PCM mixtures can be rationalised by taking this into account. The additive mixtures of salt hydrate loaded nanocapsules enhance thermoinsulating properties during each phase transition process, where one encapsulated component can reduce thermal transfer to the second component during phase transition. NanoPCM4 does not absorb heat during the phase transition of $Na_2SO_4.10H_2O$ in the NanoPCM5 core. Hence, NanoPCM4 acts as a heat insulator for NanoPCM5 capsules at 10-35°C. An increased amount of NanoPCM4 in the mixture causes a greater degree of supercooling in NanoPCM5. Likewise, during the phase transition of $Mg(NO_3)_2.6H_2O$ in the NanoPCM4 core at 70-100°C, the $Na_2SO_4.10H_2O$ inside NanoPCM5 capsules remains liquid and not active for heat transfer. Supercooling for NanoPCM4 increases with NanoPCM5 content. This is the most evident explanation of the supercooling effect observed in the additive mixtures of energy storage nanocapsules. Contrary to the additive mixtures, when NanoPCM4 and 5 are used individually, the single crystallohydrate cores undergo phase transition over the same temperature range across the whole sample and remain thermally active for heat transfer.

The magnitude of the change in supercooling can also be rationalised. When doubling the amount of the other component, T_M and T_F values for $Mg(NO_3)_2.6H_2O$ are more heavily affected than those for $Na_2SO_4.10H_2O$. When the ratio of NanoPCM4:NanoPCM5 is 1:2, the T_M and T_F for $Mg(NO_3)_2.6H_2O$ are +4°C and -10°C respectively, compared with when the ratio is 2:1. For $Na_2SO_4.10H_2O$, T_M and T_F are +1°C and -3°C when the ratio is 2:1 compared with when the ratio is 1:2. This can be rationalised by considering the phases of each component. During any $Mg(NO_3)_2.6H_2O$ phase change, $Na_2SO_4.10H_2O$ will necessarily be in the liquid phase. Liquid phases have lower thermal conductivity than the solid phase. Therefore, heat transfer from the liquid core NanoPCM5 capsules into the solid core NanoPCM4 capsules will be poor, and leads to lower amount of heat uptake and a higher T_M for NanoPCM4. During melting of the NanoPCM4 core, the decreased amount of heat uptake by NanoPCM5 means that NanoPCM4 will absorb more heat energy which causes it to remain in the liquid phase and decrease T_F.

Likewise, during any $Na_2SO_4.10H_2O$ phase transition, $Mg(NO_3)_2.6H_2O$ will be in the solid phase, therefore giving increased heat transfer to the $Na_2SO_4.10H_2O$ during melting. During freezing, more heat energy will flow to NanoPCM4 rather than NanoPCM5, allowing more rapid temperature decrease in NanoPCM5. T_M and T_F values for NanoPCM5 are therefore not as heavily affected. These supercooling effects must be accounted for when designing a CLHS system for encapsulated salt hydrates. Supercooling may be reduced by the incorporation of conductive particles into the matrix of the NanoPCMs.

3.3.14 Salt hydrate mixtures and eutectics

An interesting phenomenon amongst salt hydrates is that of eutectics. As salt hydrates are mixed, their T_M is adjusted, due to inhibition of crystallisation processes in each component[47]. The melting of the first component in the mixture initiates dissolution of components with higher transition

temperatures due to the liberation of excess non-bounded water molecules[48]. The mixture ratio with the lowest possible T_M is known as a eutectic. At this ratio, crystallohydrates reach equilibrated conditions, giving a defined T_M lower than that of all single components[49], while single phases of the individual hydrates disappear[49,50]. This effect is potentially extremely useful in tailoring the T_M to suit potential applications. It must be noted however that mixtures at ratios other than the eutectic mixture will have reduced latent heat due to the release of water. The direct application of eutectics in thermal energy storage has been hindered by similar shortcomings to single salt hydrates, but to a greater extent. High temperature salt eutectics have been investigated for CSP storage, although these are currently used as sensible heat storage materials. Salt hydrate eutectics are not prominent in the literature and not fully understood. Nagano *et al*[51] investigated a mix of magnesium nitrate hexahydrate and magnesium chloride hexahydrate, being able to modulate the T_M between 60-90°C. These eutectic mixtures have great potential in practical applications due to their T_Ms which can be as low as <30°C, rare in pure salt hydrates, and high latent heat.

$Mg(NO_3)_2.6H_2O$ and $Na_2SO_4.10H_2O$ were mixed by simply blending them together, causing a reaction and some melting of the crystallohydrates. The mixtures were then left in the freezer to form a solid. SEM images of the mixtures at 2:1, 1:1 and 1:2 ratios of $Mg(NO_3)_2.6H_2O$:$Na_2SO_4.10H_2O$ are shown in Fig 3.23. The mixtures form micrometre sized block formations, in contrast to the flakes and sheets seen in the single crystallohydrates. Non-eutectic ratios (1:1, 2:1) in Fig 3.23a-b and e-f respectively form cubic blocks of approximately 1-10µm in size. The blocks do not have uniform sizes and appear to form randomly, suggesting many phases are present, as seen in DSC data for the 1:1 mixture. The eutectic 1:2 ratio in Fig 3.23c and d also forms similar blocks, but these are mostly smaller – many are 1µm or below. This suggests a more uniform phase has formed, which gives rise to the more consistent behaviour seen in its thermal properties.

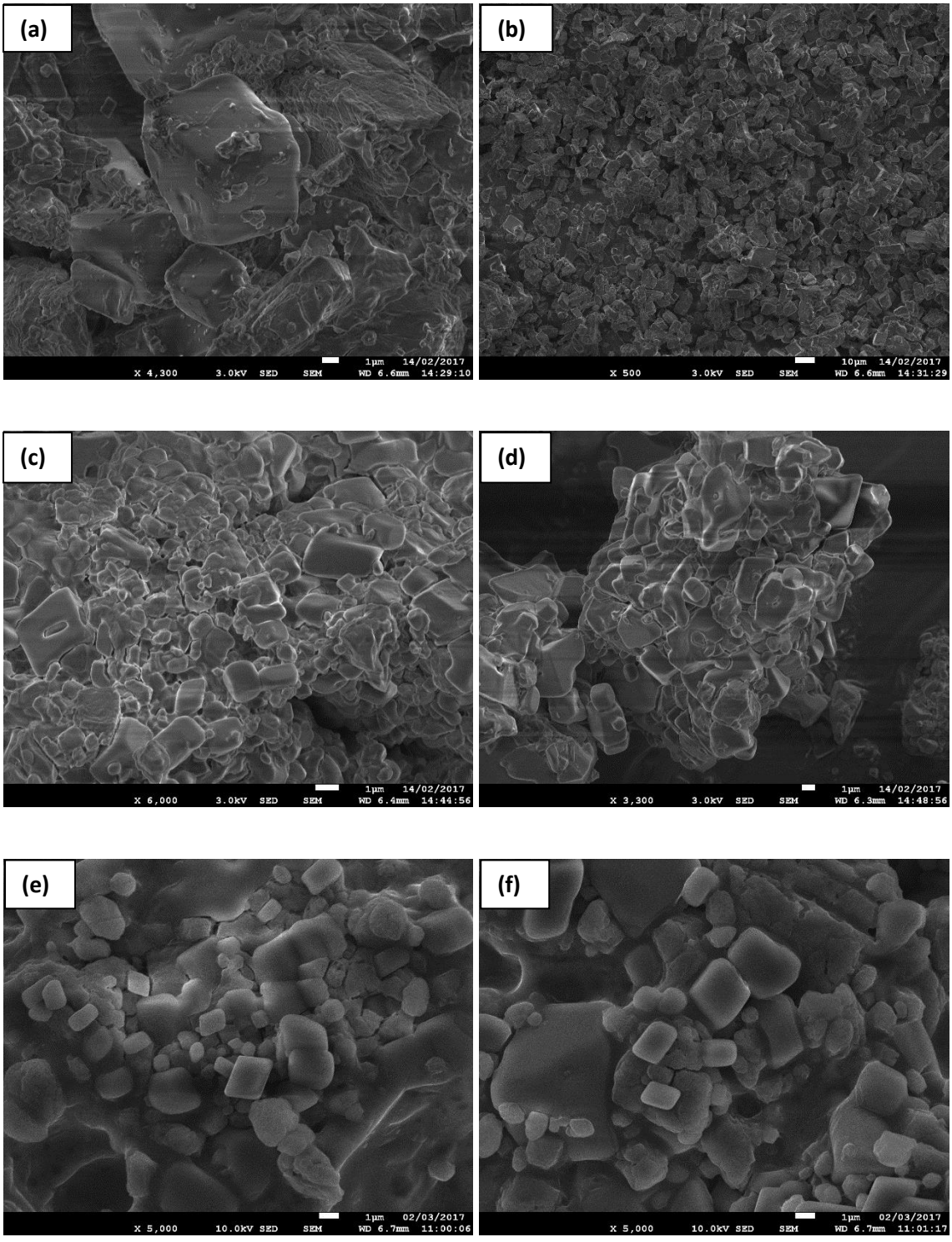

Fig 3.23 SEM images of **(a)** & **(b)** 1:1 mixture $Mg(NO_3)_2.6H_2O$:$Na_2SO_4.10H_2O$, **(c)** & **(d)**, 1:2 eutectic mixture and **(e)** & **(f)** 2:1 mixture

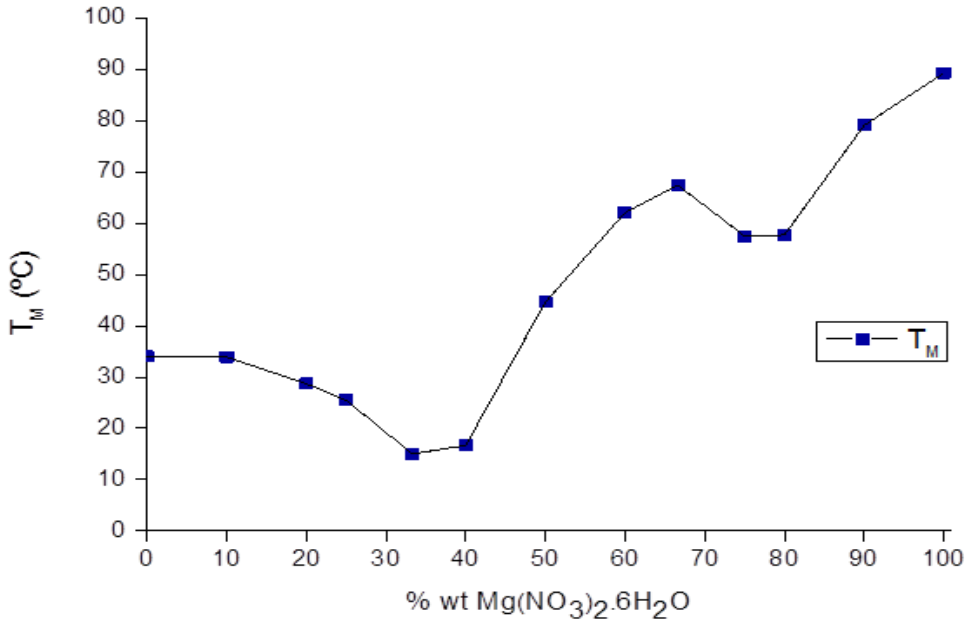

Fig 3.24 Influence of the $Mg(NO_3)_2 \cdot 6H_2O$:$Na_2SO_4 \cdot 10H_2O$ wt.% ratio on melting temperature of the corresponding mixture.

DSC results show how T_M of the non-encapsulated bulk salt hydrates is influenced by ratio, shown in Fig 3.24. T_Ms for both pure salt hydrates were taken from Zalba *et al*[43] as these values are widely accepted by researchers, and our values differed by several degrees. All mixtures give a lower T_M than pure $Mg(NO_3)_2.6H_2O$. At 100 %wt $Na_2SO_4.10H_2O$, the T_M is 32°C. Addition of $Mg(NO_3)_2.6H_2O$ causes this to decrease until the eutectic point (T_M = 15.0°C) is reached at 33.3 %wt $Mg(NO_3)_2.6H_2O$. The T_M increases sharply from 40 %wt to 66.6 %wt $Mg(NO_3)_2.6H_2O$ (16.7 to 67.4°C). The T_M then decreases again at 75 and 80 %wt $Mg(NO_3)_2.6H_2O$ (57.5 and 57.7°C) exhibiting a pseudo-eutectic ratio, before again increasing at 90 %wt $Mg(NO_3)_2.6H_2O$ (79.1°C). A similar 'double bell' shaped curve for salt hydrate mixtures has been observed using $Mg(NO_3)_2.6H_2O$ and aluminium nitrate nonahydrate[52]. The results show a wide range of T_Ms can be developed using only two crystallohydrates. It is possible to develop mixtures of three or more salts, although clearly this will

lead to large amounts of research needing to be done. Developing a molecular modelling strategy to estimate how mixtures will affect T_M would be of great benefit.

3.3.15 Encapsulated salt hydrate mixtures and eutectics

Encapsulation of multiple salts inside the same capsule was of interest to see if eutectic character could be maintained on a nanoscale level. It also provides an interesting contrast in behaviour with the additive mixtures of single salt hydrate cored NanoPCMs. Methodology to obtain the capsules is described in detail in Fig 3.25, the multi-salt hydrate core is made in step d. The eutectic blend of 1:2 $Mg(NO_3)_2.6H_2O$:$Na_2SO_4.10H_2O$ (T_M = 15.0°C, NanoPCM7) was chosen along with the 1:1 ratio (T_M = 45.5°C, NanoPCM6) to observe behaviour of a non-eutectic ratio.

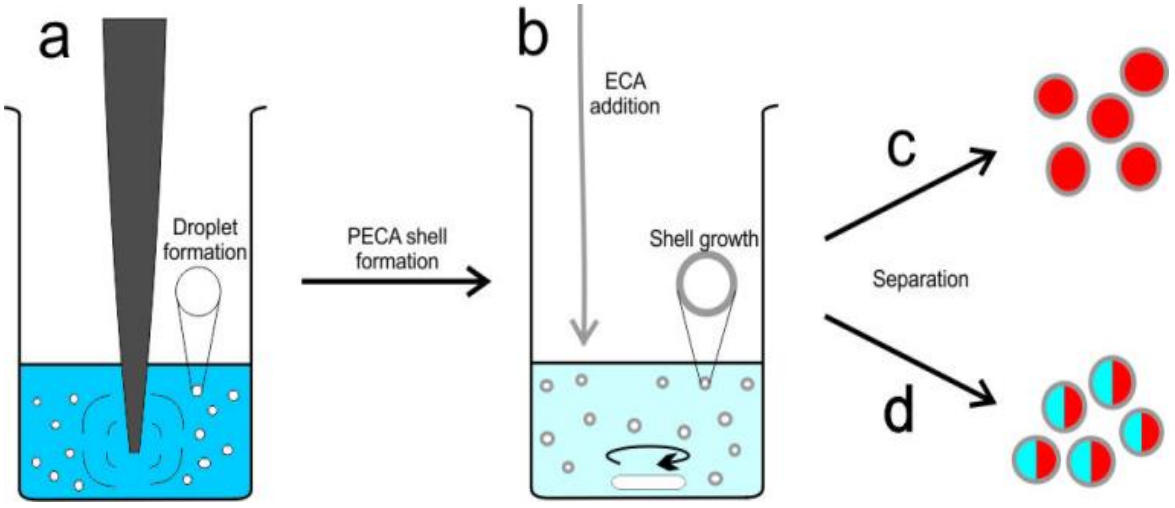

Fig 3.25 Formation of salt hydrate loaded capsules. **(a)** macroemulsion sheared by sonication to form inverse miniemulsion. **(b)** ECA dissolved in chloroform dropped in to form the PECA shell around aqueous phase. Depending on aqueous phase, nanocapsules are fabricated with **(c)** single salt hydrate core or **(d)** salt hydrate mixture core.

DSC measurements were obtained for these mixtures in both their bulk non-encapsulated and encapsulated forms. Both bulk crystallohydrates are not stable during prolonged heat uptake and release, with signals by the 10th cycle being almost negligible. During their first cycle, different thermal properties arise. The 1:1 ratio of $Mg(NO_3)_2.6H_2O$:$Na_2SO_4.10H_2O$ displays 3 peaks upon heating (Fig 3.26a). The first peak around 0°C can be assigned to the melting of free water. The other two peaks clearly show the formation of multiple crystallohydrate phases. These are formed during crystallisation processes where an excess of water for the higher T_M crystallohydrate and a water deficit for the phases with lower transition temperatures may occur. This can lead to the formation of numerous crystallohydrate phases in non-equilibrated conditions to each other and their weight balance may alter in each melting/freezing cycle. A sharp peak appears at 45.2°C and a broad peak at 67.1°C is also present. Compared to the data in Fig 3.24, these phases show character from both the 1:1 ratio and 2:1 ratio of $Mg(NO_3)_2.6H_2O$:$Na_2SO_4.10H_2O$. A broad freezing signal with a peak at 4.3°C is due to the incongruent nature of the mixture as well as water loss during thermal cycling between

-20 to 120°C. Latent heat capacity of the 1:1 mixture is 103.3 $J \cdot g^{-1}$, which is lower than the additive sum of the crystallohydrates in the mixture (194.3 $J \cdot g^{-1}$).

The 1:2 mixture of $Mg(NO_3)_2.6H_2O$:$Na_2SO_4.10H_2O$ has only one endothermic peak, melting at 15.9°C (Fig 3.26b). A single eutectic phase has formed, with high latent heat of 189.3 $J \cdot g^{-1}$, almost equal to the additive sum of crystallohydrates in the mixture (205.5 $J \cdot g^{-1}$). The high latent heat can further be rationalised by taking into account the possibility of additional thermochemical heat[48]. The shoulder of the peak until approximately 45°C is most likely due to excess water. The eutectic mixture also has a more defined freezing point than the 1:1 mixture, with a T_F of -11.4°C. Supercooling for the eutectic is therefore 27.1°C, and the latent heat is not stable during prolonged thermal cycling.

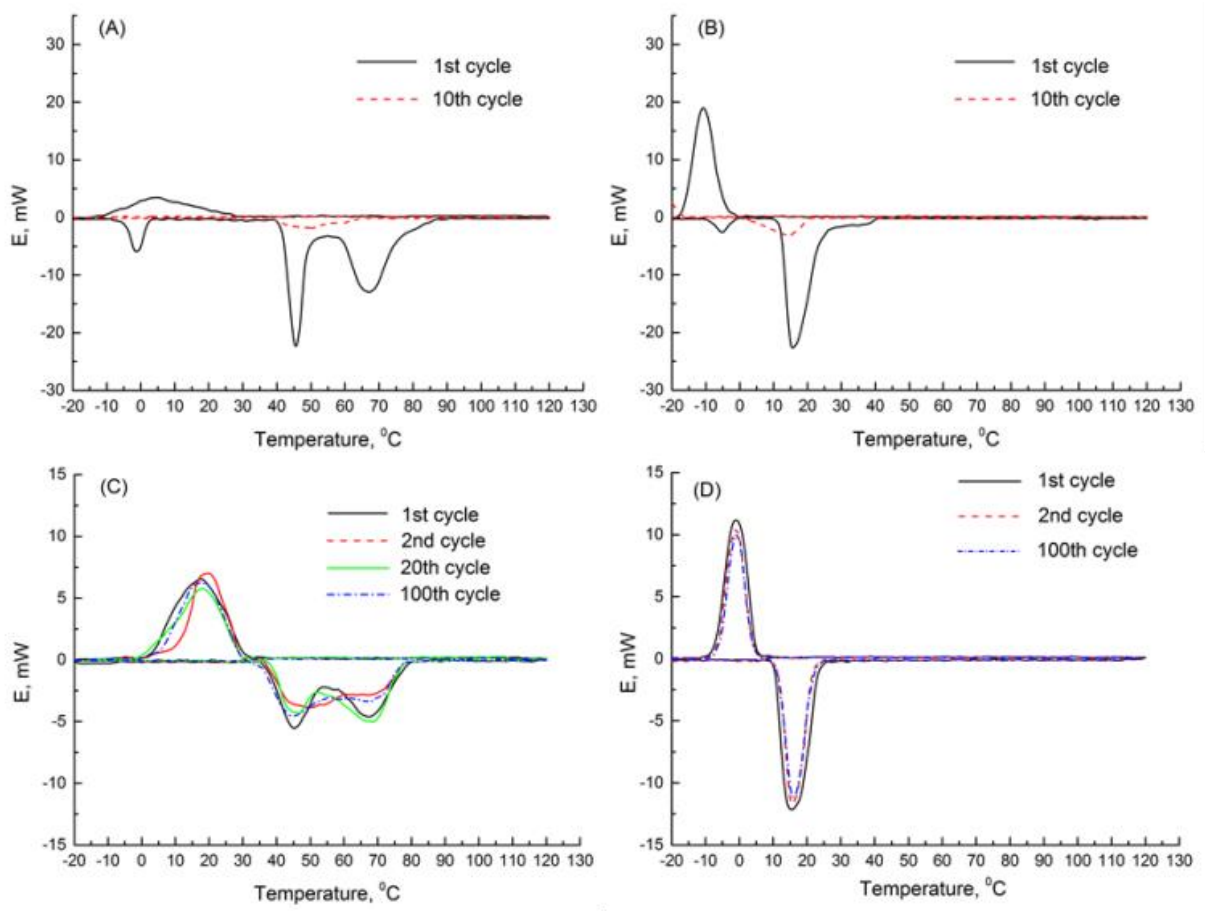

Fig 3.26 DSC thermograms for **(A)** 1:1 wt.% $Mg(NO_3)_2{\cdot}6H_2O$:$Na_2SO_4{\cdot}10H_2O$ bulk mixture, **(B)** 1:2 wt.% $Mg(NO_3)_2{\cdot}6H_2O$:$Na_2SO_4{\cdot}10H_2O$ bulk mixture, encapsulated 1:1 wt.% $Mg(NO_3)_2{\cdot}6H_2O$:$Na_2SO_4{\cdot}10H_2O$ (**(C)**, NanoPCM6) and encapsulated 1:2 wt.% $Mg(NO_3)_2{\cdot}6H_2O$:$Na_2SO_4{\cdot}10H_2O$ (**(D)**, NanoPCM7).

Encapsulation of each of the mixtures prevents loss of water during prolonged thermal cycling and reduces supercooling. NanoPCM6 (encapsulated 1:1 $Mg(NO_3)_2.6H_2O$:$Na_2SO_4.10H_2O$ core) displays numerous phases during its melting cycle (Fig 3.26c), due to the same crystallisation processes described for the bulk 1:1 mixture. During heating, two endothermic peaks appear at 45 and 67°C, and one broad peak appears during crystallisation at around 3°C. Transition temperatures are not stable and may change during any of the thermal cycles, being difficult to predict. This behaviour is caused by the multiple crystallohydrate phases in the capsule core, which have an uncertain nature. The ratio of the phases is dependent on stochastic nucleation processes. Despite this non-ideal

behaviour, the mixture still has large peaks for both melting and freezing after 100 cycles, once again showing the benefits of encapsulation.

NanoPCM7 (encapsulated eutectic 1:2 $Mg(NO_3)_2.6H_2O$:$Na_2SO_4.10H_2O$ ratio) again behaves differently, similar to the bulk mixtures (Fig 3.26d). It has one well defined transition temperature for both endothermic and exothermic processes, with $T_{M,\ onset}$ = 9.3°C, T_M = 15.4°C, $T_{F,\ onset}$ = 6.8°C and T_F = -1.1°C. Supercooling is therefore reduced to 16.5°C, 10.6°C lower than the supercooling inherent in the non-encapsulated eutectic. Difference between $T_{M,\ onset}$ and $T_{F,\ onset}$ is only 2.5°C. Like the other nanoencapsulated salt hydrates, NanoPCM7 is stable over 100+ thermal cycles and has a latent heat of 126.8 $J{\cdot}g^{-1}$. Encapsulation efficiency is 67%. The effect of nanoencapsulation on salt hydrate mixtures is similar to the effects on single crystallohydrates, producing chemically and thermally stable energy storage materials with boosted heat transfer properties. A summary of thermal parameters for the NanoPCMs is shown in Table 3.4.

Table 3.4 Thermal properties of NanoPCMs.

Sample	T_M (°C)	T_F (°C)	Supercooling (°C)	ΔH (J·g^{-1})	Encapsulation Efficiency
NanoPCM4	92	82	10	88.4	54%
NanoPCM5	32	17	15	138.6	61%
NanoPCM6*	N/A	N/A	N/A	N/A	N/A
NanoPCM7	15.4	-1.1	16.5	126.8	67%

*Data for NanoPCM6 is not available due to the incongruent nature of the melting and crystallisation processes in the mixed phases of the capsule core forming unstable phases at each cycle, see Fig. 8c.

3.3.16 Chemical stability of NanoPCMs

Clearly, NanoPCMs encapsulated in a PECA shell display excellent thermal conductivity far superior to the bulk material. Indeed, to the best of our knowledge, these are the most stable encapsulated salt hydrates found in the literature[53]. In order to further prove chemical stability of the capsules, all were subjected to FTIR analysis after 100 thermal cycles, spectra are shown in Fig 3.27. The thermally cycled NanoPCMs have largely identical spectra to those before cycling, with no peak shifting. The only minor differences are in the intensities of the peaks. NanoPCM6 has the most prominent differences, with the peaks at 2361 and 1651 cm^{-1} having reduced intensity. The FTIR results show that the shell and core materials of the NanoPCMs are chemically stable during the 100 thermal cycles from -20 to 120°C, which is of great benefit to energy storage nanocapsules.

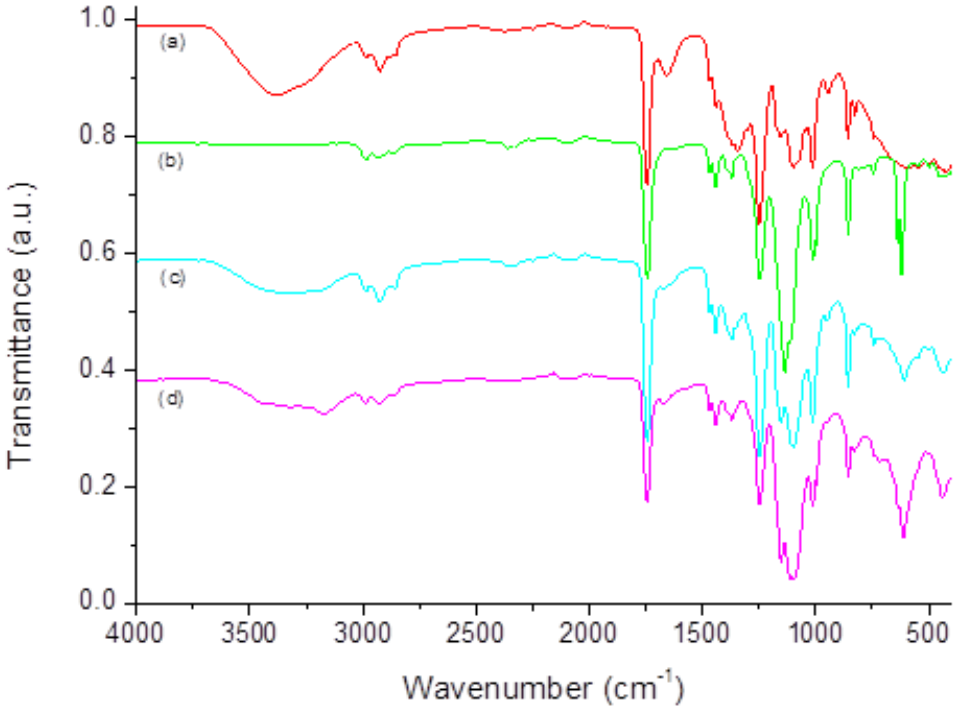

Fig 3.27 FTIR spectra for **(a)** NanoPCM1, **(b)** NanoPCM2, **(c)** NanoPCM3 and **(d)** NanoPCM4 samples after 100 DSC thermal cycles.

3.3.17 Capsule reproducibility

Clearly for any industrial application, reliable methodology is paramount to obtain products with consistently beneficial properties. After remaking NanoPCMs 3-7, properties were retested. NanoPCM3 and 4 had the same synthesis, and all chemical and thermal properties were measured. NanoPCMs 5-7 were remade and retested for their chemical structure by FTIR, shown in Fig 3.28.

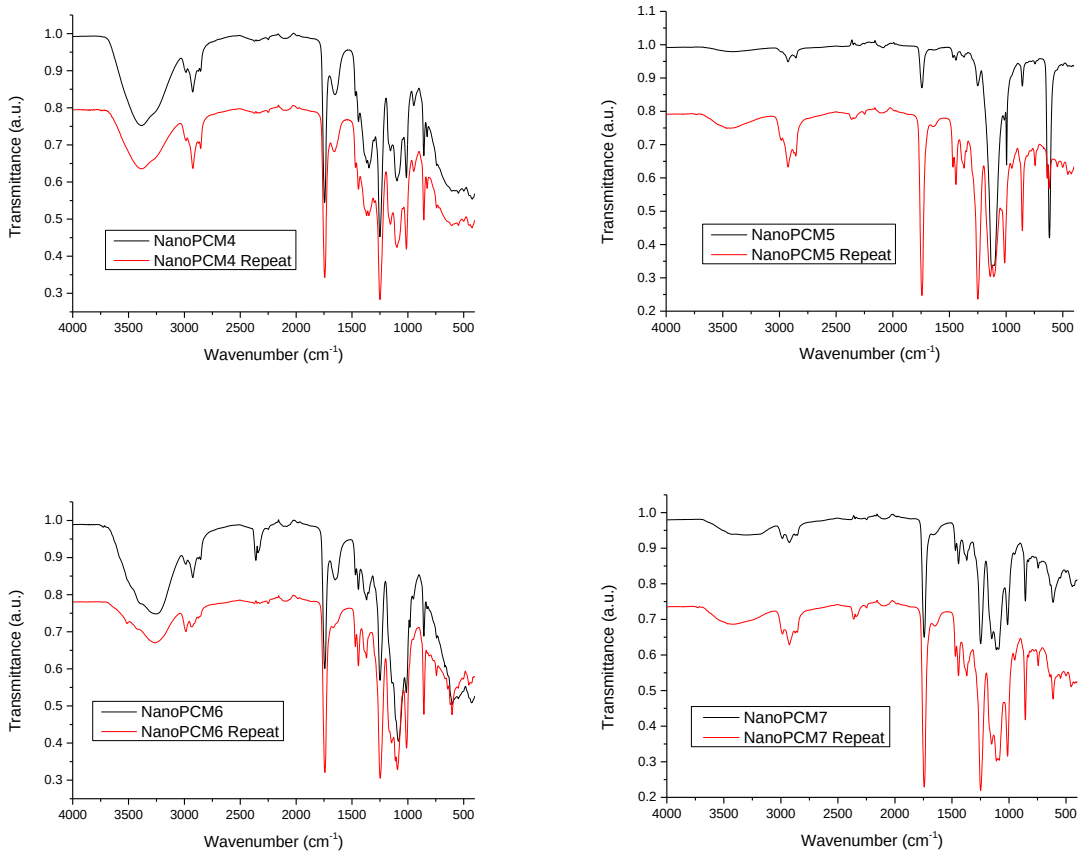

Fig 3.28 FTIR spectra from the different batches of the PCM-loaded capsules demonstrating the reproducibility of crystallohydrate encapsulation methodology

As can be seen, all spectra are nearly identical, with the only difference being the intensities of the peaks. No peak shifting occurs. NanoPCM6 contains a CN peak indicating ECA residue was present, however for the repeat this peak was eliminated due to more thorough washing.

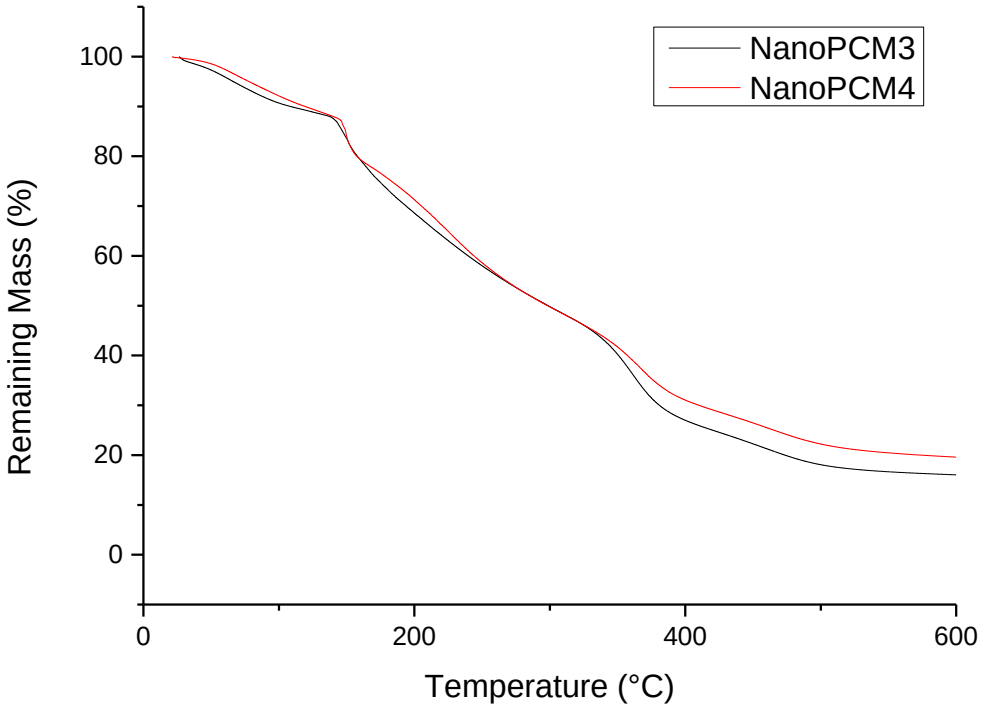

Fig 3.29 Comparison of TGA data between NanoPCM3 and 4

NanoPCM3 and 4 were synthesised with identical methodology, and were both fully analysed so a better comparison can be obtained. They are shown as similar sizes in the SEM images, 100-300nm. TGA data seen in Fig 3.29 displays a comparison between the thermal curves for NanoPCM3 and 4. As can be seen, the curves are almost identical, the major difference seen after heating above 300^{o}C due to the increased encapsulation efficiency of NanoPCM4. By 150°C, NanoPCM3 loses 12% mass, whilst NanoPCM4 loses 16%. By 300°C, both samples had lost 50% mass; and by 600°C, NanoPCM3 had lost 84% mass compared with 80% for NanoPCM4. The higher amount of salt hydrate contained in NanoPCM4, confirmed by its higher latent heat, means more MgO is present in the residual sample. A comparison of DSC data is shown below in Table 3.5. As can be seen, reproducible capsule properties are clearly achieved *via* the employment of a PECA shell with nearly identical properties for different batches.

Table 3.5 Comparison of the DSC properties obtained for NanoPCM3 and 4, which had an identical synthesis

Thermal Parameter	NanoPCM3	NanoPCM4
$T_{M,\ onset}$ *(°C)*	87	88
T_M *(°C)*	91	92
$T_{F,\ onset}$ *(°C)*	86	86
T_F *(°C)*	83	82
Supercooling (°C)	8	10
$\Delta H\ (J \cdot g^{-1})$	83.2	88.4
Thermal cycling stability	100+ cycles	100+ cycles
EE	51.9%	54%

3.3.18 PECA NanoPCMs in textile applications

Textiles are an application benefitting greatly from the addition of PCMs, increasing thermal comfort in clothing. Upon direct addition to fibres, encapsulated PCMs may be removed from the textiles during washing. To combat this, we attempted to anchor our nanocapsules to nanocellulose before addition to textiles.

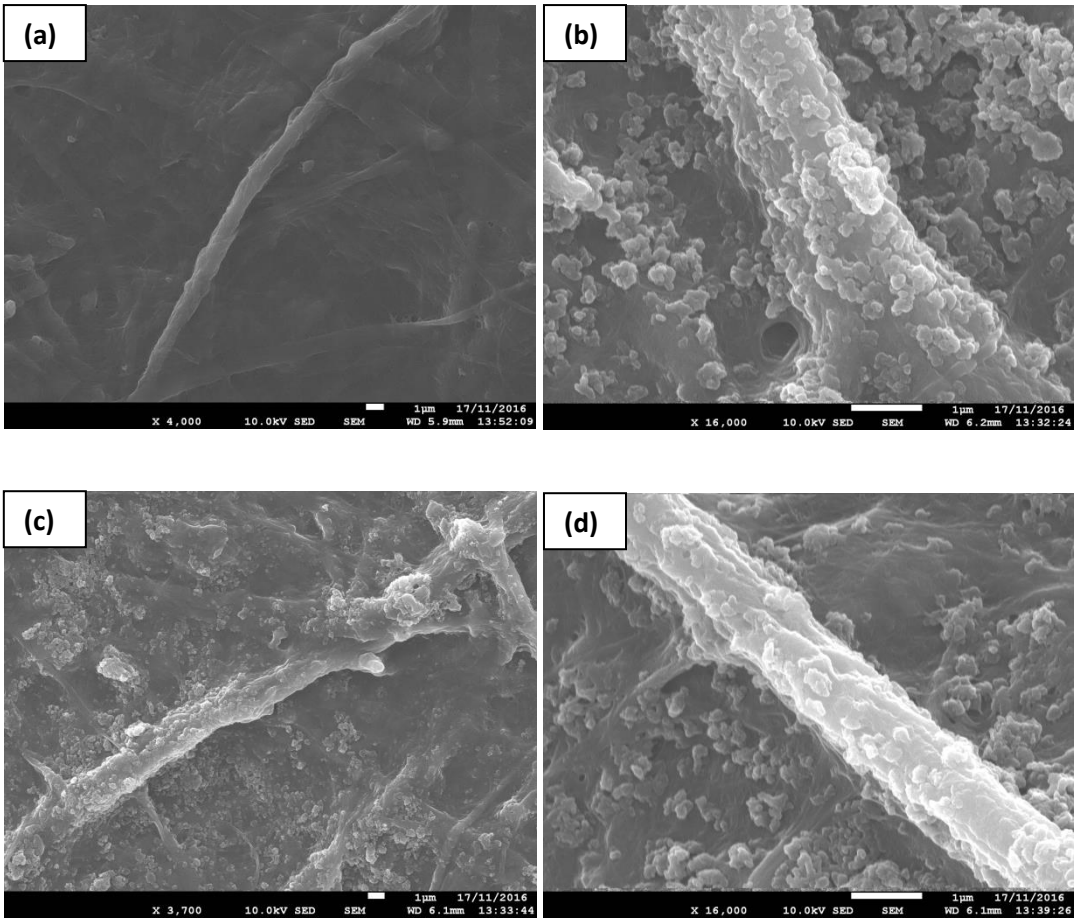

Fig 3.30 SEM images of **(a)** nanocellulose and **(b)** – **(d)** nanocellulose with adsorbed PECA NanoPCMs

SEM images of the neat nanocellulose and nanocellulose treated with PECA capsule dispersion are shown in Fig 3.30. The neat nanocellulose in Fig 3.30a appears as long strands many microns in length, with a width of around 1µm. Fig 3.30b – d show that once a solution of the nanocellulose in water in mixed with a PECA nanocapsule dispersion, some capsules adsorb on the surface of the fibres. Simply dipping textiles in the resulting solution should cause the NanoPCM-loaded nanocellulose to adhere to the textile. The use of nanocellulose as an 'anchor' for the PCM capsules is anticipated to prevent the capsules being removed during washing, which has been a problem for PCMs in textile applications[54,55].

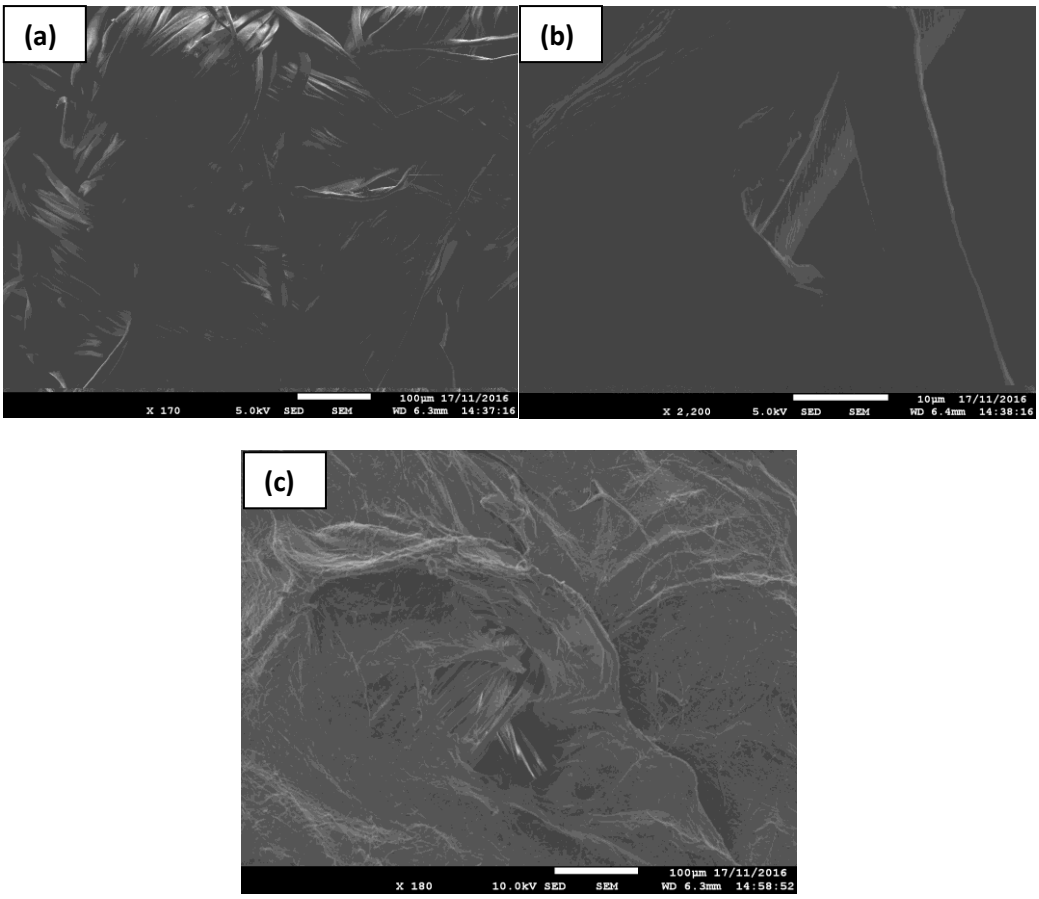

Fig 3.31 SEM images of **(a)** and **(b)** neat textile, and **(c)** textile treated with nanocellulose and PECA nanocapsule solution

Nanocellulose fibres with the adsorbed PECA nanocapsules were added to textiles by dipping the textile fabrics in a nanocellulose and capsule solution. SEM images are shown in Fig 3.31. The textiles consist of long strands of around 10µm in diameter. Nanocellulose adheres to the textile (Fig 3.31c), however the nanocapsules have not sufficiently anchored themselves to the nanocellulose fibres. Stronger interaction between the nanocapsules and nanocellulose is vital if they are to be used in thermoregulating textiles.

3.4 References

1 J. M. Asua, *Prog. Polym. Sci.*, 2014, **39**, 1797–1826.

2 N. Behan, C. Birkinshaw and N. Clarke, *Biomaterials*, 2001, **22**, 1335–1344.

3 M. G. Schwab, B. Fassbender, H. W. Spiess and A. Thomas, 2009, 7216–7217.

4 F. Fawaz, M. Guyot, A. M. Lagueny and J. P. Devissaguet, *Int. J. Pharm.*, 1997, **154**, 191–203.

5 B. Seijo, E. Fattal, L. Roblot-Treupel and P. Couvreur, *Int. J. Pharm.*, 1990, **62**, 1–7.

6 S. Vrignaud, J. P. Benoit and P. Saulnier, *Biomaterials*, 2011, **32**, 8593–8604.

7 J. L. Arias, M. A. Ruiz, M. López-Viota and Á. V. Delgado, *Colloids Surfaces B Biointerfaces*, 2008, **62**, 64–70.

8 M. R. Gasco and M. Trotta, *Int. J. Pharm.*, 1986, **29**, 267–268.

9 S. Vrignaud, N. Anton, C. Passirani, J. P. Benoit and P. Saulnier, *Drug Dev. Ind. Pharm.*, 2013, **39**, 1706–1711.

10 A. Sari, C. Alkan, D. Kahraman Doguscu and A. Bicer, *Sol. Energy Mater. Sol. Cells*, 2014, **126**, 42–50.

11 A. P. Kafka, B. J. McLeod, T. Rades and A. McDowell, *J. Control. Release*, 2011, **149**, 307–313.

12 A. Musyanovych and K. Landfester, *Prog. Colloid Polym. Sci.*, 2007, **134**, 120–127.

13 T. Pitaksuteepong, N. M. Davies, I. G. Tucker and T. Rades, *Eur. J. Pharm. Biopharm.*, 2002, **53**, 335–342.

14 S. Watnasirichaikul, N. M. Davies, T. Rades and I. G. Tucker, *Pharm. Res.*, 2000, **17**, 684–689.

15 S. Watnasirichaikul, T. Rades, I. G. Tucker and N. M. Davies, *Int. J. Pharm.*, 2002, **235**, 237–246.

16 P. B. Salunkhe and P. S. Shembekar, *Renew. Sustain. Energy Rev.*, 2012, **16**, 5603–5616.

17 T. Makuta, K. Kadoya, H. Izumi and M. Miyatake, *Chem. Eng. J.*, 2015, **273**, 192–196.

18 Z. H. Chen, F. Yu, X. R. Zeng and Z. G. Zhang, *Appl. Energy*, 2012, **91**, 7–12.

19 M. J. Graham, E. Shchukina, P. Felix De Castro and D. G. Shchukin, *J. Mater. Chem. A*, 2016, **4**, 16906–16912.

20 M. J. Graham, J. A. Coca-Clemente, E. Shchukina and D. Shchukin, *J. Mater. Chem. A*, 2017, **5**, 13683–13691.

21 T. Khadiran, M. Z. Hussein, Z. Zainal and R. Rusli, *Sol. Energy Mater. Sol. Cells*, 2015, **143**, 78–98.

22 A. Solé, L. Miró, C. Barreneche, I. Martorell and L. F. Cabeza, *Renew. Sustain. Energy Rev.*, 2013, **26**, 425–436.

23 C. Rathgeber, L. Miró, L. F. Cabeza and S. Hiebler, *Thermochim. Acta*, 2014, **596**, 79–88.

24 Q. Chen, Z. Gan, J. Wang and G. Chen, *Chem. - A Eur. J.*, 2011, **17**, 12458–12464.

25 J. Xu, L. Zhang and G. Chen, *Sensors Actuators, B Chem.*, 2013, **182**, 689–695.

26 P. Felix De Castro and D. G. Shchukin, *Chem. - A Eur. J.*, 2015, **21**, 11174–11179.

27 P. Felix De Castro, A. Ahmed and D. G. Shchukin, *Chem. - A Eur. J.*, 2016, **22**, 4389–4394.

28 M. G. Han, S. Kim and S. X. Liu, *Polym. Degrad. Stab.*, 2008, **93**, 1243–1251.

29 M. K. Tiwari, I. S. Bayer, G. M. Jursich, T. M. Schutzius and C. M. Megaridis, *Macromol. Mater. Eng.*, 2009, **294**, 775–780.

30 D. Z. Yin, L. Ma, J. J. Liu and Q. Y. Zhang, *Energy*, 2014, **64**, 575–581.

31 M. M. Farid, A. M. Khudhair, S. A. K. Razack and S. Al-Hallaj, *Energy Convers. Manag.*, 2004, **45**, 1597–1615.

32 D. R. Biswas, *Sol. Energy*, 1977, **19**, 99–100.

33 A. A. El-Sebaii, S. Al-Heniti, F. Al-Agel, A. A. Al-Ghamdi and F. Al-Marzouki, *Energy Convers. Manag.*, 2011, **52**, 1771–1777.

34 A. Abhat, *Sol. Energy*, 1983, **30**, 313–332.

35 L. F. Cabeza, A. Castell, C. Barreneche, A. De Gracia and A. I. Fernández, *Renew. Sustain. Energy Rev.*, 2011, **15**, 1675–1695.

36 J. Zhang, S. S. Wang, S. D. Zhang, Q. H. Tao, L. Pan, Z. Y. Wang, Z. P. Zhang, Y. Lei, S. K. Yang and H. P. Zhao, *J. Phys. Chem. C*, 2011, **115**, 20061–20066.

37 D. Crespy, M. Stark, C. Hoffmann-Richter, U. Ziener and K. Landfester, *Macromolecules*, 2007, **40**, 3122–3135.

38 G. Wang, W. Xu, Q. Hou and S. Guo, *Ultrason. Sonochem.*, 2015, **27**, 403–407.

39 C. Alkan, A. Sari, A. Karaipekli and O. Uzun, *Sol. Energy Mater. Sol. Cells*, 2009, **93**, 143–147.

40 A. Solé, I. Martorell and L. F. Cabeza, *Renew. Sustain. Energy Rev.*, 2015, **47**, 386–398.

41 D. Platte, U. Helbig, R. Houbertz and G. Sextl, *Macromol. Mater. Eng.*, 2013, **298**, 67–77.

42 C. Scott, D. Wu, C. C. Ho and C. C. Co, *J. Am. Chem. Soc.*, 2005, **127**, 4160–4161.

43 B. Zalba, J. M. Marin, L. F. Cabeza and H. Mehling, *Appl. Therm. Eng.*, 2003, **23**, 251–283.

44 H. Michels and R. Pitz-Paal, *Sol. Energy*, 2007, **81**, 829–837.

45 Y. Tian and C. Y. Zhao, *Appl. Energy*, 2013, **104**, 538–553.

46 L. Solomon and A. Oztekin, *J. Energy Storage*, 2016, **8**, 12–26.

47 P. W. Stott, A. C. Williams and B. W. Barry, *J. Control. Release*, 1998, **50**, 297–308.

48 K. Posern and C. Kaps, *Thermochim. Acta*, 2010, **502**, 73–76.

49 S. S. Chandel and T. Agarwal, *Renew. Sustain. Energy Rev.*, 2017, **67**, 581–596.

50 K. Pielichowska and K. Pielichowski, *Prog. Mater. Sci.*, 2014, **65**, 67–123.

51 K. Nagano, K. Ogawa, T. Mochida, K. Hayashi and H. Ogoshi, *Appl. Therm. Eng.*, 2004, **24**, 221–232.

52 Y. Marcus, A. Minevich and L. Ben-Dor, *Thermochim. Acta*, 2004, **412**, 163–170.

53 Y. E. Milián, A. Gutiérrez, M. Grágeda and S. Ushak, *Renew. Sustain. Energy Rev.*, 2017, **73**, 983–999.

54 Y. Shin, D. I. Yoo and K. Son, *J. Appl. Polym. Sci.*, 2005, **96**, 2005–2010.

55 Y. Shin, D. I. Yoo and K. Son, *J. Appl. Polym. Sci.*, 2005, **97**, 910–915.

4.

Polyurethane Micro- and Nanocapsules

4.1 Introduction

Although PECA nanocapsules have excellent promise for low temperature applications, they still have limitations. ECA is reasonably expensive and highly moisture sensitive. It must be kept below 5°C and hermetically sealed. PECA also has a low degradation temperature (150°C) in contrast with other polymers. It is also permeable to water[1], which would hinder any applications requiring a suspension of nanocapsules in aqueous solution. It is possible to develop aqueous core nanocapsules which can be suspended in water by developing impermeable shell materials. PECA is also soluble in many organic solvents, which may hinder some applications. For instance, we attempted to add the PECA capsules to a xylene based paint for thermal regulation, but the capsules dissolved. Other polymers show greater thermal and chemical stability. It is also beneficial to demonstrate that several shells can be used for the encapsulation of PCMs, so that specific properties can be chosen for energy storage systems.

Polyurethane (PU) is a highly versatile polymer and one of the most common – accounting for roughly 5% of the total polymer market[2]. It can be hard or soft depending on the building blocks used to form it and the way that they are blended. PU was discovered by Bayer and co-workers in 1937[3]. It is used in many diverse applications such as rigid foams, condoms, rollercoaster wheels, mattresses, surface coatings etc. It has excellent thermal properties, which have led to it being used in flame retardant coatings[4]. PU is synthesised by the interfacial polymerisation of hydrophilic (a diol, such as hexanediol; or polyol, such as polyvinyl alcohol (PVA)) and hydrophobic (diisocyanate) monomers, which join *via* a carbamate (urethane) link. If a diamine is used in place of the di-/polyol, a polyurea is formed instead. The wide variety of monomers mean different properties can be achieved, such as hard or soft polymer formation. Isocyanates are highly reactive monomers, ensuring good yields can be achieved on an industrial scale[3]. The reactivity of the isocyanate group can also lead to unwanted side reactions, such as with water present in reactants or with any condensation products[2]. Although the electron density of the carbamate group is not fully

understood, researchers agree that the least electron density is at the carbon atom[5]. The higher the positive charge on the carbon, the higher the reactivity of the isocyanate[3]. Isocyanates must be fully removed from the final product as they are highly toxic and potentially carcinogenic. PU however is entirely non-toxic. PU has the potential to form aqueous core nanocapsules which can be dispersed in water; aqueous PU dispersions have been used commercially since the 1970s[6]. When sufficiently crosslinked, hydrophilic groups remain attached to the PU shell even when submersed in water, demonstrating shell stability and meaning surfactants are not required to stabilise PU capsule dispersions[7]. The large range of applications for PU is possible due to two physical processes; phase separation between hard and soft segments, and hydrogen bonding between carbamate links.

PU can also be used for long-life 'self-healing' capsules. Isocyanates can be encapsulated in the core of PU capsules along with active materials[8]. When the PU shell becomes damaged, isocyanates are released and react to reform the shell. This is especially useful for advanced coating materials, as it greatly extends material lifespan. It is also possible to encapsulate corrosion inhibitors, which are released into the damaged region. Corrosion causes huge expense in maintenance costs, so these materials are of great commercial value. With the potential for the formation of multi-compartmental capsules[9], it may be possible to synthesise compartments with PCMs along with self-healing materials or corrosion inhibitors for long lasting energy storage capsules.

Environmentally friendly materials are highly desirable for industrial production; especially as the general public becomes increasingly aware of issues such as global warming and the huge amount of unnecessary waste produced by human activity. A challenge for industrial PU is that they are traditionally produced using petrochemical reactants. Petrochemicals release large amounts of emissions and are non-renewable, as they are obtained by distilling crude oil. PU can be sustainably produced from many renewable, recycled or otherwise sustainable feedstocks, such as vegetable oils[10]. Vegetable oils are cheap and abundant, and can be treated to obtain different polyols leading to a variety of properties for the PU[11]. Various methods of treatment can be used to obtain the

polyols, such as reactions involving ester groups or C-C bonds[12]. Vegetable oil-based polymers experience a performance gap compared to those that are petrochemically produced, including their processing, thermal and mechanical properties[13]. More research is therefore required to narrow this gap and ensure renewable feedstocks become economically viable. Javni *et al*[14] showed that vegetable oil-based PU can be more thermally stable than those produced with polypropylene oxide.

It is possible to remove isocyanates from PU synthesis altogether; they can be replaced by cyclic carbonates, which are non-toxic. Cyclic carbonates can be produced from renewable natural resources such as soybean oil[15]. These non-isocyanate PUs often have some superior properties to regular PU, such as increased porosity and water adsorption; but perform more poorly in other areas, for example their elasticity is not good enough to produce effective elastomers[16]. Polyhydroxyurethanes (PHUs) may be a suitable alternative to PU, synthesised from the reaction of cyclic carbonates with diamines by a nucleophilic addition[2]. PHUs were patented by Groszos in 1957.

Isocyanates are used for commercial PU synthesis due to low cost and availability, and they are suitable for continued use at high yields of PU formation which eliminates toxicity. We used methylene diphenyl diisocyanate (MDI) as our hydrophobic hard segment monomer of choice. MDI is one of the most common isocyanates used for PU production, along with toluene diisocyanate. For our hydrophilic soft segment monomer, polyvinyl alcohol (PVA) or polyethylene glycol (PEG) were used. These are both cheap and abundant polymers which are widely used in many applications.

Due to its low biotoxicity and biodegradability, much research in PU chemistry has focused on medical applications. An article in *Science* from Boretos and Pierce in 1967[17] focused on PU being used for components in a heart-assistance system. They found the PU was useful as a coating for stainless steel tubing as it was highly stable when in contact with the bloodstream, displaying no biotoxicity. PU can also be reinforced by deposition of layers of clay or other materials which enhance rigidity[18], reduce permeability and improve solvent resistance.

PU micro- and nanocapsules are prominent in literature, often used to encapsulate drugs. Rosenbauer *et al*[19] synthesised their own custom diol for addition to toluene diisocyanate, further demonstrating how PU properties can be tuned. They found they could trigger release of any active core material by decomposition of the polymer shell by several external stimuli, such as pH or temperature change. Poorly water soluble drugs, such as α-tocopherol[20] and curcumin[21] have been encapsulated in PU. These studies found by varying experimental conditions, encapsulation efficiency and nanocapsule size could be influenced.

Several researchers have used PU to encapsulate PCMs. Commonly used shell materials for PCMs such as urea formaldehyde[22,23] and melamine formaldehyde[24,25] can lead to toxic chemicals being released upon decomposition. PU is more inert and non-toxic. Su *et al*[26] made PU microcapsules containing octadecane. These capsules displayed good thermal stability and latent heat. By adding a dispersant, the capsules could be suspended in ethanol solution with reduced leakage of core material. Felix *et al*[27,28] made two studies on PU microcapsules containing docosane. By altering the speed of homogenisation to form their initial emulsion, they showed capsule size could be controlled. The largest capsules produced were 10µm from a homogenisation speed of 6000 RPM, whilst increasing the speed to 20000 RPM decreased capsule size to 2µm. The 10µm capsules had an encapsulation efficiency of 19.2%, for the 2µm capsules this was increased to 31.6%.

PU has also been used to encapsulate crystallohydrates. Schoth and collaborators[29] synthesised PU nanocapsules containing sodium sulphate decahydrate, using a Pickering emulsion template. Resulting capsules were an average of 860nm, although had a wide size range, and had a latent heat of 58 $J \cdot g^{-1}$. They also demonstrated versatility of their method by also encapsulating a water-soluble dye.

In addition to encapsulation, PU foams can be used as a supporting material for PCMs. Either PCM-loaded capsules can be dispersed within the PU matrix, or a form-stable PCM can be synthesised. Borreguero *et al*[30,31] synthesised PU foam containing microcapsules with a Rubitherm RT27 core, a

commercial PCM based on paraffin wax. They found catalyst selection to be important in the formation of foams, and showed that larger amounts of incorporated Rubitherm led to better thermal storage but decreased mechanical properties. Therefore, a balance between the two must be struck. Aydin and Okutan[32] noted how PU foams are considered the best thermal insulation material due to its superior thermal insulation per unit thickness. By adding a fatty acid-based PCM to the PU foam they could further improve thermal insulation by 34%, displaying the compatibility of PU with PCMs. Sarier and Onder[33] impregnated PU foams with various PEG polymers for use in insulating concrete. Best results were achieved by having inner and outer layers containing different types of PEG, which increased heat collection ability of the material. Zhu *et al*[34] demonstrated the suitability of PU as superhydrophobic sponges for use in oil recovery. The foams were robust and highly reusable, showing PU foams can be effective in numerous applications.

PEG-based PU can be used as form-stable PU PCM. PEG acts as the soft phase change component with solid-liquid transitions, and PU acts as a solid support and prevents leakage. Numerous researchers[35–37] have reported the synthesis of form stable bulk PU PCMs, with latent heats from 100-140 $J \cdot g^{-1}$. Leakage will still occur at high loading capacities. Form-stable PCMs are not considered for future energy saving applications however, due to the expense of synthesis and the fact that encapsulation is more effective at preventing leakage. Emulsion polymerisation is also available for industrial scale-up[38], so it is possible to form capsules on a larger scale.

The large amount of research on polyurethane shows it is a highly promising candidate for the encapsulation of inorganic PCMs, with good thermal stability and encapsulation efficiencies. We sought simple methods based on miniemulsion polymerisations, and were able to form both microcapsules and nanocapsules depending on the methodology used. Promising heat storage abilities were observed, with good thermal stability and simple synthetic procedures.

4.2 Polyurethane microcapsules

PU is a good candidate for the encapsulation of salt hydrates. Saihi *et al*[39,40] encapsulated ammonium phosphate, a non-hydrated salt, in PU microcapsules (PUMCs) for flame retardant coatings. The intumescent system protects from fire by expanding upon heating which protects the material underneath. A carbonaceous residue is formed after decomposition of the system which is thermally stable. During decomposition, ammonium phosphate degrades to form NH_3 and H_3PO_4 which catalyse the char formation. They reported the success of both a coacervation technique and an interfacial polymerisation in separate studies to form the capsules. Their coacervation technique required more steps but led to smaller capsules. Coacervation is the formation of a liquid polymer rich phase in equilibrium with another liquid phase of core material. The coacervate is then treated to form a shell around the core. The method consisted of coating the salt core with the polyol monomer, which was then crosslinked by adding a diisocyanate. We adapted their methods, using $Mg(NO_3)_2.6H_2O$ as core material. The method involves a reaction between the isocyanate groups of MDI and the OH groups of polyol PVA.

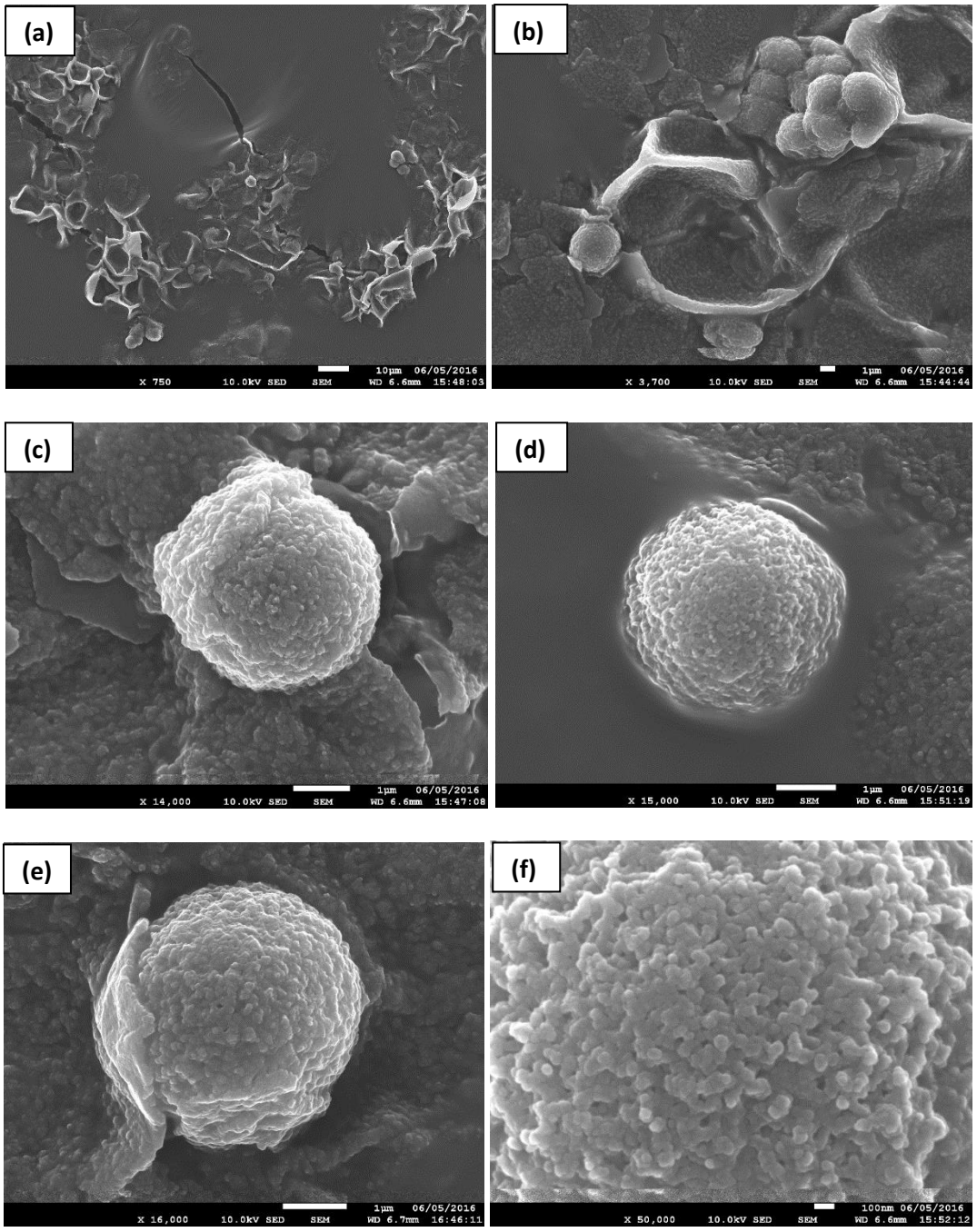

Fig 4.1 SEM images of PUMCs washed with toluene and water. Scale bars are 10µm for **(a)**, 1µm for **(b) – (e)** and 100nm for **(f)**

From the coacervation method, microcapsules were produced containing a core with 70 %wt $Mg(NO_3)_2.6H_2O$ and 30 %wt water. SEM images are shown in Fig 4.1. The capsules are spherical in shape, showing they are robust enough to withstand the SEM high vacuum, although some collapsed

capsule structures are shown in Fig 4.1a and b. Some of the capsules have also aggregated. They are 3.5-4µm in size, which fits in perfectly with Saihi *et al*'s results[39]; their capsules had an average diameter of 3.8µm. As can be seen from the images, the capsules are monodisperse. This shows the emulsification step using the Ultraturrax homogeniser led to stable emulsions. A high speed (30000 RPM) was employed for homogenisation to reduce droplet size and promote monodispersity. The morphology changes depending on the method of washing. The washing step was undertaken to remove any excess oil, surfactants and any residual reactants, especially the toxic MDI; the wash was achieved by vortexing in various solvents. Excess surfactant can be seen partially covering the shell in Fig 4.1e. After washing in water and toluene, the capsules developed a rough morphology with the surface coated in nanoparticles, as seen in the close-up in Fig 4.1f.

Other solvents were used for washing, but were less successful than the wash in water and toluene. Few capsules were observed on the SEM images for these washes, but single microparticles are shown in Fig 4.2a and b. When washed with ethanol (Fig 4.2a), the capsule has a smooth surface and looks like it has imploded with the shell cracked; The capsule is around 1.2µm in diameter, much smaller than the fully formed capsules shown in Fig 4.1 a-f. The cracked shell will release the core material, causing shrinkage. Washing in water and acetone led to the capsule seen in Fig 4.2b. Again, the morphology of the capsule is smooth, although it is clearly not spherical. Diameter is approximately 4µm. The jagged effect of the shell may be caused by the solidified crystallohydrate in the core. It may also be from implosion induced by the high vacuum of the SEM chamber.

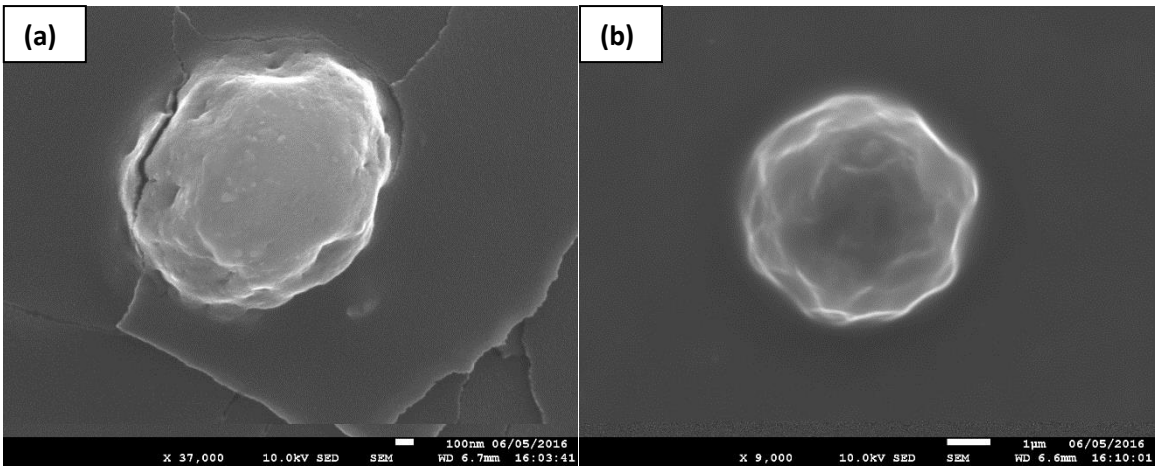

Fig 4.2 SEM images showing PUMCs washed with **(a)** ethanol and **(b)** water and acetone

The synthesis was also tested without using the PVA monomer. It was hypothesised a shell may still form due to the many OH groups present in the surfactant Span 85. SEM images from this synthesis are shown in Fig 4.3. Some capsule structures are present, however are not fully developed. When washed in toluene and water, some nanoparticles are observed on the surface, akin to the PUMCs observed when PVA was used as monomer. The capsules are not spherical in shape, showing they are not of sufficient strength to withstand the SEM high vacuum. Lack of robustness is due to poor shell formation, which can be explained by considering two possible reaction mechanisms. Either Span 85 is not as good a crosslinker for reaction with MDI compared with PVA; or, as the urethane-forming reaction occurs, Span 85 is withdrawn from the initial surfactant shell formed during emulsification and destabilises the droplets.

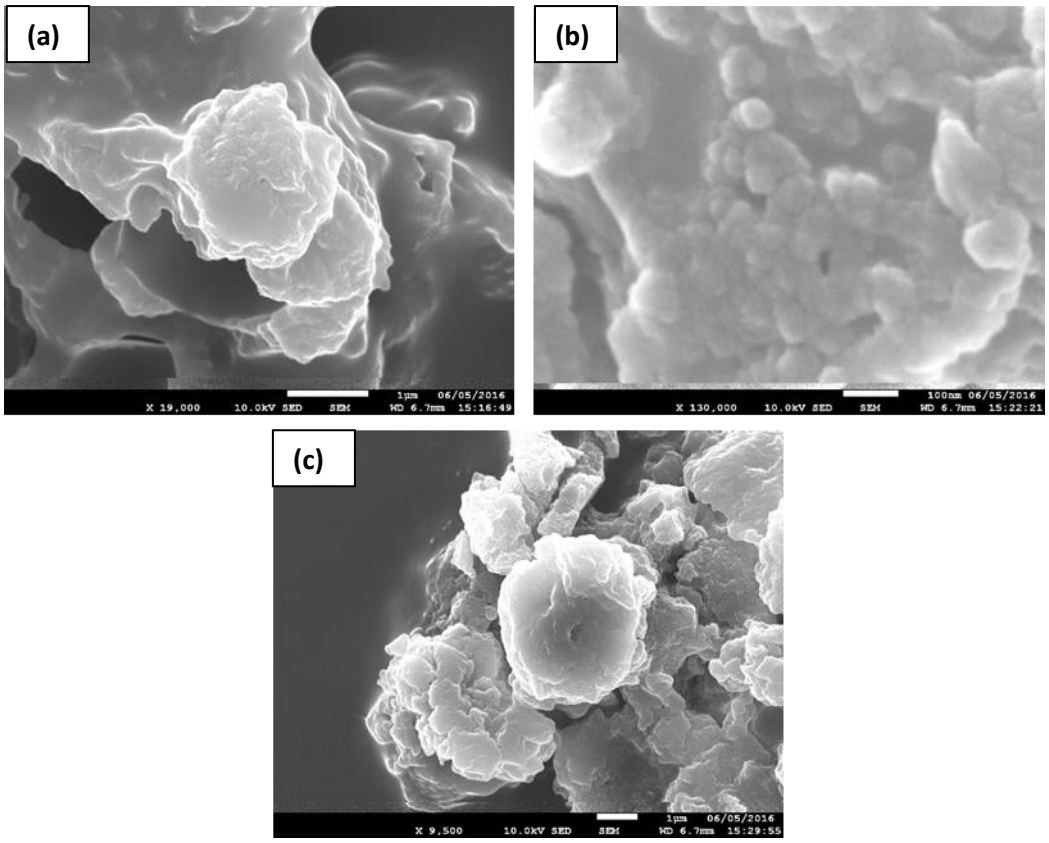

Fig 4.3 SEM images of PUMCs produced without PVA in the synthesis. **(a)** and **(b)** were washed with toluene and water, and **(c)** with ethanol

FTIR spectrum for $Mg(NO_3)_2.6H_2O$ and the PUMCs washed in toluene and water (same sample as displayed in Fig 4.1) is shown in Fig 4.4. $Mg(NO_3)_2.6H_2O$ has characteristic peaks for O-H stretching at 3356 cm^{-1}, N=O bending at 1646 cm^{-1}, a mixture of N-O stretching and bending and N=O stretch in the broad peak at 1365 cm^{-1}, plus a sharp peak at 819 cm^{-1} for the NO_3^- ion. The PUMCs spectrum contains characteristic peaks for the PU shell, along with $Mg(NO_3)_2.6H_2O$ in the core. Peaks are observed for O-H at 3400 cm^{-1}, C-H at 2900 cm^{-1}, NCO group at 2300 cm^{-1}, N-H at 1600 cm^{-1}, C=C 1500 cm^{-1}, C-H bending at 1300 cm^{-1}, C-O at 1000 cm^{-1}. The NO_3^{2-} peak at 818 cm^{-1} is present in the PUMC sample, showing that $Mg(NO_3)_2.6H_2O$ has been encapsulated.

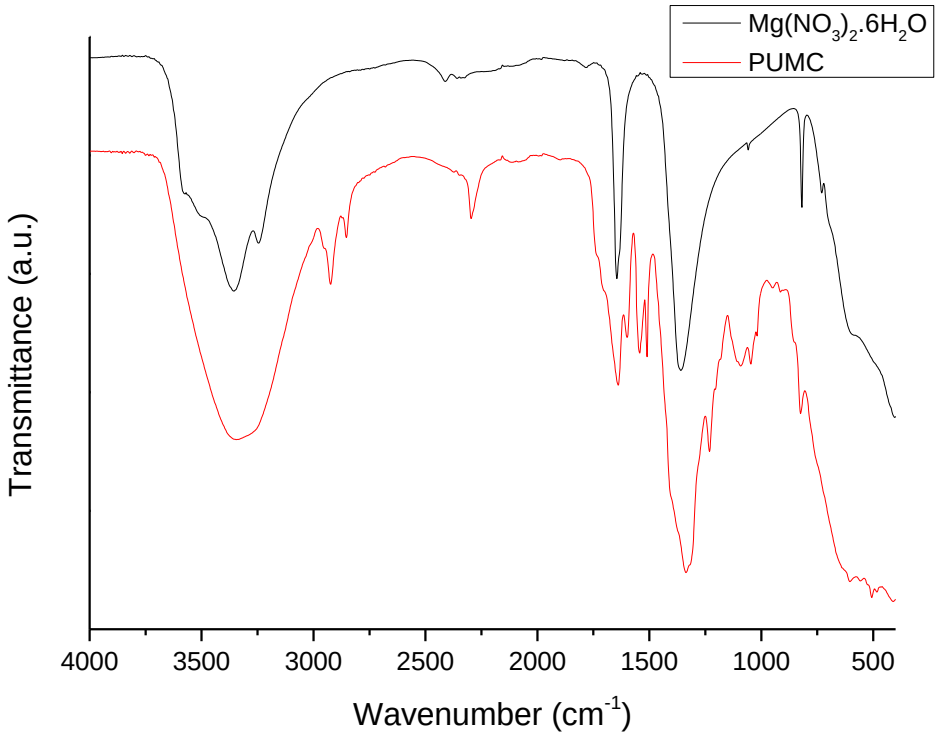

Fig 4.4 FTIR spectra for pure $Mg(NO_3)_2.6H_2O$ and PU microcapsules containing $Mg(NO_3)_2.6H_2O$

4.2.1 Stability of PUMCs

After being left in an open vial for around 6 months, the PUMC samples were again dispersed and SEM images taken. Displayed in Fig 4.5 are the PUMCs washed with toluene and water (initially shown in Fig 4.1). The capsules were no longer coated by nanoparticles. The capsules are 3µm or less, showing they have shrunk due to evaporation from the aqueous core of the microcapsules. Loss of water from the core dehydrates the contained crystallohydrate, decreasing its latent heat and reducing thermal cycling stability.

It can be concluded that the nanoparticles originally coating the capsule surface (Fig 4.1) have a stabilising effect. When coated with nanoparticles, the capsules have a more spherical shape and an increased number of capsules are observed. All SEM images of microcapsules without the adsorbed

nanoparticles are smaller in comparison, due to loss of core material. Overall, these results show that microcapsules do not give the necessary stability required for long lasting heat storage energy capsules, due to shell degradation and loss of core material.

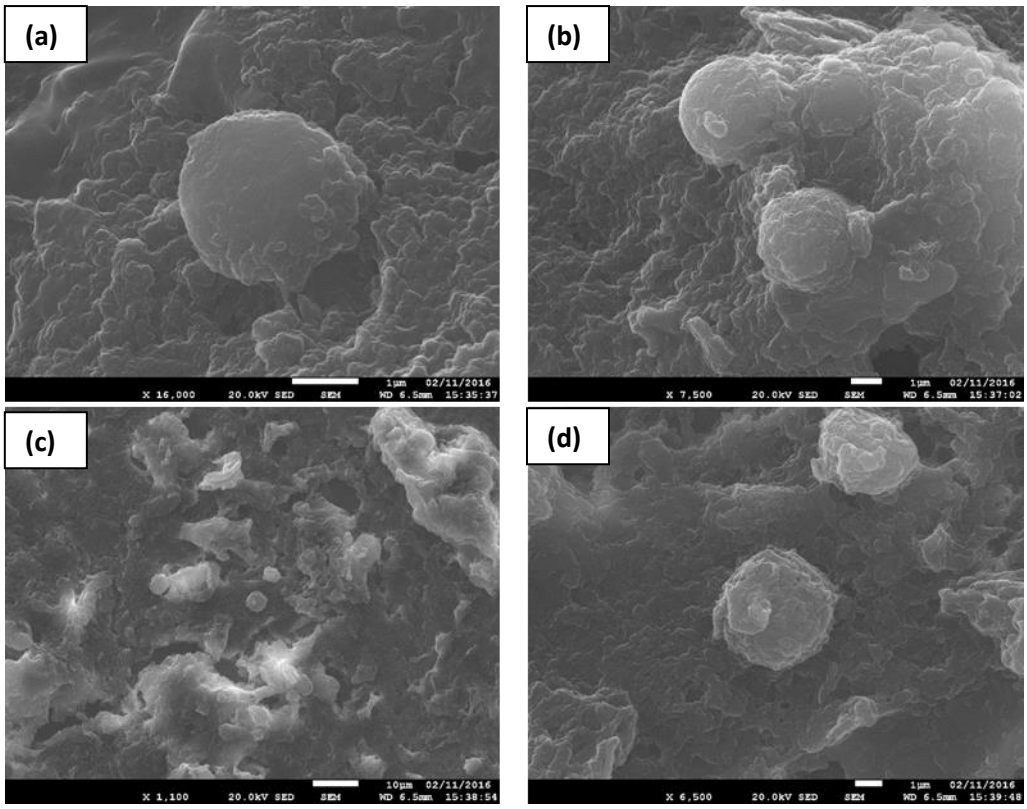

Fig 4.5 Retaken SEM images of PUMCs after 6 months drying in an open vial. Scale bars are 1µm for **(a)**, **(b)** and **(d)**; and 10µm for **(c)**

4.3 Polyurethane Nanocapsules

Clearly the PUMCs do not show the necessary stability for thermal energy storage. New methods were then sought. Due to the success of our PECA nanocapsules described in the previous chapter, we wanted to synthesise nanocapsules using PU as shell material (PUNCs). Ultrasonication was used to emulsify the reactants rather than homogenisation, in order to reduce the size of emulsion droplets.

Hamberger *et al*[41] precipitated non-water-soluble salts inside PU nanocapsules by introducing two separate W/O miniemulsions containing water-soluble salts. These salts then reacted to form non-water-soluble salts within the capsule core. We condensed their method to form one W/O miniemulsion containing crystallohydrates. As with our method to produce PUMCs, the process involves the reaction of diisocyanate with a polyol. The proposed reaction mechanism is shown in Fig 4.6.

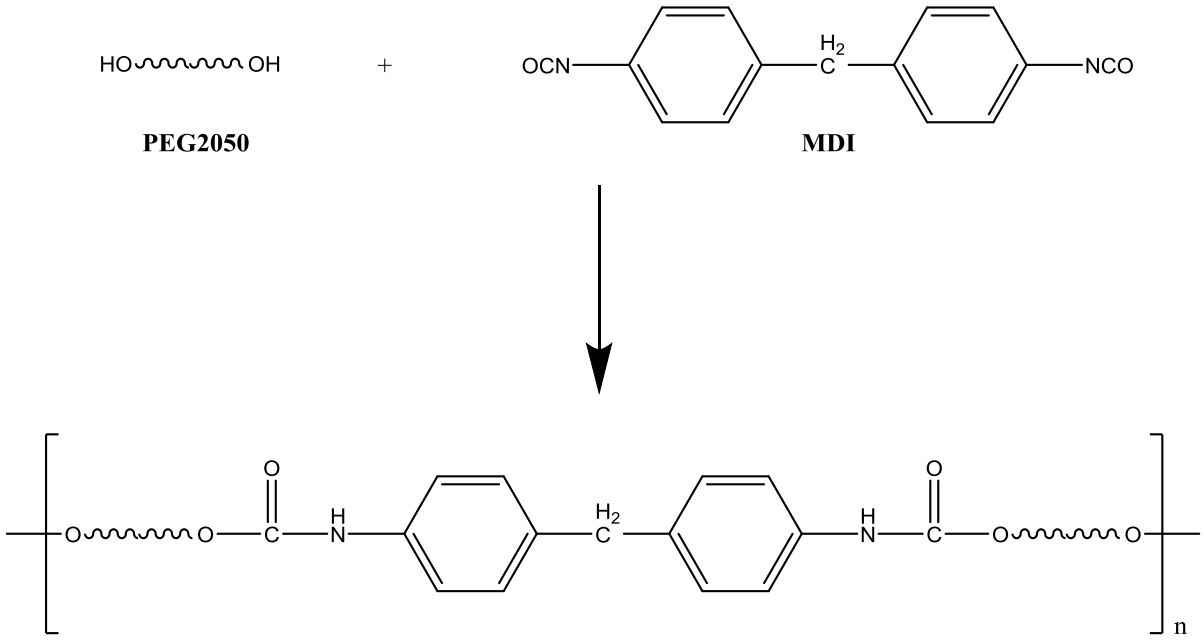

Fig 4.6 Proposed structure of PU formed by reaction of polyol PEG2050 and diisocyanate MDI (proposed by Felix de Castro *et al*[27])

Initially we used an oil phase of 5 %wt surfactants in cyclohexane. The surfactant blend of 3:2 Tween 80:Span 20 was again used, as it was so effective in the formation of PECA nanocapsules. Stable W/O miniemulsions are formed when the oil and aqueous phases are sheared by ultrasonication. Capsules from this formulation are observed in the SEM images shown in Fig 4.7, which were synthesised using PVA as polyol monomer. Although single capsules are difficult to make out as they are heavily agglomerated, they are between 100-300nm in diameter. Hamberger *et al* reported that using their similar method, capsules prepared with glycerol as polyol monomer were 300nm in size; when using PVA, capsules were an average of 800nm in diameter. Our nanocapsules were smaller, at approximately 200-300nm in diameter. This shows the importance in choosing reactants to formulate the nanocapsules as they can have a profound effect on size.

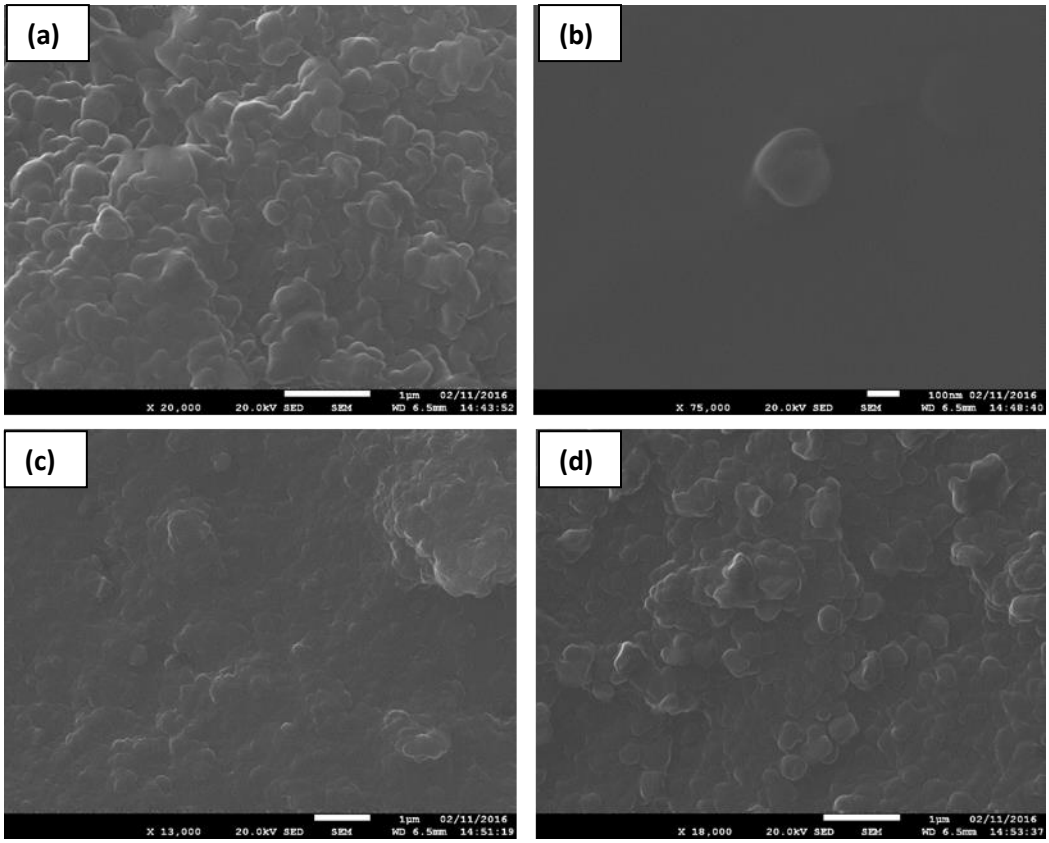

Fig 4.7 SEM images of PUNCs synthesised using 5 %wt surfactants. Scale bars are 1µm for **(a)**, **(c)** and **(d)** and 100nm for **(b)**

For easier and more accurate analysis, a powder sample needs to be formed. By reducing the amount of surfactant in the oil phase, this was achieved. We used 1 %wt 2:1 Span 85:PEGDO in cyclohexane as the oil phase. We also used a different polyol monomer, PEG2050 (M_n = 2050), as it was less viscous in aqueous solution than PVA, and had performed well in the formation of microcapsules in previous work done within the group[27,28]. Resulting miniemulsions were cloudy, meaning the aqueous phase was not fully solubilised. The nanocapsule product produced using this method was a white powder. Photographs to compare the appearance of PUNCs synthesised with 5%wt surfactants and 1 %wt surfactants, along with the PUMCs (from Fig 4.1) are shown in Fig 4.8. The PUMCs are agglomerated into a sticky solid, with some white powder around the outside. Using 5 %wt surfactants for PUNCs makes it very difficult to remove any excess surfactant from the product, giving an agglomerated, sticky and off-colour product. Reducing the amount of surfactants

to 1 %wt of the continuous phase resulted in a powder sample, seen on the right of Fig 4.8. A simple way of ensuring PU has formed is to add the product to acetone. MDI is highly soluble in acetone, whereas PU is insoluble.

Fig 4.8 Photographs documenting macroscale appearance of PUMCs (left), PUNCs made with 5 %wt surfactants (centre) and PUNCs made with 1 %wt surfactants (right)

Table 4.1 Formulations of PUNCs synthesised using 1 %wt surfactants

Sample	*Aqueous Phase*	*Oil Phase*
PUNC1	$Mg(NO_3)_2.6H_2O$ (0.5g), H_2O (0.5g), PEG2050 (0.1g)	1 %wt 2:1 Span 85:PEGDO in cyclohexane (7.5g), MDI (0.262g)
PUNC2	$Mg(NO_3)_2.6H_2O$ (0.5g), H_2O (0.5g), PEG2050 (0.2g)	1 %wt 2:1 Span 85:PEGDO in cyclohexane (7.5g), MDI (0.1g)
PUNC3	$Na_2SO_4.10H_2O$ (0.2g), H_2O (0.8g), PEG2050 (0.1g)	1 %wt 2:1 Span 85:PEGDO in cyclohexane (7.5g), MDI (0.262g)
PUNC4	$Mg(NO_3)_2.6H_2O$ (0.5g), H_2O (0.5g), PEG200 (0.1g)	1 %wt 2:1 Span 85:PEGDO in cyclohexane (7.5g), MDI (0.262g)
PUNC5	$Mg(NO_3)_2.6H_2O$ (0.5g), H_2O (0.5g), PEG2050 (0.1g)	1 %wt 2:1 Span 85:PEGDO in cyclohexane (15g), MDI (0.262g)

4.3.1 Formulation of PUNCs, morphology and chemical analysis

Yields for PUNCs were between 0.15-0.2g per reaction. The yield seems rather low considering the amount of monomers used (0.2-0.4g), and the core material consisted of 1g crystallohydrate solution. Any reactants left unreacted after synthesis were removed by centrifugation. By adding a catalyst to the reaction, dibutyltin dilaurate (DBDL), the yield was increased to 0.67g. However, no thermal data could be collected from this sample.

SEM images for PUNCs are shown in Fig 4.9. The capsules are 200-400nm in size, with a smooth morphology. They are slightly larger than capsules made with 5 %wt surfactants, as the decreased amount of surfactants results in a higher polydispersity of miniemulsion droplets. The shell material is completely intact and provides full coverage of the core material. This is essential to prevent any leakage from occurring. The capsules were fully isolated by taking them directly out of solution straight after synthesis and dispersing by sonication, rather than drying them before dispersion. This prevents agglomeration. The capsules remain a roughly spherical shape with none collapsing, in contrast to the PUMCs. This demonstrates the robustness of nanomaterials compared with larger capsules.

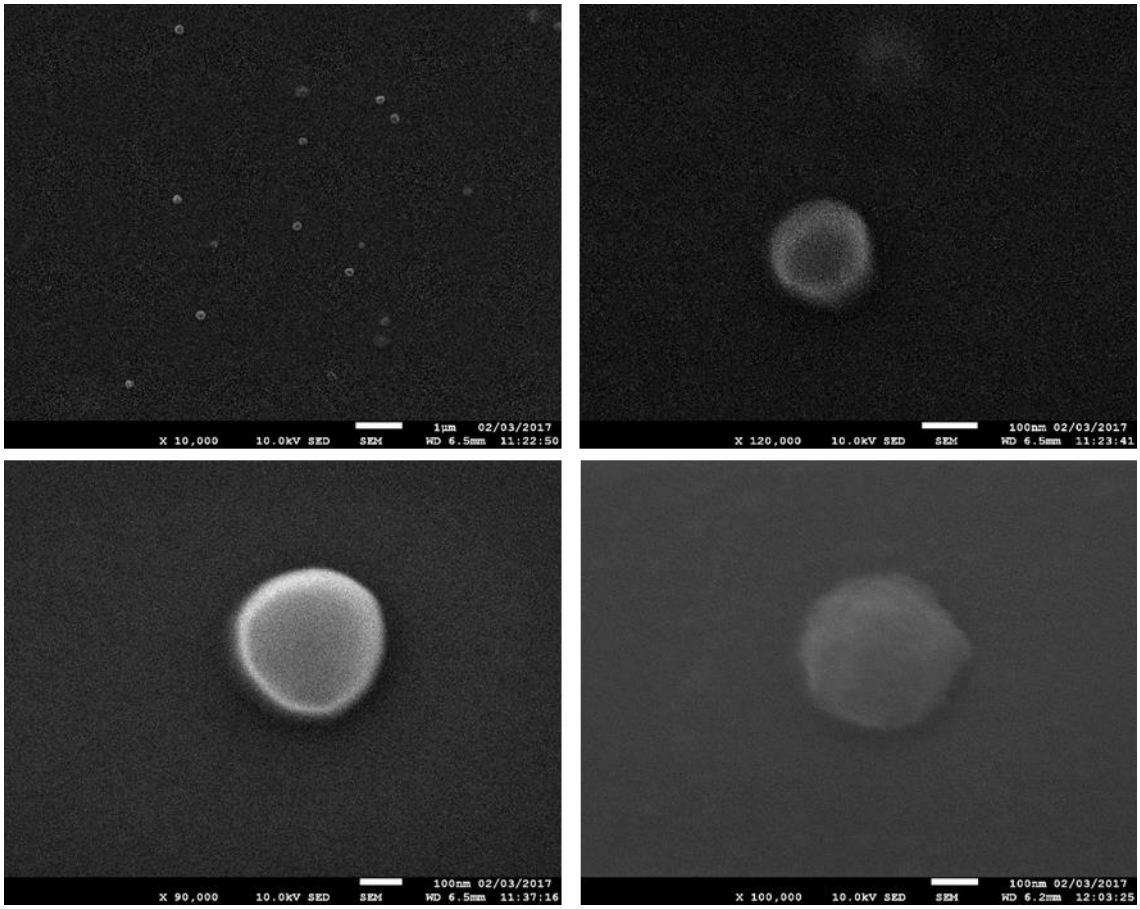

Fig 4.9 SEM images of PUNCs synthesised with 1 %wt surfactants

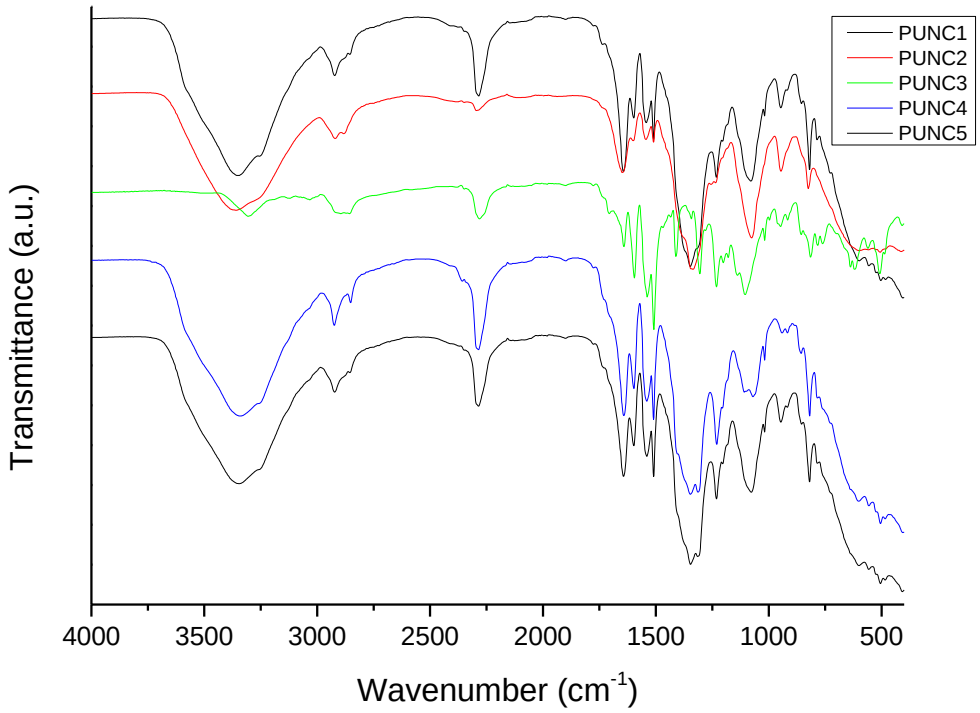

Fig 4.10 FTIR spectra of PUNCs with different formulations

Chemical analysis of the PUNCs was undertaken with FTIR (Fig 4.10). Despite differences in synthesis conditions, each PU sample has a similar spectrum. Each contains the characteristic peaks for PU, for O-H at ≈3350 cm^{-1} C-H at ≈2920 cm^{-1}, NCO group at ≈2280 cm^{-1}, C=O at ≈1640 cm^{-1}, N-H at ≈1600 cm^{-1}, two peaks for C=C from benzene at ≈1540 and 1509 cm^{-1}, C-H bend at ≈1345 cm^{-1} and C-O from the ester group at ≈1070 cm^{-1}. The main differences occur in PUNC3, which was the only sample to contain $Na_2SO_4.10H_2O$ rather than $Mg(NO_3)_2.6H_2O$. Especially, the O-H peak is much smaller and has shifted to a lower wavenumber. The smaller peak for H_2O correspond with the lower amount of water loss seen in the TGA curve (please see below). PUNCs 1, 2, 4 and 5 contained a peak at ≈818 cm^{-1} for NO_3^{2-}, whilst PUNC3 has a peak at 619 cm^{-1} for SO_4^{2-}. These correspond to the specific salt hydrates contained in their cores. Full listings of the peaks for FTIR spectra are presented in Table 4.2.

Table 4.2 FTIR peaks for PUNCs synthesised with 1 %wt surfactants

Functional Group	**PUNC1 wavenumbers (cm^{-1})**	**PUNC2 wavenumbers (cm^{-1})**	**PUNC3 wavenumbers (cm^{-1})**	**PUNC4 wavenumbers (cm^{-1})**	**PUNC5 wavenumbers (cm^{-1})**
O-H	3354	3354	3302	3354	3354
C-H	2920	2920	2895	2920	2920
NCO	2283	2294	2280	2283	2283
C=O	1642	1649	1640	1642	1642
N-H	1598	1598	1594	1598	1598
C=C aromatic	1542 & 1509	1543 & 1509	1538 & 1509	1538 & 1509	1538 & 1509
C-H bend	1345	1345	1342	1345	1345
C-O	1076	1076	1105	1069	1076
NO_3^{2-}	819	825	n/a	819	819
SO_4^{2-}	n/a	n/a	619	n/a	n/a

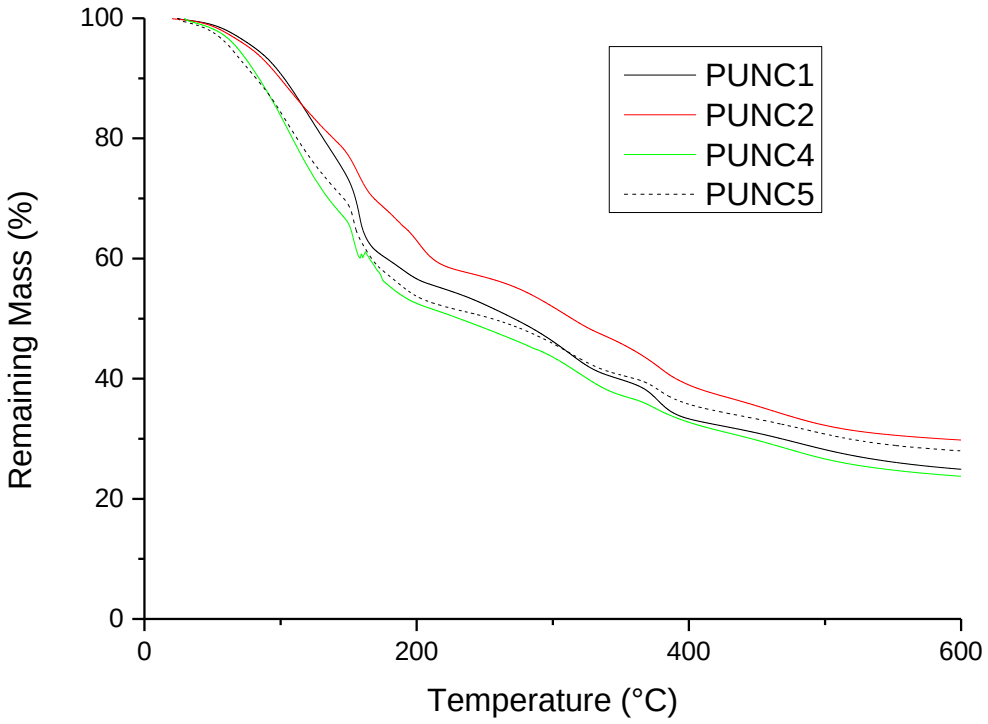

Fig 4.11 TGA curves for PUNCs 1, 2, 4 and 5 taken at 10°C/min from room temp. to 600°C

4.3.2 Thermal stability of PUNCs

TGA curves for PUNCs 1-5 are shown in Fig 4.11. PUNCs 1, 2, 4 and 5 all contain 50 %wt $Mg(NO_3)_2.6H_2O$ in the core, and differ only in synthesis conditions (listed in Table 4.1). All have very similar TGA curves, demonstrating that altering the amount of monomer, type of polyol used or increasing the amount of oil phase has minimal effect on the mechanism of PU shell formation. This corresponds with the FTIR analysis, which gave similar spectra for each of the PUNC samples.

The PUNCs start losing mass at around 90°C, corresponding to the T_M of $Mg(NO_3)_2.6H_2O$. Water is lost from the core up until approximately 200°C for all samples. By this temperature, the samples have lost between 40% (PUNC2) and 50% mass (PUNC4). At approximately 200°C, the PU shell starts to degrade, up until around 500°C. PU is clearly more thermally stable than PECA, which degraded

between 150-300°C. After heating to 600°C, the PUNCs have lost between 69% (PUNC2) and 75% (PUNC4) mass.

PUNC2 was synthesised using an excess of PEG2050 compared to the other samples, leading to the highest thermal stability. The excess of PEG may promote further crosslinking of the shell, leading to a higher MW polymer with better thermal stability. PUNC4 used a lower MW PEG (PEG200) monomer, and is the least thermally stable sample. This shows a high MW polyol is best for PU synthesis of energy storage nanocapsules. The high MW PEG molecules have more OH groups, aiding crosslinking during urethane formation resulting in increased thermal stability. No TGA curve was obtained for PUNC3 due to the lack of concordant results, possibly caused by impurities in the sample.

The PU TGA curves are similar to those of PECA nanocapsules displayed in Chapter 3 (Fig 3.9). The major differences are that PU has a higher degradation temperature (200°C compared to 150°C), but also that PUNCs have more mass loss between 100-150°C. By 150°C, PECA nanocapsules containing $Mg(NO_3)_2.6H_2O$ have lost 10% mass; corresponding PUNCs have lost 30%. Mass loss over this temperature range is attributed to water loss from the core crystallohydrate. It can be concluded that the PUNCs contain more water in the core in comparison to PECA. This was further confirmed by DSC results showing PUNCs had a lower encapsulation efficiency for the salt hydrates compared with PECA.

4.3.3 Latent heat storage of PUNCs

The key property of any thermal storage energy capsule is their latent heat storage capacity. DSC thermal cycling was undertaken on PUNC1 and PUNC3 (new samples were synthesised for these measurements, using 0.2g of MDI rather than 0.262g). It should be noted that DSC measurements for PUNC were taken on a less sophisticated instrument compared with the PECA samples, so results

may be less accurate due to less isolation and control of sample conditions. The samples were cycled between -20 to 120°C at 10°C/min. PUNC1 underwent 10 cycles. Full values obtained are shown in Table 4.3, while selected curves are shown in Fig 4.12. Melting peaks are broad, containing a small initial peak at around 79°C, which can be associated with a solid-solid transition of the crystalline structure. The peak melting temperature (T_M) changes during increased cycling, from 83.9°C in cycle 1 to 89.1°C by cycle 10, which is the literature value for $Mg(NO_3)_2.6H_2O$. Noticeable is the formation of multiple phases in the core of the PUNCs. Many peaks are present for the crystallisation of the crystallohydrate core, indicating these processes are non-homogeneous. As nucleation for freezing is a random process, it is difficult to achieve when the material is confined within a nanosized core. The PUNCs also display a large degree of supercooling, from 41.5°C in cycle 1 to 30.5°C in cycle 5. This is in stark contrast to the PECA nanocapsules, which practically eliminated supercooling. There are several possible explanations for the difference in supercooling seen in crystallohydrate-loaded nanocapsules. Supercooling results from poor nucleation properties. The inner shell surface composition can affect nucleation, so it is probable that nucleation occurs from the inner shell rather than the centre of the capsule, resulting in the difference between the two polymer shells. The PU polymerisation may also result in a thicker shell than PECA, reducing heat transfer and hindering crystallisation processes.

Latent heat actually increases from cycle 1 to cycle 10, which is unusual. Usually, a PCM decreases its latent heat over time, as the crystallohydrate gradually dehydrates. The increase can be explained by considering the non-homogeneous crystallisation. During each cycle, more of the crystallohydrate freezes into its hexahydrate form, leading to a more uniform core material, higher latent heat and the T_M equilibrating to the expected value. Latent heat after 10 cycles is 57.4 $J \cdot g^{-1}$, giving an encapsulation efficiency of 35.8%. The core material contained 50 %wt of $Mg(NO_3)_2.6H_2O$, so this is lower than expected, and can be explained by the poor nucleation inside the capsule core along with minimal heat transfer across the shell. Previous work in our group encapsulating paraffin wax docosane in PU had resulted in similar encapsulation efficiencies[28].

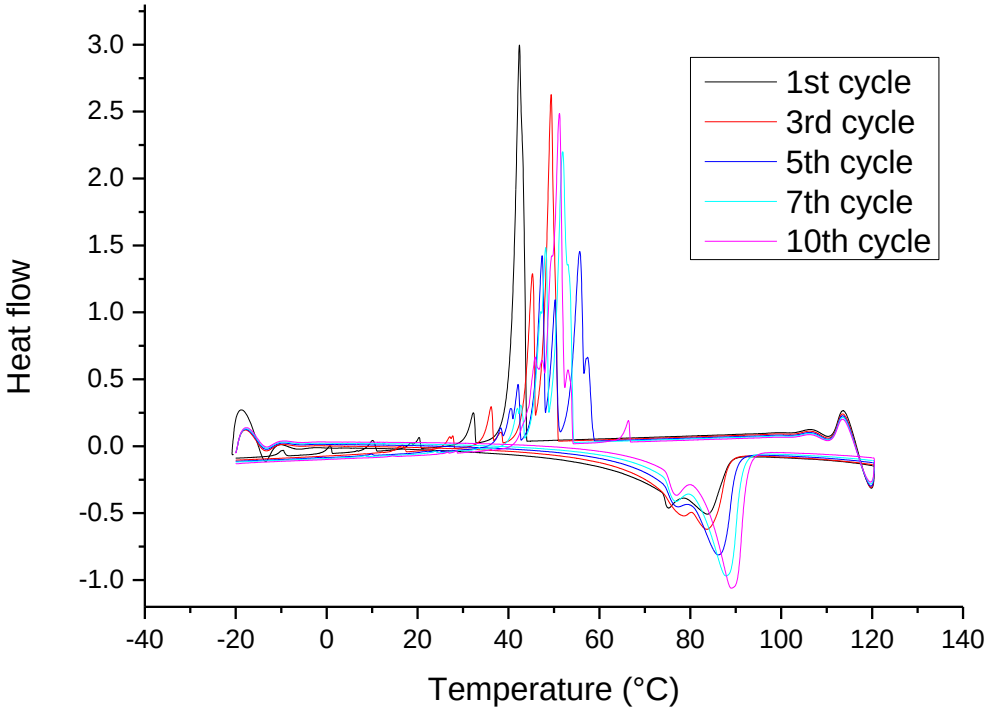

Fig 4.12 DSC curves for 10 thermal cycles between -20-120°C for PUNC1

Table 4.3 DSC results for PUNC1

Cycle	$T_{M, onset}$ (°C)	T_M (°C)	$T_{M, end}$ (°C)	$T_{F, onset}$ (°C)	T_F (°C)	$T_{F, end}$ (°C)	ΔH_M ($J \cdot g^{-1}$)	ΔH_F ($J \cdot g^{-1}$)
1	73.4	83.9	88.7	44.0	42.4	40.5	41.5	42.7
3	71.8	83.6	88.4	50.6	49.4	45.9	45.7	51.7
5	79.1	86.2	90.1	56.8	55.7	48.1	50.5	59.6
7	81.8	87.9	91.4	54.3	51.9	48.8	56.9	60.7
10	83.4	89.1	92.5	52.3	51.2	49.3	57.4	57.5

PUNC3 contains $Na_2SO_4.10H_2O$, but shows similar behaviour to PUNC1. The material was cycled 3 times, and melts between 32.9 and 36.5°C. Literature value for the T_M is 32°C. Again, latent heat increases from cycle 1 to cycle 3. After 3 cycles, latent heat is 67 $J \cdot g^{-1}$, giving an encapsulation efficiency of 29.4%. The core material contained 20 %wt of $Na_2SO_4.10H_2O$, so the latent heat is higher than expected. The melting peaks are fairly sharp, with only 1 peak present, showing $Na_2SO_4.10H_2O$ is the dominant phase present in the core. Thermal parameters are fully described in Table 4.4, DSC curves for PUNC3 are shown in Fig. 4.13.

Crystallisation is non-homogeneous with several peaks, and has a latent heat that is much smaller than that of the melting process. This can be explained that the material has not fully frozen during the measurement cycle. After the completion of each cycle, the material was set with an isothermal step at -20°C allowing the core PCM to fully freeze, leading to the higher latent heat seen in the melting cycle.

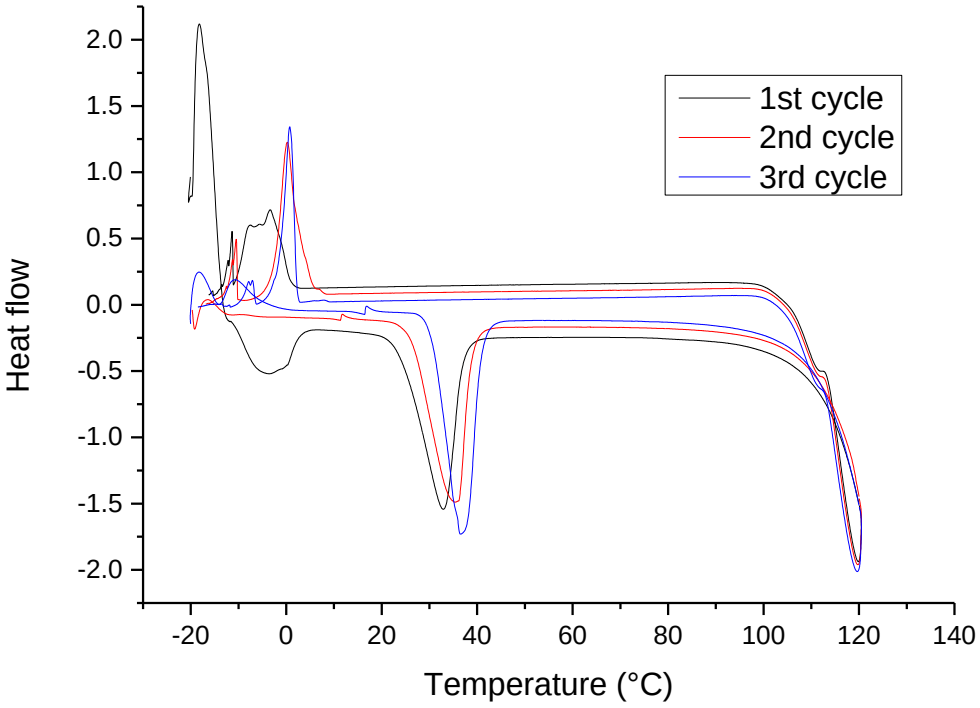

Fig 4.13 DSC curves for 3 thermal cycles between -20-120°C for PUNC3

Table 4.4 DSC results for PUNC3

Cycle	$T_{M, onset}$ (°C)	T_M (°C)	$T_{M, end}$ (°C)	$T_{F, onset}$ (°C)	T_F (°C)	$T_{F, end}$ (°C)	ΔH_M ($J \cdot g^{-1}$)	ΔH_F ($J \cdot g^{-1}$)
1	24.3	32.9	37.0	1.0	-3.4	n/a	62.6	33.2
2	26.2	35.4	38.8	3.0	0.2	-10.3	66.8	33.8
3	30.6	36.5	40.9	2.2	0.7	-1.5	67.0	22.4

From these results, it is clear PU can be used for the encapsulation of crystallohydrate PCMs. Thermal stability of the shell is improved compared to PECA nanocapsules in the previous chapter, with a higher degradation temperature for PU. PU is also more chemically resistant to many common solvents than PECA, including acetone and toluene, making it a good candidate for addition to oil-based host materials. The major drawback found in the results is supercooling of the core crystallohydrates and non-homogeneous nucleation, leading to unpredictable heat storage abilities. This problem is exacerbated by poor thermal conductivity of the PU shell, and possible issues of nucleation within the core. Future work to improve this is to add conductive carbon nanoparticles to the nanocapsule shell. Salt hydrate eutectics will also be encapsulated for modulation of the melting temperature.

4.4 References

1 T. Pitaksuteepong, N. M. Davies, I. G. Tucker and T. Rades, *Eur. J. Pharm. Biopharm.*, 2002, **53**, 335–342.

2 B. Nohra, L. Candy, J. F. Blanco, C. Guerin, Y. Raoul and Z. Mouloungui, *Macromolecules*, 2013, **46**, 3771–3792.

3 E. Delebecq, J. P. Pascault, B. Boutevin and F. Ganachaud, *Chem. Rev.*, 2013, **113**, 80–118.

4 D. K. Chattopadhyay and D. C. Webster, *Prog. Polym. Sci.*, 2009, **34**, 1068–1133.

5 A. A. Caraculacu and S. Coseri, *Isocyanates in polyaddition processes. Structure and reaction mechanisms*, 2001, vol. 26.

6 B. K. Kim, *Colloid Polym. Sci.*, 1996, **274**, 599–611.

7 F. Cheng, Y. Wei, Y. Zhang, F. Wang, T. Shen and C. Zong, *J. Appl. Polym. Sci.*, 2013, **130**, 1879–1889.

8 J. Yang, M. W. Keller, J. S. Moore, S. R. White, N. R. Sottos, J. Yang, M. W. Keller, J. S. Moore, S. R. White and N. R. Sottos, *Macromolecules*, 2008, **41**, 9650–9655.

9 X. Huang and B. Voit, *Polym. Chem.*, 2013, 435–443.

10 C. Zhang, S. A. Madbouly and M. R. Kessler, *ACS Appl. Mater. Interfaces*, 2015, **7**, 1226–1233.

11 Z. Petrovic, *Polym. Rev.*, 2008, **48**, 109–155.

12 G. Lligadas, J. C. Ronda, M. Galià, V. Cádiz, M. Galiá, V. Cádiz, M. Galià, V. Cádiz, M. Galiá and V. Cádiz, *Biomacromolecules*, 2010, **11**, 2825–2835.

13 C. Zhang, T. F. Garrison, S. A. Madbouly and M. R. Kessler, *Prog. Polym. Sci.*, 2017, **71**, 91–143.

14 I. Javni, Z. S. Petrović, A. Guo and R. Fuller, *J. Appl. Polym. Sci.*, 2000, **77**, 1723–1734.

15 B. Tamami, S. Sohn and G. L. Wilkes, *J. Appl. Polym. Sci.*, 2004, **92**, 883–891.

16 J. Guan, Y. Song, Y. Lin, X. Yin, M. Zuo, Y. Zhao, X. Tao and Q. Zheng, *Ind. Eng. Chem. Res.*, 2011, **50**, 6517–6527.

17 J. W. Boretos and W. S. Pierce, *Science (80-.).*, 1967, **158**, 1481–1482.

18 Z. Wang and T. J. Pinnavaia, *Chem. Mater.*, 1998, **10**, 3769–3771.

19 E.-M. Rosenbauer, M. Wagner, A. Musyanovych and K. Landfester, *Macromolecules*, 2010, **43**, 5083–5093.

20 K. Bouchemal, S. Briançon, E. Perrier, H. Fessi, I. Bonnet and N. Zydowicz, *Int. J. Pharm.*, 2004, **269**, 89–100.

21 H. Souguir, F. Salaün, P. Douillet, I. Vroman and S. Chatterjee, *Chem. Eng. J.*, 2013, **221**, 133–145.

22 X. X. Zhang, Y. F. Fan, X. M. Tao and K. L. Yick, *J. Colloid Interface Sci.*, 2005, **281**, 299–306.

23 J. P. Wang, X. P. Zhao, H. L. Guo and Q. Zheng, *Langmuir*, 2004, **20**, 10845–10850.

24 J. F. Su, L. X. Wang and L. Ren, *J. Appl. Polym. Sci.*, 2005, **97**, 1755–1762.

25 J. Su, L. Wang and L. Ren, *J. Appl. Polym. Sci.*, 2006, **101**, 1522–1528.

26 J. F. Su, L. X. Wang and L. Ren, *Colloids Surfaces A Physicochem. Eng. Asp.*, 2007, **299**, 268–275.

27 P. Felix De Castro and D. G. Shchukin, *Chem. - A Eur. J.*, 2015, **21**, 11174–11179.

28 P. Felix De Castro, A. Ahmed and D. G. Shchukin, *Chem. - A Eur. J.*, 2016, **22**, 4389–4394.

29 A. Schoth, K. Landfester and R. Muñoz-Espí, *Langmuir*, 2015, **31**, 3784–3788.

30 A. M. Borreguero, J. F. Rodriguez, J. L. Valverde, R. Arevalo, T. Peijs and M. Carmona, *J. Mater. Sci.*, 2010, **45**, 4462=4469.

31 A. M. Borreguero, J. F. Rodriguez, J. L. Valverde, R. Arevalo, T. Peijs and M. Carmona, *J. Mater. Sci.*, 2011, **46**, 347–356.

32 A. A. Aydin and H. Okutan, *Energy Convers. Manag.*, 2013, **68**, 74–81.

33 N. Sarier and E. Onder, *Thermochim. Acta*, 2008, **475**, 15–21.

34 Q. Zhu, Y. Chu, Z. Wang, N. Chen, L. Lin, F. Liu and Q. Pan, *J. Mater. Chem. A*, 2013, **1**, 5386.

35 J. C. Su and P. S. Liu, *Energy Convers. Manag.*, 2006, **47**, 3185–3191.

36 W. Kong, X. Fu, Z. Liu, C. Zhou and J. Lei, *Appl. Therm. Eng.*, 2016, **117**, 622–628.

37 X. Du, H. Wang, Y. Wu, Z. Du and X. Cheng, *J. Appl. Polym. Sci.*, 2017, **134**, 1–8.

38 J. M. Asua, *Prog. Polym. Sci.*, 2014, **39**, 1797–1826.

39 D. Saihi, I. Vroman, S. Giraud and S. Bourbigot, *React. Funct. Polym.*, 2005, **64**, 127–138.

40 D. Saihi, I. Vroman, S. Giraud and S. Bourbigot, *React. Funct. Polym.*, 2006, **66**, 1118–1125.

41 A. Hamberger, U. Ziener and K. Landfester, *Macromol. Chem. Phys.*, 2013, **214**, 691–699.

5. Materials and Methods

5.1 Materials

All chemicals were purchased from Sigma Aldrich (UK) except where noted. All were used as received without further purification.

5.1.1 Oils and solvents

Toluene (anhydrous, 99.8%) and cyclohexane (anhydrous, 99.5%) were employed as oils for W/O emulsion continuous phases. Chloroform (99.8%) and dichloromethane (anhydrous, 99.8% with 50-150ppm amylene as stabiliser) were used as solvents. Technical grade acetone and technical grade ethanol, along with Milli-Q water were used throughout.

5.1.2 Surfactants

Various commercial surfactants were used: Span 20 (sorbitan laurate), Span 80 (sorbitan monooleate) and Span 85 (sorbitan trioleate); Tween 20 BioXtra (polyethylene glycol sorbitan monolaurate) and Tween 80 (polyethylene glycol sorbitan monooleate); Igepal CO520 (branched polyoxyethylene nonylphenyl ether, average M_n 441); polyethylene glycol dioleate (PEGDO, average M_n 914) and Aerosol OT (AOT, dioctyl sulfosuccinate sodium salt, 97%).

5.1.3 Monomers/polymers and initiators etc.

Methyl methacrylate (MMA, 99%) was used for several polymerisation reactions, including crosslinking with ethyl acrylate (EA, 99.5% with 220ppm antioxidant as stabiliser). Ethyl-2-cyanoacrylate liquid was used as monomer for inverse micro-/miniemulsion *in situ* polymerisation. Methylene diphenyl diisocyanate (MDI, 98%) was used as diisocyanate monomer for PU crosslinking,

along with polyethylene glycol (PEG) 200 (average MW 200), PEG2050 (average M_n 2050) and polyvinyl alcohol (PVA, average MW 9000-10000 80% hydrolysed) as polyol monomers. Benzoyl peroxide (75%, remainder water) and dibutyltin dilaurate (DBDL, 95%) were used as initiators. Crosslinked sodium polyacrylate and stearic acid (98.5%) were used as lubricant and stabilisers for MMA/EA crosslinking.

5.1.4 Salt hydrates

Salt hydrates used as core materials for PCM emulsions and PCM capsules were magnesium nitrate hexahydrate ($Mg(NO_3)_2.6H_2O$, BioUltra 99%), sodium sulphate decahydrate ($Na_2SO_4.10H_2O$, 99%), calcium chloride hexahydrate ($CaCl_2.6H_2O$, 98%) and aluminium sulphate octadecahydrate ($Al_2(SO_4)_3.18H_2O$, 98%).

5.1.5 Nanocellulose

Nanocellulose was gratefully received as a gift from the Minko group at the University of Georgia, USA.

5.2 Methods

5.2.1 Chapter 2 methods

5.2.1.1 Microemulsion formation

To test the solubility of water in AOT, AOT was dissolved at different weight percentages in oil (either toluene or cyclohexane). Overall the oil phase was 10g. Water was then added in 100µL aliquots and vortexed until a permanent turbidity of the solution appeared, which indicated a saturated emulsion.

To solubilise large amounts of PCM, a high quantity of surfactants was required. 60 %wt of a surfactant blend of 3:2 Tween:Span was dissolved in toluene. Either solid (100 %wt) or 70 %wt (in water) $Mg(NO_3)_2.6H_2O$ (1g) was added and stirred mechanically overnight at 600 RPM.

5.2.1.2 Miniemulsion formation

A 20 %wt solution of salt hydrate ($Mg(NO_3)_2.6H_2O$ or $Na_2SO_4.10H_2O$) (1g) was added to a solution of 3:2 Tween:Span in cyclohexane (9g), and stirred for 30 min at 600RPM. The resulting macroemulsion was ultrasonicated for 10 min (1/2" tip, 70% amplitude; 30s on, 20s off pulse regime) in an ice bath to prevent evaporation of solvent, using a QSonica Q700-220 sonicator (700 W). After sonication, the previously milky solution became transparent/translucent and stable against agglomeration.

5.2.1.3 PMMA suspension copolymerisation

PMMA suspension copolymerisation was based on the method of Huang *et al*[1]. An aqueous phase (15g) of 70 %wt $Na_2SO_4.10H_2O$ in water was added to a solution of Span 80 (0.2g) in toluene (50mL). The solution was homogenised for 30 min at approximately 30000 RPM. The resulting emulsion was

milky and contained some precipitated salt hydrate. The emulsion was poured into a round-bottom flask, and a solution of MMA (10g) and EA (1.5g) in acetone (50mL) was added. Benzoyl peroxide (0.004g), stearic acid (0.007g) and sodium polyacrylate (0.003g) were added. The temperature was rose to 85^{o}C in a water bath and the reaction mixture left to polymerise for 5 hours. Product was separated by centrifugation at 12000 RPM for 30 mins and filtering under vacuum. The same procedure was also attempted but instead of the step of adding benzoyl peroxide for initiation, sonication was instead used. Sonication has been used to initiate MMA monomers previously[2].

5.2.1.4 PMMA nanoprecipitation

Nanoprecipitation of preformed polymer was based on the methods of Paiphansiri *et al*[3]. PMMA (MW = 996000 gmol^{-1}) was dissolved in DCM (2.25g) and added to a solution of 5 %wt 3:2 Tween80:Span20 in cyclohexane (13g), DCM (7.25g) and 70 %wt $Mg(NO_3)_2.6H_2O$ in water (0.5g). This was stirred for 30 minutes before sonicating for 2 mins (1/2" tip, 90% amplitude) in an ice bath. The resulting mixture was stirred at 50^{o}C overnight.

5.2.1.5 PMMA miniemulsion polymerisation

Miniemulsion polymerisation of PMMA was based on a method by Zhang *et al*[4]. A 70 %wt solution of $Mg(NO_3)_2.6H_2O$ was added to a surfactant blend of 1 %wt 2:1 Span 85:PEGDO in cyclohexane (15g), along with MMA (0.25g). This mixture was stirred at 600 RPM for 30 min at room temperature. Benzoyl peroxide (1.9mg) was added and the mixture sonicated for 10 min (1/2" tip, 50% amplitude; 30s on, 10s off pulse regimen) in an ice bath, yielding a milky solution. This was added to a sealed round-bottom flask and stirred at 600 RPM for 30 min under N_2 bubbling to deoxygenate the solution. Temperature was then increased to 70^{o}C and stirred at 600 RPM with N_2 bubbling for 24 hr.

The reaction mixture turned bright yellow due to the homolysis of benzoyl peroxide, and was left to dry in the fume hood to evaporate solvent and residual monomer.

5.2.2 Chapter 3 methods

5.2.2.1 PECA inverse microemulsion polymerisation

PECA nanocapsules were prepared according to the method used by Kafka *et al*[5], which was in turn based on a well-established procedure[6–8]. An aqueous phase (1g) consisting of different $Mg(NO_3)_2.6H_2O$:water ratios, either solid or solubilised in water, was added to the continuous oil phase (9g) consisting of 60 %wt surfactants (3:2 blend of Tween 80:Span 20) and 40 %wt toluene. The mixture was stirred overnight at 600 RPM to create a W/O miniemulsion. Then, ECA was dissolved in 3 times the amount of chloroform and added to the mixture dropwise. This was left to stir at 600 RPM overnight in an open vial. As chloroform evaporates, the polymerisation occurs around the microemulsion droplets. This procedure is outlined in Fig 3.4 (Method 1). The capsules were separated by centrifugation (11000 RPM for 10 mins at 10^{o}C) and washed by redispersing in cyclohexane *via* sonication. The capsules were again centrifuged (6000 RPM for 5 mins at 10^{o}C), and the product left to dry at room temperature, giving a white powder.

5.2.2.2 PECA inverse miniemulsion polymerisation

In order to decrease the amount of surfactants required, ultrasound was employed to create a W/O miniemulsion based on the method of Musyanovych *et al*[9]. An aqueous phase (1g) containing single or mixed crystallohydrates in water was added to an oil phase (9g) consisting of 5%wt surfactants and 95%wt cyclohexane. The mixture was mechanically stirred for 10 minutes at 600RPM to create a

macroemulsion. This was then sonicated for 12 mins (30s on, 20s off pulse regime, 70% amplitude) with ice bath cooling, using a Qsonica Q700-220 sonicator (700W) equipped with a micro tip. During sonication the cloudy solution became almost transparent, signifying a stable W/O miniemulsion had formed. After sonication, ECA dissolved in 3 times the amount of chloroform was added dropwise and left to stir at 600 RPM in an open vial for around 2 hours. This procedure is outlined in Fig. 3.4 (Method 2) and Fig 3.25. The product was separated by centrifugation (11000RPM for 10 mins at 10^{o}C) and left to dry at room temperature, yielding a translucent sticky solid. This was then redispersed in ethanol by sonication and centrifuged (6000 RPM for 5 mins at 10^{o}C). After drying at room temperature, a powder sample was obtained.

5.2.2.3 Formation of salt hydrate mixtures and eutectics

Salt hydrates were mixed together thoroughly, which resulted in partial melting due to the release of water. The mixtures were then frozen.

5.2.2.4 Addition of PECA nanocapsules to nanocellulose and textiles

1 %wt of dried PECA nanocapsules were dispersed in water by bath sonication for 20 min. The resulting dispersion was added to a 2 %wt nanocellulose fibre solution in water, at a ratio of 1:1. The mixture was stirred at 550 RPM for 2 hours.

To adsorb the nanocellulose on to textiles, the textile was dipped in the nanocellulose solution for 5 minutes, before curing at 70^{o}C overnight in an oven.

5.2.3 Chapter 4 methods

5.2.3.1 Complex coacervation of PU microcapsules

Pu microcapsules were synthesised based on the method of Saihi *et al*[10]. A solution of Span 85 (1g), PEGDO (0.38g) and toluene (45mL) was added to a second solution of $Mg(NO_3)_2.6H_2O$ (10.5g) in water (4.5mL). These were homogenised at approximately 30000 RPM for 1 min. A solution of MDI (1.25g) and DBDL (5 drops) dissolved in 10mL of Span 85 and PEGDO in toluene was added and sheared at 70^{o}C for 1 min at 30000 RPM. The temperature was reduced to 63^{o}C and the mixture left to react in a closed vial for 4 hours. The resulting microcapsules were washed with various solvents and centrifuged to separate.

5.2.3.2 Interfacial polymerisation of PU nanocapsules

PU nanocapsule preparation was based on the method of Hamberger *et al*[11]. An aqueous solution (1g) of crystallohydrate in water and hydrophilic monomer (PEG or PVA) (0.1g) was prepared. The solution was added to the oil phase (7.5g) consisting of 1 %wt surfactants (2:1 ratio of Span 85 to PEGDO) in cyclohexane. The mixture was stirred at 600 RPM for 30 min, creating a macroemulsion. The macroemulsion was ultrasonicated for 10 min (1/2" tip, 30s on, 10s off pulse regimen, 50% amplitude) in an ice bath to prevent evaporation of oil. The resulting miniemulsion contained no precipitate.

The miniemulsion was stirred at around 800RPM at 50^{o}C and a solution of MDI (approx. 0.2g) in 1%wt surfactants in cyclohexane (5g) was added dropwise over 15 min at 50^{o}C. The mixture was allowed to react for 2 hr to form a PU shell *via* carbamate links from the –NCO groups of the diisocyanate and the –OH groups of the polyol. The nanocapsules were separated by centrifugation (12000RPM, 10 min), and allowed to dry in a fume hood under ambient conditions.

5.2.4 Characterisation techniques

5.2.4.1 FTIR

Chemical analysis of the samples was made using a Bruker TENSOR II FTIR spectrometer equipped with an all-reflective diamond ATR. Transmittance measurements were taken on powder samples with 64 scans from 400 to 4000 cm^{-1}. The same procedure was used for liquid samples of PCM emulsions.

5.2.4.2 SEM and TEM

To analyse morphology of samples, along with capsule size, SEM measurements were taken with a JEOL JSM-7001F scanning electron microscope; whilst TEM images were obtained using a JEOL 2100FCs with a Schottky Field Emission Gun TEM (200 kV accelerating voltage). SEM samples were prepared as follows. Salt hydrates were crushed using a pestle and mortar and added directly to carbon tape attached to an SEM stub. Micro-/nanocapsule samples were diluted to approximately 0.1 %wt solid content in ethanol by bath sonication for 20 minutes. Best results are obtained when dispersing the reaction mixture directly from solution, rather than after centrifugation and drying. 50 µL of the resulting dispersion was added to a glass cover slide attached to SEM stub, and dried at room temperature overnight. The samples were coated by chromium sputtering (100 amp, 60s coating time) before measurement. To prepare TEM samples the same procedure was carried out but at 0.05 %wt solid content, before allowing samples to dry on a copper TEM grid.

5.2.4.3 TGA

Thermogravimetric analysis was taken using a TA Instruments SDT Q600, providing data on thermal degradation behaviour of both bulk and encapsulated salt hydrates. Measurements were taken from room temperature up to 600^{o}C, with a ramp of 10^{o}C min^{-1} under an N_2 atmosphere.

5.2.4.4 DSC

DSC measurements of PECA nanocapsules were taken using a DSC6 (Perkin Elmer, USA) to study cycling stability of the energy nanocapsules during heat uptake and release. 100 cycles were undertaken between -20 to 120^{o}C with a ramp of 5^{o}C under a nitrogen atmosphere. Measurements of the salt hydrate mixture T_Ms, along with DSC curves for PUNCs were taken using a DSC 214 (NETZSCH, Germany) with a ramp of 10^{o}C under a nitrogen atmosphere. T_Ms of salt hydrate mixtures were averaged over the 2nd and 3rd cycles between -20 to 120^{o}C.

5.2.4.5 XPS

X-ray Photoelectron Spectroscopy (XPS) measurements were made for NanoPCM1 and 2, using an PSP Electron Energy Analyser with Al Ka X-ray source (hn ¼1486.6 eV, 12 kV, 144 W, pass energy ¼ 20 eV). The base pressure of the system was <2 x 10^{-10} mbar with H2 as the main residual gas. The NanoPCM samples were crushed to form a fine powder before measuring.

5.2.4.6 XRD

X-ray diffraction measurements were taken using a Bruker diffractometer. Fine powder samples were scanned in transmission mode from 4 to 50 degrees (2θ) for 60 min.

5.3 References

1 J. Huang, T. Y. Wang, P. P. Zhu and J. B. Xiao, *Thermochim. Acta*, 2013, **557**, 1–6.

2 B. Teo, S. Prescott, M. Ashokkumar and F. Grieser, *Ultrason. Sonochem.*, 2008, **15**, 89–94.

3 U. Paiphansiri, P. Tangboriboonrat and K. Landfester, *Macromol. Biosci.*, 2006, **6**, 33–40.

4 G. H. Zhang, S. A. F. Bon and C. Y. Zhao, *Sol. Energy*, 2012, **86**, 1149–1154.

5 A. P. Kafka, B. J. McLeod, T. Rades and A. McDowell, *J. Control. Release*, 2011, **149**, 307–313.

6 M. R. Gasco and M. Trotta, *Int. J. Pharm.*, 1986, **29**, 267–268.

7 S. Watnasirichaikul, N. M. Davies, T. Rades and I. G. Tucker, *Pharm. Res.*, 2000, **17**, 684–689.

8 N. Behan, C. Birkinshaw and N. Clarke, *Biomaterials*, 2001, **22**, 1335–1344.

9 A. Musyanovych and K. Landfester, *Prog. Colloid Polym. Sci.*, 2007, **134**, 120–127.

10 D. Saihi, I. Vroman, S. Giraud and S. Bourbigot, *React. Funct. Polym.*, 2005, **64**, 127–138.

11 A. Hamberger, U. Ziener and K. Landfester, *Macromol. Chem. Phys.*, 2013, **214**, 691–699.

6. Conclusions and Future Work

6.1 General conclusions

This thesis details the importance of thermal energy storage within the context of humanity's energy problem. Increased demand and importance of energy, coupled with potential catastrophe of climate change mean new and non-polluting sources of energy are vital. Thermal energy storage using phase change materials (PCMs) is a cheap and efficient method to reduce energy problems associated with renewable energies and thermal regulation. Salt hydrates are the most promising PCM due to their high energy storage density, but suffer from chemical instability and thermal transfer issues. We found that confining them on the nanoscale within polymer capsules could vastly improve their thermal and chemical properties for potential domestic applications. Miniemulsions were found to be optimal templates for nanocapsule formation.

6.2 Chapter 2 conclusions

Surfactants can be employed as stabilisers for PCM emulsions. Aerosol OT (AOT) was the first surfactant investigated, using water to test for optimum parameters. Increasing the concentration of AOT led to an increase in solubilisation capacity in a non-linear fashion. Adding a co-surfactant led to a synergistic effect, increasing solubilisation capacity.

Using inverse microemulsions with large amounts of commercial Tween and Span surfactants (60 %wt of the continuous oil phase), it was possible to solubilise pure $Mg(NO_3)_2.6H_2O$ by stirring the mixture overnight. The amount of surfactant required could be greatly decreased by using ultrasonication for high energy processing to form miniemulsions, which have similar sized droplets to microemulsions but are kinetically, rather than thermodynamically, stable. Fully stable miniemulsions could be formed with only 5 %wt surfactants in the continuous phase. The miniemulsion technique also allowed the formation of PCM emulsions containing other salt hydrates such as $Na_2SO_4.10H_2O$ and $CaCl_2.6H_2O$.

It was not possible to isolate PCM emulsions for further analysis, however they provided an excellent template for polymerisation reactions to create polymer nanocapsules. Our first attempts at adding a polymer shell were using poly(methyl methacrylate). It was not possible to initiate the monomers however despite using several methods, so new polymer shell materials were sought.

6.3 Chapter 3 conclusions

To increase stability of our salt hydrate-loaded emulsions, we added a polymer shell. This was achieved with the *in situ* polymerisation of ethyl-2-cyanoacrylate around inverse micro-/miniemulsion droplets. The micro- and miniemulsions we had formulated using Tween and Span surfactants in Chapter 2 were useful as templates for the polymerisation. SEM and TEM showed the capsules were 100-300nm in size with complete coverage of the core material. Chemical analysis by FTIR, XPS and XRD showed salt hydrate was present within the sample. The microemulsion templates using large amount of surfactants were not as useful in producing salt hydrate loaded capsules. Although $Mg(NO_3)_2.6H_2O$ could be solubilised within the nanocapsule core and was stable over 100 cycles, it partially dehydrated to its dihydrate due to incongruent melting. This leads to 2 separate melting temperatures on the DSC curves, which is problematic for applications requiring a narrow temperature range. It was also discovered adding extra water to the aqueous core material promoted continued hydration of the salt, leading to higher latent heat.

Employing ultrasound to form miniemulsions led to improved results. Similarly sized capsules of 100-300nm were formed, but with $Mg(NO_3)_2.6H_2O$ remaining fully hydrated in the core, leading to a single melting point with high latent heat. Supercooling was also practically eliminated. Chemical and thermal stability over at least 100 melting/freezing cycles for these capsules was a great improvement over the bulk salt hydrates, which lose latent heat storage ability after around 5 cycles. The lower amount of surfactants needed for miniemulsions in comparison to microemulsions also led to a more thermally stable polymer shell. The work on salt hydrate-loaded PECA nanocapsules was summarised in a publication featured in Journal of Materials Chemistry A, 'Nanocapsules containing salt hydrate phase change materials for thermal energy storage' (DOI: 10.1039/c6ta06189c)[1]. An image we created was also featured on the inside back cover of the journal seen in Fig 6.1.

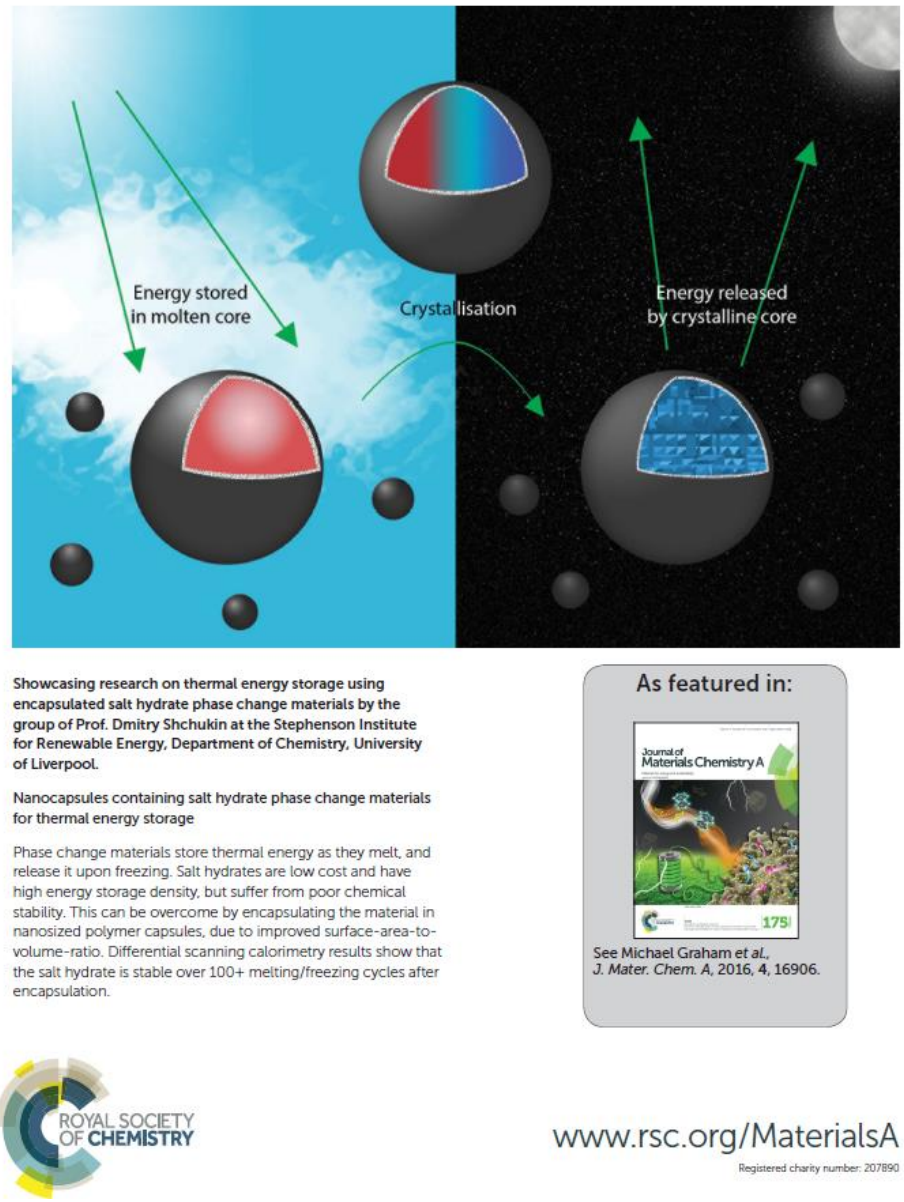

Fig 6.1 Image for inside back cover of Journal of Materials Chemistry A, Vol. 4, 2016

Further work using poly(ethyl-2-cyanoacrylate) (PECA) focused on encapsulating multiple salt hydrates. We found it was possible to encapsulate $Na_2SO_4.10H_2O$ using the same methodology; again the produced capsules were stable over 100+ cycles. Clearly, if a crystallohydrate can be solubilised within a miniemulsion, it is then possible to encapsulate it within a PECA shell and maintain stoichiometry for long-term use.

Two kinds of salt hydrate mixtures were investigated (i) additive mixtures of capsules containing single salt hydrates (ii) capsules containing mixed $Mg(NO_3)_2.6H_2O$ and $Na_2SO_4.10H_2O$ cores. The additive mixtures can prove highly useful in designing multi-temperature heat storage systems with different components reacting to different transition temperatures. Encapsulating salt hydrate mixtures can be very beneficial when encapsulated at the eutectic ratio – giving synergistic effects of low transition temperature, single defined melting temperature and high latent heat. However, when encapsulating at ratios other than the eutectic point, predictable melting and freezing was not achieved due to the formation of several crystallohydrate phases within the core. The work on salt hydrate mixtures led to a follow up publication in Journal of Materials Chemistry A, entitled 'Nanoencapsulated crystallohydrate mixtures for advanced thermal energy storage' (DOI: 10.1039/c7ta02494k)[2].

6.4 Chapter 4 conclusions

PECA nanocapsules showed the benefit of encapsulating crystallohydrates with a polymer shell. However, PECA is unstable at temperatures of 150°C and above, and can dissolve in several common organic solvents. Polyurethane (PU) is a commonly used commercial polymer with excellent durability. Many researchers have used PU as capsule shell material. We adapted two methods from the literature; a complex coacervation method yielding microcapsules, and an interfacial polymerisation reaction resulting in nanocapsules.

PU microcapsules were shown to be spherical in shape with diameters around 4µm. Chemical analysis suggested salt hydrate was present within the capsule core. Thermal properties were not fully analysed, however SEM images showed the capsules shrunk over time due to loss of core material. Methods to produce nanocapsules were then sought, as they are more durable as well as providing improved thermal performance.

PU nanocapsules were shown to have superior properties compared to the microcapsules. Using 1 %wt surfactants in the continuous phase led to powder samples being formed, which could be fully analysed. Both $Mg(NO_3)_2.6H_2O$ and $Na_2SO_4.10H_2O$ could be encapsulated. Again, chemical analysis from FTIR showed the presence of salt hydrate in the capsule samples. Thermal analysis from TGA showed the PU was more thermally stable than PECA, with shell degradation starting at approximately 200°C. DSC curves displayed promising results, with $Mg(NO_3)_2.6H_2O$ stable over 10 cycles and $Na_2SO_4.10H_2O$ over 3. Despite promising results, supercooling was a problem with PU capsules, which may be due to a thick shell forming, preventing thermal transfer. Poor nucleation inside the core was also an issue, as several phases formed.

6.5 Future Work

Generally, polymer shells have poor thermal conductivity, which can lead to poor thermal transfer to core materials. Conductive particles such as graphite may be added into the shell material to improve thermal transfer. Improved thermal conductivity leads to faster melting and freezing and a reduction of supercooling. PU nanocapsules studied in Chapter 4 will require prolonged thermal cycling tests to ensure long-term stability. Supercooling properties of PU nanocapsules may be due to a thick shell deposited on the miniemulsion droplets. This may be alleviated by varying the amount of monomers used in the synthesis. The effects of using a catalyst on the formation of PU nanocapsules will also be investigated, as it has the potential to greatly increase yield. Maximising encapsulation efficiency to maximise latent heat is also a priority.

As PU is a chemically and thermally durable polymer, it has great promise for addition to thermopaint, which is commercial paint with thermal storage abilities. PCM capsules may also be added to textiles for use in air-conditioned garments.

The work also has an impact for other researchers. Once salt hydrate-loaded capsule properties are optimised, they can be used in such applications as passive air conditioning in building walls. Creating stable capsules is also a goal for high temperature inorganic PCMs. Inorganic salts with T_Ms of 300^{o}C or more are planned for encapsulation using thermally resistant polymers or other shell material. Long term thermal energy storage materials have great potential for energy saving applications, with large chemical companies such as BASF interested in their use. These materials are vital as nations and companies attempt to fully realise an emission-free future, which will preserve our environment for future generations.

6.6 References

1 M. J. Graham, E. Shchukina, P. Felix De Castro and D. G. Shchukin, *J. Mater. Chem. A*, 2016, **4**, 16906–16912.

2 M. J. Graham, J. A. Coca-Clemente, E. Shchukina and D. Shchukin, *J. Mater. Chem. A*, 2017, **5**, 13683–13691.